

Washington University in St. Louis

## Washington University Open Scholarship

---

All Theses and Dissertations (ETDs)

---

January 2009

### Structurally diverse Cu-64-labeled RGD peptide conjugates for PET imaging of $\alpha v \beta 3$ expression

Ashley Fiamengo

*Washington University in St. Louis*

Follow this and additional works at: <https://openscholarship.wustl.edu/etd>

---

#### Recommended Citation

Fiamengo, Ashley, "Structurally diverse Cu-64-labeled RGD peptide conjugates for PET imaging of  $\alpha v \beta 3$  expression" (2009). *All Theses and Dissertations (ETDs)*. 407.

<https://openscholarship.wustl.edu/etd/407>

This Dissertation is brought to you for free and open access by Washington University Open Scholarship. It has been accepted for inclusion in All Theses and Dissertations (ETDs) by an authorized administrator of Washington University Open Scholarship. For more information, please contact [digital@wumail.wustl.edu](mailto:digital@wumail.wustl.edu).

WASHINGTON UNIVERSITY IN ST. LOUIS

Department of Chemistry

Dissertation Examination Committee

Carolyn J. Anderson, Chair

Samuel I. Achilefu

Joseph J. H. Ackerman

John R. Bleeke

Buck E. Rogers

John-Stephen A. Taylor

STRUCTURALLY DIVERSE Cu-64-LABELED RGD PEPTIDE

CONJUGATES FOR PET IMAGING OF  $\alpha_v\beta_3$  EXPRESSION

by

Ashley Lauren Fiamengo

A dissertation presented to the  
Graduate School of Arts and Sciences  
of Washington University in  
partial fulfillment of the  
requirements for the degree  
of Doctor of Philosophy

August 2009

Saint Louis, Missouri

copyright by  
Ashley Lauren Fiamengo  
2009

## ABSTRACT OF THE DISSERTATION

Structurally Diverse Cu-64-Labeled RGD Peptide Conjugates

for PET imaging of  $\alpha_v\beta_3$  Expression

by

Ashley Lauren Fiamengo

Doctor of Philosophy in Chemistry

Washington University in St. Louis, 2009

Professor Carolyn J. Anderson, Chair

Radiolabeled receptor-binding peptides have emerged as an important class of radiopharmaceuticals for diagnostic imaging and cancer therapy. Following radionuclide labeling, the specific receptor-binding properties of the ligand can be exploited to guide the radioactivity to tissues expressing a particular receptor. This dissertation reports on the development of integrin  $\alpha_v\beta_3$ -targeting radiopharmaceuticals for medical imaging applications from the perspective of both the radiometal-labeled chelator as well as the targeting peptide. Several macrocyclic copper(II) chelators have been studied with the goal of improving kinetic and *in vivo* stability. Structurally diverse bifunctional RGD (arginine-glycine-aspartic acid) peptides were investigated for  $\alpha_v\beta_3$  integrin affinity *in vitro* and *in vivo*. The goal of accomplishing higher binding affinity through multivalency has been pursued by evaluating the binding affinity of nanoparticles presenting multiple peptides on their surface.

Copper radionuclides have been the subject of considerable research effort because they offer a varying range of half-lives and positron energies, making them useful for diagnostic imaging and/or targeted radiotherapy. Ensuring the stability of metal

complexes *in vivo* remains a challenge in the development of radiometal-based radiopharmaceuticals. Reported here are data on the *in vitro* and *in vivo* evaluation of three macrocyclic chelators, C3B-DO2A, CB-TR2A, and NOTA. These studies were performed to improve Cu(II) complexation kinetics while retaining the high *in vivo* stability of our lead chelating agent, CB-TE2A. Optimal radiolabeling conditions were established for the  $^{64}\text{Cu}$ -labeled radiometal chelators and their *in vivo* biodistribution and excretion were studied in normal rats.

Integrin  $\alpha_v\beta_3$  is upregulated in tumor vasculature, osteoclasts, and areas of collateral circulation following ischemic injury. A series of structurally diverse bifunctional RGD (arginine-glycine-aspartic acid) peptides were investigated for  $\alpha_v\beta_3$  affinity *in vitro* and *in vivo*. The RGD-peptide analogs were screened for affinity to the  $\alpha_v\beta_3$  integrin and specificity compared to  $\alpha_v\beta_5$  and  $\alpha_{IIb}\beta_3$ . Extent of internalization of these peptides by an  $\alpha_v\beta_3$  expressing cell line, U87MG human glioblastoma cells, was determined. The compounds were screened via biodistribution studies and microPET imaging of a murine U87MG tumor model.

Polyvalence has known to have a profound effect on receptor-binding affinity and *in vivo* kinetics of radiolabeled multimers. The goal of accomplishing higher binding affinity through multivalency has been pursued by evaluating the binding affinity of shell cross-linked (SCK) nanoparticles presenting multiple RGD peptides on their surface. Difficulties encountered in obtaining nanoparticles with high levels of bioavailable targeting peptide on the surface led to a systematic study of methods of shell functionalization and particle purification with chemical, physical, and biological evaluation of each compound.

The development of radiometal-labeled peptides is a relatively slow process, thus in this research, optimization of various aspects was studied in parallel. Each chapter presents a small contribution, but the knowledge gained from these studies can be taken together to produce radiopharmaceuticals with optimal properties—high *in vivo* stability, high uptake in tumors, low uptake in non-target tissues, and rapid blood clearance, preferably through renal excretion.

## **Acknowledgements**

I have been blessed to have a multitude of wonderful people in my life who have helped me to become the young woman I am today. I will not name them all here, but that does not make their contributions to my life thus far any less meaningful.

I am thankful that from an early age my parents taught me the value of an education. Without my mother's support I don't know how I would have endured the many trials and tears that have been a part of the journey to where I am today. My siblings shaped me through our childhood antics and continue to play an invaluable role in my life. From my grandmother to aunts, uncles, and a whole host of cousins, my family has always shown me love and support and assured me that they always will.

During graduate school I have developed a diverse network of support, both at Washington University and from a multitude of other places. This community keeps me grounded and has enriched my life. I have dedicated friends, whom I can rely upon for encouragement, commiseration, distraction, and judicious advice (even when it's not what I want to hear). And the best cheerleader anyone could want.

Throughout the years many remarkable role models, teachers, and mentors have been part of my life, encouraging and inspiring me. My advisor, Dr. Carolyn Anderson, is the most recent of these individuals. She has taught me a great deal while challenging me to solve problems, accomplish goals, and seek balance.

Over the years many people in the Anderson, Welch, and Mach labs have taught me so much—fellow graduate students, post-docs, faculty. Interacting with them has enriched my graduate school career. The capable technicians and staff have been invaluable in making things run as smoothly as possible.

I have been fortunate to have Drs. Joe Ackerman, John Bleeke, and Sam Achilefu on my dissertation advisory committee. Each is an expert in his field. All have challenged me to think about important aspects of my thesis and have helped to direct me to its completion.

This research was supported through a Department of Defense Breast Cancer Research Program Predoctoral Fellowship (W81XWH-04-1-0396), a National Cancer Institute grant (R01 CA93375), and a National Heart, Lung and Blood Institute Program of Excellence in Nanotechnology (U01 HL080729). The production of  $^{64}\text{Cu}$  at Washington University School of Medicine is supported by a grant from the National Cancer Institute (R24 CA86307).

<b>Table of Contents</b>	
<b>Abstract of Dissertation</b>	i
<b>Acknowledgements</b>	iv
<b>Table of Contents</b>	vi
<b>List of Figures, Tables, and Schemes</b>	viii
<b>List of Abbreviations</b>	x
<b>Chapter 1: Introduction</b>	1
Molecular Imaging	2
Positron Emission Tomography	4
Targeted Radiopharmaceuticals	7
Copper-64	8
Design of Copper-64-labeled Radiopharmaceuticals	11
Integrin $\alpha_v\beta_3$	15
RGD Peptides	17
Nanotechnology	18
Summary of Research	19
<b>Chapter 2: Preparation and <i>In Vivo</i> Investigation of <math>^{64}\text{Cu}</math>-Labeled Cross-Bridged Tetraazamacrocyclic Complexes, C3B-DO2A and CB-TR2A: Comparison with NOTA</b>	21
Abstract	22
Introduction	23
Experimental Procedures	28
Results	31
Discussion	43
<b>Chapter 3: <i>In Vitro</i> and <i>In Vivo</i> Investigation of Structurally Diverse <math>^{64}\text{Cu}</math>-Labeled RGD Peptides for PET Imaging of <math>\alpha_v\beta_3</math> Expression</b>	44
Abstract	45
Introduction	46
Experimental Procedures	54
Results	60
Discussion and Conclusions	74

<b>Chapter 4: Preparation, Purification, and <i>In Vitro</i> Characterization of RGD-Functionalized Shell Crosslinked Nanoparticles</b>	78
Abstract	79
Introduction	80
Experimental Procedures	82
Results and Discussion	82
Conclusions	96
<b>Chapter 5: Concluding Remarks and Future Directions</b>	97
<b>Appendix I: Chapter 2 Supplemental Information</b>	102
<b>Appendix II: Chapter 3 Supplemental Information</b>	111
<b>Appendix III: Chapter 4 Supplemental Information</b>	114
<b>Appendix IV:</b>	128
Sprague, JE; Peng, Y; Fiamengo, AL; Wooden, KS; Southwick, EA; Weisman, GR; Wong, EH; Golen, JA; Rheingold, AL; Anderson, CJ. "Synthesis, characterization and in vivo studies of <sup>64</sup> Cu(II)-labeled cross-bridged tetraazamacrocyclic-amide complexes as models of peptide conjugate imaging agents." <i>J. Med. Chem.</i> <b>2007</b> ; 50 (10): 2527-2535.	
<b>References</b>	138
<b>Curriculum Vitae</b>	156

## List of Figures and Tables

Chapter 1		
Figure 1	Positron annihilation	5
Figure 2	PET scanner	6
Table 1	Decay characteristics of copper radionuclides	9
Figure 3	Bifunctional chelator	11
Figure 4	Tetraazamacrocyclic chelators and their Cu complexes	13
Figure 5	Integrin receptor family	16
Chapter 2		
Figure 1	Metalloradiopharmaceutical	24
Figure 2	Poylamine and polyaminocarboxylate chelators	25
Figure 3	C3B-DO2A, CB-TR2A, and NOTA	27
Figure 4	Structures of Cu-C3B-DO2A and Cu-CB-TR2A	32
Table 1	Acid-decomplexation half-lives and reduction potentials	34
Table 2	Initial Cu-64-C3B-DO2A radiolabeling attempts in acetate buffer	36
Table 3	Secondary radiolabeling attempts in acetate buffer	36
Table 4	Further radiolabeling attempts in acetate buffer	36
Table 5	Attempted radiolabeling in alternate aqueous buffers	37
Table 6	Radiolabeling with radiolytic scavengers	37
Table 7	Radiolabeling in ethanol with excess base	38
Table 8	Radiolabeling in ethanol with excess cesium carbonate	38
Table 9	Microwave assisted radiolabeling of Cu-64-C3B-DO2A	39
Figure 5	Organ biodistribution comparisons	42
Table 10	Excretion data	42
Chapter 3		
Figure 1	Tumor imaging targets based on integrin $\alpha_v\beta_3$	47
Figure 2	Standard RGD sequence compared to high affinity ligands	51
Figure 3	Structurally diverse RGD peptides	53
Figure 4	IC <sub>50</sub> binding curves for GRGDS	64
Table 1	Binding affinity values	64
Figure 5	Cellular internalization and cell-associated activity	66
Figure 6	Comparison of cellular binding and uptake at 60 min	67
Figure 7	Comparison of bidistribution in murine U87MG tumor model	68
Figure 8	Tumor:background tissue ratios	70
Figure 9	PET/CT images of Cu-64-DOTA-KCRGDC in U87MG tumor	71

Figure 10	PET/CT images of Cu-64-DOTA-GGRGDS in U87MG tumor	72
Figure 11	Comparison of SUV for Cu-64-DOTA-RGD peptides in U87MG tumor	73
Figure 12	Post-PET biodistribution comparison	73
Chapter 4		
Scheme 1	Post-labeling KCRGDC peptide to micelle/SCK	85
Table 1	IC <sub>50</sub> values of KCRGDC-micelle/SCKs prepared by post-labeling method	86
Table 2	IC <sub>50</sub> values of PEGylated SCKs, post-conjugated with PEG-RGD	87
Scheme 2	Post-conjugation of NH <sub>2</sub> -PEO <sub>113</sub> -5-FAM-KCRGDC onto SCKs	88
Figure 1	TEM images of PEGylated micelle/SCK nanoparticles	89
Scheme 3	Pre-labeling PEGylated SCKs with KCRGDC	90
Table 3	Characterization and IC <sub>50</sub> values of RGD-labeled micelle/SCKs	92
Figure 2	FPLC traces	93
Scheme 4	Synthesis of KCRGDC-labeled micelles and SCKs by post-labeling	95
Table 4	Characterization and IC <sub>50</sub> values of post-labeled nanoparticles	96
Appendix I		
Scheme 1	Synthesis of cyclo[RGDyK(DOTA)]	104
Scheme 2	Synthesis of DOTA-K-cyclo(CRGDC)-NH <sub>2</sub> .	106
Scheme 3	Synthesis of cyclo[RADyK(DOTA)]	108
Appendix III		
Scheme 1	Synthesis of NH <sub>2</sub> -PEG5000-5-FAM-KCRGDC	104
Scheme 2	Preparation of HOOC-PEG3000 <sub>4.0</sub> -g-DOTA-lysine <sub>3.2</sub> -g-PAA <sub>60</sub> -b-PS <sub>60</sub>	106
Scheme 3	Cleavage of disulfide bond on KCRGDC	108

## List of Abbreviations

%ID/g	Percentage injected dosage per gram
%ID/organ	Percentage injected dosage per organ
AA	Ascorbic acid
AFM	Atomic force microscopy
ANOVA	Analysis of variance
ATRP	Atom transfer radical polymerization
BFC	Bifunctional chelator
BSA	Bovine serum albumin
C3B-DO2A	4,10-bis(carboxymethyl)-1,4,7,10-tetraazabicyclo[5.5.3]pentadecane
CB-TE2A	4,11-bis(carboxymethyl)-1,4,8,11-tetraazabicyclo[6.6.2]hexadecane
CB-TR2A	4,11-bis(carboxymethyl)-1,4,8,11-tetraazabicyclo[6.5.2]pentadecane
CT	Computed tomography
$D_{av}$	Average particle diameters
DCC	<i>N,N</i> -Dicyclohexylcarbodiimide
DCM	Dichloromethane
Dde	1-(4,4-Dimethyl-2,6-dioxocyclohexylidene)ethyl
$D_h$	Hydrodynamic diameter
DIC	Diisopropylcarbodiimide
DIPEA	<i>N,N</i> -Diisopropylethylamine
DLS	Dynamic light scattering
DMF	<i>N,N</i> -Dimethylformamide
DOTA	1,4,7,10-tetraazacyclotetradecane- <i>N,N',N'',N'''</i> -tetraacetic acid
DOTA-(3OBu <sup>t</sup> )-COOH	1,4,7,10-tetraazacyclododecane-1,4,7-tris( <i>t</i> -butyl acetate)-10-acetic acid
DSC	Differential scanning calorimetry
DTPA	Diethylenetriaminepentaacetic acid
DTT	Dithiothreitol
ECM	Extracellular matrix
EDCI	1-[3'-(Dimethylamino)propyl]-3-ethylcarbodiimide methiodide
EDTA	Ethylenediaminetetraacetic acid
ES-MS	Electrospray-mass spectrometry
Fn	Fibronectin
FDG	[ <sup>18</sup> F]-fluoro-D-deoxyglucose
FITC	Fluorescein isothiocyanate
Fmoc	9-Fluorenylmethoxycarbonyl

FPLC	Fast protein liquid chromatography
FT-IR	Fourier transform infrared
GA	Gentisic acid
GPC	Gel permeation chromatography
H <sub>av</sub>	Average particle heights
HBSS	Hank's balanced salt solution
HBTU	2-(1H-Benzotriazole-1-yl)-1,1,3,3-tetramethyluronium hexafluorophosphate
HEPES	4-(2-Hydroxyethyl)piperazine-1-ethanesulfonic acid
HOBt	Hydroxybenzotriazole
HPLC	High performance liquid chromatography
HUVEC	Human umbilical vein endothelial cells
HYNIC	6-Hydrazinopyridine-3-carboxylate hydrochloric acid
IR	Infrared
IV	Intravenous
MaCaF	Mammary carcinoma
MAP	Maximum a posteriori
MBTE	Methyl tert-butylether
MEM	Minimum essential medium
MRI	Magnetic resonance imaging
NHS	<i>N</i> -Hydroxysuccinimide
NMR	Nuclear magnetic resonance
NNLS	Non-negatively constrained least-squares
NOTA	1,4,7-Triazacyclononane- <i>N,N',N''</i> -triacetic acid
PAA	Poly(acrylic acid)
PBS	Phosphate buffered saline
PEG	Poly(ethylene glycol)
PET	Position emission tomography
PI	Post-injection
PMDETA	<i>N,N,N',N',N''</i> -Pentamethyldiethylenetriamine
PMT	Photomultiplier tube
PS	Polystyrene
PTA	Phosphotungstic acid
P <i>t</i> BA	Poly( <i>t</i> -butyl acrylate)
P <i>t</i> BA- <i>b</i> -PS	Poly( <i>t</i> -butyl acrylate)- <i>b</i> - polystyrene
PyBOP	Benzotriazole-1-yl-oxy-tris-pyrrolidino-phosphonium hexafluorophosphate
RGD	Arginine-glycine-aspartic acid
ROI	Region of interest
RT	Room temperature
SCK	Shell crosslinked knedel-like
SDS	Sodium dodecylsulfate

SOD	Superoxide dismutase
SPECT	Single photon emission computed tomography
Sulfo-NHS	<i>N</i> -Hydroxysulfosuccinimide
SUV	Standard uptake value
TACN	1,4,7-Triazacyclononane
TEM	Transmission electron microscopy
TETA	1,4,8,11-Tetraazacyclotetradecane-1,4,8,11-tetraacetic acid
TFA	Trifluoroacetic acid
THF	Tetrahydrofuran
TLC	Thin layer chromatography
UV-Vis	Ultraviolet-visible
Vn	Vitronectin

## **CHAPTER 1**

Introduction

## **Molecular Imaging**

Molecular imaging has distinguished itself as an interdisciplinary field drawing from chemistry, biology, physics, and medicine. The fact that a collaborative effort among several professional societies was undertaken to define molecular imaging emphasizes its broad reach. "Molecular imaging is the visualization, characterization, and measurement of biological processes at the molecular and cellular levels in human and other living systems. To elaborate: Molecular imaging typically includes 2- or 3-dimensional imaging as well as quantification over time. The techniques include radiotracer imaging/nuclear medicine, MR imaging, MR spectroscopy, optical imaging, ultrasound, and others."<sup>1</sup> It has impacted clinical medicine and pharmaceutical development. Physicians can generate high-resolution images of the human body non-invasively, diagnose ailments, and prescribe or monitor treatment regimens based on them. Scientists involved in drug discovery can accelerate the screening process in pre-clinical drug development. Molecular imaging can facilitate determinations of desired and undesired pharmaceutical side effects, analyze drug-target interactions, and evaluate delivery absorption, distribution, metabolism, and elimination *in vivo*. Its utility in studying drug action, establishing dosing regimens and treatment strategies will eventually provide the means to accomplish "personalized medicine" by monitoring individual response to drug delivery.<sup>2</sup>

Molecular imaging differs from traditional imaging in that biomarkers are used to help image particular targets or pathways. Biomarkers are characteristics that are objectively and quantitatively measured and evaluated as an indicator of normal biological processes, pathogenic processes, or pharmacologic responses to a therapeutic intervention. They interact chemically with specific components in their surroundings allowing imaging of physiological changes, altering the image according to molecular changes occurring within the area of interest. This process is markedly different from older methods of imaging, such as x-ray and magnetic resonance imaging (MRI), which primarily image differences in qualities such as

density or water content. The ability to image fine molecular changes opens up numerous exciting possibilities for medical and research applications. Furthermore, molecular imaging allows for quantitative tests, imparting a greater degree of objectivity to these imaging studies.

Nuclear medicine is a medical field that employs molecular imaging through the use of radioactive agents (e.g. radiopharmaceuticals) for the purpose of diagnosis and therapy of disease. By imaging the distribution of radioactivity in the subject, physicians can non-invasively provide useful information about metabolism, blood flow, inflammation, and receptor status as well as location, size, and extent of diseased tissues. Radiopharmaceuticals are created by the incorporation of radionuclides into compounds tailored for biological targeting. This non-invasive imaging relies on the external detection of the emitted radiation by cameras surrounding the subject. The intrinsic properties of the radionuclide utilized determine the value of an agent for imaging or therapy, in addition to determining the appropriate imaging modality—gamma camera, single photon emission computed tomography (SPECT) or positron emission tomography (PET). A gamma camera gives planar images, whereas SPECT and PET provide three-dimensional images. In the research described here, PET imaging, which utilizes positron-emitting radionuclides, is used to investigate *in vivo* biological processes non-invasively.

## Positron Emission Tomography

PET allows for non-invasive construction of static anatomical images as well as the collection of dynamic, real-time images of a biochemical process. PET images are obtained following intravenous (IV) injection of a positron ( $\beta^+$ ) emitting radiopharmaceutical whose biochemical behavior and biological distribution are well characterized. The development of novel positron-emitting radiopharmaceuticals with desirable clearance and pharmacokinetic properties is a growing field of research.<sup>3</sup>

Radioactive decay occurs as part of the process of balancing an unstable nucleus' proton/neutron ratio. Proton-rich isotopes undergo a process that will lower this ratio and result in a stable nucleus. One method is through the addition of energy to convert a proton ( $p$ ) into a neutron ( $n$ ), neutrino ( $\nu$ ) and a positron ( $\beta^+$ ) (Equation 1).



The new element recoils from the event, and the positron and neutrino are emitted at high speed. The positron, a positively charged electron, collides with electrons as it travels through the surrounding matter losing kinetic energy. Once most of the energy has been lost, the positron associates with an electron, which has an opposite charge but equal mass, and both particles annihilate. The particles' masses are converted into energy in the form of two 511 keV photons, emitted in opposite directions, almost  $180^\circ$  apart from each other (Figure 1). These annihilation photons can be detected by coincidence circuitry consisting of a solid scintillation crystal coupled to a photomultiplier tube (PMT). The energy of the positron determines the distance traveled by the particle prior to annihilation. Higher ejection energy corresponds to a greater distance traveled before annihilation. This distance, known as the positron range, affects image resolution.

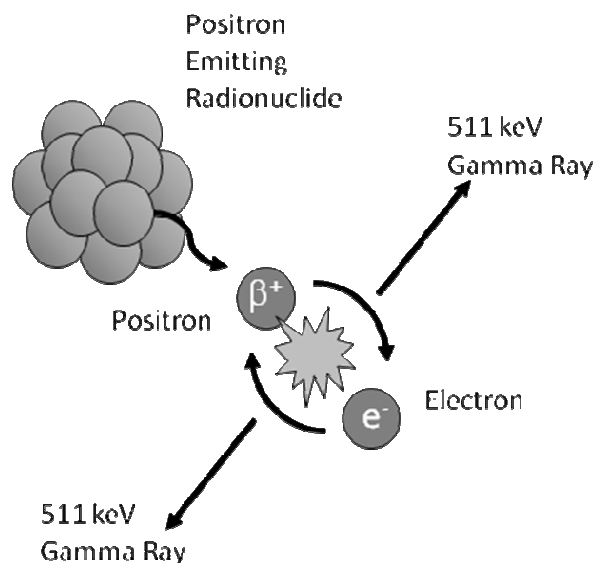


**Figure 1.** A positron is emitted from an unstable proton-rich nucleus. After traveling a short distance, it annihilates upon contact with an electron. This releases two photons approximately 180° apart.

A PET scanner consists of an array of detectors surrounding the subject, connected through coincidence circuitry. A decay event is recorded when a pair of photons are received at connected detectors within a certain time frame (Figure 2). The exact site of the annihilation is unknown, but by acquiring a large number of coincidence events recorded across all detector combinations, sufficient information is obtained for complex computer algorithms to reconstruct the numerous events that have been registered into an image with information on the spatial distribution of radioactivity as a function of time. Several factors affect image resolution, including positron range, photon attenuation, and random coincidences from scattered and random photons. Once corrections for photon attenuation and random, scattered radiation have been made, the measured tissue radioactivity can be reported in absolute units, such as Becquerel (Bq)/mL. Correlation of PET images with anatomical imaging modalities, such as CT and MRI, can aid in accurate identification of tissues with enhanced uptake.<sup>4</sup>

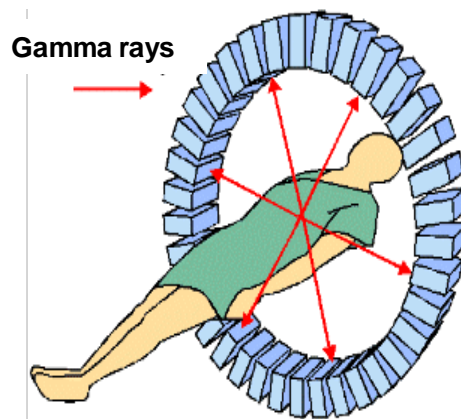


**Figure 2.** Cartoon of a human PET scanner. A circular array of detectors surrounds the patient and records sets of co-incident photon pairs.

Biomedical research usually involves extensive pre-clinical evaluation prior to approval for human use. Animal models are employed in radiopharmaceutical development. Human PET scanners have insufficient resolution for small animal, such as rodent, imaging. A small animal PET scanner called microPET has better sensitivity and image resolution for imaging in rodent or other small animal models.<sup>5</sup> Additionally, microPET systems are more compact and cost less than clinical PET systems. As with human PET images, microPET and micro-computed tomography (microCT) images can be co-registered to enhance anatomical resolution in small animal imaging.

## Targeted Radiopharmaceuticals

Radiopharmaceuticals are radioactive compounds used in nuclear medicine for diagnosis and therapy. There are two broad categories of radiopharmaceuticals: substrate specific and non-substrate specific agents. The more common, substrate-specific radiopharmaceuticals are designed to target a specific biological process, receptor or other type of protein expressed in distinct regions of the body. Radiolabeled peptides have been extensively investigated for targeting over-expressed receptors on tumor cells and at sites of cardiovascular injury and repair. Targeted radiopharmaceuticals are useful for diagnostic imaging as well as for predicting response to a therapeutic regimen such as chemotherapy or targeted radiotherapy. Depending on the mode of radioactive decay of the radionuclide, these or analogous compounds can also be used for targeted radiotherapy.

Selection of the proper radionuclide in radiopharmaceutical design is important and depends on several factors. The half-life should allow for sufficient uptake and decay to yield contrast and quality images.<sup>6</sup> The mode of decay and energies of the radionuclide emission should be suitable for detection by the chosen imaging modality. Radiopharmaceuticals incorporating  $\beta^+$  or  $\gamma$  emitting radionuclides are useful for PET or SPECT imaging, respectively. Cost and availability should also be considered.

There are a variety of commonly used positron emitting radionuclides with various energy profiles and half-lives. The most widely used isotope for PET radiopharmaceuticals is  $^{18}\text{F}$  due to practicality of transport with a half-life of 109.8 min and ideal average  $\beta^+$  energy.<sup>7</sup> The only FDA approved tracer for oncologic imaging is [ $^{18}\text{F}$ ]2-fluoro-D-deoxyglucose (FDG), a radiolabeled glucose derivative.<sup>8</sup> FDG, the most common targeted PET imaging radiopharmaceutical, is taken up by glucose-utilizing cells and retained following phosphorylation by hexokinase. It is used for studying cerebral, myocardial, and tumor glucose metabolism; however, the

specificity of FDG is compromised due to uptake by inflamed and infected tissues as well as by metabolically active tumors.

Radiolabeled peptides are good alternatives to FDG, as certain peptide-based agents specifically target receptors that are overexpressed by specific tumor cells. Peptides have many of the favorable characteristics of small molecule radiotracers, namely rapid blood clearance and tissue penetration, and low antigenicity. However,  $^{18}\text{F}$  cannot be readily incorporated into peptides and antibodies as targeted radioligands.<sup>8</sup> The short 119 min half-life of  $^{18}\text{F}$ , typical 2 h synthesis that includes HPLC purification, and resultant low yield are not ideal for radiopharmaceutical production. Due to the larger size of peptides, metals can be more readily attached to peptides via coordination by covalently bound chelators. This additional functional group typically has well established radiolabeling chemistry and its attachment often has no significant effect on peptide binding to target receptors. Also, the diversity of half-lives of radiometals allows the physical half-life of the isotope to be matched to the biological half-life of the radiopharmaceutical.<sup>9</sup> Therefore, the development of radiometal-based agents is an active area of research.

### **Copper-64**

Copper radionuclides have been the subject of considerable research effort because they offer a varying range of half-lives and positron energies, making them useful for diagnostic imaging and/or targeted radiotherapy (Table 1).<sup>10, 11</sup> Their half-lives range from 10 minutes to 62 hours; they decay by positron ( $\beta^+$ ) and/or beta-minus ( $\beta^-$ ) emission. The biodistribution of these copper radionuclides can be assessed externally via clinical positron or gamma imaging techniques.

**Table 1.** Decay characteristics of copper radionuclides.<sup>8</sup>

Isotope	$t_{1/2}$	$\beta^-$ MeV (%)	$\beta^+$ MeV (%)	EC (%)	$\gamma$ MeV (%)
<sup>60</sup> Cu	23.4 min	---	2.00 (69%)	7.4%	0.511 (186%)
			3.00 (18%)		0.85 (15%)
			3.92 (6%)		1.33 (80%)
					1.76 (52%)
<sup>61</sup> Cu	3.32 h	---	1.22 (60%)	40%	2.13 (6%)
					0.284 (12%)
					0.38 (3%)
<sup>62</sup> Cu	9.76 min	---	2.91 (97%)	2%	0.511 (120%)
<sup>64</sup> Cu	12.7 h	0.573 (38.4%)	0.655 (17.8%)	41%	0.511 (34.8%)
					1.35 (0.6%)
<sup>67</sup> Cu	62.0 h	0.395 (45%)	---	---	0.184 (40%)
		0.484 (35%)			
		0.577 (20%)			

Positron-emitting radionuclides are produced on either accelerators or cyclotrons. Typically, a target material is bombarded with a proton beam to produce a (p, n) nuclear reaction. A proton is incorporated into the nucleus followed by the release of a neutron, resulting in a proton rich, unstable radionuclide that undergoes  $\beta^+$  decay, as previously described. At Washington University, no-carrier-added <sup>64</sup>Cu is produced on a biomedical cyclotron in high yield and high specific activity.<sup>12</sup> Briefly, a gold disk target electroplated with enriched <sup>64</sup>Ni is irradiated with 14.5 MeV protons on a CS-15 biomedical cyclotron. The target is introduced to an automated processing system, and the nickel is dissolved in heated 6 M hydrochloric acid (HCl).<sup>13</sup> The dissolved nickel is loaded on an ion chromatography column and recovered for recycling. Copper-64 is eluted off using 0.5 M HCl and blown down under argon.<sup>14</sup>

Copper-64 has a long history of applications as a biomedical tracer because of its longer half-life and short positron range. The 12.7 hour half-life allows for distribution of this nuclide from regional production centers to imaging centers that do not have direct access to a cyclotron. Copper-64 decays 17.8% by positron emission and has a  $\beta^+$  maximum energy of 0.655 MeV with an average energy of 0.28 MeV. It

also decays by electron capture and  $\beta^-$ ; therefore, it has been studied as both a diagnostic and therapeutic radionuclide.<sup>15</sup> The  $\beta^+$  maximum energy of 0.655 MeV is similar to  $^{18}\text{F}$ , so the resulting PET images are of high quality.<sup>16</sup>

Copper coordination chemistry is well described in the literature, facilitating the development of copper-based radiopharmaceuticals.<sup>12</sup> Copper is a first-row transition metal that primarily exists in two oxidation states: Cu(I) and Cu(II). The coordination geometry for Cu(I) complexes is almost always tetrahedral and remains stable in aqueous solution when coordinated to soft donors, such as phosphines and thioethers. The labile nature of most Cu(I) complexes in solution makes them unsuitable for radiopharmaceutical applications. The coordination number for Cu(II) ranges from 4 to 6 depending on the denticity of the chelator. Four-coordinated Cu(II) complexes are normally square planar while 5-coordinated Cu(II) complexes are often square pyramidal. The 6-coordinated Cu(II) complexes have a distorted octahedral arrangement with the apical donor atoms weakly bound to the Cu(II). Jahn-Teller distortion causes axial elongation or tetragonal compression in these complexes.<sup>17, 18</sup> While Cu(II) complexes are often kinetically labile, they are less labile to ligand exchange and are favored for incorporation in radiopharmaceuticals.

### **Design of Copper-64-labeled Radiopharmaceuticals**

For target agents with a long biological half-life or those intended for targeted radiotherapy, it is imperative that the complexes formed are highly kinetically and thermodynamically stable to minimize accumulation of the radiometal in non-target tissues. Ligands that form radiocopper complexes with superior kinetic inertness to Cu(II) decomplexation are favored over thermodynamic stability because this is more significant following injection of the radiopharmaceutical into a living organism. Reduction of Cu(II) to Cu(I) followed by Cu(I) loss may be another mode of radiocopper loss, so resistance of the complex to Cu(II)/Cu(I) reduction and reversibility can also be important. Rapid complexation kinetics are favored to allow

for easy formation of the metal-chelator complex. Finally, the design of chelators should incorporate available functional groups for covalent linking to targeting peptides, proteins, and antibodies. A ligand consisting of a functional group for attachment to the targeting moiety and a metal complexing ligand is a bifunctional chelator (BFC) (Figure 3).<sup>9, 19, 20</sup>

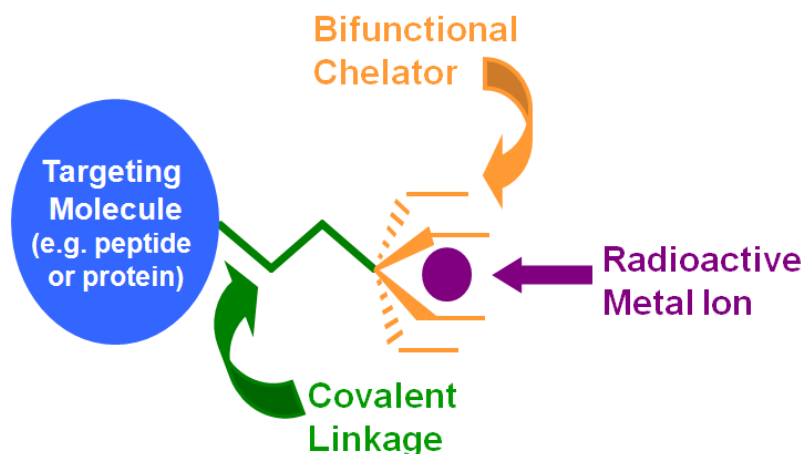


**Figure 3.** Schematic of a radiopharmaceutical showing a bifunctional chelator (BFC) to complex the radioactive metal ion attached to a targeting moiety, such as a peptide.

The design of BFCs for copper has focused on macrocyclic chelators that form kinetically stable and kinetically inert Cu(II) complexes. Copper(II) complexes of linear polyaminopolycarboxylate ligands such as ethylenediaminetetraacetic acid (EDTA) and diethylenetriaminepentaacetic acid (DTPA) have been shown to have rapid transchelation of the Cu(II) to human serum albumin despite having high thermodynamic stability.<sup>21, 22</sup> Tetraazamacrocyclic chelators, such as cyclen (1,4,7,10-tetraazacyclododecane) and cyclam (1,4,8,11-tetraazacyclotetradecane) as well as their derivatives, have been shown to be significantly more stable *in vivo*.<sup>23</sup> Two N-functionalized derivatives of cyclen and cyclam, 1,4,7,10-tetraazacyclotetradecane-*N,N',N'',N'''*-tetraacetic acid (DOTA) and 4,11-bis(carboxymethyl)-1,4,8,11-tetraazabicyclousexahexadecane (TETA) respectively, are

commonly used examples (Figure 4).<sup>24</sup> These BFCs can be covalently attached to the peptide by formation of an amide bond between one carboxylate arm of the chelator and the peptide's N-terminus, leaving three carboxylates for possible coordination to the radiometal. Both TETA and DOTA have been attached to peptides and proteins for labeling with copper radionuclides. Their kinetic stability *in vivo* is far from ideal, with dissociation leading to higher concentrations of <sup>64</sup>Cu in the blood and liver, which decreases the efficacy for imaging and therapy.<sup>24</sup>

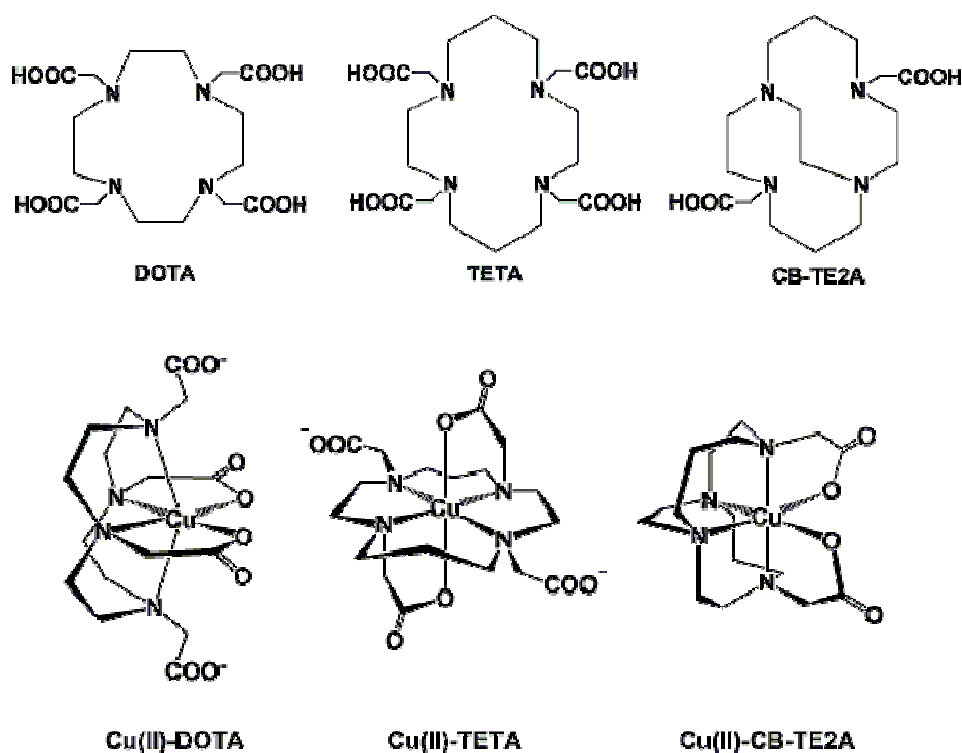


**Figure 4.** Structures of tetraazamacrocyclic chelators, and three dimensional representations of Cu(II)-DOTA, Cu(II)-TETA, and Cu(II)-CB-TE2A based on crystal structures.

Endeavoring to develop more stable BFCs for copper radionuclides, a new class of bicyclic tetraamines featuring ethylene cross-bridges has been recently reported.<sup>25</sup> The radiocopper complex of one such compound, CB-TE2A (4,11-bis(carboxymethyl)-1,4,8,11-tetraazabicyclo[6.6.2]hexadecane), demonstrates improved blood, liver, and kidney clearance and more favorable biodistribution

compared to the standard copper chelates  $^{64}\text{Cu}$ -DOTA and  $^{64}\text{Cu}$ -TETA.<sup>26, 27</sup> Metabolism studies in rats show that, compared to  $^{64}\text{Cu}$ -DOTA and  $^{64}\text{Cu}$ -TETA,  $^{64}\text{Cu}$ -CB-TE2A has increased stability and reduced transchelation of  $^{64}\text{Cu}$  to liver superoxide dismutase (SOD).<sup>28</sup>

Comparison of the structures of the Cu(II) complex of CB-TE2A with DOTA and TETA shows distorted octahedral coordination geometry with the copper being chelated by four nitrogens and two oxygens for each complex (Figure 4).<sup>27</sup> However, the coordinating atom arrangement around each Cu(II) is different. Cu(II)-TETA has two trans-axial oxygens while the coordinating oxygens for Cu(II)-DOTA and Cu(II)-CB-TE2A have a *cis* conformation. Cu(II)-CB-TE2A adopts a low strain conformation with all four nitrogen lone pairs coming together in a cleft, allowing the Cu(II) to be fully enveloped in a “clamshell” arrangement.<sup>27</sup> Both Cu(II)-DOTA and Cu(II)-TETA have two non-coordinating carboxylate arms that remain free for potential conjugation to a targeting moiety, whereas Cu(II)-CB-TE2A has no free carboxylate arms. While this affects the net charge of the cross-bridged macrocyclic complex, it has been demonstrated that a single carboxylate arm is sufficient for *in vivo* stability.

Cross-bridged chelators have demonstrated improved kinetic and *in vivo* stability; however, the radiolabeling conditions required for formation of  $^{64}\text{Cu}$ -CB-TE2A and  $^{64}\text{Cu}$ -CB-TE2A-peptide conjugates are harsh. Biologically compatible aqueous conditions are sufficient for radiocopper complexation by TETA (0.5 M  $\text{NH}_4\text{OAc}$ , pH 6.5 for 30 min at room temperature (RT)).<sup>29</sup> For formation of radiocopper cross-bridged chelator complexes, the chelator must be pre-incubated for 30 min with excess  $\text{Cs}_2\text{CO}_3$  in EtOH at 75° C with constant mixing before the addition of  $^{64}\text{CuCl}_2$  and then complexation is achieved by heating for 30 min at 75° C.<sup>30</sup> Cross-bridged chelator-peptide conjugates require somewhat milder labeling conditions (0.1 M  $\text{NH}_4\text{OAc}$ , pH 6.5 - 8 for 45-90 min at 95° C).<sup>31</sup> In order to be compatible with larger peptides or antibodies,  $^{64}\text{Cu}$ -radiolabeling conditions would require aqueous solution near physiological pH at or below 43° C. Thus,

development of other kinetically stable and kinetically inert BFCs with favorable labeling kinetics remains an active area of research.

### **Integrin $\alpha_v\beta_3$**

Integrins are best understood to constitute an important class of cell adhesion receptors. They are responsible for cell-matrix adhesion and signaling across the membrane. Integrins and their ligands play key roles in development, immune response, leukocyte traffic, hemostasis, cellular entry and exit, and cancer.<sup>32</sup> The 18 known  $\alpha$  subunits and 8 known  $\beta$  subunits associate non-covalently to form 24 integrin heterodimers (Figure 5).<sup>33, 34</sup> Each of these appears to have a distinct, non-redundant function, as concluded from their ligand specificities and from phenotypes of knockout mice.<sup>35</sup>

The  $\alpha_v\beta_3$  integrin is expressed on the surface of a variety of cell types including endothelial cells,<sup>36-39</sup> platelets,<sup>40</sup> osteoclasts,<sup>41</sup> melanoma,<sup>42</sup> and smooth muscle.<sup>43</sup> Although known as the “vitronectin receptor,” it binds a variety of extracellular matrix proteins with the exposed RGD sequences including fibrinogen, fibronectin, laminin, collagen, Von Willibrand’s factor and osteopontin.<sup>42</sup> From these diverse sites of expression and ligands, it should not be surprising the diversity of physiological roles ascribed to it: angiogenesis,<sup>44</sup> apoptosis,<sup>45</sup> and bone resorption.<sup>46</sup> Induction of angiogenesis by a tumor or cytokine promotes the expression of  $\alpha_v\beta_3$ . Angiogenesis is essential for the proliferation and metastatic properties of human tumors. Unregulated neovasculature is also responsible for a variety of other pathological processes such as restenosis,<sup>47</sup> rheumatoid arthritis, and retinopathy.<sup>48</sup> <sup>49</sup> Due to integrin  $\alpha_v\beta_3$ ’s key role in many physiological processes, it has been evaluated extensively as a drug target.<sup>50</sup>

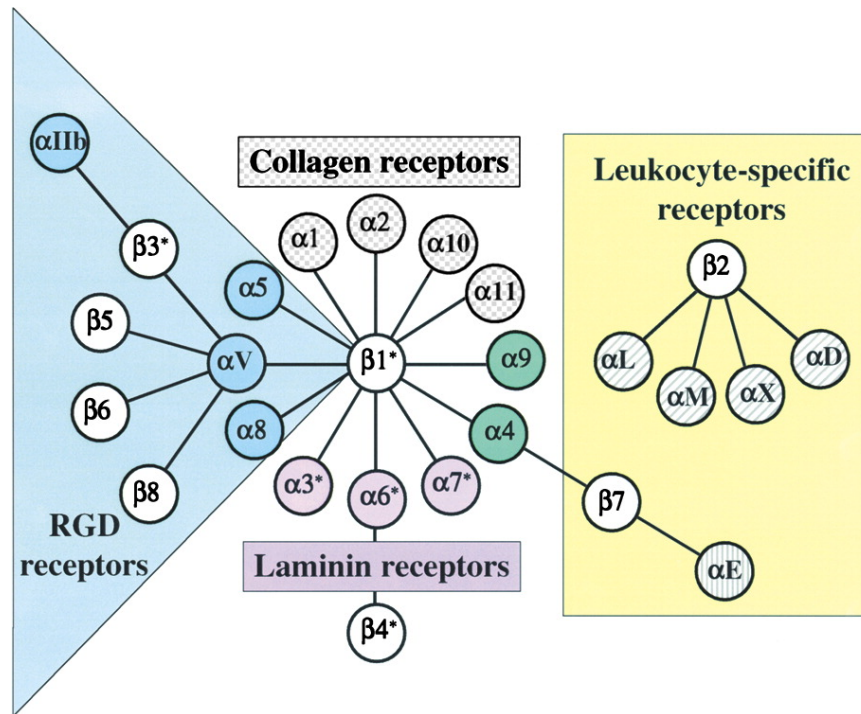


**Figure 5.** The integrin receptor family. Schematic representation of the mammalian subunits and their  $\alpha\beta$  associations which can be considered in several subfamilies based on evolutionary relationships and ligand specificity. RGD receptors are indicated on the left-hand side. (Reprinted with permission from R.O. Hynes.<sup>51</sup>)

The  $\alpha_v\beta_3$  integrin has been targeted with RGD (Arginine-Glycine-Aspartic acid) peptides for PET imaging because of its expression on neovasculature as well as some tumor cells.<sup>52</sup> At least one report demonstrates the ability to image  $\alpha_v\beta_3$  on neovasculature in an  $\alpha_v\beta_3$ -negative tumor, but other reports indicate that only  $\alpha_v\beta_3$ -positive tumors are detected following injection of a radiolabeled RGD-peptide. Neither the mechanism of  $\alpha_v\beta_3$  involvement in tumor neoangiogenesis nor the ability to image  $\alpha_v\beta_3$  specifically on blood vessels is well-established. Additionally, osteoclasts have high levels of  $\alpha_v\beta_3$  expression where it is required for bone resorption. Peptidomimetic  $\alpha_v\beta_3$  antagonists have been found to reduce bone resorption *in vitro* and *in vivo*. Administration of an  $\alpha_v\beta_3$  antagonist prevented hypercalcemia of malignancy in a mouse model of Leydig cell tumor, an effect due to

inhibition of tumor cell secretion of osteoclast activating factors or direct inhibition of osteoclasts.<sup>36</sup>

### **RGD Peptides**

Proteins that express the RGD attachment sit together with the integrins that serve as receptors for them and comprise a major recognition system for cell adhesion. Because of its small structure, the RGD site can easily be reproduced with peptides. Short peptides containing the basic RGD sequence can mimic cell adhesion proteins in two ways. When coated on a surface, they can promote cell adhesion, while in solution they block adhesion by serving as decoys. RGD peptides that have not been specifically designed to be selective for binding to certain integrins mimic a number of adhesion proteins and bind to more than one receptor. The peptide can be quite specific in its activity, however. Conformation of the amino acids is known to be important; changing the aspartic acid residue to the D-form inactivates the peptide. Replacing the aspartic acid with a glutamic acid or the glycine residue with an alanine reduces the activity of the peptide in cell attachment assays by 100-fold or more.

Since the RGD-sequence is conserved in all native ligands, differences in binding affinities and specificity can be obtained from slight modifications. The flanking amino acid residues, especially the two positions following the aspartic acid, are known to change binding affinity both by direct interaction of the residues with the integrin as well as influencing peptide folding. Cyclization is a common technique to improve binding properties because it confers rigidity on the structure. All selective RGD peptides have at least one ring structure. Linear RGD peptides are highly susceptible to degradation, due to reaction of the aspartic acid residue with the peptide backbone. Non-natural peptide modifications, such as the introduction of D-amino acids and replacement with peptidomimetic structures, have yielded RGD peptide ligands with greater specificity and nanomolar or higher affinities. Multivalent

RGD-protein conjugates demonstrate subnanomolar affinity for  $\alpha_v\beta_3$ -expressing human umbilical vein endothelial cells (HUVEC), a 250-fold increase versus the monomer. Furthermore, multivalency has been shown to facilitate internalization. Carrier systems like liposomes, nanoparticles, and proteins bearing multiple RGD peptides are therefore more likely to be internalized via receptor-mediated endocytosis than single peptide constructs.

## **Nanotechnology**

Nanotechnology is a rapidly expanding field, benefiting from multidisciplinary efforts in research, development, and education. It is a broad field encompassing everything from nanoscale phenomena and processes to societal studies of the benefits and risks of nanotechnology. Conventionally, nanoscale materials are defined as being man-made and having a size of 1 to 100 nm in at least one dimension. Unusual physical, chemical, and biological properties can emerge in materials at the nanoscale. These properties may differ in important ways from the properties of bulk materials and single atoms or molecules. The size of nanoparticles makes them capable of imitating many features of biological species, including proteins, a feature being taken advantage of by scientists to probe cell structure and function at the sub-cellular level. Advances in nanotechnology and medicine in the past decade are allowing researchers to take advantage of many unique properties of nanoscale materials for improved diagnosis and treatment of disease.

Nanomedicine is the application of nanotechnology to disease treatment, diagnosis, monitoring and control of biological systems, as defined by the National Institutes of Health (NIH). The goal of nanomedicine is to develop safer and more effective therapeutic and diagnostic modalities. Because of the size and supramolecular structure of nanoparticles, technologies utilizing nanoparticles have much potential for improving cancer therapy. A primary attribute of nanoparticle

delivery systems is their potential to enhance the tumor accumulation of anticancer agents in tumor cells than healthy tissues.

Polymeric nanoparticles have attracted interest for their potential applications in nanomedicine. Shell crosslinked nanoparticles (SCKs) mimic the amphiphilic core-shell morphology with a hydrophobic core contained within a hydrogel network. They are prepared from self-assembly of amphiphilic block copolymers which are subsequently crosslinked between the polymer chains located within a shell. SCKs present many available sites for surface functionalization by attachment of a variety of compounds, such as receptor-targeting ligands, cell penetrating peptides, and chelators for radiolabeling. Guest molecules can be encapsulated by the hollowing of the core by selective degradation of the polymer chains. The properties of SCKs are tunable by control of size, shape, and particle composition, as has been demonstrated previously by Murthy *et al.*<sup>52</sup>

Through a multidisciplinary collaboration between physicians and scientists at Washington University, a concerted effort is underway to develop a group of well-characterized and versatile nanoscale agents for targeted drug delivery. Novel SCKs with the peptide KCRGDC have been evaluated for their affinity for the  $\alpha_v\beta_3$  integrin.

### **Summary of Research**

Molecular imaging plays an increasingly important role in disease management, from screening and diagnosis to treatment and follow-up. This is dependent upon the development of robust and specific image contrast agents. The goal of this dissertation is to develop novel radiometal-based radiopharmaceuticals for medical imaging. This has been addressed from the perspective of both the bifunctional chelators as well as the targeting moiety.

Stability of metal chelates *in vivo* is a considerable challenge but consideration must also be paid to the complex formation kinetics. In this work,

several macrocyclic copper(II) chelators have been studied with the goal of developing a BFC with good complex formation kinetics and *in vivo* stability.

Integrin  $\alpha_v\beta_3$  is implicated in many disease processes—angiogenesis, proliferation of vascular smooth muscle following injury, tumor metastasis, inflammation, and osteolysis. With so many potential disease targets, it is an interesting molecular target for diagnostic and therapeutic imaging. This work reports on the investigation of structurally diverse bifunctional RGD peptides for affinity for integrin  $\alpha_v\beta_3$  *in vitro* and *in vivo*. *In vitro* characterization of RGD-functionalized nanoparticles is also presented.

## CHAPTER 2

Preparation and *In Vivo* Investigation of  $^{64}\text{Cu}$ -Labeled Cross-Bridged  
Tetrazamacrocyclic Complexes, C3B-DO2A and CB-TR2A: Comparison with NOTA

## Abstract

Copper radionuclides have been the subject of considerable research effort because they offer a varying range of half-lives and positron energies, making them useful for diagnostic imaging and/or targeted radiotherapy. Ensuring the stability of metal complexes *in vivo* remains a challenge in the development of radiometal-based radiopharmaceuticals. A new class of structurally reinforced macrocycles, “cross-bridged” cyclam derivatives, form highly stable complexes with Cu(II) that are resistant to dissociation in strong acid and have rapid tissue clearance in biodistribution studies; however, their radiolabeling is inefficient and requires harsh conditions that are unsuitable for larger biomolecules. Here, we report the evaluation of three macrocyclic chelators--C3B-DO2A, CB-TR2A, and NOTA—as we seek more rapid Cu(II) complexation kinetics while retaining the high *in vivo* stability of CB-TE2A. The <sup>nat</sup>Cu complexes were characterized by structure evaluation, inertness to acid decomplexation, and electrochemical properties. The inertness of Cu-C3B-DO2A to decomplexation is remarkable, exceeding that of CB-TE2A. Electrochemical reduction of Cu-CB-TR2A is quasi-reversible; Cu-C3B-DO2A and Cu-NOTA are irreversible. The reaction conditions for preparing <sup>64</sup>Cu-C3B-DO2A (microwaving at high temperature) and <sup>64</sup>Cu-CB-TR2A (basic ethanol) are relatively harsh compared to those for the conventional complexes, such as DOTA. The *in vivo* behavior of <sup>64</sup>Cu-ligand complexes was evaluated in normal rats. Rapid and continual clearance of <sup>64</sup>Cu-CB-TR2A and <sup>64</sup>Cu-NOTA through the blood, liver, and kidneys suggests good *in vivo* stability, although inferior to <sup>64</sup>Cu-CB-TE2A. Although <sup>64</sup>Cu-C3B-DO2A clears continually, the initial uptake is high and only about half is excreted within 22 h, suggesting poor stability and transchelation of <sup>64</sup>Cu to proteins in the blood and/or liver. These data suggest that *in vitro* stability of a chelator may not always be a good indicator of *in vivo* stability. Furthermore, a macrocyclic chelator with rapid complexation kinetics which also demonstrates kinetic inertness

comparable to the previously studied  $^{64}\text{Cu}$ -CB-TE2A, under physiological conditions, has not yet been identified.

## **Introduction**

Radiopharmaceuticals, drugs containing a radionuclide, are routinely used in nuclear medicine for the diagnosis and therapy of various diseases.<sup>9, 53-55</sup> An ideal radiopharmaceutical would be injected intravenously, travel via the blood stream to the target tissue or cells, and interact in an effective manner and with only the desired molecular pathway.<sup>56</sup> Excretion of any radiopharmaceutical that did not reach the intended target would occur rapidly, leaving in the body only the fraction of the radiotracer which localized to the target site. While an ideal compound may never exist, the objective in radiopharmaceutical design is to come as close as possible.

Substrate-specific radiopharmaceuticals are designed to target a specific biological process, protein, or receptor expressed in distinct regions of the body. Generally, a substrate-specific metalloradiopharmaceutical is composed of four parts: a targeting biomolecule, a linker, a bifunctional chelator (BFC), and a metallic radionuclide (Figure 1).<sup>18, 57</sup> Each of these components must be considered in light of each other and optimized as a whole. Thus, the design of novel BFCs and their characterization with specific radiometals is an area of ongoing research.

BFCs must form a very stable metal chelate, demonstrating kinetic inertness at physiological pH. Its solution stability in biological medium depends primarily on a slow rate of dissociation. This is important to avoid a loss of radiometal from the chelate, resulting in the accumulation of radioactivity in non-target tissue that obscures imaging of the desired target and increases the radiation dose the subject receives. Rapid complexation kinetics are also favored to allow for easy formation of the metal-chelator complex.

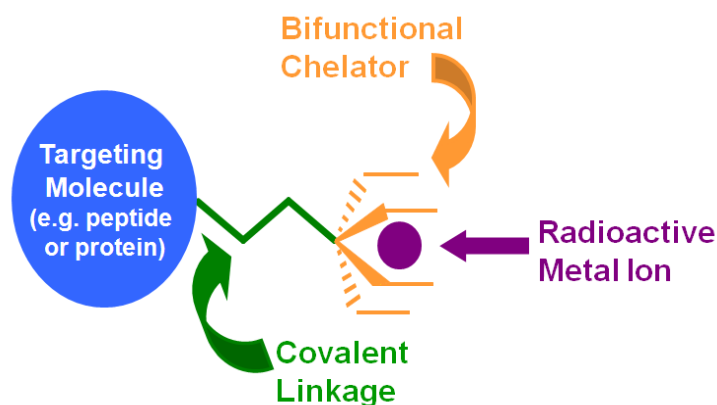


**Figure 1.** Conceptual diagram of a substrate specific metalloradiopharmaceutical.

As discussed in the introduction (chapter 1), copper radionuclides have been the subject of considerable research effort because they offer a varying range of half-lives and positron energies, making them useful for diagnostic imaging and/or targeted radiotherapy. Their half-lives range from 10 minutes to 62 hours, and they decay by positron ( $\beta^+$ ) and/or beta-minus ( $\beta^-$ ) emission. The biodistribution of these copper radionuclides can be assessed externally via clinical positron or gamma imaging techniques. Copper-64 has a long history of applications as a biomedical tracer because of its longer half-life and short positron range ( $T_{1/2}=12.7$  h;  $\beta^+$ : 0.656 MeV, 17.8%;  $\beta^-$ : 0.573 MeV, 38.45%).<sup>58</sup>

Kinetic stability of Cu(II) complexes has been shown to be more predictive of *in vivo* stability than thermodynamic stability.<sup>22, 59</sup> Since the coordination chemistry of copper radionuclides has been extensively reviewed,<sup>15, 57</sup> only a brief summary will be given here. Macrocyclic chelators of Cu(II) such as TETA (1,4,8,11-tetraazacyclotetradecane-1,4,8,11-tetraacetic acid) demonstrate higher kinetic and thus *in vivo* stability relative to acyclic chelators such as EDTA (ethylene diamine tetraacetic acid).<sup>12, 59, 60</sup> However, biodistribution and metabolism studies of  $^{64}\text{Cu}$ -TETA in rats have demonstrated significant transchelation of  $^{64}\text{Cu}$  to superoxide dismutase and metallothionein in liver and albumin in blood resulting in high background radioactivity.<sup>61, 62</sup> Cu(II) complexes with a class of chelators called the

cross-bridged macrocycles, in particular CB-TE2A (4,11-bis(carboxymethyl)-1,4,8,11-tetraazabicyclo[6.6.2]hexadecane), have shown much greater *in vivo* stability;<sup>62, 63</sup> however, a disadvantage of CB-TE2A is that labeling with copper radionuclides requires heating to 95 °C, and this precludes the use of this chelator with proteins or other heat-sensitive compounds.

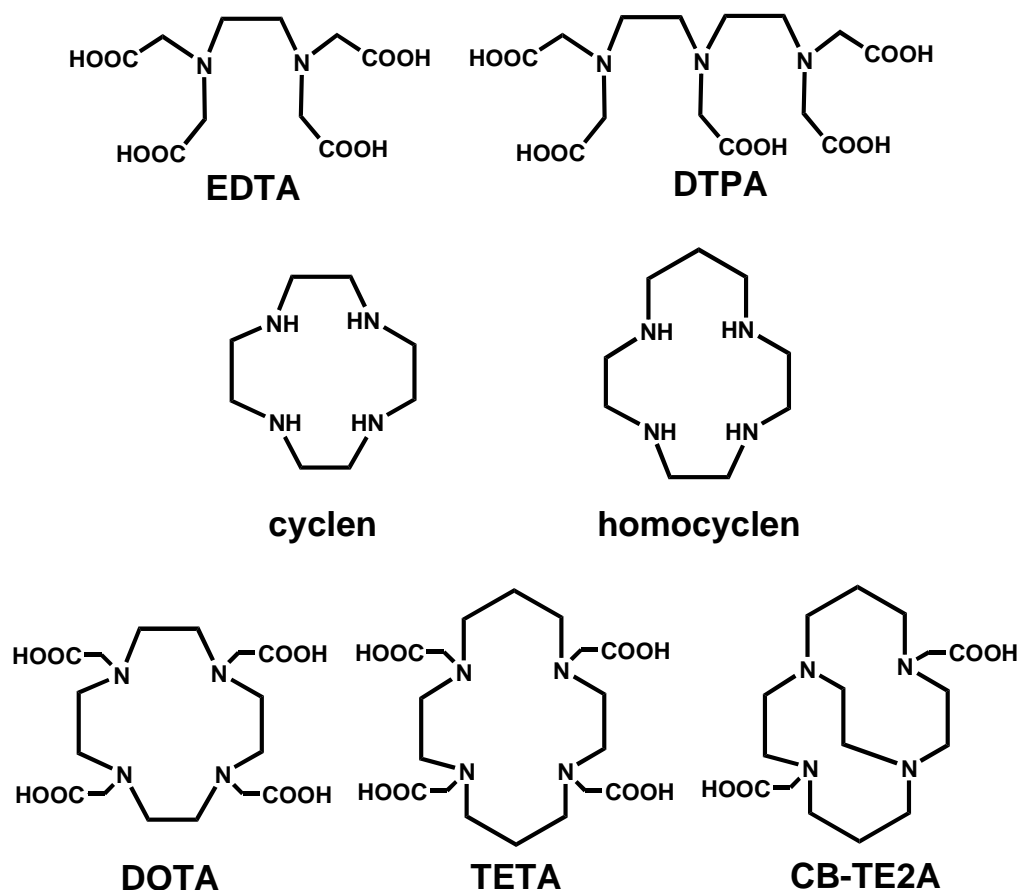


**Figure 2.** Structures of representative polyamine and polyaminocarboxylate acyclic and cyclic chelators for radiometal complexation.

To design cross-bridged chelators that complex Cu(II) with faster kinetics while retaining the high *in vivo* stability of CB-TE2A, different ring sizes of cross-bridged tetraazamacrocycles were designed. First, a dicarboxylate analog of Springborg's trimethylene-cross-bridged cyclen<sup>64, 65</sup> was proposed. This DOTA analog, 4,10-bis-(carboxymethyl)-1,4,7,10-tetraazabicyclo[5.5.3]pentadecane

(C3B-DO2A), has one more methylene unit in the cross-bridge than the previously studied CB-DO2A.<sup>62</sup> The biodistribution of <sup>64</sup>Cu-CB-DO2A demonstrated rapid clearance of the agent through the blood, liver, and kidneys. It is hypothesized that the increased ring size of C3B-DO2A will improve the radiolabeling kinetics while retaining the *in vivo* stability of CB-DO2A.

Homocyclen has a ring size falling between that of cyclen and cyclam. Just as C3B-DO2A was chosen for its slightly larger ring size than the previously studied CB-DO2A, a two-carbon cross-bridged dicarboxylate analog of homocyclen, 4,11-bis-(carboxymethyl)-(1,4,8,11-tetraazabicyclo[6.5.2]pentadecane (CB-TR2A), was proposed.

Prasanphanich *et al.* recently reported <sup>64</sup>Cu-labeled bombesin analogs using 1,4,7-triazacyclononane-N,N',N''-triacetic acid (NOTA) as a chelator. The reduced liver and intestinal accumulation suggested high *in vivo* kinetic stability of <sup>64</sup>Cu-NOTA-bombesin vectors with little or no dissociation of <sup>64</sup>Cu from NOTA.<sup>66</sup> This chelator has been used multiple times as a BFC for <sup>64/67</sup>Cu and <sup>68</sup>Ga attachment to antibodies<sup>67</sup> and peptides<sup>68, 69</sup>; however, an evaluation of the *in vivo* stability of the <sup>64</sup>Cu-NOTA complex has not previously been reported. Stability constants for several metal-NOTA complexes are found in literature<sup>70, 71</sup> as well as crystal structures for Cu(II)-NOTA and Ga(III)-NOTA.<sup>72, 73</sup> NOTA deviates from most of the macrocyclic chelators that we investigate because it is a triazamacrocycle and not cross-bridged; however, its reported high *in vivo* stability and rapid labeling kinetics drive our interest in this molecule.

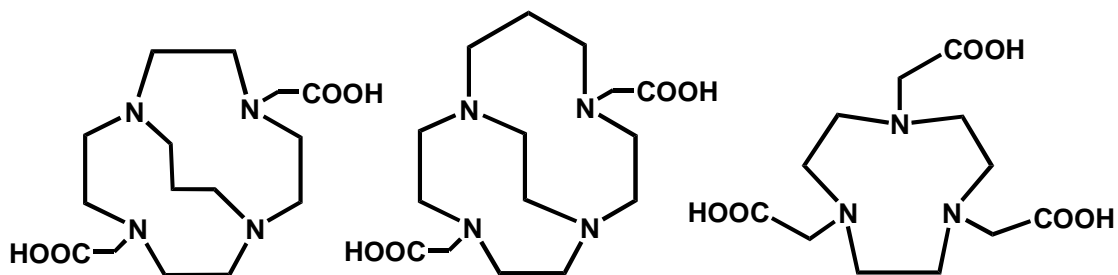


**Figure 3.** Structures of cross-bridged tetraazamacrocyclic chelators, C3B-DO2A and CB-TR2A, as well as triazamacrocyclic chelator, NOTA.

Here we present the results of our efforts to develop kinetically stable cross-bridged azamacrocycles. We synthesized a three-carbon cross-bridged DO2A, 4,10-bis-(carboxymethyl)-1,4,7,10-tetraazabicyclo[5.5.3]pentadecane (C3B-DO2A), and a two-carbon cross-bridged TR2A, 4,11-bis-(carboxymethyl)-(1,4,8,11-tetraazabicyclo[6.5.2]pentadecane (CB-TR2A). These novel BFCs were investigated for their potential use in constructing new PET imaging agents with improved properties. Copper(II) complexes were synthesized and characterized by structure, acid decomplexation and electrochemistry. Optimized  $^{64}\text{Cu}$ -radiolabeling conditions were established for each chelator. The biodistribution of  $^{64}\text{Cu}$ -C3B-DO2A and  $^{64}\text{Cu}$ -CB-TR2A in normal rats was compared to another highly stable macrocyclic chelator that has been used to complex  $^{64}\text{Cu}$  to biological molecules, 1,4,7-triazacyclononane-*N,N,N'*-triacetic acid (NOTA).

## Experimental Procedures

**Materials and methods.** Unless otherwise specified all chemicals were purchased from Sigma-Aldrich Chemical Co. (St. Louis, MO) and used as received. All solutions were prepared using water which had been distilled and then deionized ( $18\text{ M}\Omega/\text{cm}^2$ ) by passing through a Milli-Q water filtration system (Millipore Corp., Bedford, MA). Trace metals were removed from all buffers used for radiolabeling by Chelex 100 resin (BioRad Laboratories, Hercules, CA). Whatman C18 silica gel TLC

plates (KC18F, 60 Å, 200 µm) were purchased from Fisher Scientific (Pittsburgh, PA). Copper-64 was prepared on a biomedical cyclotron at Washington University Medical School by the  $^{64}\text{Ni}(p,n)^{64}\text{Cu}$  nuclear reaction at high specific activity as previously described.<sup>74</sup> Male Lewis rats were purchased from Charles River Laboratories (Boston, MA).

Radio-TLC was accomplished using a Bioscan 200 imaging scanner (Bioscan, Inc., Washington, DC). Analytical reversed-phase HPLC was performed on a Waters 600E (Milford, MA) chromatography system with a Waters 991 photodiode array detector and an Ortec Model 661 radioactivity detector (EG&G Instruments, Oak Ridge, TN). Radioactive samples were counted with a Beckman 8000 automated well-type gamma counter (Beckman Instruments, Inc., Fullerton, CA) or a Wallac Wizard 1480 automatic gamma counter (Perkin Elmer, Gaithersburg, MD).

**Optimization of radiolabeling conditions for preparation of  $^{64}\text{Cu}$ -C3B-DO2A.** A solution of C3B-DO2A (1 µg/µL) was prepared by dissolving the ligand in 0.1 M ammonium acetate, pH 7.0, or ethanol. Except for microwave assisted reaction, all reactions were carried out in 1.5 mL acid washed conical vials and shaken for the duration of the incubation. A variety of aqueous reaction conditions were tested, with incubation times, ligand concentrations, buffer concentration and pH, temperatures, and radiochemical yields reported in the results section (Tables 2-6). The method for radiolabeling described by Boswell *et al.* for the synthesis of  $^{64}\text{Cu}$ -CB-TE2A<sup>62</sup>, and described below for the production of  $^{64}\text{Cu}$ -CB-TR2A, was tested for formation of  $^{64}\text{Cu}$ -C3B-DO2A (Tables 7-8). At several time points, the outcome of the labeling experiment was assessed by radio-TLC ( $R_f \sim 0.8$ , C18 silica plates, eluent: methanol/10% ammonium acetate 7:3,  $R_f$  ( $^{64}\text{Cu}$ -acetate) = 0). Radio-TLC results for some reactions were confirmed by radio-HPLC (Agilent C8 column; isocratic, 0.1% formic acid in water; 0.5 mL/min). When radiolytic stabilizers were used, a final concentration of 1 mM gentisic acid (GA) or ascorbic acid (AA) was added prior to incubation. For carrier-added reactions, a 100 mM solution of  $\text{CuCl}_2$  in milliQ water or

absolute EtOH was added to the ligand solution prior to addition of the  $^{64}\text{CuCl}_2$ . Microwave assisted reactions were carried out using a Biotage Initiator closed vessel reactor (Biotage AB, Uppsala, Sweden). Solvent, pH, temperature, and length of reaction were varied to find conditions that resulted in consistent radiochemical purity of  $\geq 98\%$  (Table 9).

The highest radiochemical purity with greatest consistency of yield was obtained using a microwave assisted reaction. A solution of  $^{64}\text{CuCl}_2$  (750  $\mu\text{Ci}$  in 50  $\mu\text{L}$  milliQ water, pH 3) was added to 4.61  $\mu\text{g}$  (14.0 nmol) C3B-DO2A dissolved in 250  $\mu\text{L}$  of milliQ water (pH 3). The sealed vial containing the reaction mixture was placed in the microwave reactor, stirred for two minutes, and then heated at 100  $^\circ\text{C}$  for 2 h. Complex formation was confirmed by radio-TLC. Radiochemical purity was determined by HPLC and found to be  $\geq 98\%$  before use in animal studies.

**Preparation of  $^{64}\text{Cu-NOTA}$ .** An aqueous solution of  $^{64}\text{CuCl}_2$  (1.3 mCi, 50  $\mu\text{L}$ , 0.1 M  $\text{NH}_4\text{OAc}$ , pH 7.0) was added to 4.17  $\mu\text{g}$  (13.7 nmol) of NOTA dissolved in 50  $\mu\text{L}$  of 0.1 M  $\text{NH}_4\text{OAc}$ , pH 7.0. The reaction mixture was incubated with shaking at 37  $^\circ\text{C}$  for 1 h. Complex formation was followed by radio-TLC ( $R_f \sim 0.75$ , C18 silica plates, eluent: methanol/10% ammonium acetate 7:3,  $R_f$  ( $^{64}\text{Cu-acetate} = 0$ )). Radiochemical purity of  $\geq 98\%$  was attained.

**Biodistribution Studies.** Animal experiments were carried out in compliance with the Guidelines for the Care and Use of Research Animals established by Washington University's Animal Studies Committee. Tissue distribution studies were performed in male Lewis rats (34-42 day old) after intravenous injection of the radiolabeled compound,  $^{64}\text{Cu-C3B-DO2A}$  (45  $\mu\text{Ci}$ ; 0.9 nmol ligand),  $^{64}\text{Cu-CB-TR2A}$  (100  $\mu\text{Ci}$ ), or  $^{64}\text{Cu-NOTA}$  (60  $\mu\text{Ci}$ ; 0.5 nmol ligand), via the tail vein (100-150  $\mu\text{L}$ ). Tissue biodistribution data were obtained at 1, 4, and 24 hours post injection (PI). Animals were sacrificed at the appropriate time points, organs of interest were removed and weighed, and the radioactivity was measured in a gamma counter. The

percent injected dose per gram (%ID/g) and percent injected dose per organ (%ID/organ) were calculated by comparison to a weighed and counted standard. Rats were allowed food and water *ad libitum*. Animals in the 24 h group for  $^{64}\text{Cu}$ -C3B-DO2A and  $^{64}\text{Cu}$ -NOTA were maintained in metabolism cages; urine and feces were collected.

**Statistical methods.** All data are presented as the mean  $\pm$  standard deviation. Group comparisons were made using standard ANOVA methods. Post hoc testing of individual group differences was accomplished with the Bonferroni test. Groups with  $p < 0.05$  were considered significantly different. GraphPad Prism software (version 5.02; San Diego, CA) was used for all statistical analyses.

**Collaborators.** The experimental procedures for work performed by collaborators are included as supplemental material Appendix I. Synthesis of C3B-DO2A was performed by Dr. Riccardo Ferdani, CB-TR2A by Yijie Peng (University of New Hampshire, Durham, NH)<sup>75</sup> and NOTA by Elizabeth Garcia (UNH). Synthesis of all  $^{\text{nat}}\text{Cu}(\text{II})$ -chelator complexes and their characterization was carried out at UNH in the laboratory of Dr. Ed Wong. The Cu-CB-TR2A work has been reported in the doctoral dissertation of Antoinette Odeendaal (UNH).<sup>76</sup> X-ray crystallography was done in the laboratory of Dr. Arnold Rheingold at the University of California—San Diego (La Jolla, CA); Cu-CB-TR2A structure solved by James Golen. Dr. Thad Wadas was responsible for radiochemistry involving CB-TR2A.

## Results

**Synthesis of Ligands.** The synthesis and characterization of the chelator and Cu(II) complex of the cyclen-based cross-bridged chelator, C3B-DO2A, and that of the homocyclen-based cross-bridged chelator, CB-TR2A, have not previously been reported. The low overall yield for the synthesis of C3B-DO2A (18%) was primarily due to the cross-bridging step which had a yield of 21%. The compound

has subsequently been synthesized by a different synthetic route in much higher yield.

**Cu-C3B-DO2A.** The complexation of Cu(II) by the ligand was relatively slow, requiring overnight reflux in 95% ethanol solution. It was found subsequently that under microwave irradiation, the complex can be more conveniently formed in aqueous solution at 85° after 1 h at pH 6. The complex co-crystallized with NaClO<sub>4</sub> as well as with waters of hydration. The solution electronic spectrum showed a visible maximum at 614 nm, typical of Cu(II)-cross-bridged complexes. Solid-state FT-IR spectrum revealed carboxylate bands at 1687 (m, s) and 1616 (s, bd) cm<sup>-1</sup>. An X-ray structural determination of crystals grown from hexafluoro-*i*-propanol revealed a distorted octahedral geometry with Jahn-Teller elongation along one N-Cu-O axis (Figure 4). The cation is only slightly distended from the chelator cavity with an “axial” N-Cu-N angle of 173.6° and “equatorial” N-Cu-N angle of 97.5°.

The inertness of Cu-C3B-DO2A (half-life = 7.2(7) days) to decomplexation in 12M HCl at 90 °C, even exceeding that of the Cu-CB-TE2A (half-life = 1.3(2) h)<sup>57</sup>, is remarkable. This attests to the optimal envelopment of the Cu(II) within the ligand's hexadentate coordination sphere. To begin the demetallation process, dislodgement of at least one pendant arm and rupture of a Cu-N bond must be followed by major chelator structural rearrangements. The kinetic barrier to such an event must be significantly higher even than that for Cu-CB-TE2A, previously the most acid-inert Cu(II)-tetraazamacrocyclic complex.

Similar inertness is not observed upon electrochemical reduction as revealed by the cyclic voltammogram of this complex. An irreversible reduction was found near -1.0 V (Ag/AgCl) with no reoxidation peak until the large stripping peak near 0 V, indicative of copper metal deposition. Thus Cu(I)-C3B-DO2A, if formed, must have low stability in aqueous solution and is thus rapidly demetallated.

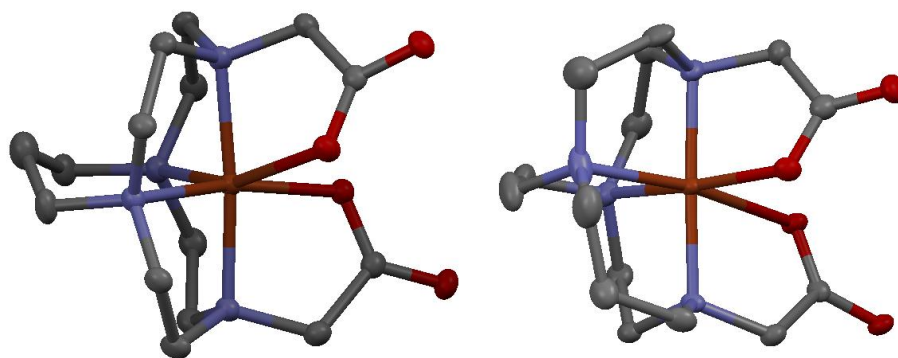


**Figure 4.** Structures of Cu-C3B-DO2A and Cu-CB-TR2A (Complex A) based on crystallographic data. For clarity, all hydrogens are omitted.

**Cu-CB-TR2A.** The complexation of Cu(II) by the ligand CB-TR2A was accomplished following overnight reflux in 95% ethanol solution. Elemental analysis of Cu-CB-TR2A was consistent with a composition of  $\text{Cu}\cdot\text{CB-TR2A}\cdot 1.2\text{Na}(\text{ClO}_4)\cdot 2\text{H}_2\text{O}$ . Two strong broad IR bands were observed, one at  $1610\text{ cm}^{-1}$ , which corresponds to the carboxylate stretching vibration, and another at  $1098\text{ cm}^{-1}$ , which corresponds to the perchlorate stretching vibration. The UV-Vis spectrum in  $\text{H}_2\text{O}$  has an absorption  $\lambda_{\text{max}}$  at 608 nm ( $\epsilon = 32.1\text{ M}^{-1}\text{cm}^{-1}$ ).

An X-ray crystal structure determination of  $\text{Cu}\cdot\text{CB-TR2A}$  was obtained after a second slow  $\text{Et}_2\text{O}$  diffusion into a solution of complex in 95% EtOH. The structure showed the presence of three unique *cis*-V-folded complexes each with a six-coordinated distorted octahedral copper, but each with a different ligand conformation (Complex A shown in Figure 4). Jahn-Teller elongated bonds were observed for each complex along one N-Cu-O axis. The metal center is only slightly distended from the chelator cavity as indicated by the “axial” N-Cu-N bond angles (Complex A: “axial” N-Cu-N  $176.8(2)^\circ$ ; Complex B:  $168.7(2)^\circ$ ).

The acid-decomplexation half-life of Cu-CB-TR2A was determined to be 10.8(4) h in 5 M HCl at 30 °C, conducted under pseudo-first order conditions. This is between the half-lives of Cu-CB-DO2A and Cu-CB-TE2A (Table 1). Although not as

kinetically inert as Cu-CB-TE2A, Cu-CB-TR2A is significantly more resistant to acid decomplexation than Cu-CB-DO2A whose ligand cavity is smaller. The cyclic voltammogram of Cu-CB-TR2A has a quasi-reversible reduction at -0.95 V (vs. Ag/AgCl) with a peak separation of 138 mV. This is between the values found for Cu-CB-TE2A and Cu-CB-DO2A (Table 1) and indicates that Cu-CB-TR2A is more resistant to reductive demetallation than Cu-CB-DO2A, though not as resistant as Cu-CB-TE2A. Quasi-reversible reduction suggests that the chelator can adapt a geometry suitable for Cu(I) coordination.<sup>77</sup>

**Table 1.** Pseudo first-order half-lives for acid-decomplexation and reduction potentials of copper(II) complexes.

Complex	12 M HCl, 90°C	5 M HCl, 90°C	5 M HCl, 30°C	E <sub>red</sub> (V) vs. Ag/AgCl	Overall Charge
Cu-C3B-DO2A	7.2(7) days	nd	nd	-1.03 (irrev)	0
Cu-CB-DO2A <sup>b</sup>	nd	nd	< 2 min	-0.85 (irrev)	0
Cu-DOTA	< 3 min <sup>a</sup>	nd	nd	-0.94 (irrev) <sup>c</sup>	-2
Cu-CB-TR2A	nd	nd	10.8(4) h	-0.95 (quasi-rev, ΔE=138 mV)	0
Cu-CB-TE2A <sup>a</sup>	1.6(2) h	154(6) h	> 1 year	-1.08 (quasi-rev, ΔE=120 mV)	0
Cu-TETA <sup>b</sup>	< 3 min	4.5(5) min	3.5(2) days	-1.18 (irrev)	+2
Cu-cyclam <sup>a</sup>	< 3 min	< 3 min	nd	-0.68 (quasi-rev)	+2
Cu-NOTA	nd	nd	< 3 min	-0.9, -1.2 (irrev)	-1

Previously published data: a=Wadas *et al.*<sup>57</sup>; b=Woodin *et al.*<sup>77</sup>; c=Boswell *et al.*<sup>62</sup>

**Cu-NOTA.** The acid inertness of this complex in 1M HCl at 30 °C is superior to that of Cu-cyclen, Cu-TACN, and Cu-CB-DO2A, all of which were completely decomplexed after 1 day. It is, however, demetallated within minutes in 5 M HCl at 30 °C, making it considerably less inert than Cu-DOTA, Cu-TETA, as well as Cu-CB-TR2A (Table 1). Among the chelators shown here, Cu-C3B-DO2A is the most

kinetically inert and Cu-NOTA one of the least. The relative order is Cu-C3B-DO2A > CB-TE2A >> Cu-TETA  $\approx$  Cu-DOTA > Cu-CB-TR2A > Cu-CB-DO2A  $\approx$  Cu-NOTA. While they only provide a qualitative estimate of comparative kinetic inertness, the resistance of a copper chelate complex to aqueous acid decomplexation generally serves as a useful first indicator of the likely *in vivo* integrity of the complex towards metal loss due to protonation, competing biometals, or biological ligands.<sup>78</sup>

The cyclic voltammogram contained two irreversible reduction peaks at -0.9 and -1.2 V (Ag/AgCl) along with the large copper stripping peak upon reoxidation. Thus Cu(I)-NOTA does not appear to be a stable species in aqueous solution. Comparison to other chelators is provided in Table 1. A threshold potential of approximately -1 V with quasi-reversibility is generally indicative of good *in vivo* stability.

**Radiochemistry.** Optimization of the radiolabeling conditions for <sup>64</sup>Cu-C3B-DO2A to be compatible with the conjugation and labeling of proteins (i.e. lower temperature) was not attained. Radiolabeling was attempted under a variety of aqueous conditions varying the buffer, pH, and temperature. The reaction conditions and <sup>64</sup>Cu-labeling yields for numerous attempts to attain rapid kinetics in aqueous ammonium acetate (NH<sub>4</sub>OAc) are presented in Tables 2-4. For reaction conditions repeated multiple times, the highest yield is reported in each series.

Phosphate and citrate buffers resulted in similarly inconsistent and disappointing yields (Table 5). Reactions were monitored over time to assess the rate of complexation. Instability of the <sup>64</sup>Cu-C3B-DO2A complex was observed in the form of secondary peak formation and yields which peaked and then declined. Although radiolysis is not commonly observed for small molecules, reactions were carried out in the presence of two different radiolytic scavengers (Table 6). Carrier-added reactions did not produce any improvement in radiolabeling.

**Table 2.** Initial radiolabeling attempts for  $^{64}\text{Cu}$ -C3B-DO2A. In all reactions 0.5  $\mu\text{g}$  C3B-DO2A was incubated with 100  $\mu\text{Ci}$   $^{64}\text{Cu}$  in a total volume of 50  $\mu\text{L}$ .

Buffer	Concentration	pH	Temp ( $^{\circ}\text{C}$ )	Yield (%)	
				30 m	7 h
$\text{NH}_4\text{OAc}$	0.1 M	8.0	25	6	9
$\text{NH}_4\text{OAc}$	0.5 M	6.0	25	6	28
$\text{NH}_4\text{OAc}$	0.5 M	8.0	25	23	52
$\text{NH}_4\text{OAc}$	1.0 M	7.0	25	4	22
$\text{NH}_4\text{OAc}$	1.25 M	4.5	25	1	3
$\text{NH}_4\text{OAc}$	0.1 M	8.0	37	3	9
$\text{NH}_4\text{OAc}$	0.5 M	6.0	37	11	9
$\text{NH}_4\text{OAc}$	0.5 M	8.0	37	23	12
$\text{NH}_4\text{OAc}$	1.0 M	7.0	37	1	10
$\text{NH}_4\text{OAc}$	1.25 M	4.5	37	1	2

**Table 3.** Secondary radiolabeling attempts for  $^{64}\text{Cu}$ -C3B-DO2A. In all reactions 1.0  $\mu\text{g}$  C3B-DO2A was incubated with 100  $\mu\text{Ci}$   $^{64}\text{Cu}$  in 0.1 M  $\text{NH}_4\text{OAc}$  (50  $\mu\text{L}$ ).

pH	Temp ( $^{\circ}\text{C}$ )	Yield (%)		
		1.5 h	3.5 h	18 h
6.0	25	47	45	32
7.0	25	27	46	82
8.0	25	72	45	40
6.0	95	30	58	90
7.0	95	19	19	35
8.0	95	34	50	90

**Table 4.** Further radiolabeling attempts for  $^{64}\text{Cu}$ -C3B-DO2A. In all reactions 1.0  $\mu\text{g}$  C3B-DO2A was incubated with 150  $\mu\text{Ci}$   $^{64}\text{Cu}$  in 0.1 M  $\text{NH}_4\text{OAc}$  (50  $\mu\text{L}$ ).

pH	Temp ( $^{\circ}\text{C}$ )	Yield (%)			
		1 h	6 h	8 h	18 h
8	25	6	8	14	54
8.5	25	8	31	43	21
9	25	11	36	56	41
8	40	4	22	7	39
8.5	40	40	12	10	32
9	40	69	5	83	13
8	95	27	53	49	46
8.5	95	26	49	37	68
9	95	21	53	66	79

**Table 5.** Alternate buffers used for attempted radiolabeling of  $^{64}\text{Cu}$ -C3B-DO2A. In all reactions 0.5  $\mu\text{g}$  C3B-DO2A was incubated with 70  $\mu\text{Ci}$   $^{64}\text{Cu}$  in a total volume of 50  $\mu\text{L}$  at 95  $^{\circ}\text{C}$ .

Buffer	Concentration	pH	Yield (%)	
			1 h	4 h
$\text{NH}_4\text{Citrate}$	0.1 M	5.5	21	23
$\text{NH}_4\text{Citrate}$	0.1 M	7.0	31	30
$\text{NH}_4\text{Citrate}$	0.1 M	8.0	64	58
$\text{NH}_4\text{Citrate}$	0.5 M	7.0	28	39
$\text{Na}_2\text{PO}_4$	0.1 M	5.5	34	18
$\text{Na}_2\text{PO}_4$	0.1 M	7.0	22	55
$\text{Na}_2\text{PO}_4$	0.5 M	7.5	27	51

**Table 6.** Radiolabeling attempts for  $^{64}\text{Cu}$ -C3B-DO2A with radiolytic scavengers. In all reactions 1.0  $\mu\text{g}$  C3B-DO2A was incubated with 100  $\mu\text{Ci}$   $^{64}\text{Cu}$  in 0.1 M  $\text{NH}_4\text{OAc}$  (50  $\mu\text{L}$ ) at 95  $^{\circ}\text{C}$ .

pH	Scavenger	Yield (%)		
		1 h	4 h	16 h
5.5	GA	7	20	33
7	GA	8	45	64
8.5	GA	21	34	61
5.5	AA	5	11	22
7	AA	17	45	42
8.5	AA	32	36	62

After such exhaustive attempts at radiolabeling under aqueous conditions, the standard CB-TE2A radiolabeling conditions<sup>79</sup> were attempted (Tables 7-8). Table 7 includes data on a radiolabeling attempt using  $\text{Li}_2\text{CO}_3$  as the base instead of  $\text{Cs}_2\text{CO}_3$ . The effect of specific activity was assessed showing limited improvement in radiochemical yield (Table 8). Again, carrier-added reactions did not generate any improvement in radiolabeling yield.

**Table 7.** Radiolabeling  $^{64}\text{Cu}$ -C3B-DO2A in ethanol with excess base. In all reactions 0.5  $\mu\text{g}$  C3B-DO2A was incubated with 100  $\mu\text{Ci}$   $^{64}\text{Cu}$ .

Time	Yield (%)		
	$\text{Cs}_2\text{CO}_3$ ; 100 $\mu\text{L}$	$\text{Cs}_2\text{CO}_3$ ; 50 $\mu\text{L}$	$\text{Li}_2\text{CO}_3$ ; 100 $\mu\text{L}$
1 h	43	70	3
3 h	60	43	5
4.5 h	70	nd	4
6 h	65	nd	3
18 h	35	nd	6

**Table 8.** Radiolabeling  $^{64}\text{Cu}$ -C3B-DO2A in ethanol with excess  $\text{Cs}_2\text{CO}_3$ . In all reactions C3B-DO2A was incubated with 130  $\mu\text{Ci}$   $^{64}\text{Cu}$  in a total volume of 80  $\mu\text{L}$ .

Time	Yield (%)		
	1 $\mu\text{g}$ C3B-DO2A	2 $\mu\text{g}$ C3B-DO2A	3 $\mu\text{g}$ C3B-DO2A
1 h	32	64	64
2.5 h	37	67	85
4 h	32	63	83
6 h	20	47	nd
18 h	30	66	74

In an attempt to speed up the reaction kinetics, the use of a microwave reactor was employed (Table 9). While reaction times can be shortened due to the concentrated heating of a microwave reactor, the sealed vial system limited the number of time points assessed for each set of reaction conditions. Shorter reaction times did not initially produce high yields, so longer reaction times were utilized until higher yields were attained. Then reaction length optimization occurred, finding the shortest reaction time required to consistently provide a minimum of 97% radiochemical purity.

**Table 9.** Microwave assisted radiolabeling  $^{64}\text{Cu}$ -C3B-DO2A. In all reactions 1.0  $\mu\text{g}$  C3B-DO2A was incubated with  $\sim 100 \mu\text{Ci}$   $^{64}\text{Cu}$  in a total volume of 300  $\mu\text{L}$ .

Solvent	pH	Temp ( $^{\circ}\text{C}$ )	Time	Yield (%)
0.1 M $\text{NH}_4\text{OAc}$	7	60	1 h	9
0.1 M $\text{NH}_4\text{OAc}$	7	60	4 h	30
0.1 M $\text{NH}_4\text{OAc}$	7	95	1 h	38
0.1 M $\text{NH}_4\text{OAc}$	7	95	4 h	50
0.1 M $\text{NH}_4\text{OAc}$	7	95	6 h	28
0.5 M $\text{NH}_4\text{OAc}$	7	60	1 h	38
0.5 M $\text{NH}_4\text{OAc}$	7	85	4 h	44
0.5 M $\text{NH}_4\text{OAc}$	7	95	1h	39
0.5 M $\text{NH}_4\text{OAc}$	7	95	4 h	55
0.1 M $\text{NH}_4\text{OAc}$	5	95	4 h	61
0.1 M $\text{NH}_4\text{OAc}$	8.5	95	4 h	82
0.1 M $\text{NH}_4\text{OAc}$	8.5	150	4 h	48
0.1 M $\text{NH}_4\text{OAc}$	8.5	180	4 h	45
0.1 M $\text{Na}_2\text{PO}_4$	7	60	4 h	39
0.1 M $\text{Na}_2\text{PO}_4$	7	95	4 h	59
0.5 M $\text{Na}_2\text{PO}_4$	7.5	95	4 h	52
milliQ water	3	95	4 h	87
milliQ water	3	100	4 h	99
milliQ water	3	100	1h	91
milliQ water	6	95	4 h	83
milliQ water	6	100	4 h	94
milliQ water	6	100	1h	85
milliQ water	3	100	2h	99

CB-TR2A was successfully labeled with  $^{64}\text{Cu}$  by the method employed for CB-TE2A and other cross-bridged chelators<sup>24, 79</sup> (radiochemical purity  $\geq 98\%$ ) at room temperature in basic ethanolic solution. A single peak corresponding to  $^{64}\text{Cu}$ -CB-TR2A was confirmed by radio-TLC.

The NOTA chelator used for comparison was successfully labeled with  $^{64}\text{Cu}$  at room temperature in neutral buffer solution, with radiochemical purity  $\geq 98\%$  attainable within one hour. A single peak corresponding to  $^{64}\text{Cu}$ -NOTA was verified by radio-TLC.

**Biodistribution Studies.** The biodistribution of  $^{64}\text{Cu}$ -C3B-DO2A,  $^{64}\text{Cu}$ -CB-TR2A, and  $^{64}\text{Cu}$ -NOTA were determined in normal, juvenile Lewis rats to examine their *in vivo* properties. The blood, liver, and kidney clearance of these agents are plotted in Figure 5 along with previously published data of  $^{64}\text{Cu}$ -CB-DO2A<sup>62</sup> and  $^{64}\text{Cu}$ -CB-TE2A<sup>63</sup> for comparison. For  $^{64}\text{Cu}$ -CB-TR2A and  $^{64}\text{Cu}$ -NOTA rapid clearance of the agent through the blood, liver, and kidneys was observed, suggesting that the intact complex is clearing because dissociated  $^{64}\text{Cu}$  binds to proteins and remains trapped in tissues, hindering clearance.<sup>61</sup> Comparable levels of clearance are observed for blood (%ID/g at 24 h PI:  $^{64}\text{Cu}$ -CB-TR2A,  $0.010\pm 0.002$ ;  $^{64}\text{Cu}$ -NOTA,  $0.016\pm 0.001$ ) and liver (%ID/g at 24 h PI:  $^{64}\text{Cu}$ -CB-TR2A,  $0.075\pm 0.014$ ;  $^{64}\text{Cu}$ -NOTA,  $0.086\pm 0.009$ ). The highest uptake in all organs is observed for  $^{64}\text{Cu}$ -C3B-DO2A at all time points. Clearance of  $^{64}\text{Cu}$ -C3B-DO2A is slow but continuous (from 1h to 22 h: blood 29.8% reduction; liver 22.2%; kidney 50.4%). All other compounds have higher percent reduction for all three organs than  $^{64}\text{Cu}$ -C3B-DO2A. The rate of clearance from liver is higher for cyclam-based cross bridged chelators and lower for non-cross-bridged NOTA (percent reduction at 22 or 24 h PI:  $^{64}\text{Cu}$ -CB-TR2A, 66.4%;  $^{64}\text{Cu}$ -NOTA, 46.3%;  $^{64}\text{Cu}$ -C3B-DO2A, 22.2%;  $^{64}\text{Cu}$ -CB-DO2A, 69.5%;  $^{64}\text{Cu}$ -CB-TE2A, 90.2%). Kidney uptake cleared by at least 50% for all complexes (percent reduction at 22 or 24 h PI:  $^{64}\text{Cu}$ -CB-TR2A, 89.2%;  $^{64}\text{Cu}$ -NOTA, 80.1%;  $^{64}\text{Cu}$ -C3B-DO2A, 50.4%;  $^{64}\text{Cu}$ -CB-DO2A, 95.6%;  $^{64}\text{Cu}$ -CB-TE2A, 99.1%). This results in

excretion of the complexes in the urine (Table 10). Excluding  $^{64}\text{Cu}$ -C3B-DO2A, the highest levels of  $^{64}\text{Cu}$  remaining in the blood and tissues at 24 h is observed for  $^{64}\text{Cu}$ -NOTA as well as the lowest percent reduction from 1 to 24 h. These data demonstrate that the  $^{64}\text{Cu}$ -labeled cross-bridged chelates are cleared more completely from the blood, liver, and kidneys than the non-cross-bridged analogues, with  $^{64}\text{Cu}$ -CB-TE2A having the lowest amount of  $^{64}\text{Cu}$  remaining in the blood and tissues after 24 h.<sup>62</sup>

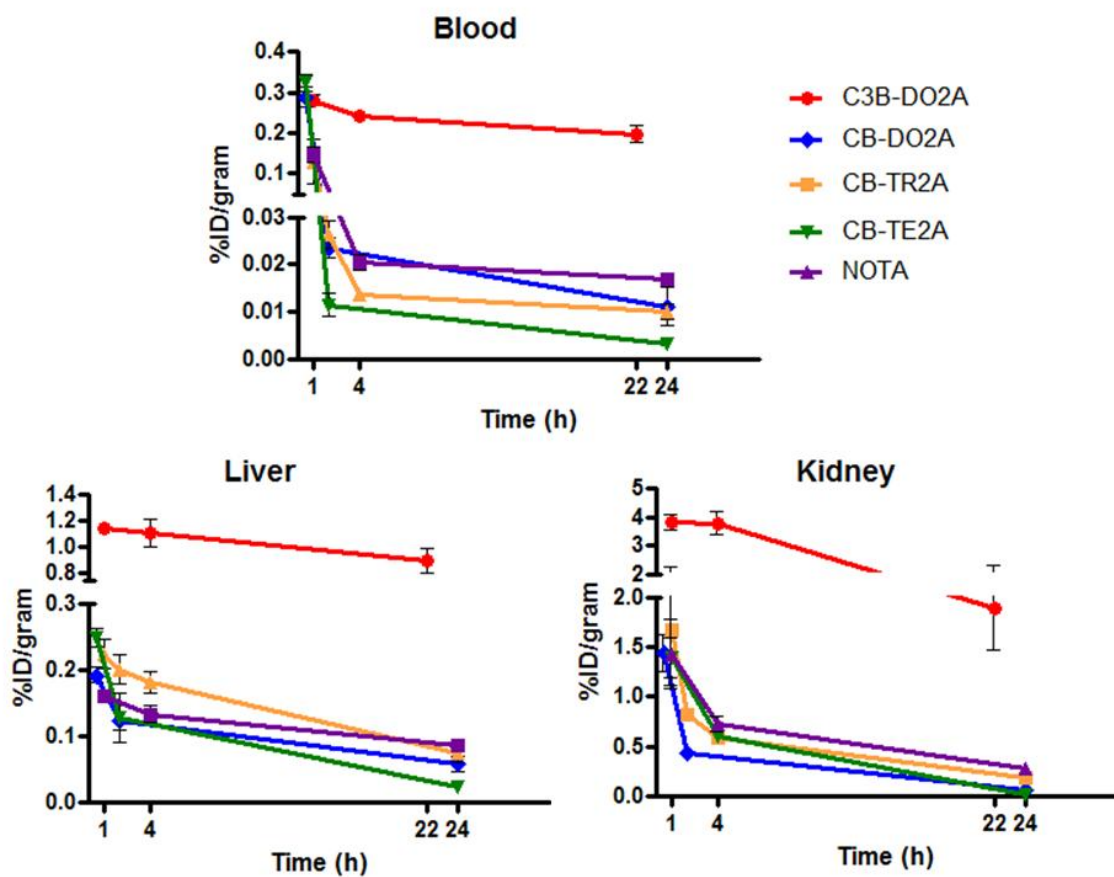


**Figure 5.** Selected organ biodistribution for  $^{64}\text{Cu}$ -C3B-DO2A,  $^{64}\text{Cu}$ -CB-TR2A, and  $^{64}\text{Cu}$ -NOTA. Plotted with previously published data for  $^{64}\text{Cu}$ -CB-DO2A<sup>62</sup> and  $^{64}\text{Cu}$ -CB-TE2A<sup>63</sup> for comparison. Note differences in scale.

**Table 10.** Excretion data for  $^{64}\text{Cu}$ -C3B-DO2A and  $^{64}\text{Cu}$ -NOTA, 0 - 24 h PI.

Complex	% ID	
	Urine	Feces
$^{64}\text{Cu}$ -C3B-DO2A	46.0 ± 5.2	5.4 ± 1.2
$^{64}\text{Cu}$ -NOTA	74.9 ± 7.1	4.4 ± 4.9

## Discussion

It was initially proposed that cross-bridged chelators would form more stable complexes with copper radionuclides thereby improving pharmacokinetics of  $^{64}\text{Cu}$ -labeled cross-bridged ligand biomolecule conjugated for enhanced imaging. Research has confirmed this hypothesis, demonstrating superior kinetic and *in vivo* stability of these chelators as carriers for copper radionuclides compared to traditional macrocyclic ligands.<sup>22, 62, 63</sup> Greater kinetic stability improved target uptake and pharmacokinetics of cross-bridged ligand-peptide conjugates for molecular imaging purposes.<sup>25</sup> In this work we investigated a second generation of cross-bridged macrocyclic chelators of copper-based radiopharmaceuticals for imaging of cancer and other diseases. Pendant-armed cross-bridged cyclen and homocyclen derivatives were designed taking into consideration the convenience of synthetic routes, radiometal binding ability, and rapid complexation kinetics to enable efficient radiolabeling of proteins under mild conditions. The kinetic and thermodynamic properties of the coordination complexes were studied and correlation between these properties and desired *in vivo* behavior was examined.

Comparison of the crystal structures of  $\text{Cu(II)-C3B-DO2A}$  and  $\text{Cu(II)-CB-TR2A}$  reveals strong similarities in the coordination geometry of these complexes. Both have *cis*-coordinating O's with Jahn-Teller distortion along the N-Cu-O bond. This is consistent with previously published structures of  $\text{Cu(II)-CB-TE2A}$  and  $\text{Cu(II)-CB-DO2A}$ .<sup>23, 62</sup> Both  $\text{Cu(II)-C3B-DO2A}$  and  $\text{Cu(II)-CB-TR2A}$  are slightly "exo," meaning that the metal protrudes from the ligand cleft, revealing the poor fit of the metal in the complex. The  $\text{Cu(II)-CB-DO2A}$  structure also reveals a protrusion of the  $\text{Cu(II)}$  from the ligand cleft.<sup>62</sup>  $\text{Cu(II)-CB-TE2A}$ , however, has been shown to have a less pronounced Jahn-Teller distortion, and the copper cation fits snugly in the cleft of the cross-bridged chelator.<sup>77</sup> Stable coordination conformation, including how well the metal fits in the chelator, contributes to good *in vivo* stability.

*In vitro* inertness of copper chelators has been investigated as a convenient indicator of *in vivo* stability. Aqueous acid-assisted decomplexation of polyazamacrocyclic copper complexes is a known indicator of their kinetic inertness.<sup>77</sup> Comparison of the decomplexation half-lives suggested that Cu-C3B-DO2A should be more stable than Cu-CB-TR2A *in vivo* although the biodistribution study did not confirm this. The acid decomplexation mechanism has not yet been elucidated, so the data should be interpreted with caution.

The coordination preferences for Cu(II) and Cu(I) are significantly different, thus *in vivo* reduction of stable Cu(II) complexes to form Cu(I) products can lead to demetallation and transchelation to a variety of copper-binding biomolecules. The quasi-reversibility of Cu(II)-CB-TR2A compared to Cu(II)-CB-DO2A's irreversible reduction, likely contributes to its superior *in vivo* behavior, relatively speaking. A quasi-reversible reduction was also reported for Cu-CB-TE2A.<sup>77</sup> The quasi-reversibility demonstrated by Cu-CB-TR2A suggests that, like CB-TE2A, the ligand is capable of adapting to a geometry suitable for Cu(I) coordination.<sup>57</sup> The quasi-reversibility is thought to stem from the ability of the molecule to adjust somewhat to the tetrahedral geometry favored by Cu(I).<sup>80</sup> This malleability on the part of the chelator enhances the stability of the chelator *in vivo*, providing resistance to metal loss from the chelator upon reduction.

The reaction conditions for preparing <sup>64</sup>Cu-C3B-DO2A (microwaving at high temperature) and <sup>64</sup>Cu-CB-TR2A (basic ethanol) are relatively harsh compared to those for the conventional complexes, such as DOTA. NOTA, however, is easily radiolabeled with <sup>64</sup>Cu using conditions compatible with protein conjugation (aqueous media at temperatures below 43 °C). The need for harsh radiolabeling conditions to form the complex is not indicative of complex stability *in vivo*. However, a positive correlation between the harshness of the conditions required for complex formation and the acid-decomplexation half-life has been observed.

Evaluation of the biodistributions of the ligands shows rapid clearance of  $^{64}\text{Cu}$ -CB-TR2A and  $^{64}\text{Cu}$ -NOTA through the blood, liver, and kidneys, consistent with what has been previously reported for  $^{64}\text{Cu}$ -labeled azamacrocyclic complexes.<sup>22, 62</sup> The initial high uptake and slow clearance of  $^{64}\text{Cu}$ -C3B-DO2A suggests poor *in vivo* stability and transchelation of  $^{64}\text{Cu}$  to proteins, as has been observed in previous studies.<sup>61, 81</sup> Biodistribution of  $^{64}\text{Cu}$ -NOTA showed similar trends to  $^{64}\text{Cu}$ -CB-TR2A and CB-TE2A, but demonstrated a lower rate of clearance from liver and blood within 24 h compared to the  $^{64}\text{Cu}$ -labeled cross-bridged complexes.

Many parameters control the behavior of radiopharmaceuticals in biological media, and some of them cannot be easily predicted requiring *in vivo* studies. CB-TE2A remains the best cross-bridged chelator for  $^{64}\text{Cu}$  and other copper radionuclides. Beyond the favorable *in vitro* characterization<sup>77</sup>, *in vivo* clearance and metabolism studies indicate the enhanced stability of  $^{64}\text{Cu}$ -CB-TE2A.<sup>62</sup> The *in vivo* stability of Cu(II)-C3B-DO2A and Cu(II)-CB-TR2A complexes could be further evaluated by examination of the radiometabolites and determination of the extent of transchelation to proteins.

Previous work correlated acid stability and resistance to electrochemical reduction in aqueous conditions to biodistribution in normal rats, showing that biological stability might be predicted by thresholds of acid stability and reduction potentials.<sup>59, 77</sup> While this does not hold for all of the compounds presented here, the *in vitro* characterization of BFCs remains a valuable tool for understanding the multifaceted *in vivo* biodistribution, stability, and metabolism of radiopharmaceuticals. A macrocyclic chelator with rapid complexation kinetics which also demonstrates kinetic inertness comparable to the previously studied  $^{64}\text{Cu}$ -CB-TE2A under physiological conditions has not yet been identified. Further research in developing Cu(II) chelators with even greater stability is clearly warranted.

## CHAPTER 3

*In Vitro* and *In Vivo* Investigation of Structurally Diverse  
<sup>64</sup>Cu-Labeled RGD Peptides for PET Imaging of  $\alpha_v\beta_3$  Expression

## Abstract

Integrin  $\alpha_v\beta_3$  is upregulated in tumor vasculature, osteoclasts and areas of collateral circulation following ischemic injury. Here, we investigate structurally diverse bifunctional RGD (Arginine-Glycine-Aspartic acid) peptides for  $\alpha_v\beta_3$  integrin affinity *in vitro* and *in vivo*. A series of peptides containing the RGD sequence were synthesized. Affinity to  $\alpha_v\beta_3$  and specificity against  $\alpha_v\beta_5$  and  $\alpha_{IIb}\beta_3$  were determined in an isolated, competitive binding assay for the peptide alone and several peptide conjugates. A lactam-cyclized peptide (c(RGDyK)) demonstrated higher affinity for  $\alpha_v\beta_3$  than disulfide-cyclized (KCRGDC) or linear peptide (GRGDS). Disulfide-cyclized peptides exhibited the best selectivity of the ligands investigated. A control, lactam-cyclized peptide (c(RADyK)) has low affinity for all three integrins. Conjugation of Cu(II)-containing chelators did not affect the binding affinity or selectivity of the peptides. Cellular uptake studies in an  $\alpha_v\beta_3$ -positive cell line (U87MG human glioblastoma cells) were performed using four different  $^{64}\text{Cu}$ -DOTA-labeled peptides. In cell studies the disulfide-cyclized peptide showed the greatest amount of internalization. Uptake of RGD peptides could be blocked by high doses of unlabeled peptide. Internalization of the control peptide was minimal although receptor-mediated surface binding was observed. Disulfide-linked KCRGDC exhibited the best *in vitro* behavior. Biodistribution studies in U87MG tumor-bearing *nu/nu* mice showed rapid uptake and retention of the  $^{64}\text{Cu}$ -labeled peptides in tumor with good tumor:blood and tumor:muscle ratios. At 4 h post-injection tumor:muscle ratios for all three compounds were similar, but  $^{64}\text{Cu}$ -DOTA-c(RGDyK) has a significantly higher tumor:blood ratio ( $p < 0.001$ ). Uptake of  $^{64}\text{Cu}$ -DOTA-c(RGDyK) can be blocked by co-administration of high doses of unlabeled peptide. Blocking of  $^{64}\text{Cu}$ -DOTA-KCRGDC and  $^{64}\text{Cu}$ -DOTA-GGRGDS uptake at 1 h was not attained with either co-injection or pre-injection (15 min or 1 h) of cold peptide. Small-animal PET/CT imaging of  $^{64}\text{Cu}$ -DOTA-KCRGDC and  $^{64}\text{Cu}$ -DOTA-GGRGDS afforded visualization of the tumor, consistent with the biodistribution profiles. There was no observed difference

between block and non-block uptake (SUV at 4 h PI:  $^{64}\text{Cu}$ -DOTA-KCRGDC,  $0.79\pm 0.17$ ;  $^{64}\text{Cu}$ -DOTA-KCRGDC + block,  $0.98\pm 0.36$ ;  $^{64}\text{Cu}$ -DOTA-GGRGDS,  $1.45\pm 0.23$ ;  $^{64}\text{Cu}$ -DOTA-GGRGDS + block,  $1.58\pm 0.075$ ). Further *in vivo* investigation is warranted to demonstrate targeting specificity of the peptides along with investigation of a different peptide as a control. Higher binding affinity is being investigated through multimeric peptides and conjugation of several peptides onto the surface of nanoparticles.

## Introduction

Cell-cell and cell-matrix interactions play an important role in tumor metastasis and are essential during three specific processes: 1) dissociation of individual cells from the primary tumor and invasion of the adjacent tissue; 2) adherence in the capillary bed of the target organ; and 3) extravasation and arrest in the foreign tissue (Figure 1).<sup>82, 83</sup> Integrins comprise one class of cell surface receptors participating in these cell adhesion processes. They are heterodimeric, transmembrane receptors composed of an  $\alpha$ - and a  $\beta$ -subunit.<sup>28</sup> There are 24 known mammalian heterodimer pairs arising from combinations of the 18 known  $\alpha$ -subunits and 8  $\beta$ -subunits. Among the most interesting members of the integrin family are  $\alpha_{\text{IIb}}\beta_3$ , also known as glycoprotein IIb/IIIa, which is involved in platelet aggregation,<sup>84</sup> and  $\alpha_v\beta_3$ , the vitronectin receptor.

Integrin  $\alpha_v\beta_3$  is expressed in a variety of cell types including endothelial cells<sup>85</sup>, platelets<sup>86</sup>, osteoclasts<sup>38, 87</sup>, melanoma, and smooth muscle cells.<sup>30</sup> This receptor is known to be over-expressed on many tumor cells, such as osteosarcomas, neuroblastomas, glioblastomas, breast, prostate, and invasive melanomas.<sup>31, 88, 89</sup> Additionally,  $\alpha_v\beta_3$  has been shown to be important during angiogenesis, tumor-induced and otherwise (Figure 1).<sup>90</sup> Consequently, many

researchers are searching for high affinity, selective  $\alpha_v\beta_3$  antagonists for diagnostic and therapeutic applications.<sup>91</sup>

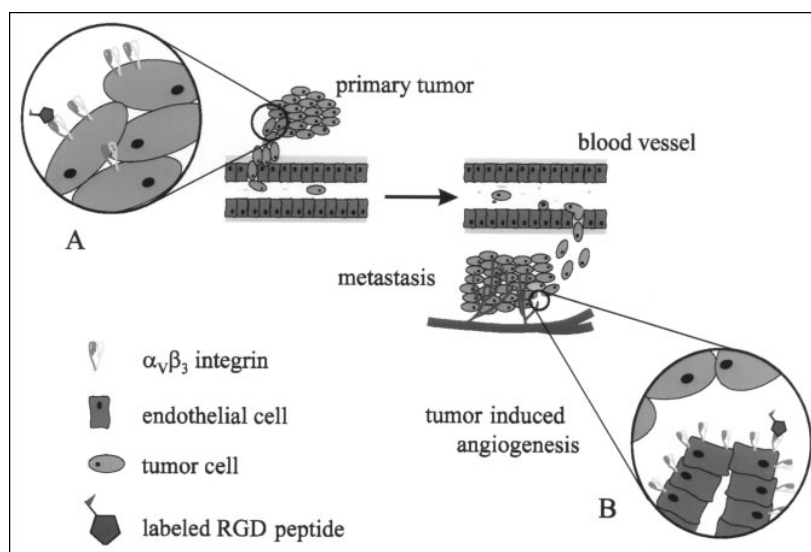


**Figure 1.** Targets for tumor imaging based on  $\alpha_v\beta_3$ -tageting tracers, such as labeled RGD peptides. Integrin  $\alpha_v\beta_3$  is highly expressed on metastatic tumors and on endothelial cells undergoing angiogenesis. (Reprinted with permission from R. Haubner.<sup>83</sup>)

The amino acid sequence arginine-glycine-aspartic acid (RGD) is common to various extracellular matrix (ECM) proteins involved in cell-matrix adhesion, e.g. vitronectin, fibronectin, fibrinogen, thrombospondin, and von Willebrand factor.<sup>92</sup> Molecular interaction between these ECM proteins and integrins are known to mediate many biological processes.<sup>93</sup> The RGD-binding site is involved in cell morphology, differentiation, proliferation, and gene expression.<sup>94</sup> Many linear and cyclic peptides incorporating the RGD sequence have been developed to take advantage of these properties.<sup>95</sup>

The most prominent lead compound for development of radiotracers for non-invasive determination of  $\alpha_v\beta_3$  expression is the lactam-cyclized pentapeptide, cyclo(Arg-Gly-Asp-D-Phe-Val), which demonstrates high affinity for  $\alpha_v\beta_3$ .<sup>96</sup> The first evaluation of this approach involved radioiodination of a series of RGD peptides.<sup>97-99</sup>

*In vitro* assays showed comparable affinity for  $\alpha_v\beta_3$  and selectivity against  $\alpha_{IIb}\beta_3$  as the lead structure. Receptor-specific tumor uptake was observed *in vivo* in nude mice bearing tumor xenografts of human melanoma (M21) and mammary carcinoma (MaCaF). Predominantly hepatobiliary clearance resulted in high activity concentration in liver and intestine. Strategies to improve pharmacokinetics of radiohalogenated peptides have been undertaken.

Glycosylation improved pharmacokinetics and increased activity uptake and retention in the tumor compared to the first-generation peptides.<sup>100</sup> Conjugation of hydrophilic D-amino acids shifted elimination to the renal pathway.<sup>101, 102</sup> However, tumor uptake was lower than observed with the glycosylated peptides. PEGylation is known to improve plasma stability, immunogenicity, and pharmacokinetics of peptides and proteins.<sup>74</sup> Chen, *et al.* systematically studied the effects of various PEG moieties on radioiodinated<sup>103</sup>, F-18<sup>104</sup>, and Cu-64-labeled<sup>105</sup> derivatives. The studies showed different effects of PEGylation on the pharmacokinetics, while tumor uptake and retention of RGD-peptides was dependent on the nature of the lead compound and minimally on the size of the PEG moiety.

Besides radiohalogenation, a variety of radiometal-based RGD tracers have been developed. Typically the  $\epsilon$ -amino function of the lysine in the lead structure cyclo(Arg-Gly-Asp-D-Xaa-Val), where Xaa is Phe or Tyr, is conjugated with a chelating moiety. Van Hagen *et al.* coupled c(RGDyK) with DTPA for <sup>111</sup>In labeling and demonstrated  $\alpha_v\beta_3$  specific binding in newly formed vessels by autoradiography using human tumor tissue sections.<sup>96</sup> Conjugation of the cystein-containing tetrapeptide sequence H-Asp-Lys-Cys-Lys-OH or macrocyclic chelator DOTA to cyclo(Arg-Gly-Asp-D-Phe-Lys) allowed for the preparation of <sup>99m</sup>Tc-, <sup>188</sup>Re- and <sup>90</sup>Y-labeled analogues.<sup>106</sup> All of these compounds exhibit high receptor affinity and selectivity as well as specific tumor accumulation. However, the pharmacokinetics of most of them need improvement.

Phage display has generated additional RGD derivatives. RGD-4C ((Cys<sup>2</sup>-Cys<sup>10</sup>, Cys<sup>4</sup>-Cys<sup>8</sup>)H-Ala-Cys-Asp-Cys-Arg-Gly-Asp-Cys-Phe-Cys-Gly-OH) contains two disulfide bridges and binds with moderate affinity to both  $\alpha_v\beta_3$  and  $\alpha_v\beta_5$ .<sup>107</sup> A shortened derivative of RGD-4C coupled with HYNIC and labeled with <sup>99m</sup>Tc was found to have only marginal tumor uptake which can be explained by the modest  $\alpha_v\beta_3$  binding affinity.<sup>108, 109</sup> Conjugation with HYNIC, deletion of the terminal amino acids, or labeling with <sup>99m</sup>Tc impairs the affinity to integrin  $\alpha_v\beta_3$  resulting in a peptide not suitable for *in vivo* imaging.

Apart from the cyclic structures, a few linear peptides have been investigated. Using a new labeling strategy allowing for <sup>18</sup>F-labeling of peptides on a solid support, 4-[<sup>18</sup>F]fluorobenzyl-Lys-Pro-Gln-Val-Thr-Arg-Gly-Asp-Val-Phe-Phe-Glu-Gly-NH<sub>2</sub> was synthesized.<sup>110</sup> Despite exhibiting high  $\alpha_v\beta_3$  binding affinity, biodistribution studies and PET images showed low activity accumulation in the tumor. Analysis of blood and urine samples revealed no intact peptide present as soon as 5 min post-injection, indicating that the linear peptide is metabolically unstable. A linear decapeptide (Arg-Gly-Asp-Ser-Cys-Arg-Gly-Asp-Ser-Tyr) containing two RGD sites and labeled with <sup>99m</sup>Tc via the Cys<sup>5</sup> within the peptide was studied in 14 patients with melanoma.<sup>111</sup> Despite a fast renal clearance rate, the peptide localized to most metastatic melanoma lesions with specific tumor accumulation. Tumor-to-background ratios were generally low due to high lung and abdomen background activity levels. Some small linear peptides, e.g. GRGDSPK, are reported to have low selectivity for distinct integrin subtypes, but the affinity and selectivity of such tracers has not been described thus far.<sup>112, 113</sup>

Multimeric compounds presenting more than one RGD site have been introduced. Janseen *et al.* synthesized a dimeric peptide by coupling two cyclo(Arg-Gly-Asp-D-Phe-Lys) units via a glutamic acid linker with DOTA or HYNIC conjugated to the free amino function of the linker moiety for radiolabeling.<sup>114, 115</sup> Technetium-<sup>99m</sup>-HYNIC-E-[c(RGDfK)]<sub>2</sub> exhibited a 10-fold higher affinity for  $\alpha_v\beta_3$  than the

monomeric  $^{99m}\text{Tc}$ -HYNIC-c(RGDfK). The groups of Kessler and Wester carried out a systematic study on the influence of multimerization on receptor affinity and tumor uptake.<sup>116, 117</sup> A PEG linker and lysine moieties connected different numbers of c(RGDfE) peptides. An *in vitro* binding affinity assay and PET images show increasing affinity in the series monomer, dimer, tetramer, and octamer. Many other groups have had varying degrees of success with multimerization.<sup>118-121</sup> Overall, multimerization leads to increased binding affinity and tumor uptake as well as retention. Through the use of appropriate linker moieties, the pharmacokinetics of the peptide-based tracer can be improved.

A wide variety of non-peptide low molecular weight compounds (petidomimetics) have been developed based on structure-activity investigations in the past decade. These will not be reported upon here, but they have been extensively reviewed elsewhere.<sup>122-127</sup>

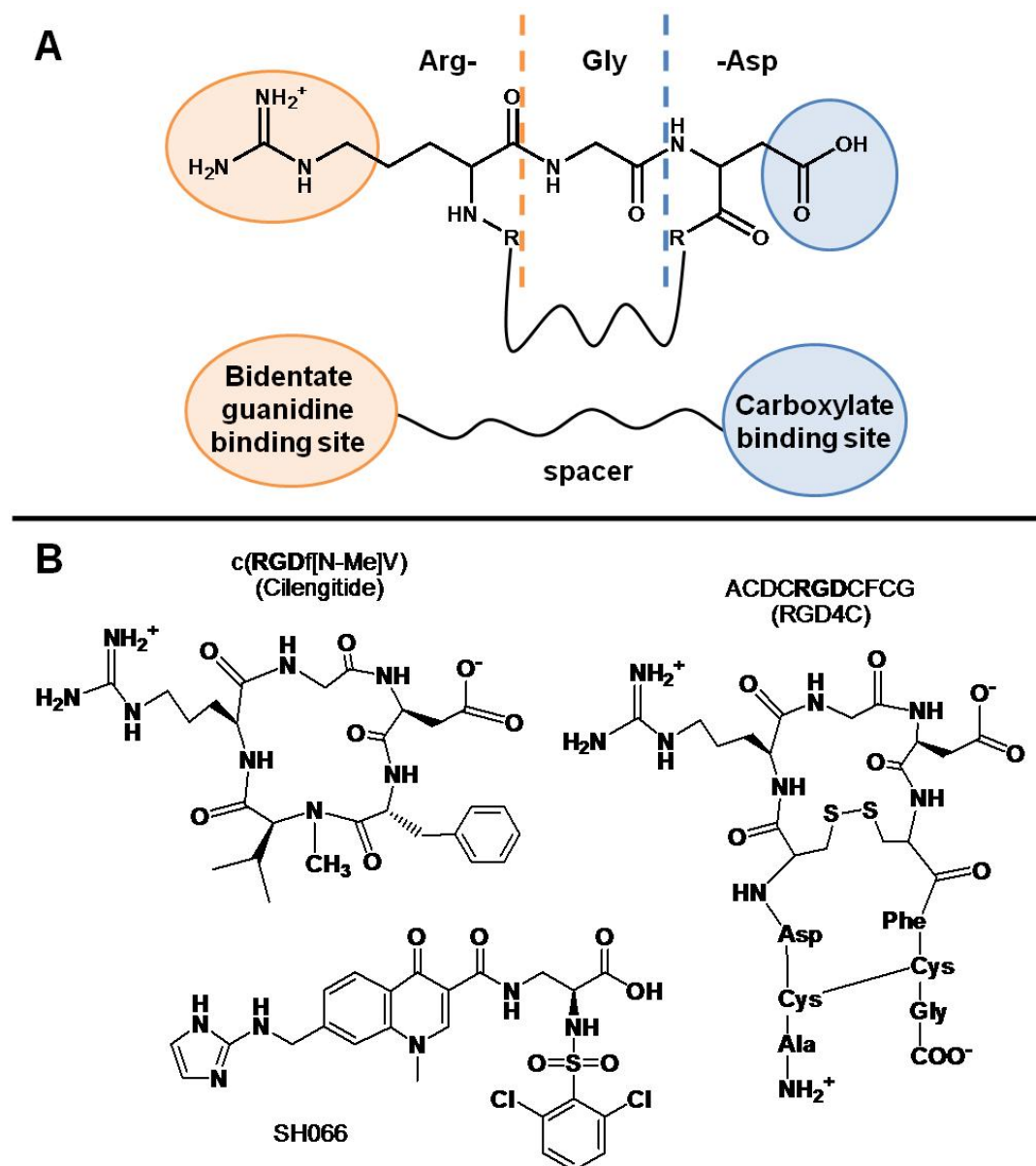


**Figure 2.** The standard RGD sequence in comparison with high affinity ligands for integrin  $\alpha_v\beta_3$ . **(A)** A schematic representation of the RGD binding motif. Specificity and affinity for  $\alpha_v\beta_3$  has been introduced in peptide ligands by ring closure and flanking amino acids, which force the arginine and aspartic acid side-chains into the proper conformation. In RGD-mimetics, the two domains that interact with the integrin (Arg and Asp) have been replaced by a guanidine binding site and carboxylate group. **(B)** Structures of c(RGDf(N-Me)V), RGD4C, and the quinolone vitronectin receptor antagonist SH066 described by Harris *et al.*<sup>128</sup> All are high affinity ligands for  $\alpha_v\beta_3$ . (Figure adapted from Temming *et al.*<sup>129</sup>)

As mentioned above, most of the integrin super-family members recognize the RGD tripeptide sequence, an epitope shared by a variety of extracellular ligands. Structural similarities within the integrin family and between their respective ligands make selectivity a major concern in the design of potential diagnostic imaging and therapeutic agents.<sup>130</sup> The affinity of RGD peptides for their ligands may be affected by steric conformation of the peptide.<sup>131-133</sup> The RGD sequence assumes very different conformations in different proteins, which have similar affinities to cell attachment<sup>134, 135</sup> and disintegrins.<sup>136-138</sup> The RGD sequences of these proteins are almost always located in flexible loop regions. Amino acids flanking RGD have also been suggested to affect the selectivity and affinity of peptides toward integrins.<sup>139, 140</sup> In addition to direct interactions between these residues and the integrin, flanking groups influence the folding of the peptide and the conformational features of the RGD-motif. Cyclization is commonly employed to improve the binding properties of RGD peptides. By conferring rigidity to structure, it improves the selectivity of the “promiscuous” RGD-sequence for a specific integrin sub-type.<sup>129</sup> Systematic substitution studies have shown that the positive and negative charges of the arginine (R) and aspartic acid (D) side chain functionalities and the unmodified glycine (G) spacer residue are critical.<sup>141, 142</sup> Most RGD peptidomimetics studied as  $\alpha_v\beta_3$  antagonists share a common pattern, consisting of a rigid, preferably achiral core unit, which links a guanidine type functionality and a carboxylic moiety.<sup>122</sup>

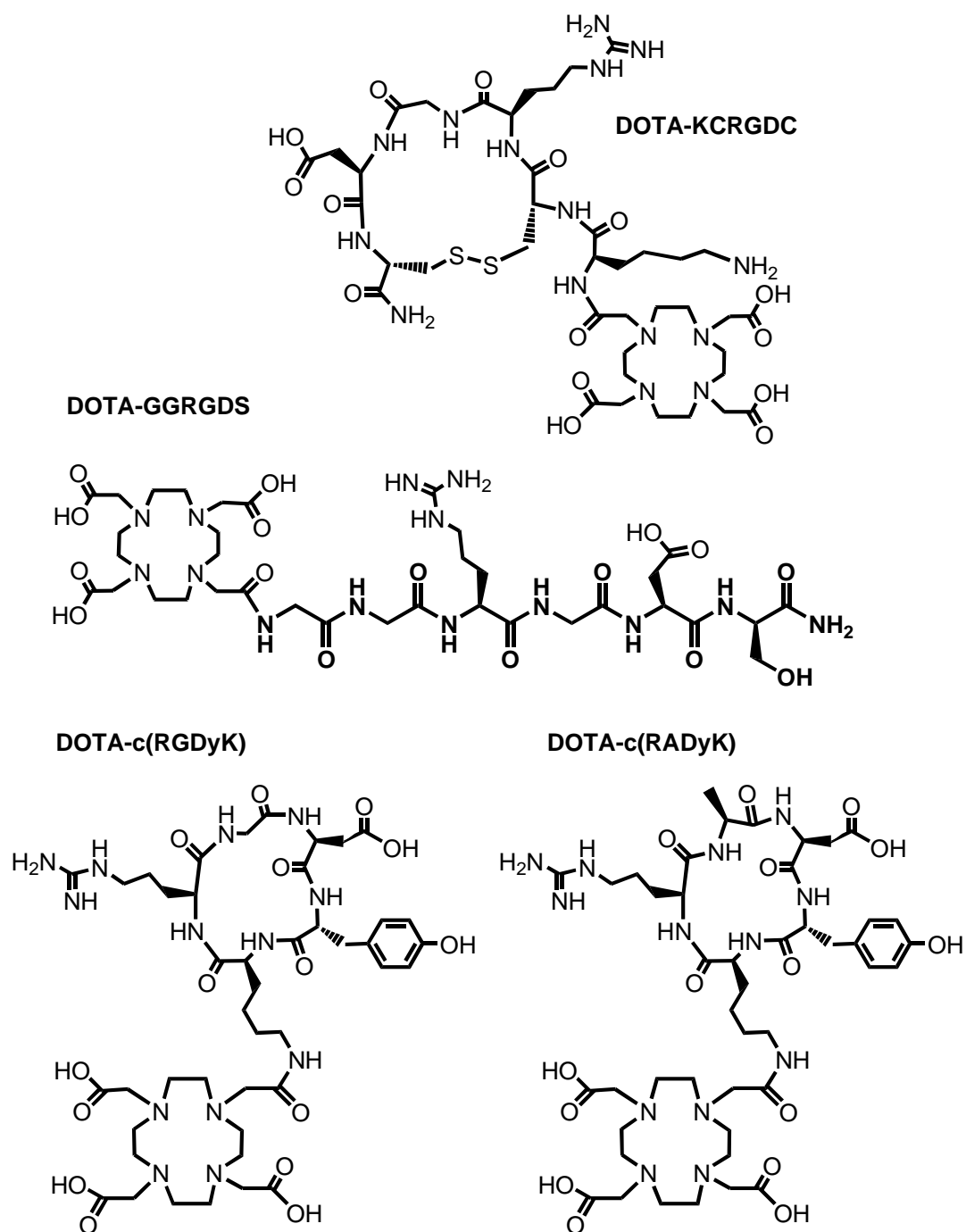


**Figure 3.** Structurally diverse RGD peptides characterized in this study, including lactam-cyclized, disulfide-cyclized, and linear RGD derivatives and a lactam-cyclized control peptide.

Here, we investigate structurally diverse bifunctional RGD peptides for  $\alpha_v\beta_3$  integrin affinity *in vitro* and *in vivo*. Lactam-cyclized, disulfide-cyclized, and linear RGD derivatives and a lactam-cyclized control peptide were synthesized or purchased with and without the macrocyclic chelator DOTA for radiolabeling with  $^{64}\text{Cu}$  (Figure 3). The *in vitro* binding affinity of the four RGD peptides towards integrin  $\alpha_v\beta_3$  was studied in a plate-based competitive binding assay as well as specificity against  $\alpha_v\beta_5$  and  $\alpha_{IIb}\beta_3$  using the same assay. Cellular uptake studies in an  $\alpha_v\beta_3$ -positive cell line (U87MG human glioblastoma cells) were performed using the four different  $^{64}\text{Cu}$ -DOTA-labeled peptides. *In vivo* properties were studied via biodistribution studies and small-animal PET imaging in U87MG tumor-bearing *nu/nu* mice.

## Experimental Procedures

**General materials and instrumentation.** All solvents and chemicals were reagent grade and used without further purification unless otherwise noted. N-hydroxybenzotriazole (HOBt) and the Fmoc-protected amino acids were purchased from AnaSpec (San Jose, CA). Trifluoroacetic acid (TFA) and N,N-diisopropylethylamine (DIEA) were purchased from Advanced ChemTech (Louisville, KY). Dichloromethane (DCM), N,N-dimethylformamide (DMF), methanol, and acetonitrile were from purchased from Fisher Scientific (Pittsburgh, PA). 1,4,7,10-Tetraazacyclododecane-1,4,7-tris(*t*-butyl acetate)-10-aceitc acid (DOTA-(3OBu<sup>t</sup>)-COOH) was purchased from Macrocyclics (Dallas, TX). Diisopropylcarbodiimide (DIC) and other commercial chemicals were purchased from Sigma-Aldrich (St. Louis, MO). The peptides and derivatives were obtained from a variety of sources: KCRGDC and GRGDS were custom synthesized by Tianma Pharma Co. (Suzhou, China); DOTA-GGRGDS was custom synthesized by C.S Bio Company, Inc. (Menlo Park, CA); and c(RGDyK) was purchased from Peptides International, Inc. (Louisville, KY). Yunpeng Ye synthesized DOTA-c(RGDyK) and DOTA-KCRGDC.

Vitronectin, fibronectin,  $\alpha_v\beta_3$  and  $\alpha_v\beta_5$  were purchased from Chemicon (a division of Millipore; Bellerica, MA). Integrin  $\alpha_{IIb}\beta_3$  was purchased from EMD Chemicals, Inc. (Gibbstown, NJ). All solutions were prepared using water which had been distilled and then deionized (18 M $\Omega$ /cm<sup>2</sup>) by passing through a Milli-Q water filtration system (Millipore Corp.; Bedford, MA). Trace metals were removed from all buffers used for radiolabeling by Chelex 100 resin (BioRad Laboratories; Hercules, CA). Whatman C18 silica gel TLC plates (KC18F, 60 Å, 200  $\mu$ m) were purchased from Fisher Scientific (Pittsburgh, PA). Copper-64 was prepared on a biomedical cyclotron at Washington University Medical School by the  $^{64}\text{Ni}(p,n)^{64}\text{Cu}$  nuclear reaction at high specific activity as previously described.<sup>103</sup> Female *nu/nu* mice were purchased from Charles River Laboratories (Boston, MA). ES-MS was accomplished using a Waters Micromass ZQ (Millford, MA). Radio-TLC was accomplished using a Bioscan 200 imaging scanner (Bioscan, Inc., Washington, DC). Analytical reversed-phase HPLC was performed on a Waters 600E (Milford, MA) chromatography system with a Waters 991 photodiode array detector and an Ortec Model 661 radioactivity detector (EG&G Instruments, Oak Ridge, TN). Radioactive samples were counted with a Beckman 8000 automated well-type gamma counter (Beckman Instruments, Inc.; Fullerton, CA) or a Wallac Wizard 1480 automatic gamma counter (Perkin Elmer; Gaithersburg, MD).

**HPLC purification and analysis for peptide synthesis.** HPLC analysis was performed with a Vydac C-18 column (250 $\times$ 4.6 mm) at a flow rate of 1.0 mL/min. Semi-preparative HPLC was performed with a Vydac C-18 column (25 $\times$ 2.2 cm) at 9.5 mL/min. HPLC eluents consist of water containing 0.05% TFA (solvent A) and acetonitrile containing 0.05% TFA (solvent B). The elution profile was monitored by UV absorbance at 254 nm and 214 nm.

**Solid phase peptide synthesis of H-DTyr(Bu<sup>t</sup>)-Lys(Dde)-Arg(Pbf)-Ala-Asp(OBu<sup>t</sup>)-OH.** The protected peptide sequence was assembled manually from H-Asp(Bu<sup>t</sup>) 2-chlorotrityl resin (0.81 g, 0.64 mmol/g) using the conventional Fmoc

chemistry in a glass reaction vessel fitted with a sintered glass frit. The coupling reactions were carried out by adding a pre-activated solution of N- $\alpha$ -Fmoc-protected amino acid (1.2 mmol), HOBT (1.2 mmol), HBTU (1.2 mmol), and DIEA (2.4 mmol) in anhydrous DMF (3 mL/g resin) into the resin and swirling for 2 h. The progress of the coupling was monitored by Kaiser test. The Fmoc protecting groups were removed with a solution of 20% piperidine in DMF (10 min, 2x). The resin was washed with methanol (1 min, 2x), followed by DMF (1 min, 6x). The penta-peptide, H-DTyr(Bu<sup>t</sup>)-Lys(Dde)-Arg(Pbf)-Ala-Asp(OBu<sup>t</sup>)-OH, was cleaved by swirling the resin in trifluoroacetic acid/dichloromethane (1:99 v:v) for 5 min. The filtrate was added to a solution of pyridine/methanol (5 mL/10 mL). The resin was washed with methanol (2x) and dichloromethane (2x). The cleavage procedure described above was repeated five more times and the combined filtrate was concentrated, washed with water, and dried to give the title compound (480 mg, 94% yield).

**Cyclo[DTyr(Bu<sup>t</sup>)-Lys-Arg(Pbf)-Ala-Asp(OBu<sup>t</sup>)].** The peptide obtained above was added dropwise into a solution of PyBOP (520 mg, 1 mmol), HOBT(135 mg, 1 mmol), and DIEA (260 mg, 2 mmol) in DMF/DCM (1000 mL, 10:90 v:v). The mixture was stirred overnight, concentrated, and washed with water, 5% aqueous potassium, and water. The solid was dissolved in methanol (100 mL) containing hydrazine (1.0 mL). The mixture was stirred for 15 min, concentrated, and washed with aqueous NaHCO<sub>3</sub> solution (5%) and water. The title compound was further purified by flash column chromatography on silica gel using a mixture of methanol, DCM, and DIEA as eluent (155 mg, 35% yield).

**Cyclo[DTyr-Lys(DOTA)-Arg-Ala-Asp].** A mixture of the peptide obtained above (80.0 mg, 0.08 mmol), DOTA(3OBu<sup>t</sup>) (82.0 mg, 0.24 mmol), HOBT (32.4 mg, 0.24 mmol), and DIC (100.8 mg, 0.80 mmol) in DMF (1.2 mL) was stirred for 72 h. The mixture was filtered, concentrated, and stirred in aqueous TFA (95:5 v:v, 3 mL) for 2 h. The resulting mixture was added to a solution of cold MBTE (10 mL). The precipitate was collected by centrifugation and purified by HPLC (gradient from 3% to

50% over a period of 20 min and then isocratic at 50% for 10 min). The desired fractions were characterized by both ES-MS and HPLC, combined, and lyophilized to afford the title compound (19 mg, ~15% yield), observed m/z for  $[MH]^+$  and  $[MH_2]^{2+}$  in ES-MS: 1019.5 and 510.25.

**Integrin binding assay.** An isolated, competitive binding assay described previously is utilized here. Briefly, vitronectin (Vn) and fibronectin (Fn) were biotinylated with N-hydroxysuccinimide biotin (2 h at room temperature) before dialysis into PBS, pH 7.4. The wells of a 96-well plate (Nunc Immuno Plate with MaxiSorp) were coated with 100  $\mu$ g integrin  $\alpha_v\beta_3$ ,  $\alpha_v\beta_5$ , or  $\alpha_{IIb}\beta_3$  in coating buffer (20 mM Tris, pH 7.4, 150 mM NaCl, 2 mM  $CaCl_2$ , 1 mM  $MgCl_2$ , 10  $\mu$ M  $MnCl_2$ ). The plates were then blocked (1 h at 4  $^\circ$ C) with bovine serum albumin (BSA) (3% in coating buffer). After washing three times with binding buffer (0.1% BSA in coating buffer), biotinylated Vn for integrins  $\alpha_v\beta_3$  and  $\alpha_v\beta_5$ , or biotinylated Fn for integrin  $\alpha_{IIb}\beta_3$ , (final concentration 14 nM) with and without serially diluted ligands was allowed to bind to the integrins (3 h at 37  $^\circ$ C). After washing (200  $\mu$ L binding buffer, 3x), bound biotinylated ligand was detected by binding ExtrAvidin alkaline phosphatase (1/35,000 dilution, 1 h at room temperature) and using the p-nitrophenyl phosphate substrate solution as the chromogen. Each concentration data point was done in triplicate, and each binding experiment was performed at least twice. Nonlinear regression was used to fit binding curves and calculate inhibitory concentrations of 50% ( $IC_{50}$  value). A control assay was performed concurrently with all experiments to ensure the accuracy of the procedure and reagents.

**Radiolabeling with  $^{64}Cu$ .** Each of the DOTA-RGD-peptide constructs was radiolabeled with  $^{64}Cu$  in aqueous solution following the general procedures for radiolabeling non-cross-bridged ligands that have been previously described.<sup>79</sup> In brief, no-carrier-added  $^{64}CuCl_2$  was added to a 5 mM solution of DOTA-peptide conjugate in 0.1 M  $NH_4OAc$ , pH 8 and heated at 37  $^\circ$ C for 45 – 90 min. Specific

activities ranging from 1 - 2.8 mCi/ $\mu$ g were obtained. Radiochemical purity of  $\geq 95\%$  was verified by radio-TLC and radio-HPLC.

**Cellular internalization assay.** The U87MG human glioblastoma cell line (integrin  $\alpha_v\beta_3$ -positive) was obtained from American Tissue Culture Collection (Manassas, VA) and maintained at 37 °C in a humidified environment containing 5 % CO<sub>2</sub> in Eagle's Minimum Essential medium (with Earle's BSS and 2mM L-glutamine) (MEM) supplemented with 10% fetal bovine serum (Invitrogen Corp., Carlsbad, CA). For cell assays, cells were grown until 65–75 % confluent before being harvested by incubation at 37 °C for two min in trypsin/EDTA solution. The cell samples were centrifuged at 110 g for 5 min. The cell pellets were rinsed with growth medium (2 x 1 mL) and resuspended in the binding medium (MEM, 1 % glutamine, 1 % BSA, 0.1 mM Mg<sup>2+</sup>, 0.1 mM Mn<sup>2+</sup>) ( $1 \times 10^6$  cells/(0.5) mL) in microfuge tubes. The <sup>64</sup>Cu-DOTA-peptide solution (1 nM, ~5  $\mu$ Ci in 20-30  $\mu$ L) was added to the cell suspension, and the samples were incubated (37 °C, 5 % CO<sub>2</sub>) with rotation for 15, 30, 60, 90 min. For block experiments the samples were administered 1  $\mu$ M non-radioactive peptide solution (50  $\mu$ L) 15 min prior to addition of the <sup>64</sup>Cu-DOTA-peptide solution. At appropriate time points, the samples were centrifuged for 1 min at 110 g and the radioactive medium was aspirated. Cell pellets were rinsed with ice cold binding buffer (0.5 mL) and centrifuged for 1 min at 110 g (2x). Suspension of the cells in acidic wash buffer (HBSS containing 20 mM NaOAc (pH 4.0)) (0.5 mL, 2x) and incubation at 37 °C for 10 min was used to isolate the surface bound fraction. The cells were separated from the surface bound fraction by centrifugation and collection of the supernatant; the resulting two acid wash fractions were combined. The cell-internalized fraction was obtained by lysing the cell pellets in lysis buffer (1 mL 0.5 % SDS in PBS). The radioactivity in each fraction was measured in a well-type gamma counter. Total protein concentration was determined using the bicinchoninic acid protein assay (Pierce Biotechnology, Rockford, IL). Uptake was normalized by

expression as % activity administered per milligram of protein. Each peptide and time point was done in triplicate.

**Biodistribution studies.** Animal experiments were carried out under humane conditions and in compliance with the Guidelines for the Care and Use of Research Animals established by Washington University's Animal Studies Committee. Female athymic nude mice (*nu/nu*) (6 wk old) were given subcutaneous injections at the nape of the neck with  $5 \times 10^6$  U87MG glioblastoma cells suspended in a minimal volume of PBS. After 3.5 weeks the tumor-bearing mice were subject to biodistribution and small-animal PET imaging studies.

Tissue distribution studies were performed after intravenous injection of the radiolabeled compound via the tail vein (20-30 mCi in 100-150  $\mu$ L). A blocking experiment was also performed by coinjecting radiotracer with a saturating dose of cold peptide (18 mg/kg mouse body weight). Tissue biodistribution data were obtained at 1, 4, and 24 h post injection (PI) and 1 h block ( $n = 5$  per time point). Animals were sacrificed at the appropriate time points, organs of interest, including tumor, were removed and weighed, and the radioactivity was measured in a gamma counter along with dose standards. The raw counts were decay corrected to a standard time, and the counts were normalized as the percent total inject dose per gram of tissue (%ID/g) and percent injected dose per organ (%ID/organ). Mice were allowed food and water *ad libitum*.

**microPET imaging.** Whole-body small animal PET imaging was performed on a microPET Focus 120 or 220 small-animal PET scanner (CTI-Concord Microsystems LLC, Knoxville, TN). Mice anesthetized with 1-2 % isoflurane were imaged for 10 min at 1, 4 and 24 h after tail vein injection of the  $^{64}\text{Cu}$ -DOTA-peptide. Co-registration of the small-animal PET images was achieved in combination with a microCAT-II small-animal CT camera (CTI-Imtek Inc., Knoxville, TN) which provides high-resolution CT anatomic images. Co-registration of microPET and microCAT images was accomplished through a landmark registration technique with image

display software (Amira, TGS Inc.) using fiducial markers directly attached to the animal bed. Maximum a posteriori (MAP) reconstruction was used for the PET component of the co-registered images. Regions of interest (ROI) were drawn manually based on co-registered small-animal CT images, and ROI activity on the corresponding small-animal PET images was measured using Amira 4.0 software (Visage Imaging Inc., San Diego, CA). These values were converted to standard uptake values (SUVs) using equation 1.

$$\text{SUV} = \frac{\text{tissue concentration } (\mu\text{Ci/g})}{\text{injected dose } (\mu\text{Ci}) / \text{body weight (g)}} \quad (\text{Eq. 1})$$

After imaging, the mice were sacrificed for post-PET biodistribution, as described above.

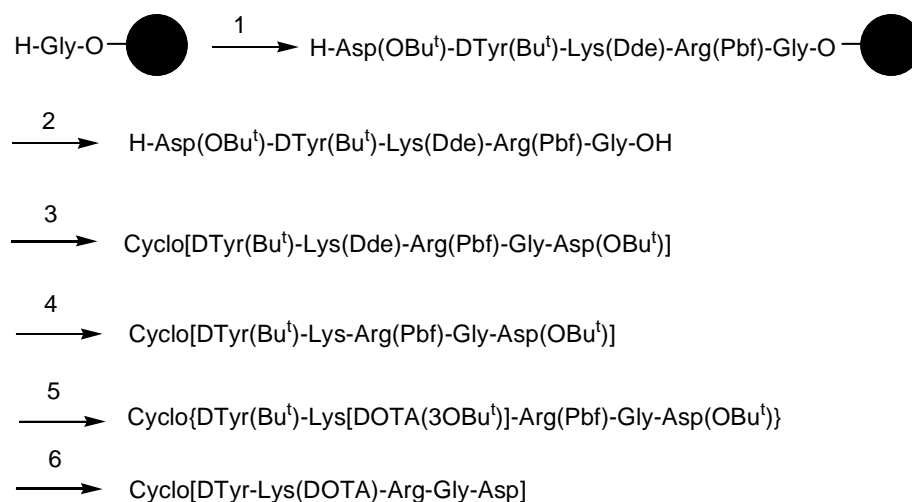
**Statistical methods.** All data are presented as the mean  $\pm$  standard deviation. Group comparisons were made using standard ANOVA methods. Post-hoc testing of individual group differences was accomplished with the Bonferroni test. Groups with  $p < 0.05$  were considered significantly different. GraphPad Prism software (version 5.02; San Diego, CA) was used for all statistical analyses.

**Collaborators.** Synthesis of the peptides described in the experimental section was carried out in the laboratory of Dr. Sam Achilefu by ALF. Details for the synthesis of DOTA-c(RGDyK) and DOTA-KCRGDC by Yunpeng Ye can be found in Appendix II.

## Results

**Solid phase peptide synthesis.** As shown in Scheme 1, the cyclic protected RGD peptide i.e. cyclo[R(Pbf)GD(OBu<sup>t</sup>)y(Bu<sup>t</sup>)K] was similarly prepared as reported previously. The linear protecting peptide H-D(OBu<sup>t</sup>)y(Bu<sup>t</sup>)K(Dde)R(Pbf)G-OH was assembled from H-Gly-2-chlorotrityl resin using conventional Fmoc chemistry and then cleaved with 1% TFA in DCM. The crude product was cyclized in the presence

of PyBOP/HOBT/DIEA in a diluted solution in DCM/DMF (90:10). The resulting cyclic protected peptide i.e. cyclo[R(Pbf)GD(OBu<sup>t</sup>)y(Bu<sup>t</sup>)K(Dde)] was further de-protected with 2% hydrazine in methanol to afford the desired amino-containing analog i.e. cyclo[R(Pbf)GD(OBu<sup>t</sup>)y(Bu<sup>t</sup>)K], which was confirmed by ES-MS. This peptide was conjugated with DOTA(3OBu<sup>t</sup>)-COOH in the presence of HOBT and DIC to give cyclo[R(Pbf)GD(OBu<sup>t</sup>)y(But)K(DOTA(3OBu<sup>t</sup>))] which was de-protected with TFA. The crude product was purified by semi-preparative HPLC to get the desired product, i.e. cyclo[RGDyK(DOTA)].



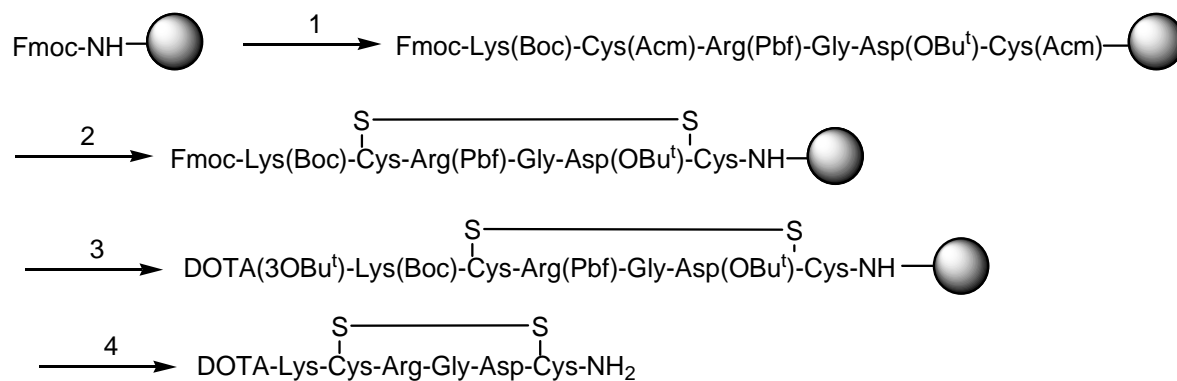
Reagents and conditions:

1. Fmoc chemistry; 2. a) TFA/DCM(1:99); b) Pyridine/DCM/Methanol;
3. PyBOP/HOBT/DIEA/DMF/DCM; 4. Hydrazine/methanol(1:100);
5. DOTA(3OBu<sup>t</sup>)-COOH/HOBT/DIC/DMF; 6. TFA/water(95:5).

### Scheme 1. Synthesis of cyclo[RGDyK(DOTA)]

As summarized in Scheme 2, the resin-bound linear protected peptide i.e. Fmoc-Lys(Boc)-Cys(Acm)-Arg(Pbf)-Gly-Asp(OBu<sup>t</sup>)-Cys(Acm)-Rink amide resin was assembled from Fmoc-Rink amide resin using Fmoc chemistry. The disulfide bond was formed with thallium trifluoroacetate in DMF on solid support. After the Fmoc at the N-terminus was deblocked with 20% piperidine in DMF, the DOTA(3OBu<sup>t</sup>)-COOH was attached in the presence of HOBT and DIC. Finally, the desired product, i.e.

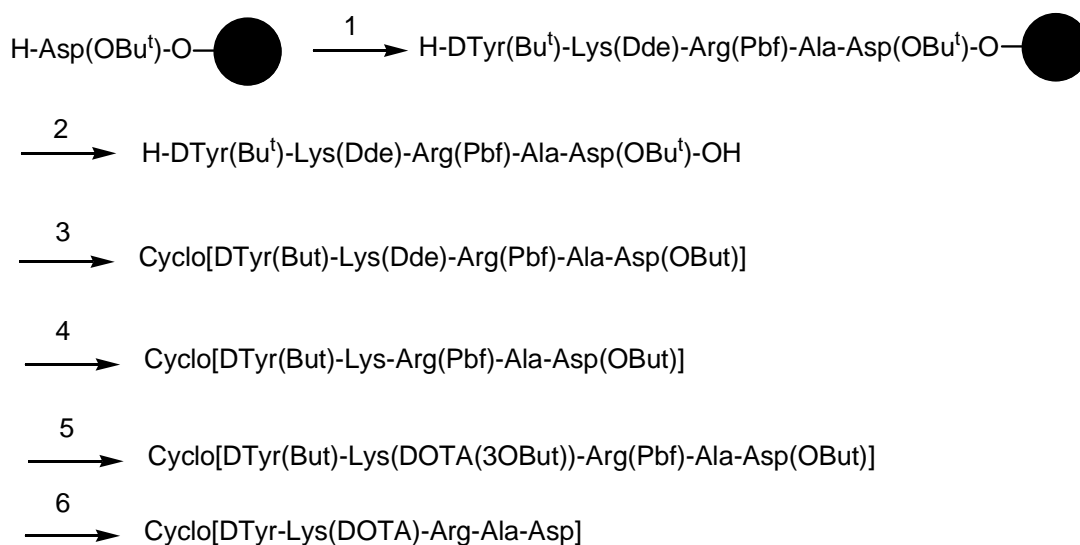
DOTA-K-cyclo(CRGDC)-NH<sub>2</sub>, was obtained by cleavage with TFA/water (95:5) was purified by HPLC. The two desired products were identified by both ES-MS and analytical HPLC.



Reagents and condition: 1. Peptide assembly using Fmoc chemistry; 2.  $\text{Ti}(\text{CF}_3\text{COO})_3/\text{DMF}$ ; 3. (a) piperidine/DMF(20%); (b) DOTA(3OBu<sup>t</sup>)/HOBt/DIC/DMF; 4. TFA/water(95:5).

**Scheme 2.** Synthesis of DOTA-K-cyclo(CRGDC)-NH<sub>2</sub>.

The cyclic control peptide was prepared in three steps consisting of solid phase peptide synthesis, intramolecular cyclization in solution, and conjugation of peptide with DOTA, as shown in Scheme 3. Briefly, the orthogonally protected linear peptide [DTyr(Bu<sup>t</sup>)-Lys(Dde)-Arg(Pbf)-Ala-Asp(OBu<sup>t</sup>)-O-Resin] was prepared on a 2-chlorotrityl resin and cleaved with 1% TFA in dichloromethane (DCM). After cyclizing the protected peptide in a solution of PyBOP (2.5 equiv), HOBt (2.5 equiv), and DIEA (5 equiv) in DMF/DCM (1:10 v:v), the Dde group was selectively removed with 1% hydrazine in methanol. DOTA(3OBu<sup>t</sup>) (3 equiv) was conjugated to the free ε-amino lysine group of the peptide (1 equiv) in the presence of DIC (10 equiv), and HOBt (3 equiv) in anhydrous DMF. All side-chain protecting groups were removed with 95% aqueous TFA solution and the crude product was purified by HPLC and identified by ES-MS.



Reagents and conditions: 1. Fmoc chemistry; 2. a) TFA/DCM(1:99); b) Pyridine/DCM/Methanol; 3. PyBOP/HOBT/DIEA/DMF/DCM; 4. Hydrazine/methanol(1:100); 5. DOTA(3OBut<sup>t</sup>)/HOBT/DIC/DMF; 6. TFA/water(95:5).

**Scheme 3.** Synthesis of cyclo[RADyK(DOTA)]

**Integrin binding assay.** Inhibitory effects of structurally diverse RGD peptides were quantified by measuring their effects on the interactions between immobilized integrin and biotinylated soluble ligands (Table 1). Figure 4 shows representative IC<sub>50</sub> binding curves of GRGDS towards integrins  $\alpha_v\beta_3$ ,  $\alpha_v\beta_5$ , and  $\alpha_{IIb}\beta_3$ . The IC<sub>50</sub> values obtained in replicate experiments were within the same confidence interval. The ability of the peptides to inhibit the binding of vitronectin to the isolated immobilized  $\alpha_v\beta_3$  and  $\alpha_v\beta_5$  receptor was compared with the previously published values for c(RGDyK). In some instances inhibitory peptides were able to suppress fully the binding of ligands to the isolated receptors. All the binding kinetics followed a classic sigmoid path and could be fit with a nonlinear regression curve. According to the IC<sub>50</sub> values obtained, KCRGDC has the best selectivity for integrin  $\alpha_v\beta_3$  and its binding specificity is comparable to c(RGDyK), which has the lowest IC<sub>50</sub> value. Whereas Haubner *et al.* found selectivity of all peptides to be similar, with biological activities about 4000 times higher for the  $\alpha_v\beta_3$  integrin over  $\alpha_{IIb}\beta_3$ , that trend was only observed here for the disulfide-cyclized KCRDGDC. The lactam-cyclized peptide,

c(RDGyK), was found to have a 30-fold better affinity for  $\alpha_{IIb}\beta_3$  compared to  $\alpha_v\beta_3$ . This was surprising but has not been further investigated. A previous study by Pfaff *et al.*, using a similar binding assay, reported a similar affinity of the linear peptide GRGDS towards  $\alpha_v\beta_3$  and  $\alpha_{IIb}\beta_3$  as was observed here (30-fold increase verse 55-fold increase).

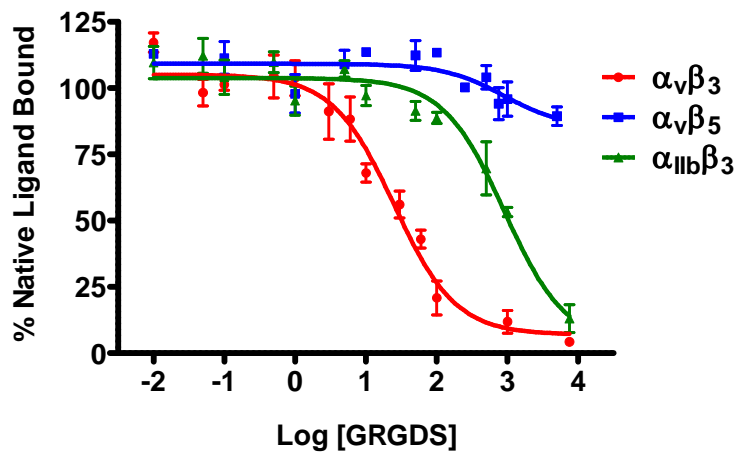


**Figure 4.** IC<sub>50</sub> binding curves for GRGDS versus vitronectin for integrins  $\alpha_v\beta_3$  and  $\alpha_v\beta_5$  and versus fibronectin for  $\alpha_{IIb}\beta_3$  (n=3).

**Table 1.** Inhibition of Vitronectin Binding to Immobilized  $\alpha_v\beta_3$  and  $\alpha_v\beta_5$  and Fibrinogen Binding to Immobilized  $\alpha_{IIb}\beta_3$  in a Competitive Heterologous Binding Assay.

	IC <sub>50</sub>		
	$\alpha_v\beta_3$ (nM)	$\alpha_v\beta_5$ (nM)	$\alpha_{IIb}\beta_3$ (nM)
c(RGDyK)	3.7 <sup>a</sup>	194 <sup>a</sup>	0.11
KCRGDC	10.4	921	> 5,000
GRGDS	15.9	> 5,000	873
c(RADyK)	1,400	> 5,000	> 5,000

a: previously published values<sup>103</sup>

**Cellular internalization assay.** Cell-based assays were performed with  $^{64}\text{Cu}$ -DOTA-peptides to measure the internalization efficiency of the peptides in U87MG glioblastoma cells. Internalization of the radioactivity as well as total cell associated activity were measured at several time-points over 90 min and normalized to protein content (Figure 5). In order to better visualize the differences between the compounds, internalization and total cell associated activity of all four compounds after 60 min are presented on one graph (Figure 6). For the three  $^{64}\text{Cu}$ -DOTA-RGD compounds, total cell associated activity continues to increase for the entire time although internalization does not. The disulfide-cyclized  $^{64}\text{Cu}$ -DOTA-KCRGDC has statistically significant higher levels of non-blocked internalization ( $p < 0.001$ ) and total cell associated activity ( $p < 0.05$ ) compared to the three other compounds. The binding and internalization trends of  $^{64}\text{Cu}$ -DOTA-GGRGDS and  $^{64}\text{Cu}$ -DOTA-c(RGDyK) are the same with slightly less uptake observed for  $^{64}\text{Cu}$ -DOTA-c(RGDyK), although not statistically significant. Binding and uptake of  $^{64}\text{Cu}$ -DOTA-RGD peptides could be blocked by addition of excess cold peptide.

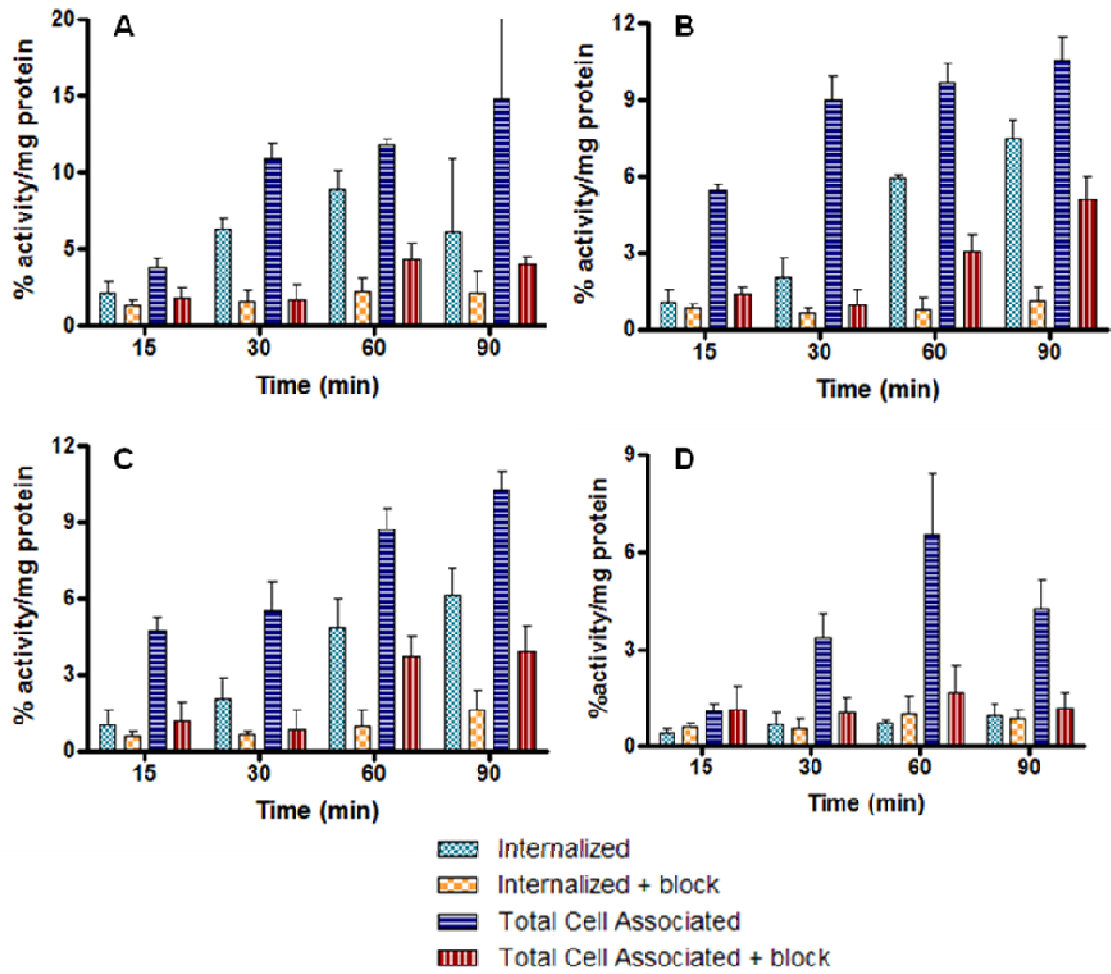


**Figure 5.** Comparison of cellular internalization and cell-associated activity in U87MG cells over time (n = 3). (A)  $^{64}\text{Cu}$ -DOTA-KCRGDC, block with KCRGDC; (B)  $^{64}\text{Cu}$ -DOTA-GGRGDS, block with GRGDS; (C)  $^{64}\text{Cu}$ -DOTA-c(RGDyK), block with c(RGDyK); (D)  $^{64}\text{Cu}$ -DOTA-c(RADyK), block with c(RGDyK). Note the different y-axis scale used for (A) and (D).

Specific, blockable cell surface binding is observed for  $^{64}\text{Cu}$ -DOTA-c(RADyK), although only minimal internalization is observed. Total cell associated ( $p < 0.001$ ) and internalization ( $p < 0.05$ ) without blocking are significantly lower for the control compared to the RGD peptides.

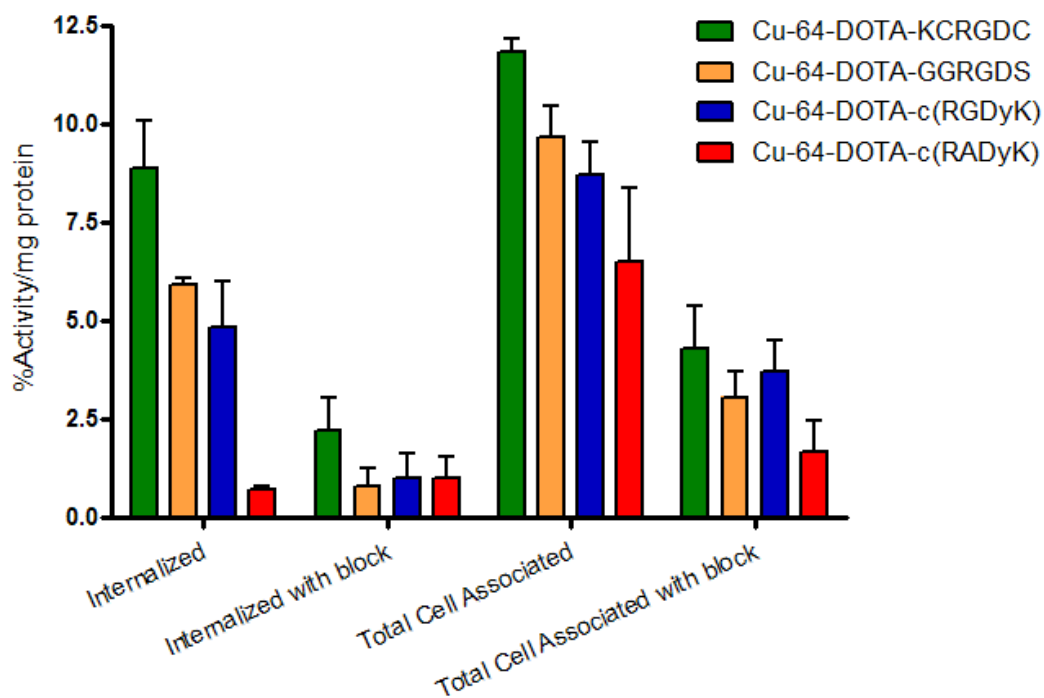


**Figure 6.** Comparison of cellular internalization and cell-associated activity at 60 min in U87MG cells for four  $^{64}\text{Cu}$ -DOTA-peptides ( $n = 3$ ).

***In vivo* characterization.** Small-animal PET and CT co-registration was performed with two of the  $^{64}\text{Cu}$ -DOTA-peptide constructs,  $^{64}\text{Cu}$ -DOTA-KCRGDC and  $^{64}\text{Cu}$ -DOTA-GGRGDS ( $n = 2$  with and without block), simultaneously with biodistribution studies. Biodistribution was also performed with  $^{64}\text{Cu}$ -DOTA-c(RGDyK). A comparison of biodistribution in selected organs is presented in Figure 7, showing rapid uptake and retention of the  $^{64}\text{Cu}$ -labeled peptides in tumor.

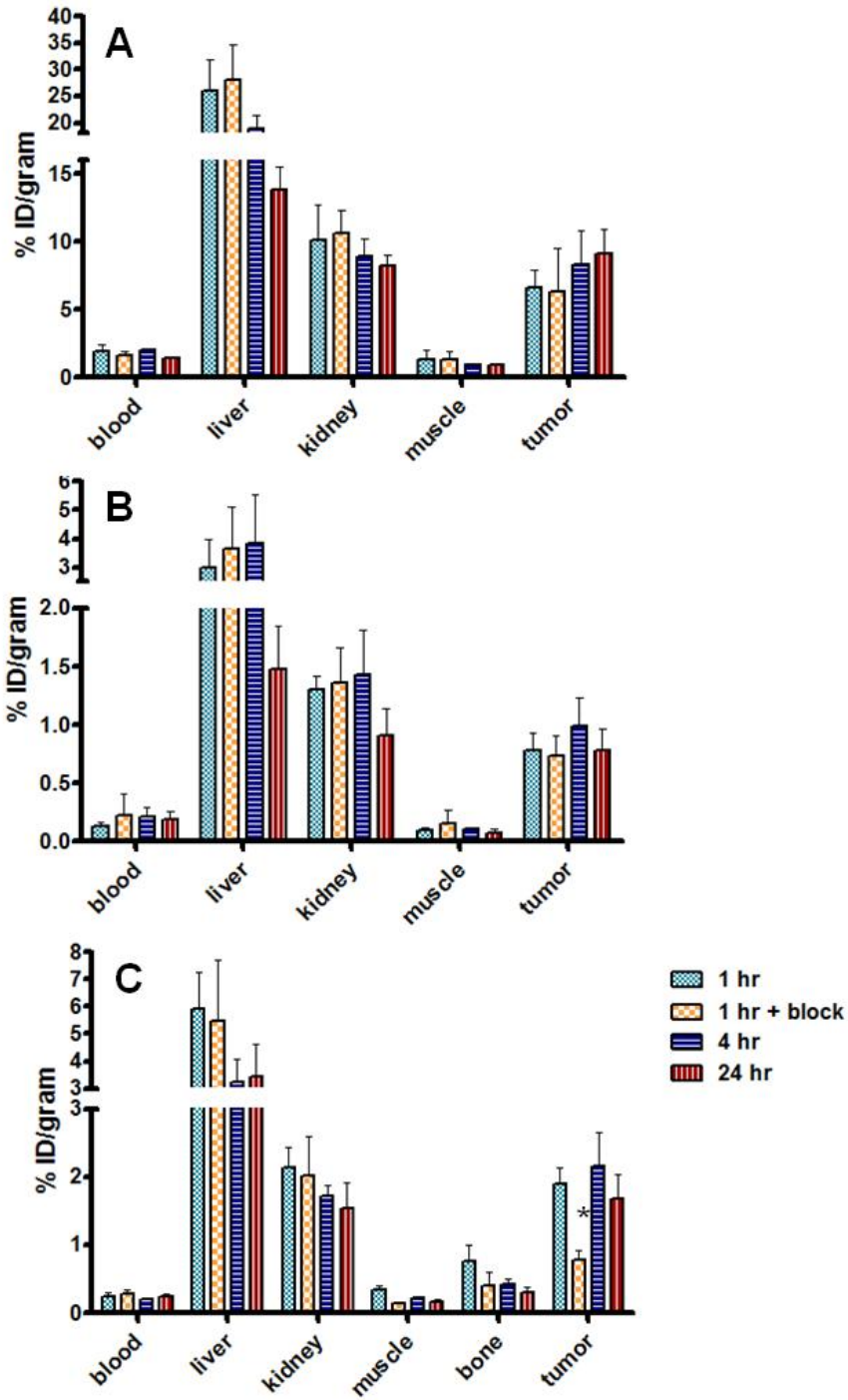


**Figure 7.** Comparison of biodistribution of selected organs in U87MG tumor-bearing *nu/nu* mice ( $n = 5$ ). (A)  $^{64}\text{Cu}$ -DOTA-KCRGDC, block with KCRGDC; (B)  $^{64}\text{Cu}$ -DOTA-GGRGDS, block with GRGDS; (C)  $^{64}\text{Cu}$ -DOTA-c(RGDyK), block with c(RGDyK). (\*  $p < 0.05$  compared to non-blocked.)

Significantly higher levels of uptake were observed for  $^{64}\text{Cu}$ -DOTA-KCRGDC across all organs. As observed in the cell studies,  $^{64}\text{Cu}$ -DOTA-GGRGDS and  $^{64}\text{Cu}$ -DOTA-c(RGDyK) have similar profiles. The disulfide-cyclized peptide was the only compound observed to have increased tumor uptake from 4 to 24 h PI ( $^{64}\text{Cu}$ -DOTA-KCRGDC, 9.4% increase;  $^{64}\text{Cu}$ -DOTA-GGRGDS, 20.4% decrease;  $^{64}\text{Cu}$ -DOTA-c(RGDyK), 22.5% decrease). This was also the only peptide to have continuous blood clearance over the 24 h period (from 1 to 24 h PI:  $^{64}\text{Cu}$ -DOTA-KCRGDC, 28.4% decrease;  $^{64}\text{Cu}$ -DOTA-GGRGDS, 28.2% increase;  $^{64}\text{Cu}$ -DOTA-c(RGDyK), 1.0% increase). The increased blood activity observed for  $^{64}\text{Cu}$ -DOTA-GGRGDS suggests that the compound is unstable *in vivo* which would contribute to its overall poor biodistribution. All three compounds have similar rates of clearance for liver and kidney (percent reduction in kidney from 1 to 24 h:  $^{64}\text{Cu}$ -DOTA-KCRGDC, 18.4%;  $^{64}\text{Cu}$ -DOTA-GGRGDS, 30.8%;  $^{64}\text{Cu}$ -DOTA-c(RGDyK), 27.9%) (percent reduction in kidney from 1 to 24 h:  $^{64}\text{Cu}$ -DOTA-KCRGDC, 46.8%;  $^{64}\text{Cu}$ -DOTA-GGRGDS, 50.4%;  $^{64}\text{Cu}$ -DOTA-c(RGDyK), 73.3%). Tumor uptake of  $^{64}\text{Cu}$ -DOTA-c(RGDyK) can be blocked by co-administration of high doses of unlabeled peptide (1 h PI: non-block,  $1.8875 \pm 0.2396$ ; block,  $0.7723 \pm 0.1458$  ( $p < 0.05$ )). Blocking of  $^{64}\text{Cu}$ -DOTA-KCRGDC and  $^{64}\text{Cu}$ -DOTA-GGRGDS uptake at 1 h was not attained with either co-injection or pre-injection (15 min or 1 h) of cold peptide (pre-blocking data not shown).

Good tumor:blood and tumor:muscle ratios were observed for the three compounds tested. At 4 h post-injection tumor:muscle ratios for all three compounds were similar (Figure 8). The lactam-cyclized  $^{64}\text{Cu}$ -DOTA-c(RGDyK) has a significantly higher tumor:blood ratio ( $p < 0.001$ ).

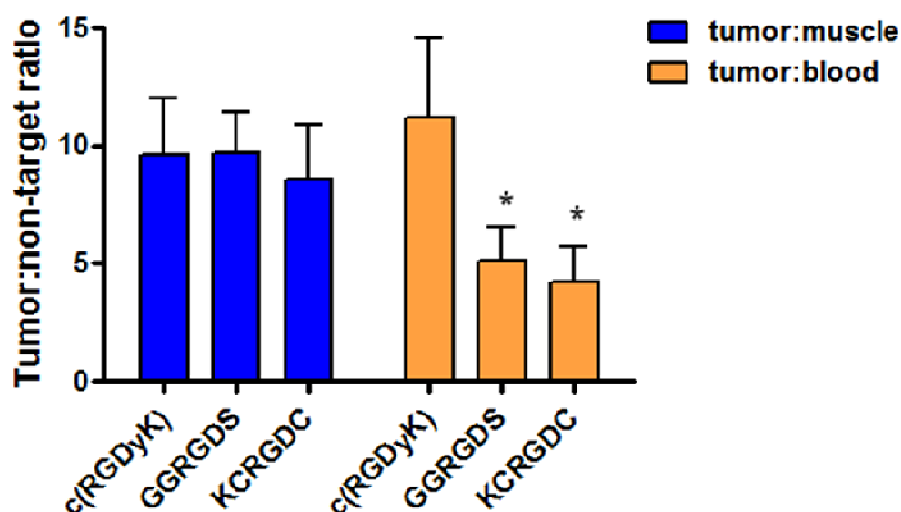


**Figure 8.** Comparison of tumor:background tissue ratios. (\*p < 0.001 compared to  $^{64}\text{Cu}$ -DOTA-c(RGDyK).)

The coregistered PET/CT images shown in Figures 9 and 10 are representative of all mice in each group (n = 2). In coronal and transaxial sections uptake in the tumor can be visualized. As observed in the biodistribution study at 1 h, there is no significant difference between those animals receiving a blocking dose of peptide or not at 1, 4, or 24 h PI (SUV at 4 h PI:  $^{64}\text{Cu}$ -DOTA-KCRGDC,  $0.79 \pm 0.17$ ;  $^{64}\text{Cu}$ -DOTA-KCRGDC + block,  $0.98 \pm 0.36$ ;  $^{64}\text{Cu}$ -DOTA-GGRGDS,  $1.45 \pm 0.23$ ;  $^{64}\text{Cu}$ -DOTA-GGRGDS + block,  $1.58 \pm 0.075$ ) (Figure 11). The best tumor visualization was obtained at 4 h PI and is supported by the highest SUV values of the three time points. Following the 24 h imaging timepoint, a post-PET biodistribution was performed (Figure 12). The activity distributions are comparable to those observed in the other biodistribution studies (Figure 7) and support the imaging observations. At 24 h there is not statistically significant difference in tracer uptake and retention between animals receiving a dose of cold peptide block at time 0 and those which did not.

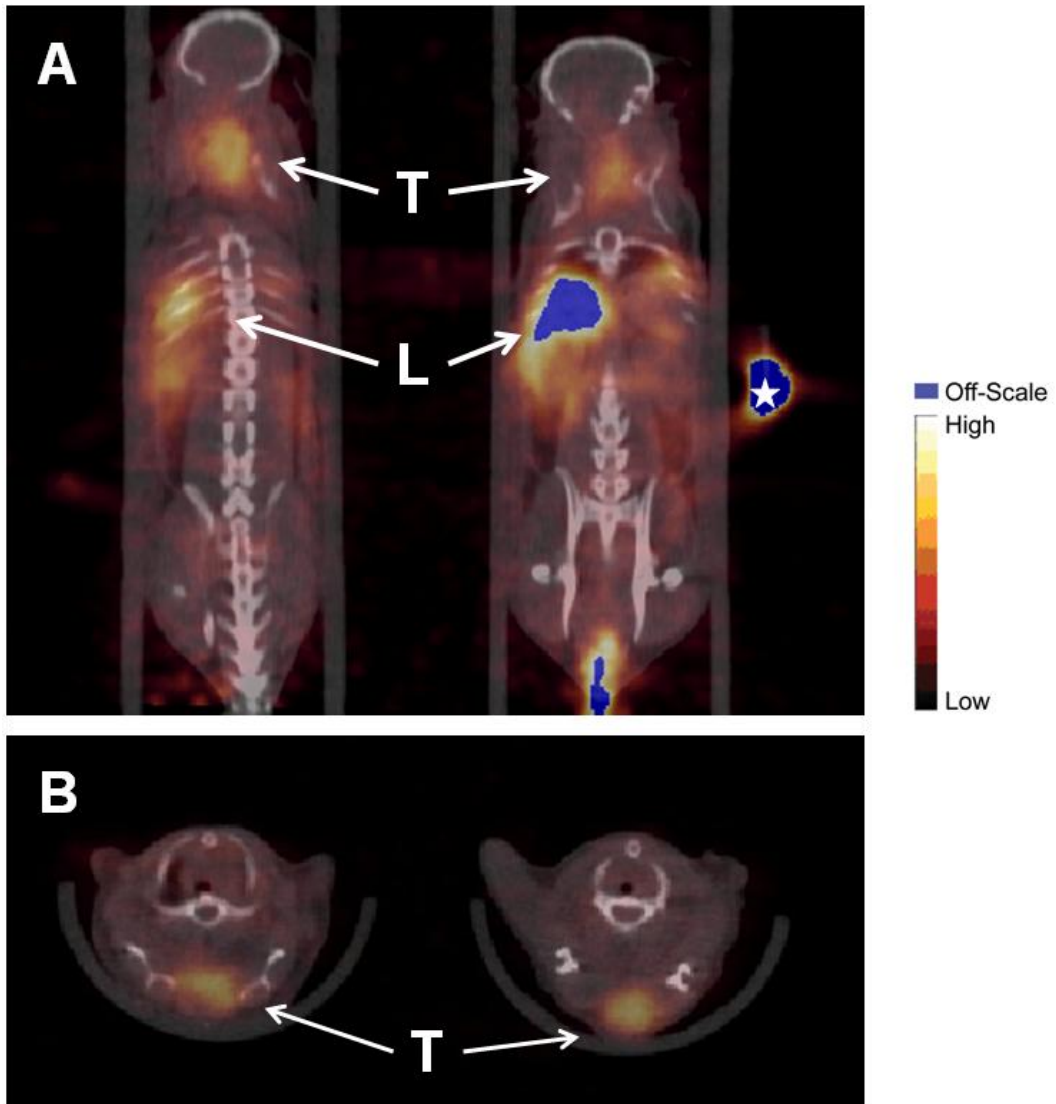


**Figure 9.** Small-animal PET/CT of  $^{64}\text{Cu}$ -DOTA-KCRGDC uptake in U87MG tumor-bearing *nu/nu* mice (static image obtained 4 h PI, 10 min scan). Block with KCRGDC on left in both panels. **(A)** Coronal slice with tumor (T), liver (L), and fiducial (\*) indicated. **(B)** Transaxial slice with tumor indicated.

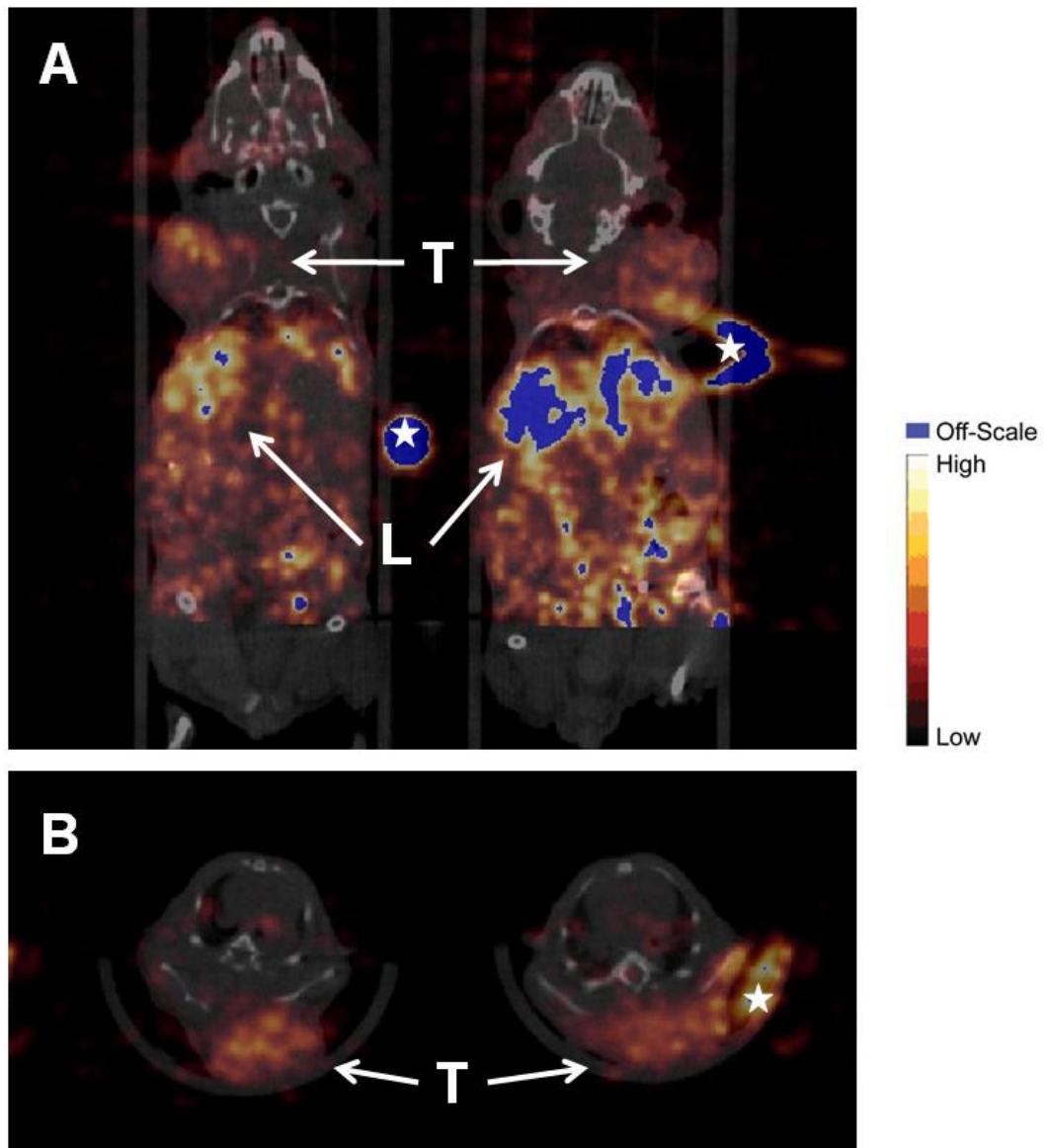


**Figure 10.** Small-animal PET/CT of  $^{64}\text{Cu}$ -DOTA-GGRGDS uptake in U87MG tumor-bearing *nu/nu* mice (static image obtained 4 h PI, 10 min scan). Block with GRGDS on right in both panels. **(A)** Coronal slice with tumor (T), liver (L), and fiducials (\*) indicated. **(B)** Transaxial slice with tumor and fiducial indicated.

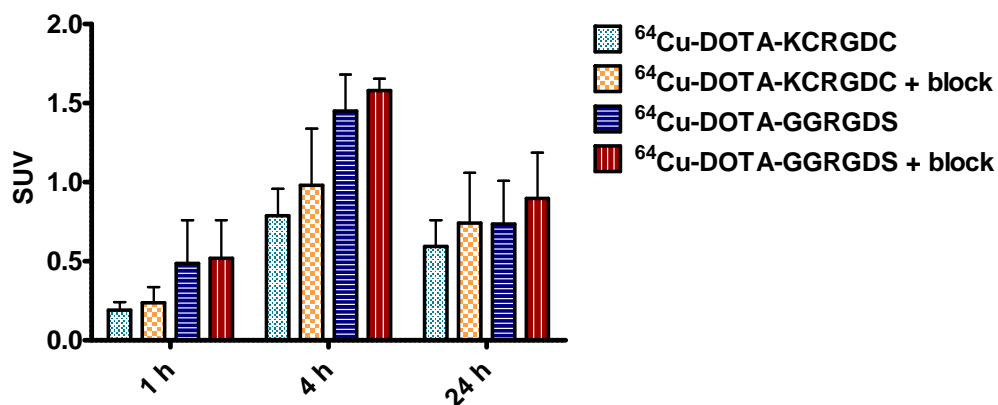


**Figure 11.** Standard uptake values for  $^{64}\text{Cu}$ -DOTA-RGD peptides in U87MG tumor.

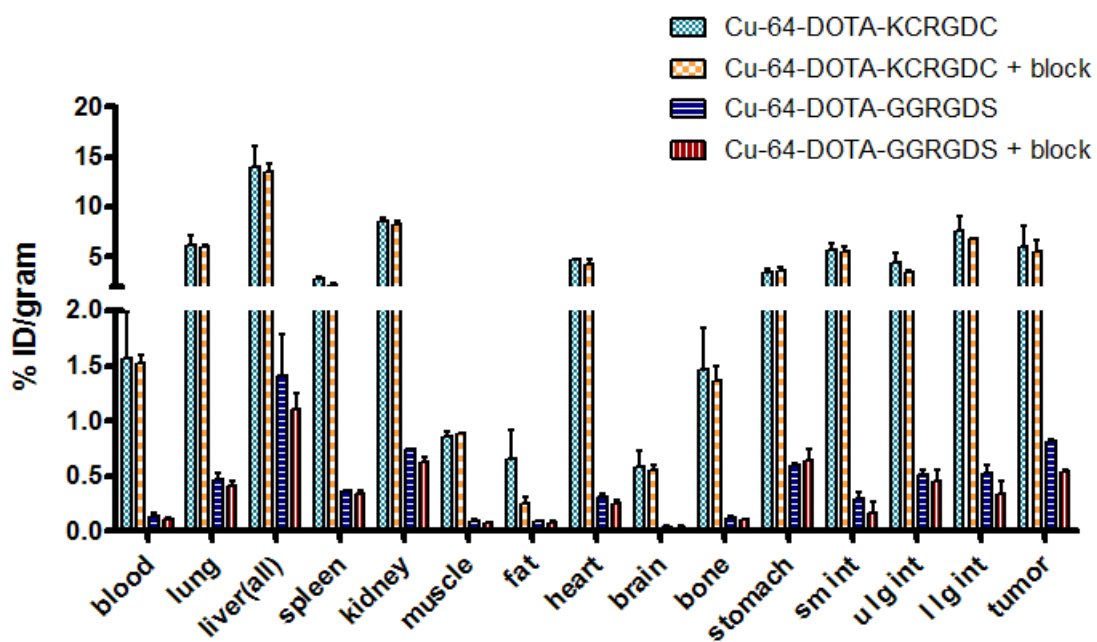


**Figure 12.** Comparison of post-PET imaging biodistribution in U87MG tumor-bearing *nu/nu* mice (24 h PI) (n = 2).

## Discussion and Conclusions

The goal of this study was to systematically evaluate the affinity, receptor specificity, cellular internalization and tumor localization properties of a series of structurally diverse RGD peptides. A lactam-cyclized, disulfide-cyclized, and linear peptide, as well as a lactam-cyclized control were selected for evaluation. While none of these peptides are novel, they have not previously been rigorously studied using the same assays to allow for direct comparison of their respective *in vitro* and *in vivo* properties. The results are useful for the design and evaluation of future integrin  $\alpha_v\beta_3$  imaging agents.

Peptides were screened against the integrins  $\alpha_v\beta_5$  and  $\alpha_{IIb}\beta_3$ , found on macrophages and platelets respectively, to evaluate the specificity of the compounds towards the integrin  $\alpha_v\beta_3$ . The cyclic lactam c(RGDyK) peptide sequence is known to possess high affinity and selectivity for  $\alpha_v\beta_3$  relative to  $\alpha_v\beta_5$ <sup>94</sup>; however, its high affinity for  $\alpha_{IIb}\beta_3$  was surprising and could contribute to high background in imaging studies. The more than five hundred-fold enhancement of binding of KCRGDC towards  $\alpha_v\beta_3$  compared with  $\alpha_{IIb}\beta_3$ , and hundred-fold compared to  $\alpha_v\beta_5$ , suggests high selectivity. The linear peptide has similarly high selectivity, with three hundred-fold higher affinity for  $\alpha_v\beta_5$  and fifty-fold higher affinity for  $\alpha_{IIb}\beta_3$ . While  $\alpha_v\beta_3$  is upregulated in angiogenesis and other disease processes, integrins  $\alpha_v\beta_5$  and  $\alpha_{IIb}\beta_3$  are upregulated in other disease processes and found on other non-disease cells. Highly selective peptide results are promising for application in clinical imaging and therapeutic settings.

The cell-based assays were performed to evaluate the internalization efficiency of the peptides in  $\alpha_v\beta_3$ -positive cells. Block experiments performed with an excess of non-radiolabeled peptide resulted in significantly lower levels of internalization for all peptides studied and is consistent with receptor mediated endocytosis of the radiotracer. Additionally, whole cell assays introduce factors not present in the isolated receptor binding assays carried out with purified proteins and

allowed for confirmation of the receptor specificity of the observed binding. Internalization of each of the RGD peptides was observed with varying extents  $^{64}\text{Cu-DOTA-KCRGDC} > ^{64}\text{Cu-DOTA-GGRGDS} \sim ^{64}\text{Cu-DOTA-c(RGDyK)}$ . Although in the isolated binding assay c(RADyK) showed low affinity for  $\alpha_v\beta_3$ , specific, blockable cell surface binding was observed. Therefore, this compound will not serve as a good negative control *in vivo*. Investigation of another variant, c(GREyK), which has also demonstrated low affinity towards the isolated integrins, is being studied.

The U87MG glioblastoma tumor model has been well-established to have a high level of integrin  $\alpha_v\beta_3$  expression.<sup>143</sup> Tumor uptake and retention of  $^{64}\text{Cu-DOTA-KCRGDC}$  was five to ten times higher than either  $^{64}\text{Cu-DOTA-GGRGDS}$  or  $^{64}\text{Cu-DOTA-c(RGDyK)}$ . This disparity led to nearly identical tumor:background ratios for each compound at all time points. The high tumor:background ratio for  $^{64}\text{Cu-DOTA-c(RGDyK)}$  combined with the observed ability to block tumor uptake with co-administration of an excess of unlabeled peptide, suggests that *in vivo* imaging would afford tumor visualization. Chen, *et al.* reported the use of  $^{64}\text{Cu-DOTA-c(RGDyK)}$  for tumor angiogenesis imaging in MDA-MB-435 tumor-bearing mice.<sup>144</sup> They observed prolonged tumor retention and persistent uptake in the liver, with strong contrast from the background tissue in microPET imaging.

Attempts to demonstrate that  $^{64}\text{Cu-DOTA-KCRGDC}$  and  $^{64}\text{Cu-DOTA-GGRGDS}$  accumulation in the tumor was receptor specific, were not successful. Coadministration of a competitive dose of KCRGDC or GGRGDS was ineffective in blocking *in vivo* tumor uptake of  $^{64}\text{Cu-DOTA-KCRGDC}$  or  $^{64}\text{Cu-DOTA-GGRGDS}$ , respectively. The chosen blocking quantity, 18 mg/kg, was based on previous work that showed it was sufficient to completely inhibit radiolabeled RGD peptide analogues in  $\alpha_v\beta_3$ -positive tissue.<sup>103, 145</sup> While we observed partial inhibition of  $^{64}\text{Cu-DOTA-c(RGDyK)}$  accumulation, neither  $^{64}\text{Cu-DOTA-KCRGDC}$  nor  $^{64}\text{Cu-DOTA-GGRGDS}$  accumulation was inhibited at this dosing level, a thousand-fold excess of the administered dose of radiolabeled peptide. While many groups have reported

successful *in vivo* blocking, we are not the first to report difficulty blocking *in vivo* accumulation despite the ability to efficiently block accumulation *in vitro*.<sup>146</sup> The lack of competitive inhibition may be due to differing clearance properties between the radiolabeled <sup>64</sup>Cu-DOTA-peptide and the peptide, extremely rapid recycling of integrin  $\alpha_v\beta_3$  following peptide-mediated internalization, or a combination of the two.<sup>147</sup>

Small-animal imaging of <sup>64</sup>Cu-DOTA-KCRGDC and <sup>64</sup>Cu-DOTA-GGRGDS in a murine U87MG tumor model demonstrated tumor uptake for both compounds. There is good correlation between the observed liver and kidney accumulation by microPET and the tissue biodistribution measurements. The images produced with the linear peptide, <sup>64</sup>Cu-DOTA-GGRGDS, have a noisy, non-uniform distribution through the tissues with radiotracer uptake, but the tumor is discernable, aided by coregistration with microCT. Neither specific activity nor injected dose has been optimized to improve tumor visualization. Previously, it has been reported that the linear peptides do not accumulate in tumor and are not clearly visualized in small-animal imaging<sup>148</sup> due to poor *in vivo* stability.<sup>110</sup> While the tumor could be visualized with <sup>64</sup>Cu-DOTA-GGRGDS on a coregistered PET/CT image, the clarity of the image is worse than that of the <sup>64</sup>Cu-DOTA-KCRGDC images. Cyclic peptides seem to be more resistant to proteolysis, and their conformationally constrained state traps them in the active conformation. Thus, cyclization improves tumor targeting efficiency.

While the disulfide-cyclized <sup>64</sup>Cu-DOTA-KCRGDC exhibits the best *in vitro* behavior, <sup>64</sup>Cu-DOTA-c(RGDyK) has better *in vivo* properties. The benefits of the synthetic simplicity afforded by a disulfide-cyclized peptide versus a lactam-cyclized one must be weighed against the improved *in vivo* performance. Future studies with new versions of RGD peptide amphiphiles may produce compounds in which these properties are not in opposition.

Further *in vivo* investigation of the compounds reported upon here is warranted to demonstrate targeting specificity of the peptides along with exploration

of a different peptide as a negative control. Improved pharmacokinetics of RGD-peptide based radiopharmaceuticals would also be necessary for successful adoption as diagnostic imaging or radiotherapeutic agents. Higher binding affinity is being investigated through multimeric peptides and conjugation of several peptides onto the surface of nanoparticles. High  $\alpha_v\beta_3$  binding affinity and specificity along with good *in vivo* pharmacokinetics would enable RGD-peptide based radiopharmaceuticals to be used for diagnostic imaging and as therapeutic agents for cancer and other  $\alpha_v\beta_3$ -expressing disease states.

## **CHAPTER 4**

Preparation, Purification, and *In Vitro* Characterization  
of RGD-Functionalized Shell Crosslinked Nanoparticles

## Abstract

In this work, micelles and shell crosslinked nanoparticles (SCKs) prepared from poly(acrylic acid)-*b*-polystyrene (PAA-*b*-PS) were labeled with the cyclic peptide KCRGDC, as nanoscale agents for non-invasive imaging and targeted drug delivery. This peptide contains the tripeptide arginine-glycine-aspartic acid (RGD) sequence as the recognition motif for the  $\alpha_v\beta_3$  integrin receptor, which is highly expressed in areas where angiogenesis occurs. Methods were developed to afford nanoparticles labeled with covalently attached and ready-to-bind KCRGDC peptide. The binding of these peptide-labeled nanoparticles was evaluated by measuring IC<sub>50</sub> values to  $\alpha_v\beta_3$ . In order to specifically target the  $\alpha_v\beta_3$  integrin, selectivity against another integrin,  $\alpha_v\beta_5$ , was also demonstrated. The best affinity to  $\alpha_v\beta_3$  was achieved by attaching the KCRGDC peptide to the micelle assembled from HOOC-PEG3000<sub>4.0</sub>-*g*-DOTAlysine<sub>3.2</sub>-*g*-PAA<sub>58.2</sub>-*b*-PS<sub>71</sub>, with IC<sub>50</sub> value being 0.49 nM, a significant enhancement from that of the KCRGDC, whose IC<sub>50</sub> value to  $\alpha_v\beta_3$  is 10.5 nM. These materials are of interest for cancer imaging and therapeutic delivery and *in vitro* cell assay experiments should be performed to determine cellular binding and internalization.

## Introduction

Angiogenesis is a physiological process involving the growth of new blood vessels from existing vasculature.<sup>149</sup> It is a normal process involved in many biological processes, e.g. embryogenesis, wound healing, and tissue remodeling; however, it is also a fundamental step in the transition of tumors from a dormant state to a malignant one. Several disorders are characterized by either an excess or insufficient number of blood vessels, e.g. rheumatoid arthritis<sup>38</sup>, psoriasis<sup>150</sup>, restenosis<sup>151</sup>, and diabetic retinopathy<sup>152</sup>.

Angiogenesis is a multi-step, invasive process, characterized by endothelial cell proliferation, modulation of the extracellular matrix (ECM), and cell adhesion/migration. Among the many angiogenic factors, integrin  $\alpha_v\beta_3$  has been found to be necessary for the formation, survival, and maturation of new blood vessels.<sup>153</sup> In human melanoma cells, the expression of  $\alpha_v\beta_3$  is correlated with malignancy grade, collagenase production, and cell growth.<sup>154, 155</sup> Due to integrin  $\alpha_v\beta_3$ 's key role in many physiological processes, it has been evaluated extensively as a drug target. The tripeptide sequence arginine-glycine-aspartic acid (RGD) is common to various ECM proteins, e.g. vitronectin, fibronectin, fibrinogen, thrombospondin, and von Willebrand factor, involved in cell-matrix adhesion.<sup>31, 156</sup> High-affinity  $\alpha_v\beta_3$  selective ligands containing RGD have been identified by phage display.<sup>157</sup> Targeted chemotherapy has been investigated using RGD peptides to deliver doxorubicin<sup>158</sup> and proapoptotic peptides<sup>159</sup> to tumor vasculature. *In vivo* imaging of sites of angiogenesis has been demonstrated using RGD-containing peptides.<sup>160, 161</sup>

Since the RGD-sequence is conserved in all native ligands, differences in binding affinities and specificity can be obtained from slight modifications. The flanking amino acid residues, especially the two positions following the aspartic acid, are known to affect binding affinity both by direct interaction of the residues with the integrin as well as influencing peptide folding.<sup>156</sup> Cyclization is a common technique

to improve binding properties because it confers rigidity on the structure.<sup>162</sup> All selective RGD peptides have at least one ring structure. It has been recently reported that multimeric RGD peptides can enhance the affinity of the receptor-ligand interaction through either multivalent binding or statistical rebinding. Polyvalency affords better targeting capability and higher cellular internalization because of increased apparent ligand concentration.<sup>163</sup> The unique structural properties of nanoscale materials provide the ability for them to carry therapeutic agents and to present numerous targeting moieties as well. Furthermore, multivalency has been shown to facilitate internalization.<sup>47</sup> Carrier systems like liposomes,<sup>164</sup> polymers,<sup>165-167</sup> nanoparticles,<sup>168</sup> and proteins<sup>169</sup> bearing multiple RGD peptides are therefore more likely to be internalized *via* receptor-mediated endocytosis than single peptide constructs.

In this work, the disulfide-cyclized KCRGDC peptide was selected as the antagonist to  $\alpha_v\beta_3$ , while shell crosslinked nanoparticles (SCKs) were used as the carrier system. SCKs are self-assembled core-shell nanomaterials, originating from crosslinking the shell domain of micelles assembled from amphiphilic block copolymers, poly(acrylic acid)-*b*-polystyrene (PAA-*b*-PS) in this work. The SCKs produced have a robust structure due to the covalent crosslinking reaction, and have controllable sizes ranging from 10 to 200 nm.<sup>170, 171</sup> SCKs conjugated with KCRGDC peptide were synthesized *via* various methods and were tested for binding affinities to  $\alpha_v\beta_3$  via *in vitro* plate-based assays. Improved binding affinities were achieved, compared to the KCRGDC peptide as a small molecule that is capable only of monovalent binding. With the enhanced blood circulation times that can be achieved by grafting poly(ethylene glycol) from the nanoparticles,<sup>172</sup> these multi-functional materials could be good candidates as carrier systems for imaging and therapeutic agents, selectively to injured or diseased tissues that overexpress  $\alpha_v\beta_3$ .

## Experimental Procedures

**General Materials and Methods.** All chemicals were purchased from Sigma-Aldrich and used without further purification unless otherwise noted. Nanopure water (18 M $\Omega$ -cm) was acquired by means of a Milli-Q water filtration system (Millipore Corp.; Bedford, MA). KCRGDC was custom synthesized by Tianma Pharma Co., Suzhou, China, and used as received.

**Integrin binding assay.** An isolated, competitive binding assay described previously<sup>83, 173</sup> is utilized here. Briefly, vitronectin (Chemicon CC080) was biotinylated with N-hydroxysuccinimide biotin (2 h at room temperature) before dialysis into PBS, pH 7.4. The wells of a 96-well plate (Nunc Immuno Plate with MaxiSorp) were coated with 100  $\mu$ g integrin  $\alpha_v\beta_3$  or  $\alpha_v\beta_5$  (Chemicon CC1019 and CC1025, respectively) in coating buffer (20 mM Tris, pH 7.4, 150 mM NaCl, 2 mM CaCl<sub>2</sub>, 1 mM MgCl<sub>2</sub>, 10  $\mu$ M MnCl<sub>2</sub>). The plates were then blocked (1 h at 4  $^{\circ}$ C) with bovine serum albumin (BSA) (3% in coating buffer). After washing three times with binding buffer (0.1% BSA in coating buffer), biotinylated vitronectin (final concentration 14 nM) with and without serially diluted ligands was allowed to bind to the integrins (3 h at 37  $^{\circ}$ C). After washing (3 times in binding buffer), bound biotinylated vitronectin was detected by binding ExtrAvidin alkaline phosphatase (1/35,000 dilution, 1 h at room temperature) using the p-nitrophenyl phosphate liquid substrate system as the chromogen. Each concentration data point was done in triplicate, and each binding experiment was performed at least twice. Nonlinear regression was used to fit binding curves and calculate inhibitory concentrations of 50% (IC<sub>50</sub> value) (Prism, version 5.02; GraphPad).

## Results and Discussion

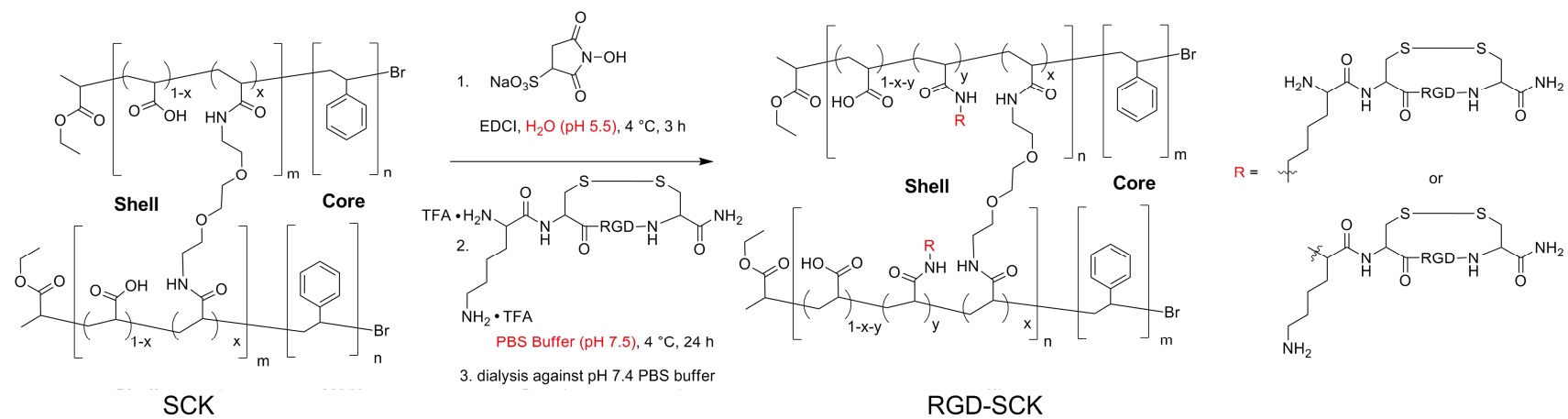
To create a functional nanomaterial that is capable of carrying imaging and/or therapeutic agents to a selective tissue site, it is imperative that the targeting ligand be accessible for binding with the receptor target. Two general approaches, the

*post-conjugation* method and the *pre-conjugation* method, were, therefore, applied to afford micelle/SCK nanoparticles functionalized with a disulfide-cyclized RGD peptide, KCRGDC. For the *post-conjugation* method, SCK nanoparticles were first prepared from the amphiphilic diblock copolymer precursors (PAA-*b*-PS), according to our established protocol, the cyclic KCRGDC peptide or the amine-terminated PEO<sub>113</sub>-5-FAM-KCRGDC were then conjugated onto the nanoparticle shell domain through carbodiimide-mediated aqueous amidation (see Experimental Section for details). For the *pre-conjugation* method, the PAA-*b*-PS block copolymers were modified with the KCRGDC peptides *via* amidation chemistry in organic solvent, followed by aqueous assembly into nanostructures and crosslinking across the shell domain of nanoparticles.<sup>172, 174</sup> Coincident with these synthetic efforts were rigorous physicochemical studies to determine the composition and structure of the resulting materials, and biological evaluations to determine the binding affinities between the ligand bound to the nanostructure and receptors either coated on a plate or presented on cells. The synthetic work and physicochemical studies were performed by collaborators and details can be found in Appendix III, whereas the biological studies were the focus of my studies.

**Integrin Binding Assay.** This assay tests the heterologous competitive binding to the integrin between biotinylated vitronectin and an RGD peptide or RGD-SCK construct and allows for calculation of the IC<sub>50</sub> value. While the integrin binding assay protocol was developed for small molecules and peptides,<sup>83</sup> this work demonstrates the applicability of this isolated integrin binding assay for nanoparticles as well. The specificity of the ligand for  $\alpha_v\beta_3$  is determined by measuring the affinity for the integrin  $\alpha_v\beta_5$ , which is expressed on macrophages. A peptide of known binding affinity, usually KCRGDC, was included as an external reference in each assay.

**Post-conjugation of KCRGDC peptide onto micelles and SCKs.** The work started with post attachment of the KCRGDC peptide onto micelles and SCKs

prepared from PAA<sub>61</sub>-*b*-PS<sub>34</sub> (Scheme 1 and Table 1). Nanoparticles with varied numbers of KCRGDC were prepared by controlling the coupling stoichiometry. Determination of the IC<sub>50</sub> values for these samples showed that the micelle/SCKs with no KCRGDC peptide attached showed no binding to either  $\alpha_v\beta_3$  or  $\alpha_v\beta_5$ , at concentrations up to 10,000 nM. For KCRGDC-labeled nanoparticles, poor binding affinity to  $\alpha_v\beta_3$  was observed for micelles and 20% crosslinked SCKs. An interesting phenomenon is that the KCRGDC-micelle samples showed very good binding to  $\alpha_v\beta_5$  instead to  $\alpha_v\beta_3$ , although KCRGDC has poor binding to  $\alpha_v\beta_5$  as a small molecule. The reason behind this phenomenon has not been investigated. Compared to micelles and 20% crosslinked SCKs, enhanced and also selective binding to  $\alpha_v\beta_3$  was achieved with 50% crosslinked SCKs. Also, as the number of peptides per SCK increased from less than 1 to *c.a.* 52, the IC<sub>50</sub> value towards  $\alpha_v\beta_3$  improved, decreasing from 380 nM to 37.8 nM. It is hypothesized that as the extent of crosslinking increases, more of the peptides attached to the nanoparticle will be located on the outer surface of the nanoparticles to be accessible for integrin binding, thus improving the nanoparticles' binding affinities as well. Increased loading of peptides also leads to better binding.



**Scheme 1.** Illustration of post-labeling KCRGDC peptide to micelle/SCK.

**Table 1.** IC<sub>50</sub> values of KCRGDC-micelle/SCKs prepared by post-labeling method.

Samples	N <sub>aggr.</sub>	Peptide per NP <sup>a</sup>	Peptide per NP <sup>b</sup>	IC <sub>50</sub> (nM) <sup>d</sup>	
				$\alpha_v\beta_3$	$\alpha_v\beta_5$
<i>KCRGDC</i>				10.5	921
<i>Micelle</i>	125	0	0	> 10,000	> 10,000
<i>20% Crosslinked SCK</i>	125	0	0	> 10,000	> 10,000
<i>50% Crosslinked SCK</i>	125	0	0	> 10,000	> 10,000
<i>KCRGDC-Micelle</i>	125	4	<i>n.d.</i> <sup>c</sup>	> 10,000	1.5
	125	40	<i>n.d.</i>	> 1,000	0.3
	125	400	<i>n.d.</i>	1,080	26.1
<i>KCRGDC-SCKs</i>	125	4	<i>n.d.</i>	> 5,000	> 10,000
	125	40	< 1	> 1,000	> 10,000
	125	400	58	> 1,000	> 5,000
<i>KCRGDC-SCKs</i>	125	4	<i>n.d.</i>	> 1,000	> 10,000
	125	40	< 1	380	> 5,000
	125	400	42	37.4	> 10,000

<sup>a</sup> nominal numbers of peptide per nanoparticle (NP) from stoichiometry; <sup>b</sup> numbers of peptide per nanoparticle measured from Ellman's assay; <sup>c</sup> not determined; <sup>d</sup> IC<sub>50</sub> values for micelle/SCKs were measured to be the concentrations of the nanoparticles in units of nM.

**Post-conjugation of NH<sub>2</sub>-PEG5000-5-FAM-KCRGDC onto PEGylated SCKs prepared from mPEG2000<sub>5.5</sub>-g-DOTA-lysine<sub>2.5</sub>-g-PAA<sub>52</sub>-b-PS<sub>60</sub>.** Relative to KCRGDC, the binding affinity for KCRGDC-labeled nanoparticles to  $\alpha_v\beta_3$  still needed to be improved. Facile ways to achieve this would be to increase the peptide density on nanoparticles or to add a spacer between KCRGDC and nanoparticles to make the peptide more accessible for binding. Meanwhile, besides good binding, nanoparticles with good biodistribution are also desired. A well known method to achieve improved biodistribution is the introduction of poly(ethylene glycol) (PEG), grafted on the surface of particles.<sup>172, 175</sup> To achieve this end, 20% and 50% crosslinked SCKs prepared from mPEG2000<sub>5.5</sub>-g-DOTA-lysine<sub>2.5</sub>-g-PAA<sub>52</sub>-b-PS<sub>60</sub> which were reported to have good blood retention times were selected. The DOTA-lysine here acts as a chelator for radiometal incorporation for PET imaging. A PEGylated KCRGDC peptide, NH<sub>2</sub>-PEG5000-5-FAM-KCRGDC, was prepared. The PEG5000 linker was used to allow the attached peptide to be more accessible for

integrin binding, and the fluorophore, 5-FAM, was incorporated for improved quantification of the peptide by UV-vis, thereby eliminating the need to perform the Ellman's assay. Scheme 2 illustrates the coupling reaction and Table 2 shows the characterization and binding affinities of samples prepared by this method.

The coupling efficiency was found to be extremely low (0.6% and 0.4% for 20% and 50% crosslinked PEGylated SCKs, respectively). The layer of poly(ethylene glycol) that surrounded the SCKs can cause the low coupling efficiencies by hindering access of the PEGylated 5-FAM-KCRGDC to the carboxyl groups in the shell of the nanoparticles. Compared to KCRGDC, both 5-FAM-KCRGDC and PEG5000-5-FAM-KCRGDC showed slightly decreased binding affinities to  $\alpha_v\beta_3$ . Due to the low peptide coupling, no appreciable binding to  $\alpha_v\beta_3$  was observed for the two PEGylated SCKs labeled with PEG5000-5-FAM-KCRGDC.

**Table 2.** IC<sub>50</sub> values of PEGylated SCKs, post-conjugated with NH<sub>2</sub>-PEG5000-5-FAM-KCRGDC.

Samples	N <sub>aggr.</sub>	Peptide per NP <sup>a</sup>	Peptide per NP <sup>b</sup>	IC <sub>50</sub> (nM) <sup>c</sup>	
				$\alpha_v\beta_3$	$\alpha_v\beta_5$
5-FAM-KCRGDC				23.0	> 1,000
PEG5000-5-FAM-KCRGDC				21.3	> 1,000
20% Crosslinked PEG-5-FAM-KCRGDC-SCK	200	1000	6.3	> 1,000	> 10,000
50% Crosslinked PEG-5-FAM-KCRGDC-SCK	200	1000	4.2	> 5,000	> 10,000

<sup>a</sup> targeted number of peptide per nanoparticle based on stoichiometry; <sup>b</sup> number of peptides per nanoparticle as determined by UV-vis ( $\epsilon(5\text{-FAM-KCRGDC})_{492\text{nm}} = 63,000 \text{ M}^{-1}\text{cm}^{-1}$ ); <sup>c</sup> IC<sub>50</sub> values for micelle/SCKs were measured to be the concentrations of the nanoparticles in units of nM.



**Pre-labeling of NH<sub>2</sub>-PEG5000-5-FAM-KCRGDC onto mPEG2000<sub>5</sub>-g-DOTA-lysine-g-PAA-b-PS, followed by micelle assembly and crosslinking into SCKs.** Due to the low peptide coupling efficiencies, NH<sub>2</sub>-PEG5000-5-FAM-KCRGDC was pre-labeled onto mPEG2000<sub>5</sub>-g-DOTA-lysine-g-PAA-*b*-PS block copolymers, in DMF, to achieve better coupling through amidation chemistry facilitated by EDCI and HOBt (Scheme 3). PAA-*b*-PS block copolymers with composition similar to PAA<sub>60</sub>-*b*-PS<sub>60</sub> were used. TEM images showed that these PEGylated micelle/SCKs were spherical nanoparticles with narrow size distributions (Figure 1). Detailed characterization data and IC<sub>50</sub> values are provided in Table 3. Compared to the post-labeling method, increased amounts of peptide were able to be incorporated onto the nanoparticles prepared through the pre-labeling method as a result from the increased coupling efficiency for amidation reactions carried out in DMF rather than water.

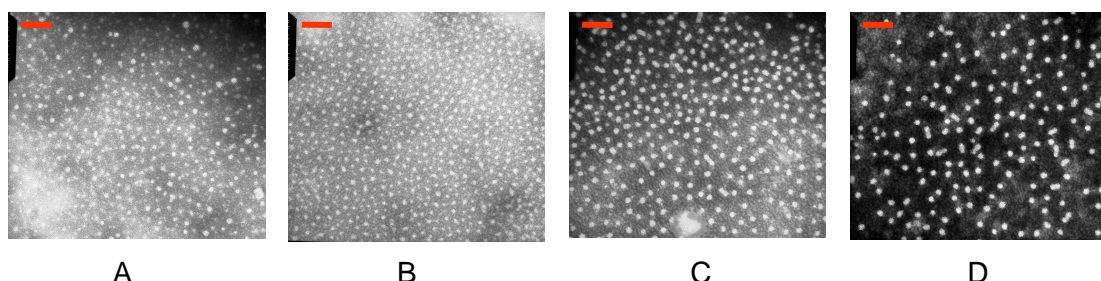
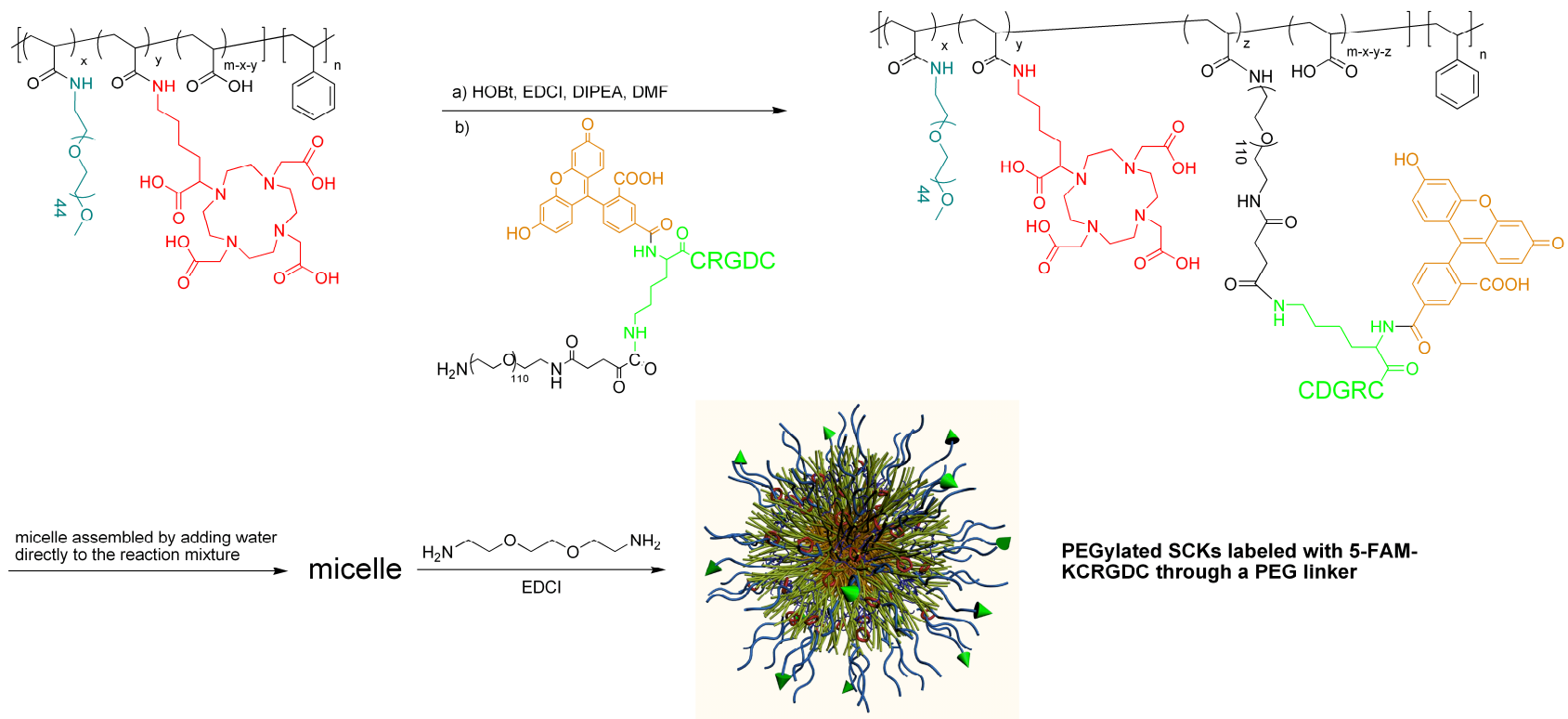


**Figure 1.** Transmission electron microscopy (TEM) images of PEGylated micelle/SCK nanoparticles, prepared from pre-labeling the NH<sub>2</sub>-PEG5000-5-FAM-KCRGDC onto the amphiphilic PAA-*b*-PS block copolymers. A, micelle from mPEG2000<sub>2.4</sub>-g-DOTA-lysine<sub>2.0</sub>-g-PEG5000-5-FAM-KCRGDC<sub>0.6</sub>-g-PAA<sub>59</sub>-*b*-PS<sub>54</sub>; B, 50% crosslinked SCK from mPEG2000<sub>2.4</sub>-g-DOTAlysine<sub>2.0</sub>-g-PEG5000-5-FAM-KCRGDC<sub>0.6</sub>-g-PAA<sub>59</sub>-*b*-PS<sub>54</sub>; C, micelle from DOTAllysine<sub>2.5</sub>-g-PEG5000-5-FAM-KCRGDC<sub>0.5</sub>-g-PAA<sub>65</sub>-*b*-PS<sub>70</sub>; D, 50% crosslinked SCK from DOTA-lysine<sub>2.5</sub>-g-PEG5000-5-FAM-KCRGDC<sub>0.5</sub>-g-PAA<sub>65</sub>-*b*-PS<sub>70</sub>. Scale bar 100 nm.



**Scheme 3.** Graphic representation of the synthesis PEGylated SCKs labeled with KCRGDC peptide by pre-labeling  $\text{NH}_2\text{-PEO}_{113}\text{-5-FAM-KCRGDC}$  onto the SCK precursor,  $\text{mPEG2000-g-DOTAlysine-g-PAA-b-PS}$ .

Initially, nanoparticle samples were purified by dialysis in MWCO 100 kDa dialysis tubings to remove non-covalently bound NH<sub>2</sub>-PEG5000-5-FAM-KCRGDC (samples 2-4 in Table 3). The IC<sub>50</sub> values of these nanoparticles towards  $\alpha_v\beta_3$  were dramatically improved compared to samples prepared by the post-labeling method. Unfortunately, fast protein liquid chromatography (FPLC) analysis of these nanoparticles clearly showed that a considerable amount of non-covalently attached NH<sub>2</sub>-PEG5000-5-FAM-KCRGDC was present. Since the shell of the nanoparticles is composed of poly(acrylic acid) as well as mPEG2000, which can result in strong van der Waals interactions such as hydrogen bonding between the free NH<sub>2</sub>-PEG5000-5-FAM-KCRGDC and the shell/surface domain area, it made the complete removal of the NH<sub>2</sub>-PEG5000-5-FAM-KCRGDC by dialysis difficult.

Centricon tubes (MWCO 10000 Da) were used to remove the free peptide, making use of the shear force centrifugation provides, but free peptide was still present. These samples were also dialyzed in high salt buffer (samples 6-8), with the expectation that high salt concentration decreases the interactions between the peptide and the nanoparticles. After 30 d dialysis, although no free peptide was observed by FPLC, the binding affinities of these nanoparticles also decreased. It's possible that the peptide might have been degraded, causing a loss of activity, during the long dialysis.

**Table 3.** Characterization data and IC<sub>50</sub> values of micelle/SCK nanoparticles labeled with RGD peptide prepared by pre-labeling the NH<sub>2</sub>-PEG5000-5-FAM-KCRGDC onto the amphiphilic PAA-*b*-PS block copolymers.

entry	Samples	Polymer Precursor					D <sub>TEM</sub> nm	N <sub>aggr.</sub>	Purification method	Peptide per NP <sup>2</sup>	IC <sub>50</sub> (nM) <sup>a</sup>	
		x	y	z	m	n					α <sub>v</sub> β <sub>3</sub>	α <sub>v</sub> β <sub>5</sub>
1	PEG5000-5-FAM-KCRGDC										21.3	> 1,000
2	PEG5000-5-FAM-KCRGDC-NP (micelle)	2.4	2.0	0.6	64	54	14 ± 2	240	Dialysis in MWCO 100 kDa tubing in 5 mM PBS, pH 7.4, for 4 d	140	11.7	> 5,000
3	PEG-5-FAM-KCRGDC-SCK-NP (50% Crosslinked SCK)	2.4	2.0	0.6	64	54	14 ± 2	240		143	29.9	> 5,000
4	PEG5000-5-FAM-KCRGDC-NP (micelle)	0	2.5	0.5	68	70	19 ± 2	364	Dialysis in MWCO 100 kDa tubing in 5 mM PBS, pH 7.4, for 4 d	192	65.7	> 5,000
5	PEG-5-FAM-KCRGDC-SCK-NP (50% Crosslinked SCK)	0	2.5	0.3	68	70	19 ± 2	364		118	71.8	> 5,000
6	PEG5000-5-FAM-KCRGDC-NP (micelle)	2.4	2.0	0.6	64	54	12 ± 2	140	Dialysis in MWCO 100 kDa tubing in 150 mM PBS, pH 7.6, for 30 d	80	> 1,000	>1,000
7	PEG-5-FAM-KCRGDC-SCK-NP (20% Crosslinked SCK)	2.4	2.0	0.6	64	54	12 ± 2	140		79	388	>1,000
8	PEG-5-FAM-KCRGDC-SCK-NP (50% Crosslinked SCK)	2.4	2.0	0.6	64	54	12 ± 2	140		76	> 1,000	>1,000
9	PEG5000-5-FAM-KCRGDC-NP (micelle)	5.5	2.0	1.6	64	54	12 ± 2	100	Sephadex <sup>®</sup> G75 (superfine) SEC column	158	>170 <sup>b</sup>	n.d
10	PEG-5-FAM-KCRGDC-SCK-NP (50% Crosslinked SCK)	5.5	2.0	1.6	64	54	12 ± 2	100		160	>141 <sup>b</sup>	n.d
11	PEG5000-5-FAM-KCRGDC-NP (micelle)	0	0	0.9	66	71	12 ± 2	118	Sephadex <sup>®</sup> G75 (superfine) SEC column	104	>148 <sup>b</sup>	n.d
12	PEG-5-FAM-KCRGDC-SCK-NP (50% Crosslinked SCK)	0	0	0.9	66	71	12 ± 2	118		101	>130 <sup>b</sup>	n.d

<sup>a</sup> IC<sub>50</sub> values for micelle/SCKs were measured to be the concentrations of the nanoparticles in units of nM.

<sup>b</sup> Limited sample size and concentration enabled a relatively low IC<sub>50</sub> value minimum value for these samples.

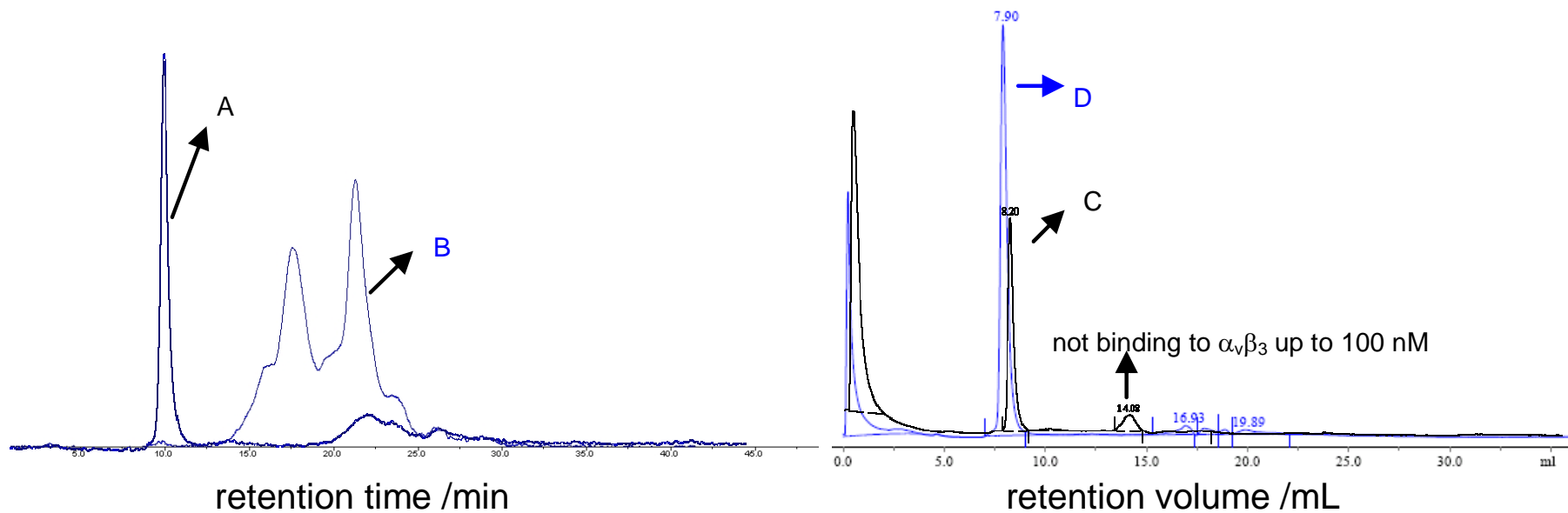
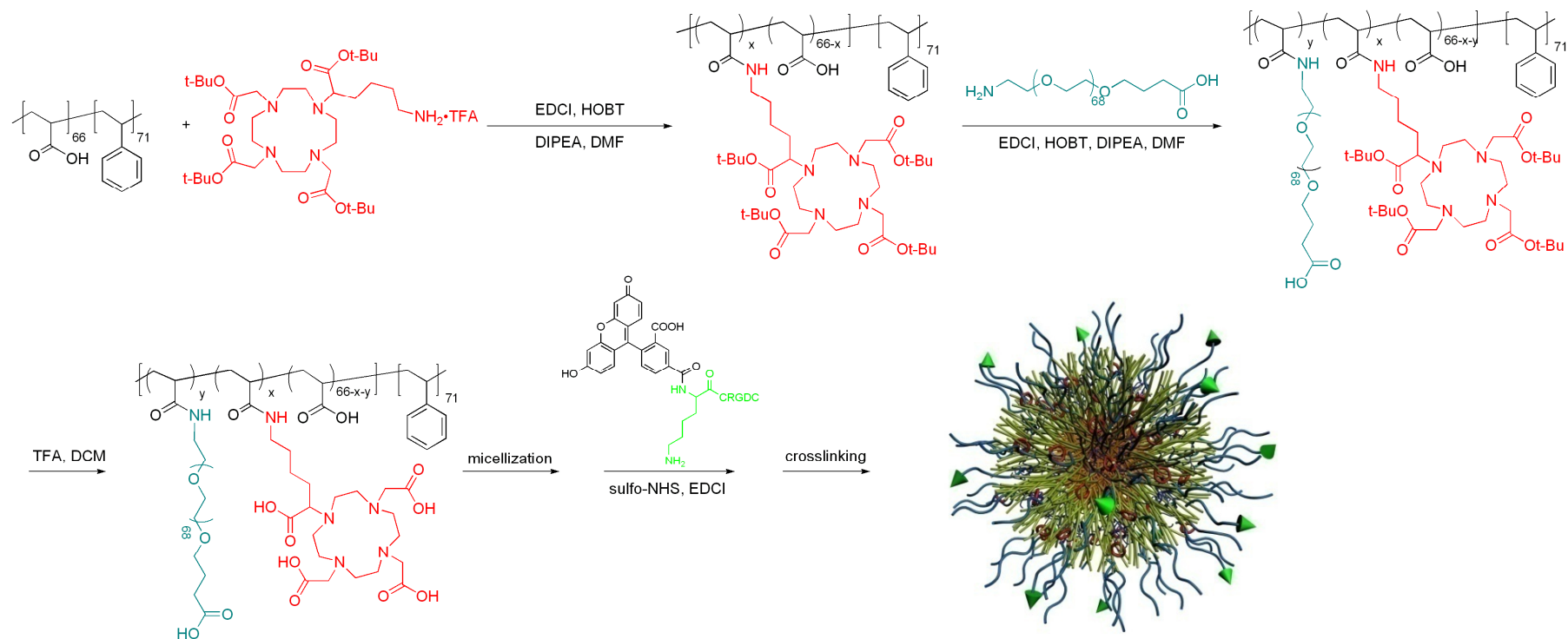


**Figure 2.** Fast protein liquid chromatography (FPLC) traces of A: control sample of RGD-NP prepared from Pre-conjugation method and purified by dialysis in 5 mM PBS (pH ~ 7.4) for 4 d; B: NH<sub>2</sub>-PEO<sub>113</sub>-5-FAM-KCRGDC; C: control sample of RGD-NP prepared from Pre-conjugation method and purified by dialysis in 150 mM PBS (pH ~ 7.4) for 30 d; D: sample 2 in Table 3.

These materials were then purified by SEC columns packed from Sephadex<sup>®</sup> G75 resin (bead size 20-50  $\mu\text{m}$ , fractionation range 1000-50000 Da (Dextrans)). Complete removal of the free peptide was confirmed by FPLC (Figure 2). Despite the fact that pure samples without free peptides were obtained, the binding affinities for  $\alpha_v\beta_3$  remain worse than that of the PEGylated RGD peptide. This indicates that the majority of the peptides attached to the nanoparticles might be located underneath the surface and not available for binding to integrin receptors.

**Post-labeling of KCRGDC to micelles functionalized with –NH-PEG-COOH chains, targeting attachment of most of the peptides to the end of the PEG chains to achieve better accessibility of the peptides for integrin binding.** A new method was then developed to afford nanoparticles with KCRGDC attached to the outer surface (Scheme 4). In this method,  $\text{NH}_2$ -PEG3000-COOH was attached onto the amphiphilic block copolymer first. The product polymer was then assembled into micelles, with some of the PEG-COOH chains expected to spread out on the surface of micelles. The peptide, 5-FAM-KCRGDC was then conjugated to the micelles by methods described above. Crosslinking the shell domain with 2,2'-(ethylenedioxy)bis(ethylamine) afforded the SCKs. One micelle and one 50% crosslinked SCK were prepared by this method.  $\text{IC}_{50}$  values to  $\alpha_v\beta_3$  were measured, as shown in Table 4. Compared to 5-FAM-KCRGDC, whose  $\text{IC}_{50}$  for  $\alpha_v\beta_3$  is 23.0 nM, greatly enhanced bindings to  $\alpha_v\beta_3$  were found with the micelle and SCKs, whose  $\text{IC}_{50}$  values were determined to be 1.38 nM and 0.49 nM, respectively.



**Scheme 4.** Graphic representation of the synthesis KCRGDC-labeled micelles and SCKs by post-labeling 5-FAM-KCRGDC onto micelles with PEG-COOH functionalities.

**Table 4.** Characterization data and IC<sub>50</sub> values of 5-FAM-KCRGDC-labeled nanoparticles by post-labeling KCRGDC onto micelles with PEG-COOH on the surface.

entry	Samples	D <sub>TEM</sub> nm	N <sub>aggr.</sub>	Purification method	Peptide per NP <sup>2</sup>	IC <sub>50</sub> (nM) <sup>a</sup> α <sub>v</sub> β <sub>3</sub>
13	Micelle-5-FAM-KCRGD	26 ± 3	825	Sephadex <sup>®</sup> G75	170	1.38
14	SCK-5-FAM-KCRGD (50% crosslinked)	26 ± 3	825	(superfine) SEC column	170	0.49

<sup>a</sup> IC<sub>50</sub> values for micelle/SCKs were measured to be the concentrations of the nanoparticles in units of nM.

## Conclusions

Methods to develop shell crosslinked nanoparticles bearing cyclic KCRGDC peptide as the nanoscale antagonist to α<sub>v</sub>β<sub>3</sub> integrin were described in this study. Nanoparticles labeled with KCRGDC prepared from post-labeling the 5-FAM-KCRGDC peptide onto micelle/SCKs assembled from HOOC-PEG3000<sub>4.0</sub>-*g*-DOTA-lysine<sub>3.2</sub>-*g*-PAA<sub>58.8</sub>-*b*-PS<sub>71</sub> showed much better binding affinities to α<sub>v</sub>β<sub>3</sub> than those nanoparticles prepared from pre-labeling the NH<sub>2</sub>-PEG5000-5-FAM-KCRGDC to amphiphilic PAA-*b*-PS block copolymers. It is hypothesized that when the NH<sub>2</sub>-PEG5000-5-FAM-KCRGDC was pre-attached to the polymer, the majority of the peptide is buried underneath the shell layer during the course of self-assembly, leading to low accessibility to bind to outside integrins. With good integrin α<sub>v</sub>β<sub>3</sub> binding affinity and selectivity, good biodistribution which has been reported<sup>172</sup>, as well as with the DOTA-lysine serving as the chelator of radiometals for imaging for PET imaging, these nanoparticles possess potential to be developed into nanoscale diagnostic and therapeutic agent delivery vehicles.

## **CHAPTER 5**

### Concluding Remarks and Future Directions

Radiolabeled receptor-binding peptides have emerged as an important class of radiopharmaceuticals for diagnostic imaging and cancer therapy.<sup>176</sup> Following radionuclide labeling the specific receptor-binding properties of the ligand can be exploited to guide the radioactivity to tissues expressing a particular receptor. This dissertation reports on the development of integrin  $\alpha_v\beta_3$ -targeting radiopharmaceuticals for medical imaging applications from the perspective of both the radiometal-labeled chelator as well as the targeting peptide. Several macrocyclic copper(II) chelators have been studied with the goal of improving kinetic and *in vivo* stability. Structurally diverse bifunctional RGD (arginine-glycine-aspartic acid) peptides were investigated for  $\alpha_v\beta_3$  integrin affinity *in vitro* and *in vivo*. The goal of accomplishing higher binding affinity through multivalency has been pursued by evaluating the binding affinity of nanoparticles presenting multiple peptides on their surface.

Copper radionuclides have been the subject of considerable research effort because they offer a varying range of half-lives and positron energies, making them useful for diagnostic imaging and/or targeted radiotherapy. Ensuring the stability of metal complexes *in vivo* remains a challenge in the development of radiometal-based radiopharmaceuticals and significant research effort has been devoted to the development of ligands which can stably chelate copper isotopes.<sup>57, 177</sup> To design cross-bridged chelators that complex Cu(II) with faster kinetics while retaining the high *in vivo* stability of CB-TE2A, different ring sizes of cross-bridged tetraazamacrocycles were designed. Optimal radiolabeling conditions were established for the <sup>64</sup>Cu-labeled radiometal chelators, and their *in vivo* biodistribution and metabolism was studied in normal rats. First, a dicarboxylate analog of Springborg's trimethylene-cross-bridged cyclen<sup>64</sup>, 4,10-bis-(carboxymethyl)-1,4,7,10-tetraazabicyclo[5.5.3]pentadecane (C3B-DO2A), exhibited high *in vitro* stability, which unfortunately did not translate to high *in vivo*

stability. A two-carbon cross-bridged dicarboxylate analog of homocyclen, 4,11-bis-(carboxymethyl)-(1,4,8,11-tetraazabicyclo[6.5.2]pentadecane (CB-TR2A), has the same ring sizes as C3B-DO2A arranged in a different conformation. This compound did not have the same high *in vitro* stability as Cu-C3B-DO2A, but had better *in vivo* stability. The triazaamacrocyclic chelator 1,4,7-triazacyclononane-N,N',N''-triacetic acid (NOTA) has been used in radiopharmaceuticals with suggested high *in vivo* kinetic stability.<sup>66, 178</sup> No study of the Cu-chelator complex alone has been reported in the literature, so the stability of <sup>64</sup>Cu-NOTA was studied.

Previously *in vitro* inertness of copper chelators has been investigated as a convenient indicator of *in vivo* stability,<sup>77</sup> but this did not hold for the Cu-chelators studied here. Many parameters control the behavior of radiopharmaceuticals in biological media, and some of them cannot be easily predicted, requiring *in vivo* studies. The *in vivo* stability of these complexes could be further evaluated by examination of the radiometabolites and determination of the extent of transchelation to proteins. Furthermore, a macrocyclic chelator with rapid complexation kinetics which also demonstrates kinetic inertness comparable to the previously studied <sup>64</sup>Cu-CB-TE2A under physiological conditions has not yet been identified. Research in developing Cu(II) chelators with even greater stability is clearly warranted.

Integrin  $\alpha_v\beta_3$  is upregulated in tumor vasculature, osteoclasts, and areas of collateral circulation following ischemic injury.<sup>28</sup> A series of structurally diverse bifunctional RGD (arginine-glycine-aspartic acid) peptides were investigated for  $\alpha_v\beta_3$  affinity *in vitro* and *in vivo*—lactam-cyclized, disulfide-cyclized, and linear RGD derivatives and a lactam-cyclized control peptide. The RGD-peptides and the control RAD-peptide were screened for integrin  $\alpha_v\beta_3$  binding affinity and specificity compared to  $\alpha_v\beta_5$  and  $\alpha_{IIb}\beta_3$  in a competitive binding assay with each integrin's native ligand. A

lactam-cyclized peptide (c(RGDyK)) demonstrated higher affinity for  $\alpha_v\beta_3$  than disulfide-cyclized (KCRGDC) or linear peptide (GRGDS). Disulfide-cyclized peptides exhibit the best selectivity of the ligands investigated. A control, lactam-cyclized peptide (c(RADyK)) has low affinity for all three integrins. Extent of internalization of the  $^{64}\text{Cu}$ -DOTA-peptides in  $\alpha_v\beta_3$ -positive U87MG human glioblastoma cells was determined. Uptake of RGD peptides could be blocked by high doses of unlabeled peptide. Internalization of the control peptide was minimal, although specific surface binding was observed. Disulfide-linked KCRGDC exhibited the best *in vitro* behavior—binding affinity, selectivity, and internalization.

Biodistribution studies of the three  $^{64}\text{Cu}$ -DOTA-RGD peptides in U87MG tumor-bearing *nu/nu* mice showed rapid uptake and retention of the  $^{64}\text{Cu}$ -labeled peptides in tumor with good tumor:blood and tumor:muscle ratios. At 4 h post-injection tumor:muscle ratios for all three compounds were similar, but  $^{64}\text{Cu}$ -DOTA-c(RGDyK) had a significantly higher tumor:blood ratio ( $p < 0.001$ ). Uptake of  $^{64}\text{Cu}$ -DOTA-c(RGDyK) can be blocked by co-administration of high doses of unlabeled peptide. Blocking of  $^{64}\text{Cu}$ -DOTA-KCRGDC and  $^{64}\text{Cu}$ -DOTA-GGRGDS uptake at 1 h was not attained with either co-injection or pre-injection (15 min or 1 h) of cold peptide. Further *in vivo* investigation is warranted to demonstrate targeting specificity of the peptides along with investigation of a different peptide as a negative control.

Polyvalency is known to have a profound effect on receptor-binding affinity and *in vivo* kinetics of radiolabeled multimers. The goal of accomplishing higher binding affinity through multivalency has been pursued by evaluating the binding affinity of SCK nanoparticles presenting multiple RGD peptides on their surface. Micelles and shell crosslinked nanoparticles (SCKs) prepared from poly(acrylic acid)-*b*-polystyrene (PAA-*b*-PS) were labeled with the disulfide-cyclized peptide KCRGDC and studied as nanoscale

agents for non-invasive imaging and targeted drug delivery. The SCKs produced have a robust structure due to the covalent crosslinking reaction and have controllable sizes ranging from 10 to 200 nm.<sup>179</sup> Difficulties encountered in obtaining nanoparticles with high levels of bioavailable radiometal macrocyclic chelator and targeting peptide on the surface led to a systematic study of methods of shell functionalization and particle purification with chemical, physical, and biological evaluation of each compound. With the good cell targeting capabilities, good biodistribution been reported,<sup>172</sup> as well as with the DOTA-lysine acting as the chelator of radiometals for imaging for PET imaging, these nanoparticles possess good potential to be developed into nanoscale diagnostic and therapeutic agent delivery vehicles.

The development of radiometal-labeled peptides is a relatively slow process, thus in this work optimization of various aspects was studied in parallel. This dissertation contains many disappointing results, but the data are very relevant in that they suggest different properties of chelator structure-activity to consider in future designs and new directions in the synthesis and characterization of nanoparticles for targeted imaging and drug delivery. Each chapter presents a small contribution, but the knowledge gained from these studies can be taken together to produce radiopharmaceuticals with optimal properties—high *in vivo* stability, high target uptake with low uptake in non-target tissues, and rapid blood clearance preferably through renal excretion.

## **APPENDIX I**

### Chapter 2 Supplemental Information

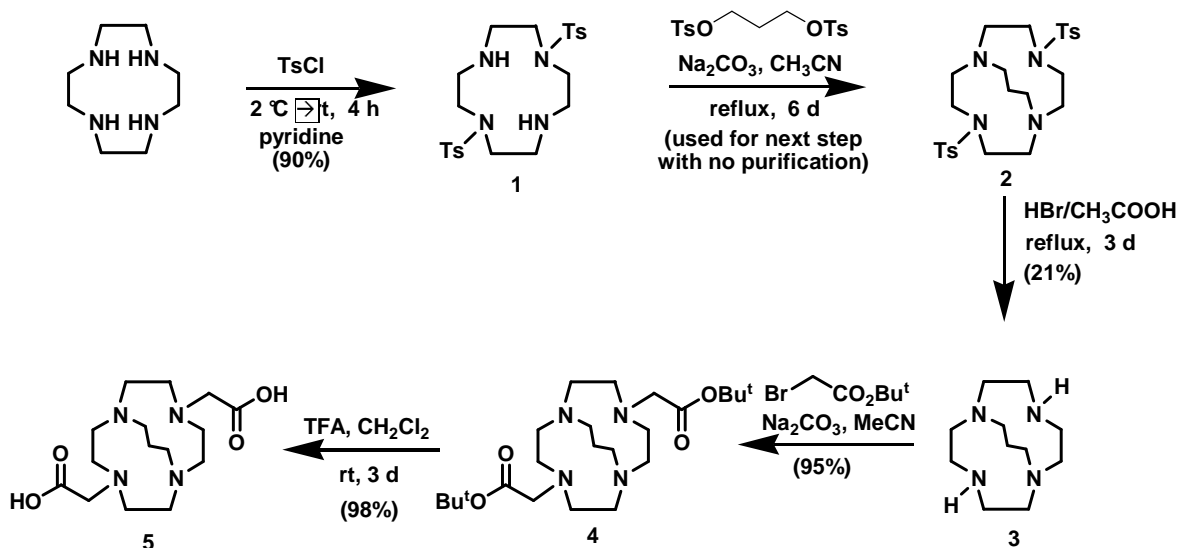
## Experimental Section

**Collaborators.** The experimental procedures for work related to Chapter 2 but performed by collaborators are included here. Synthesis of C3B-DO2A was performed by Dr. Riccardo Ferdani, CB-TR2A by Yijie Peng (University of New Hampshire, Durham, NH)<sup>75</sup> and NOTA by Elizabeth Garcia (UNH). Synthesis of all <sup>nat</sup>Cu(II)-chelator complexes and their characterization was carried out at UNH in the laboratory of Dr. Ed Wong. The Cu-CB-TR2A work has been reported in the doctoral dissertation of Antoinette Odeendaal (UNH).<sup>76</sup> X-ray crystallography was done in the laboratory of Dr. Arnold Rheingold at the University of California—San Diego (La Jolla, CA); Cu-CB-TR2A structure solved by James Golen. Dr. Thad Wadas was responsible for radiochemistry involving CB-TR2A.

**Materials and methods.** Unless otherwise specified all chemicals were purchased from Sigma-Aldrich Chemical Co. (St. Louis, MO) and used as received. Cyclen was purchased from Macrocyclics (Dallas, TX). Copper chloride (CuCl<sub>2</sub>) was purchased from Johnson Matthey (West Deptford, NJ). All solutions were prepared using water which had been distilled and then deionized (18 MΩ/cm<sup>2</sup>) by passing through a Milli-Q water filtration system (Millipore Corp., Bedford, MA).

Infrared spectra were obtained as KBr pellets on a Nicolet MX-1 FTIR spectrophotometer. Electronic spectra were recorded on a Carey 50 Bio UV/Vis spectrophotometer. NMR spectra were taken using a Varian 300 MHz instrument and referenced against internal trimethylsilane. ES-MS was accomplished using a Waters Micromass ZQ (Millford, MA). Elemental analyses were carried out by Galbraith Laboratories, Inc. (Knoxville, TN).

**Synthesis of C3B-DO2A.** CB3-DO2A (**5**) was synthesized according to the scheme shown in Scheme 1. Note that compound **3** was synthesized according to a procedure previously published by Springborg *et al.* in 1995.<sup>65</sup>



**Scheme 1.** Synthesis of CB3-DO2A.

Briefly, cyclen was treated with 2 equivalents of *p*-toluene-sulfonyl chloride (TsCl) in pyridine: the only product obtained was the 1,7-bis-tosylated derivative **1**. The 3-carbon cross bridge was then introduced by alkylation of the 2 secondary nitrogen atoms with 1 equivalent of 1,3-propanediol di-*p*-tosylate. Compound **2** was used in the following step with no further purification: the protecting tosyl groups were removed upon refluxing **2** in a HBr/CH<sub>3</sub>COOH mixture for 3 days. Recrystallization of the crude product yielded compound **3** that was alkylated with 2 equivalents of *tert*-butyl bromoacetate. The final product was obtained by removing the *tert*-butyl protecting groups in TFA/CH<sub>2</sub>Cl<sub>2</sub>.

**4,10-bis-(carbo-*tert*-butoxymethyl)-1,4,7,10-tetraazabicyclo[5.5.3]pentadecane (4).** Compound **3**\*3HBr (0.45 g, 1.0 mmol) was dissolved in acetonitrile (25 mL) and then Na<sub>2</sub>CO<sub>3</sub> (0.45g, 4.2 mmol) and *tert*-butyl

bromoacetate (0.34 mL, 2.3 mmol) were added and the reaction was heated to 60 °C for 3 days. After cooling, the solid was filtered off and the solution was evaporated under reduced pressure. The crude was dried at the high vacuum pump and then triturated with ethyl ether to give **4** in a 95% yield. <sup>1</sup>H-NMR (DMSO-d<sub>6</sub>, 300 MHz): δ 1.32 (s, 18H, C(CH<sub>3</sub>)<sub>3</sub>), 1.68 (m, 2H, NCH<sub>2</sub>CH<sub>2</sub>CH<sub>2</sub>N), 2.65-3.05 (m, 20H, NCH<sub>2</sub>CH<sub>2</sub>N and NCH<sub>2</sub>CH<sub>2</sub>CH<sub>2</sub>N), 3.38 (s, 4H, NCH<sub>2</sub>C(O)). <sup>13</sup>C NMR (DMSO-d<sub>6</sub>, 75 MHz): δ 21.4, 28.5, 50.2, 53.3, 54.1, 55.8, 81.0, 171.4. MS (ESI+): m/z 441.1 (MH<sup>+</sup>), 385.1 (MH<sup>+</sup>- 1tBu), 329.1 (MH<sup>+</sup>- 2tBu).

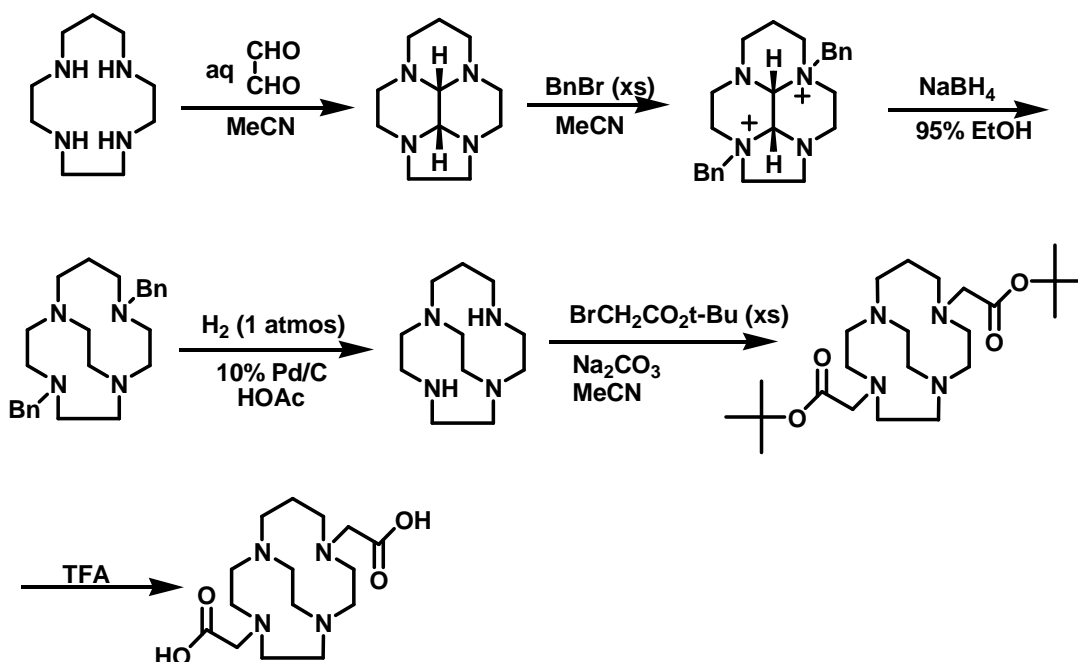
**4,10-bis-(carboxymethyl)-1,4,7,10-tetrazabicyclo[5.5.3]pentadecane (5).**

Compound **4** (0.47 g, 1.1 mmol) was dissolved in a 1:1 mixture of dichloromethane (15 mL) and trifluoroacetic acid (15 mL) and the reaction was stirred at room temperature under argon for 3 days. The solvent was then evaporated and the remaining oil was dissolved in ethanol and slowly precipitated with ethyl ether. The final compound, CB3-DO2A (**5**) was obtained, after drying at the high vacuum pump) as a slightly off-white solid in a 98% yield. <sup>1</sup>H-NMR (D<sub>2</sub>O, 300 MHz): δ 1.82 (m, 2H, NCH<sub>2</sub>CH<sub>2</sub>CH<sub>2</sub>N), 2.95-3.25 (m, 20H, NCH<sub>2</sub>CH<sub>2</sub>N and NCH<sub>2</sub>CH<sub>2</sub>CH<sub>2</sub>N), 3.61 (s, 4H, NCH<sub>2</sub>C(O)). <sup>13</sup>C NMR (D<sub>2</sub>O, 75 MHz): δ 18.2, 51.7, 53.8, 53.9, 60.2, 173.1. MS (ESI+): m/z 329.1 (MH<sup>+</sup>). Elem. analysis: calcd for C<sub>15</sub>H<sub>28</sub>N<sub>4</sub>O<sub>4</sub>\*1.4 NaCl: C 43.92, H 6.88, N 13.64; found: C 43.94, H 6.92, N 13.30.

**Synthesis of Cu-C3B-DO2A.** An amount of 100 mg (0.203 mmol) of the ligand (**5**) as a trifluoroacetate salt was combined with 75 mg (0.203 mmol) of Cu(ClO<sub>4</sub>)<sub>2</sub>•6H<sub>2</sub>O in 8 mL of 95% ethanol. The pH was adjusted to 8.5 with 0.1 N NaOH. The suspension was refluxed under nitrogen for 24 h to give a dark blue solution. After thorough removal of volatiles under reduced pressure, a dark-blue sticky solid was obtained. This was extracted with 4 mL methanol and centrifuged. The supernatant was then placed in vials

inside a glass container for diethylether diffusion. A total crop of 75 mg of dendritic dark-blue crystals formed. Elem. analysis: calcd for  $C_{15}CuH_{26}N_4O_4 \cdot 1.33NaClO_4 \cdot 1.33H_2O$ : C 31.24, H 5.01, N 9.71, Cl 8.18%. Found: C 31.05, H 5.21, N 9.45, Cl 8.06%. Electronic spectrum (aq.)  $\lambda_{max}$  614 nm ( $\epsilon = 84.6 M^{-1}cm^{-1}$ ). FT-IR (KBr)  $\nu_{COO}$  1687, 1616  $cm^{-1}$ . X-ray crystals were grown from a hexafluoro-*i*-propanol solution upon diethylether diffusion.

**Synthesis of CB-TR2A.** The 4,11-bis(carbo-*tert*-butoxymethyl)-1,4,8,11-tetraazabicyclo[6.5.2]pentadecane was prepared from homocyclen according to the procedure of Peng (Scheme 2).<sup>75, 180</sup>

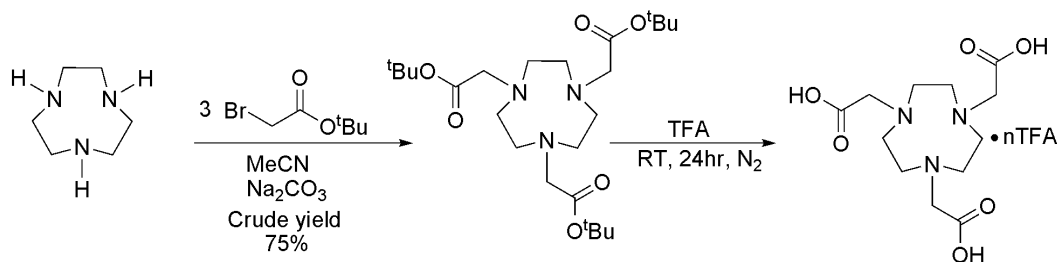


**Scheme 2.** Synthesis of CB-TR2A.<sup>75</sup>

**Synthesis of Cu-CB-TR2A.**<sup>76</sup> A solution of 4,11-bis(carbo-*tert*-butoxymethyl)-1,4,8,11-tetraazabicyclo[6.5.2]pentadecane (96.0 mg, 0.2179 mmol) in trifluoroacetic acid (3.4 mL, 0.046 mol) and  $CH_2Cl_2$  (3.4 mL) was stirred under  $N_2$  for 2 days. The reaction mixture was then concentrated under aspirator pressure and the residual

solvent was removed under vacuum to give 0.1635 g (0.2179 mol, 100%) of CB-TR2A as a brown oil containing 3.7 equivalents of TFA by mass. To the solution of CB-TR2A•3.7 TFA in 95% EtOH (15 mL) was added  $\text{Cu}(\text{ClO}_4)_2 \cdot 6\text{H}_2\text{O}$  (135.5 mg, 0.3657 mmol) and the pH of the reaction mixture was adjusted to 8 with 1 M NaOH. The reaction was then refluxed under  $\text{N}_2$  for approximately 23 hours. The reaction mixture was centrifuged and the supernatant collected and concentrated down under aspirator pressure. Residual solvent was removed under vacuum to give 263.7 mg of a blue solid. The solid was dissolved in 95% EtOH (15 mL) and the blue solution was placed in a diethylether diffusion chamber. A powdery blue solid was collected to give 55.3 mg (44%) of  $\text{Cu} \cdot \text{CB-TR2A} \cdot 2(\text{H}_2\text{O}) \cdot 1.2(\text{NaClO}_4)$ . Elem. analysis: calcd for  $\text{Cu}(\text{C}_{15}\text{H}_{26}\text{N}_4\text{O}_4) \cdot 2(\text{H}_2\text{O}) \cdot 1.2\text{NaClO}_4$ : C, 31.45; H, 5.28; N, 9.78; Cl, 7.43. Found C, 31.49; H, 5.14, N, 9.68, Cl, 7.10; IR (KBr) 3536, 3490, 3430, 3394, 3364, 1610, 1485, 1437, 1397, 1320, 1098, 631  $\text{cm}^{-1}$ . UV-Vis ( $\text{H}_2\text{O}$ )  $\lambda_{\text{max}}$  608 ( $\epsilon = 32.1 \text{ M}^{-1}\text{cm}^{-1}$ ); Cyclic voltammetry conducted in 0.1 sodium acetate: indicated a quasi-reversible reduction with  $E_p = -0.950 \text{ V}$  (Ag/AgCl). A 0.13 M solution of  $\text{Cu} \cdot \text{CB-TR2A} \cdot 2(\text{H}_2\text{O}) \cdot 1.2(\text{NaClO}_4)$  in 95% EtOH was placed in a diethylether diffusion chamber. Plate-like blue crystals were collected for X-ray structural analysis, which yielded an empirical formula of  $\text{Cu} \cdot \text{CB-TR2A} \cdot \text{H}_2\text{O} \cdot \text{NaClO}_4$ .

**Synthesis of NOTA.** Pendant arming of 1,4,7-Triazacyclononane (TACN) was achieved by using adapted procedure of functionalization of cross-bridged cyclams.<sup>181</sup> Then, the elimination of t-butyl groups was carried out with approximately 600 equivalents of trifluoroacetic acid (TFA) (Scheme 3).



**Scheme 3.** Synthesis of NOTA.

**1,4,7-Triazacyclononane-1,4,7-tri-tertbutylacetate.** Compound **3** (0.113 g, 0.875 mmol) was dissolved in MeCN (4.0 mL). Anhydrous  $\text{Na}_2\text{CO}_3$  (0.283 g, 2.67 mmol) and t-butyl bromoacetate (0.509 g, 2.61 mmol) were added sequentially to the solution. The mixture was heated and stirred under  $\text{N}_2$  at 50 °C for 24 h. Then, solvent was removed and the yellow residue was dissolved in cold solution of 20 % aq NaOH (30 mL). Keeping an ice bath temperature below 5 °C, solution extractions with cold  $\text{CHCl}_3$  (3× 50 mL), organic layers were collected and dried with  $\text{NaSO}_4$ . Chloroform was removed to give (0.308 g, 75%).  $^1\text{H}$  NMR (400 MHz,  $\text{CDCl}_3$ ; TMS):  $\delta_{\text{H}}$  3.33(6H, s), 2.87(12H, s), 1.45(27H, s).

**1,4,7-Triazacyclononane-1,4,7-tri-acetic acid.** Compound **8** (0.308 g, 0.653 mmol) was dissolved in TFA (29 mL) and reflux for 24 hours under  $\text{N}_2$ . The solution was concentrated to give brownish crude (0.446 g) which was then triturated with  $\text{Et}_2\text{O}$  (2× 50 mL). Evaporation of  $\text{Et}_2\text{O}$  produced yellow brownish solid (0.390 g). Final product was dissolved in warm MeOH (20 mL) and then cooling down to room temperature allowed the precipitation of white crystals.  $^1\text{H}$  NMR (400 MHz,  $\text{D}_2\text{O}$ ; MeCN):  $\delta_{\text{H}}$  3.35 (6H, s), 3.40 (12H, s);  $^{13}\text{C}\{^1\text{H}\}$  NMR (500 MHz,  $\text{D}_2\text{O}$ ; MeCH):  $\delta_{\text{C}}$  173.5 ( $\text{C}_{\text{Carbonyl}}$ ), 58.14 ( $\text{C}_{1(\text{Ethylene})}$ ), 50.96 ( $\text{C}_{2(\text{Ethylene})}$ ).

**Synthesis of Na[Cu-NOTA].** This compound was synthesized by a modified version of the method reported by Wieghardt *et al.* in 1982.<sup>72</sup> An amount of 0.16 mmol of NOTA (as the trifluoroacetate salt) and an equimolar amount of  $\text{CuCl}_2 \cdot 2\text{H}_2\text{O}$  (28 mg) was dissolved in 0.40 mL water. The solution pH was adjusted to neutral using 0.1N NaOH, followed by addition of 1 mL of ethanol. After cooling overnight at 0°C, light-blue crystals formed.

**Acid-decomplexation studies.** The acid inertness assay was carried out for each of the Cu(II)-ligand complexes, according to previously published methods.<sup>77</sup> Briefly, a cuvette containing a sample of the complex in aqueous HCl was monitored by its time-dependent electronic spectrum in a Cary 50 spectrophotometer. Cu-C3B-DO2A was found to be inert to 5 M HCl at both 60 °C and 90 °C for at least one day. In 12 M HCl at 90 °C, it decomplexed with a *pseudo*-first order half life of 7.2(7) days. Cu-CB-TR2A was determined to have a half-life of 10.8(4) h in 5 M HCl at 30 °C. Cu-NOTA was found to be inert to 1 M HCl at both 30 °C and 60 °C for at least one day but decomplexed within minutes in 5 M HCl at 30 °C.

**Electrochemical studies.** This assay was carried out for each of the Cu(II)-ligand complexes, according to previously published methods.<sup>77</sup> Briefly, a 3 mM solution of the complex in 0.1 N NaOAc was examined in a BAS 100B Electrochemical Analyzer using a glassy carbon working electrode, a platinum wire auxiliary electrode, and a Ag/AgCl reference electrode. CV sweeps were performed at 200 mV/s. For Cu-C3B-DO2A an irreversible reduction peak was observed at ~ -1.03 V with a large copper stripping peak upon reoxidation. A quasi-reversible reduction was seen at -0.95 V for Cu-CB-TR2A. For Cu-NOTA irreversible reduction peaks were observed at ~ -0.9 and -1.2 V along with a large copper stripping peak upon return scanning.

**Preparation of  $^{64}\text{Cu}$ -CB-TR2A.** Preparation of this compound was similar to radiolabeling conditions for CB-TE2A.<sup>62, 79</sup> To a 1.5 mL acid washed conical vial, was added CB-TR2A (100  $\mu\text{L}$  of a 17 mM solution in ETOH), 150  $\mu\text{L}$  of absolute EtOH and excess  $\text{Cs}_2\text{CO}_3$ . This solution was heated at 98  $^\circ\text{C}$  for 2-3 h. After cooling and centrifugation,  $^{64}\text{CuCl}_2$  was added (10 mCi, 2.5 mCi/ $\mu\text{L}$ ). The solution was sealed, vortexed, and incubated for 2 h with shaking at 98  $^\circ\text{C}$ . After cooling, radio-TLC was performed on regular silica plates with an eluent mixture of 1:1 MeOH:10%NH4OAc. Once 95+% was achieved, the supernatant was placed in a second 1.5 mL centrifuge tube and heated to reduce the volume of EtOH. When the volume was reduced by 75%, 200  $\mu\text{L}$  of NH4OAC (pH 7, 0.1 mM) was added to the remaining liquid and the resulting solution was mixed and heated again for 15 minutes to remove any remaining EtOH. The sample was again re-analyzed using the same TLC conditions.

## **APPENDIX II**

### Chapter 3 Supplemental Information

## Experimental Procedures

**Collaborators.** The experimental procedures for work related to Chapter 3 but performed by Yunpeng Ye are included here. Cells were cultured by Susan Adams and Alex Zheleznyak. All cell implants and animal dissections were performed by Chris Sherman. Small-animal imaging and post-imaging animal dissections were performed by the Radiological Sciences Small Animal Imaging Facility staff.

**Cyclo[Asp(OBu<sup>t</sup>)-DTyr(Bu<sup>t</sup>)-Lys-Arg(Pbf)-Gly].** The resin-bound protected peptide (H-Asp(OBu<sup>t</sup>)-DTyr(Bu<sup>t</sup>)-Lys-Arg(Pbf)-Gly-resin) was assembled manually from H-Gly-2-chlorotrityl resin (1.0 g, 0.54 mmol/g) via Fmoc chemistry as described above. The linear protected peptide H-Asp(OBu<sup>t</sup>)-DTyr(Bu<sup>t</sup>)-Lys-Arg(Pbf)-Gly-OH was cleaved by mixing the resin with 1% TFA in dichloromethane (DCM) for 2 min. The filtrate was added to a solution of pyridine (5 mL) / methanol (10 mL) and the resin was washed with methanol (1x) and dichloromethane (3x). This cleavage procedure was repeated for 5 times. The combined filtrate was concentrated by evaporation. The product was precipitated by adding water (100 mL) and collected by filtration. The linear peptide was dissolved in DMF (20 mL) and added drop-wise into a solution of benzotriazole-1-yl-oxy-tris-pyrrolidino-phosphonium hexafluorophosphate (PyBOP, 520 mg, 1.0 mmol), HOBT (135 mg, 1.0 mmol), and DIEA (260 mg, 2.0 mmol) in DMF (80 mL) / DCM (720 mL). The mixture was stirred overnight, concentrated, and washed with water to give the crude product cyclo[Asp(OBu<sup>t</sup>)-DTyr(Bu<sup>t</sup>)-Lys(Dde)-Arg(Pbf)-Gly] (ES-MS: [MH]<sup>+</sup> 1148.3). The solid was dissolved in methanol (50 mL), followed by adding hydrazine (1 mL). The mixture was stirred for 15 min, concentrated, washed with water, and dried. The product, cyclo[Asp(OBu<sup>t</sup>)-DTyr(Bu<sup>t</sup>)-Lys-Arg(Pbf)-Gly], was further purified by flash column chromatography to afford the desired compound (320 mg, 60% yield) ES-MS: [MH]<sup>+</sup> 984.5.

**Cyclo[DTyr-Lys(DOTA)-Arg-Gly-Asp].** A mixture of tri-tert-butyl  $N',N'',N''',N''''$ -dodecyltetraacetic acid (DOTA-(3OBu<sup>t</sup>)-COOH) (114.6 mg, 0.2 mmol), the protecting cyclic RGD obtained above (98.5 mg, 0.1 mmol), DIC (50.4 mg, 0.4 mmol), and HOBT (27.0 mg, 0.2 mmol) was stirred in anhydrous DMF (5 mL) for 8 h and concentrated under high vacuum. ES-MS confirmed the formation of DOTA-RGD peptide conjugation ( $[MH]^+/[MH_2]^{2+}$ : 1538.7 / 770.4). The residue was dissolved in 4 mL of TFA/water (95 %) and kept at room temperature for about 3h and the solution was concentrated. This step was repeated for another time. Half of the crude product was purified by semi-preparative HPLC. The desired fractions identified by ES-MS were combined and lyophilized to afford the title compound (31 mg, ~40% yield). ES-MS:  $[MH_2]^{2+}$  503.7.

**DOTA-Lys-cyclo(Cys-Arg-Gly-Asp-Cys)-NH<sub>2</sub>.** The resin-bound protected peptide Fmoc-Lys(Boc)-Cys(Acm)-Arg(Pbf)-Gly-Asp(OBut)-Cys(Acm)-NH-Rink amide resin was assembled manually from Fmoc-Rink amide resin (0.2 g, ~0.20 mmol/g) as described above. Thallium trifluoroacetate (2 equiv) in DMF (5 mL) was added and the mixture was swirled for 1.5 h. The resin was washed with methanol (2x) and DMF (3x). The resin was swirled with piperidine in DMF (20 %) and washed with methanol (2x) and DMF (5x). A mixture of DOTA(3OBu<sup>t</sup>)-COOH (3 equiv), HOBT (3 equiv), and DIC (9 equiv) in DMF was added into the resin and swirled overnight. The mixture was filtrated and washed with DMF (2x) and methanol (3x). The resin obtained was mixed with TFA/water (95:5, 3 mL) for 2 and filtered. This step was repeated for another 3 times. The filtrate was combined and concentrated to give the crude product. Similarly, HPLC purification followed by both ES-MS and analytical HPLC identifications gave the title compound (13 mg, ~20% yield). ES-MS:  $[MH_2]^{2+}$  532.6.

## **APPENDIX III**

### Chapter 4 Supplemental Information

## Experimental Procedures

**Collaborators.** All nanoparticles were synthesized by Zicheng Li from polymer precursors synthesized by Jinqi Xu, Andreas Nyström, Guorong Sun, and Zicheng Li in the laboratory of Dr. Karen L. Wooley. Yongjian Liu, Aviv Hagooly and Tetsuya Mori assisted with FPLC analysis. Mike G. Veith assisted with TEM imaging using the facilities of the Department of Otolaryngology at Washington University in St. Louis.

**General Materials and Methods.** Nitrogen (99.99%) was used for polymerization. All chemicals were purchased from Sigma-Aldrich and used without further purification unless otherwise noted. Prior to use, styrene (St; 99%) and *t*-butyl acrylate (*t*-BA; 98%), purchased from Aldrich, were distilled over calcium hydride. *N,N,N',N',N''*-pentamethyldiethylenetriamine (PMDETA; 99%), ethyl-2-bromopropionate (99%), copper(I) bromide (99.999%; Aldrich), trifluoroacetic acid (TFA; 95%), 2,2'-(ethylenedioxy)-bis(ethylamine) (97%), 1-(3'-dimethylaminopropyl)-3-ethylcarbo-diimide methiodide (EDCI; 98%), palladium on carbon (10 wt% loading), *N*-hydroxysuccinimide (NHS; 98%), *N*-Hydroxysulfosuccinimide sodium salt (sulfo-NHS; 98.5), *N,N'*-Dicyclohexylcarbodiimide (DCC; 99%), Succinic anhydride (99%), were used as received. Supor 25 mm 0.1  $\mu$ m Spectra/Por Membrane tubes (molecular weight cutoff (MWCO) 3,500 or 6-8000 Da), purchased from Spectrum Medical Industries Inc., were used for dialysis. Nanopure water (18 M $\Omega$ -cm) was acquired by means of a Milli-Q water filtration system (Millipore Corp.; Bedford, MA). KCRGDC was custom synthesized by Tianma Pharma Co., Suzhou, China, and used as received. 5-FAM-KCRGDC was custom synthesized by Chengdu Kaijie Biopharmaceuticals Co. Ltd., Chengdu, China, and was used as received. Poly(ethylene glycol) (PEG) and derivatives were purchased from Rapp Polymere GmbH, Germany. Superfine Sephadex<sup>®</sup> G75 resin (bead

diameter: 20-50  $\mu\text{m}$ ; Fractionation range: 1000-50000 Da (Dextrans)) was purchased from GE Healthcare and was used to purify aqueous nanoparticle samples.

$^1\text{H}$  NMR spectra were recorded on a Varian 300 MHz spectrometer interfaced to a UNIX computer using Mercury software. Chemical shifts are referred to the solvent proton resonance. Infrared spectra were acquired on a Perkin-Elmer Spectrum BX FT-IR instrument using KBr pellets.

Absolute molecular weight and molecular weight distribution were determined by Gel Permeation Chromatography (GPC). GPC was performed on a Waters 1515 HPLC system (Waters Chromatography Inc., Medford, MA), equipped with a Waters 2414 differential refractometer, a PD2020 dual-angle ( $15^\circ$  and  $90^\circ$ ) light scattering detector (Precision Detector, Inc.), and a three-column series PL gel 5  $\mu\text{m}$  Mixed columns (Polymer Laboratories Inc.). The system was equilibrated at  $35^\circ\text{C}$  in anhydrous THF, which served as the polymer solvent and eluent (flow rate set to 1.00 mL/min then determined gravimetrically). All instrumental calibrations were conducted using a series of nearly monodispersed polystyrene standards. Data were collected upon an injection of a 200  $\mu\text{L}$  of polymer solution in THF (ca. 5.0 mg/mL), and then analyzed using Discovery 32 software (Version, Precision Detectors Inc). Inter-detector delay volume and the light scattering detector calibration constant were determined by calibration using a nearly monodispersed polystyrene standard (Pressure Chemical Co.,  $M_p = 90$  kDa,  $M_w/M_n < 1.04$ ). The differential refractometer was calibrated with standard polystyrene reference material (SRM 706 NIST), of known specific refractive index increment  $dn/dc$  (0.184 mL/g). The  $dn/dc$  values of the analyzed polymers were then determined from the differential refractometer response.

Differential scanning calorimetry (DSC) measurements were performed with a DSC822<sup>e</sup> instrument (Mettler-Toledo, Inc.) in a temperature range of  $-100$  to  $180^\circ\text{C}$  with

a ramp rate of 10 °C/min under nitrogen. Data were acquired and analyzed using STAR<sup>e</sup> software (Mettler-Toledo, Inc.). The glass transition temperature,  $T_g$ , was determined at the midpoint of the inflection tangent upon the third heating scan.

Samples for transmission electron microscopy (TEM) measurements were diluted with 1 wt% of phosphotungstic acid (PTA) stain solution (v/v, 1:1). Carbon grids were exposed to oxygen plasma treatment to increase the surface hydrophilicity. Micrographs were collected at 100,000 magnifications. The number average particle diameters ( $D_{av}$ ) and standard deviations were generated from the analysis of a minimum of 150 particles from at least three different micrographs.

The average heights for the nanoparticles were determined by performing tapping-mode AFM under ambient conditions in air. The AFM instrumentation consisted of a Nanoscope III BioScope system (Digital Instruments, Veeco Metrology Group; Santa Barbara, CA) and standard silicon tips (type, OTESPA-70; L, 160  $\mu\text{m}$ ; normal spring constant, 50 N/m; resonance frequency, 246-282 kHz). Samples for AFM imaging analysis were prepared through spin-coating *c.a.* 2.0  $\mu\text{L}$  of the nanoparticle solution (typical concentration: 0.2 mg/mL) onto freshly cleaved mica plates (Ruby clear mica, New York Mica Co.) and allowed to dry freely in air. The number-average particle heights ( $H_{av}$ ) values and standard deviations were generated from the sectional analysis of more than 150 particles from several different regions.

Hydrodynamic diameters ( $D_h$ ) and size distributions for the SCKs in aqueous solutions were determined by dynamic light scattering (DLS). The DLS instrument consisted of a Brookhaven Instruments Limited (Worcestershire, U.K.) system, including a model BI-200SM goniometer, a model BI-9000AT digital correlator, a model EMI-9865 photomultiplier, and a model 95-2 Ar ion laser (Lexel Corp., Farmindale, NY) operated at 514.5 nm. Measurements were made at 20 °C. Prior to analysis, solutions were filtered

through a 0.22  $\mu\text{m}$  Millex GV PVDF membrane filter (Millipore Corp., Medford, MA) and then centrifuged in a model 5414 microfuge (Brinkman Instruments, Inc., Westbury, NY) for 10 min to remove dust particles. Scattered light was collected at a fixed angle of 90°. The digital correlator was operated with 522 ratio spaced channels, and initial delay of 5  $\mu\text{s}$ , a final delay of 100 ms, and a duration of 10 min. A photomultiplier aperture of 400  $\mu\text{m}$  was used, and the incident laser intensity was adjusted to obtain a photon counting of between 200 and 300 kcps. Only measurements in which the measured and calculated baselines of the intensity autocorrelation function agreed to within 0.1% were used to calculate particle sizes. The calculations of the particle size distributions and distribution averages were performed with the ISDA software package (Brookhaven Instruments Company), which employed single-exponential fitting, cumulants analysis, non-negatively constrained least-squares (NNLS) and CONTIN particle size distribution analysis routines. All determinations were made in triplicate. The results were analyzed by UNICORN 3.10.11.

Fast protein liquid chromatography (FPLC) was performed on an AKTA (GE) system, including a P-920 pump, Columns of Superose 12 10/300 GL, and a UV detector with 254 nm wavelength. The eluent was 20 mM HEPES with 150 mM NaCl and flow rate was 0.8 mL/min. UV- *vis* spectra were acquired on a Varian Cary 1E UV- *vis* system (Varian, Inc., Palo Alto, CA) using polystyrene cuvettes.

**General Procedures for Diblock Copolymer Preparation.** Poly(*t*-butyl acrylate) (P*t*BA) homopolymer was first prepared by atom transfer radical polymerization (ATRP). P*t*BA was further used as a macroinitiator to grow the second block, polystyrene (PS), through the same polymerization method, to afford poly(*t*-butyl acrylate)-*b*-polystyrene (P*t*BA-*b*-PS). The resulting P*t*BA-*b*-PS was then treated with trifluoroacetic acid in methylene chloride to remove the protecting *t*-butyloxy groups, as

monitored by  $^1\text{H}$  NMR. After the removal of the solvent, the residue was dissolved in tetrahydrofuran and purified by dialysis against water. PAA-*b*-PS diblock copolymer was obtained after lyophilization.

PtBA<sub>61</sub>-*b*-PS<sub>34</sub>: 0.83 g (67% yield).  $^{\text{GPC}}M_n = 11,600$  Da from GPC,  $M_w/M_n = 1.08$ .  $T_g$  (PtBA) = 53 °C,  $T_g$  (PS) = 82 °C. IR: 3433, 3100-2870, 1943, 1870, 1802, 1734, 1601, 1493, 1452, 1392, 1368, 1259, 1164, 846, 757, 704, 542  $\text{cm}^{-1}$ .  $^1\text{H}$  NMR ( $\text{CDCl}_3$ , 300 MHz, ppm):  $\delta$  7.25-6.27 (m, 5Ar-**H**), 2.37-2.02 (br, **CH** of the polymer backbone), 1.99-1.08 (br, **CH<sub>2</sub>** of the polymer backbone and C(**CH<sub>3</sub>**)<sub>3</sub>).  $^{13}\text{C}$  NMR ( $\text{CDCl}_3$ , 75 MHz, ppm):  $\delta$  174.0, 125.8-129.7, 108.1, 80.3, 40.4-41.5, 35.5-36.8, 27.9.

PAA<sub>61</sub>-*b*-PS<sub>34</sub>: 0.44 g (88% yield).  $M_n = 8,200$  Da.  $T_g$  (PAA) = 126 °C,  $T_g$  (PS) = 105 °C. IR: 3405, 3047-2914, 1942, 1875, 1722, 1601, 1492, 1450, 1245, 762, 701  $\text{cm}^{-1}$ .  $^1\text{H}$  NMR ( $\text{THF-d}_8$ , 300 MHz, ppm):  $\delta$  11.6-10.0 (br, COO**H**), 7.25-6.30 (m, 5Ar-**H**), 2.60-2.20 (br, **CH** of the polymer backbone), 2.15-1.10 (br, **CH<sub>2</sub>** of the polymer backbone).  $^{13}\text{C}$  NMR ( $\text{THF-d}_8$ , 75 MHz, ppm):  $\delta$  177.5, 124.8-129.5, 41.5-42.6, 35.5-37.2.

PtBA<sub>60</sub>-*b*-PS<sub>60</sub>: 4.1 g (80% yield);  $^{\text{GPC}}M_n = 14,000$  Da,  $M_w/M_n = 1.15$ .  $T_g$  (PtBA) = 49 °C,  $T_g$  (PS) = 93 °C. IR: 3430, 3100-2890, 1940, 1860, 1800, 1734, 1600, 1490, 1452, 1390, 1370, 1260, 1164, 845, 756, 700, 540  $\text{cm}^{-1}$ .  $^1\text{H}$  NMR ( $\text{CDCl}_3$ , 300 MHz, ppm):  $\delta$  7.23-6.24 (m, 5Ar-**H**), 2.35-2.05 (br, **CH** of the polymer backbone), 1.98-1.07 (br, **CH<sub>2</sub>** of the polymer backbone and C(**CH<sub>3</sub>**)<sub>3</sub>).  $^{13}\text{C}$  NMR ( $\text{CDCl}_3$ , 75 MHz, ppm):  $\delta$  173.6, 126.0-130.2, 108.0, 80.1, 40.6-41.7, 35.5-36.6, 28.0.

PAA<sub>60</sub>-*b*-PS<sub>60</sub>: 1.1 g (90% yield).  $M_n = 10,600$  Da.  $T_g$  (PAA) = 126 °C,  $T_g$  (PS) = 104 °C. IR: 3407, 3040-2915, 1940, 1873, 1722, 1600, 1492, 1453, 1242, 760, 700  $\text{cm}^{-1}$ .  $^1\text{H}$  NMR ( $\text{THF-d}_8$ , 300 MHz, ppm):  $\delta$  12.6-10.4 (br, COO**H**), 7.20-6.35 (m, 5Ar-**H**), 2.58-2.18 (br, **CH** of the polymer backbone), 2.20-1.10 (br, **CH<sub>2</sub>** of the polymer

backbone).  $^{13}\text{C}$  NMR (THF- $d_8$ , 75 MHz, ppm):  $\delta$  177.0, 125.3-130.5, 42.0-42.9, 35.7-37.0.

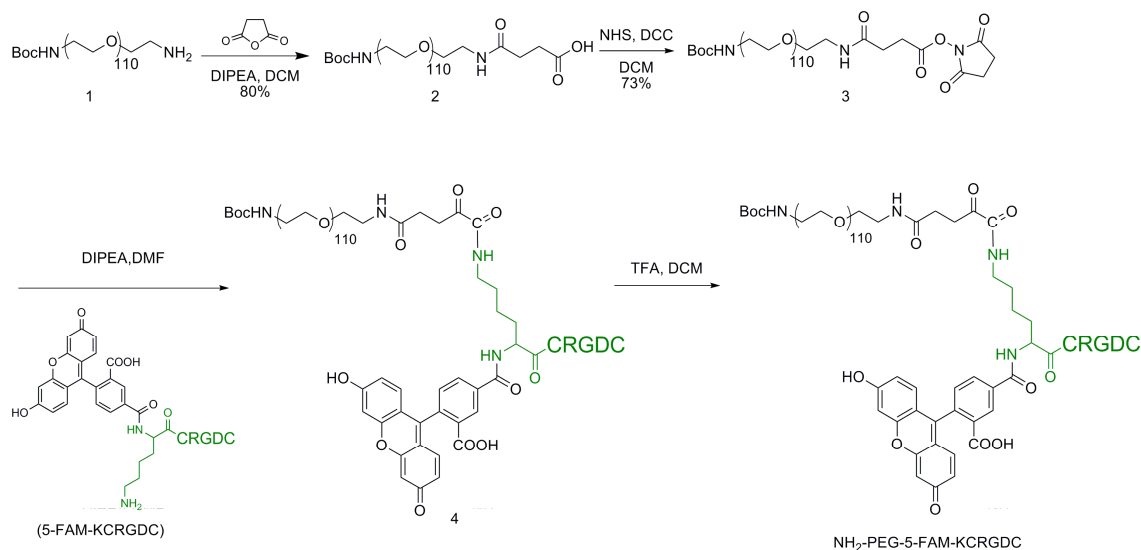
**Preparation of  $\text{NH}_2$ -PEG5000-5-FAM-KCRGDC.** Three steps were involved to prepare  $\text{NH}_2$ -PEG<sub>5000</sub>-5-FAM-KCRGDC, as shown in Scheme 1. BocNH-PEG5000- $\text{NH}_2$  (compound 1, 300 mg, 0.0600 mmol), was dissolved in 13 mL of dichloromethane and stirred at room temperature for *c.a.* 0.5 h. Succinic anhydride (24.6 mg, 0.246 mmol) and DIPEA (21.0  $\mu\text{L}$ , 15.5 mg, 0.120 mmol) were added. The reaction mixture was allowed to stir at room temperature for 24 h. The reaction mixture was then concentrated and precipitated into cold ether (40 mL) twice. The precipitate was dried under vacuum to afford 238 mg of white solid as compound 2, BocNH-PEG5000-NHCOCH<sub>2</sub>CH<sub>2</sub>COOH (yield 80%).

Compound 2 (201 mg, 0.0402 mmol) was dissolved in 10 mL of dichloromethane and stirred at room temperature for *c.a.* 0.5 h. *N*-hydroxysuccinimide (23.6 mg, 0.205 mmol) and *N,N*-Dicyclohexylcarbodiimide (43.7 mg, 0.211 mmol) were added. The solution was allowed to stir at room temperature for 24 h before being concentrated and precipitated into cold ether (40 mL) twice. The precipitate was then dried under vacuum to afford a white solid, compound 3 (151 mg, yield: 73%).

5-FAM-KCRGDC (40.6 mg, 0.0390 mmol) was dissolved in 5 mL of dry DMF, to this solution were also added Compound 3 (104 mg, 0.0201 mmol) and DIPEA (10  $\mu\text{L}$ , 7.3 mg, 0.057 mmol). The reaction mixture was allowed to stir at room temperature for 24 h. The reaction mixture was precipitated into cold ether (45 mL) once. The solid was then dissolved in DCM and precipitated into cold ether (45 mL) twice to afford a yellow solid as compound 4 (100 mg, yield: 80%).

Compound 4 (100 mg, 15.9  $\mu\text{mol}$ ) was dissolved in 6 mL of DCM. TFA (4.8 mL, 7.1 g, 62.3 mmol) was added. The reaction mixture was allowed to stir at room

temperature for 12 h, concentrated and precipitated into cold ether. The precipitate was dried under vacuum to afford NH<sub>2</sub>-PEG5000-5-FAM-KCRGDC as a yellow solid (80 mg, yield: 79%).



**Scheme 1.** Synthesis of NH<sub>2</sub>-PEG5000-5-FAM-KCRGDC.

*General procedures for preparation of mPEG2000-g-PAA-b-PS Block Copolymers.*

Grafting mPEG2000 onto PAA-*b*-PS involved the following: to a solution of PAA<sub>60</sub>-*b*-PS<sub>60</sub> block copolymer in anhydrous (DMF), 1-[3'-(dimethylamino)propyl]-3-ethylcarbodiimide methiodide (EDCI), and 1-hydroxybenzotriazole (HOBt) were added, and the reaction mixture was allowed to stir for 1 h at room temperature. Then DIPEA and a solution of monoamine terminated mPEG2000 in anhydrous DMF were added and the reaction mixture was further stirred for 30 h at room temperature. The relative ratios of PAA<sub>60</sub>-*b*-PS<sub>60</sub> block copolymer/EDCI/HOBt/mPEG-NH<sub>2</sub> were varied to alter the grafting densities, whereby to achieve grafting densities of 2.5 and 5.5 mPEGs per macromolecule, the stoichiometry were 1.0:3.5:3.5:3.5, and 1.0:7.0:7.0:7.0, respectively. The final grafted

block copolymers were isolated by transferring the reaction mixtures to presoaked dialysis tubing (MWCO 6000-8000 Da) and dialyzing against nanopure water for 4 d to remove the organic solvent and the small molecular byproduct. The aqueous solutions were then lyophilized to afford the products as white solid.  $^1\text{H}$  NMR ( $\text{CD}_2\text{Cl}_2$ , 500 MHz, ppm):  $\delta$  1.20-2.40 (br,  $-\text{CH}_2-$  and  $-\text{CH}-$  of the polymer backbone), 3.34 (s, mPEG terminal  $-\text{OCH}_3$  protons), 3.42-3.80 (br, mPEG backbone  $-\text{OCH}_2\text{CH}_2\text{O}-$  protons), 6.16-7.11 (br, aromatic protons).

*mPEG2000*<sub>2.5</sub>-*g-PAA*<sub>57.5</sub>-*b-PS*<sub>60</sub>. *PAA*<sub>60</sub>-*b-PS*<sub>60</sub> (120.0 mg, 11.3  $\mu\text{mol}$ ), EDCI (11.8 mg, 39.6  $\mu\text{mol}$ ), HOBt (5.4 mg, 40.0  $\mu\text{mol}$ ), and monoamine terminated mPEG2000 (79.2 mg, 39.6  $\mu\text{mol}$ ) in anhydrous DMF (15.0 mL). Yield: 75%.

*mPEG2000*<sub>5.5</sub>-*g-PAA*<sub>54.5</sub>-*b-PS*<sub>60</sub>. *PAA*<sub>60</sub>-*b-PS*<sub>60</sub> (110.0 mg, 10.4  $\mu\text{mol}$ ), EDCI (21.6 mg, 72.8  $\mu\text{mol}$ ), HOBt (9.9 mg, 73.3  $\mu\text{mol}$ ), and monoamine terminated mPEG2000 (145.6 mg, 72.8  $\mu\text{mol}$ ) in anhydrous DMF (15.0 mL). Yield: 75%.

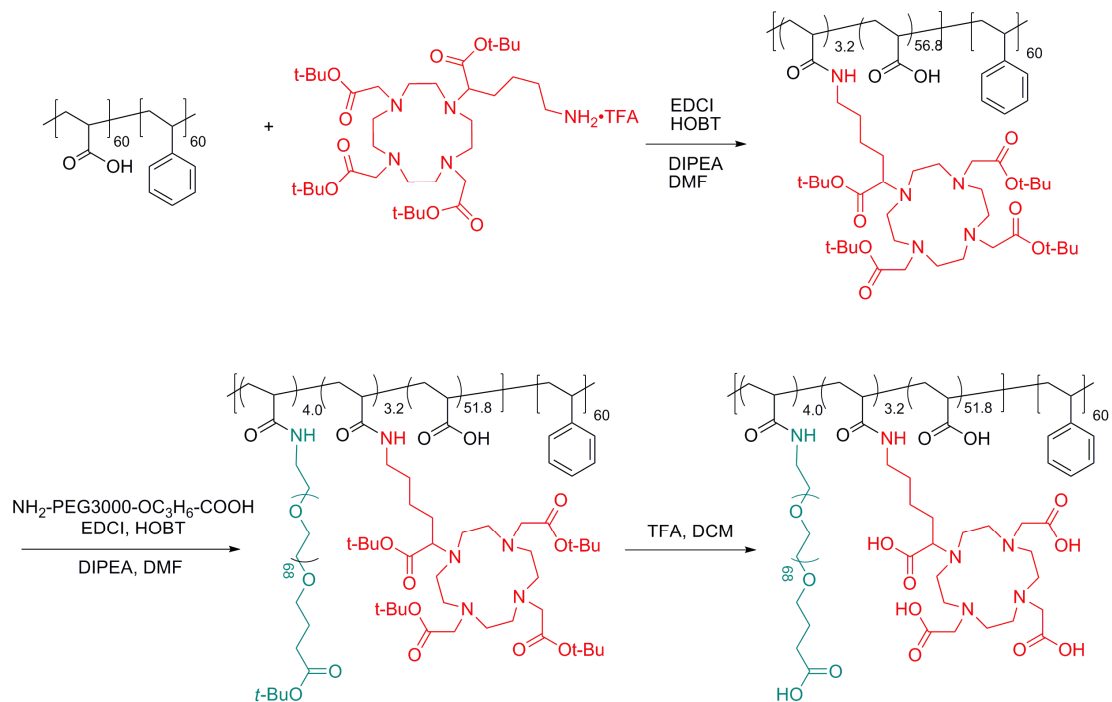
*Preparation of mPEG2000-g-DOTA-lysine-g-PAA-b-PS Block Copolymers.* The DOTA-lysine (a lysine derivative for 1,4,7,10-tetraazocyclododecane-*N,N,N',N''*-tetraacetic acid, DOTA) was grafted onto mPEG2000-*g-PAA-b-PS* by following a procedure similar to that used to graft mPEG2000 (described above). To a solution of mPEG2000-*g-PAA-b-PS* block copolymer (10.3  $\mu\text{mol}$ ) in anhydrous DMF (10.0 mL), EDCI (11.6 mg, 39.1  $\mu\text{mol}$ ) and HOBt (5.3 mg, 39.3  $\mu\text{mol}$ ) were added and the reaction mixture was allowed to stir for 1 h at room temperature. Then a solution of DOTA-lysine (trifluoroacetic acid (TFA) salt, 23.1 mg, 39.2  $\mu\text{mol}$ ) and *N,N*-diisopropylethylamine (DIPEA, 25.4 mg, 0.196 mmol) in anhydrous DMF (2.0 mL) was added and the reaction mixture was further stirred for 30 h at room temperature. The final grafted block copolymers were isolated by transferring the reaction mixtures to presoaked dialysis

tubing (MWCO 6000-8000 Da) and dialyzing against nanopure water for 5 d to remove the organic solvent and the small molecular byproduct. The aqueous solutions were then lyophilized to afford the products as white solid. Yield: 65%.  $^1\text{H}$  NMR (500 MHz,  $\text{CD}_2\text{Cl}_2$  with 2 drops of  $\text{CF}_3\text{CO}_2\text{D}$ , ppm):  $\delta$  1.20-2.40 (br,  $-\text{CH}_2-$  and  $-\text{CH}-$  of the polymer backbone, overlapped with DOTA-lysine protons), 2.40-2.70 (br, DOTA-lysine macrocyclic protons), 3.34 (s, mPEG terminal  $-\text{OCH}_3$  protons), 3.42-3.80 (br, mPEG backbone  $-\text{OCH}_2\text{CH}_2\text{O}-$  protons), 6.16-7.11 (br, aromatic protons).

**Preparation of PEG-5-FAM-KCRGDC-g-mPEG2000-g-DOTA-lysine-g-PAA-b-PS Block Copolymers.** The PEG-5-FAM-KCRGDC was grafted onto mPEG2000-g-DOTA-lysine-g-PAA-b-PS by following the procedures similar to used to graft mPEG2000 or DOTA-lysine (described above). The relative ratio of mPEG2000-g-DOTA-lysine-g-PAA-b-PS block copolymer/EDCI/HOBt/mPEG-NH<sub>2</sub> was 1:20:20:4. To a solution of mPEG2000-g-PAA-b-PS block copolymer (0.80  $\mu\text{mol}$ ) in anhydrous DMF (7.5 mL), EDCI (4.96 mg, 16.7  $\mu\text{mol}$ ) and HOBt (2.27 mg, 16.8  $\mu\text{mol}$ ) were added and the reaction mixture was allowed to stir for 1 h at room temperature. Then a solution of PEG-5-FAM-KCRGDC (trifluoroacetic acid (TFA) salt, 21.1 mg, 3.36  $\mu\text{mol}$ ) and *N,N*-diisopropylethylamine (DIPEA, 100 mg, 0.85 mmol) in anhydrous DMF (2.0 mL) was added and the reaction mixture was further stirred for 24 h at room temperature. The polymer concentration of the reaction mixture was then adjusted to 1.00 mg/mL by adding appropriate amount of DMF for future use. Micelles were directly prepared from the reaction mixture and impurities were later removed by dialysis against nanopure water in MWCO 50000 Da dialysis tubings.

**Preparation of HOOC-PEG3000<sub>4,0</sub>-g-DOTA-lysine<sub>3,2</sub>-g-PAA<sub>60</sub>-b-PS<sub>60</sub> Block Copolymer.** Similar procedures were followed as mentioned above, except for the attaching sequence, as shown in the scheme below: DOTA-lysine (tetra-*t*-butyl ester)

was first grafted onto the block copolymer PAA<sub>60</sub>-*b*-PS<sub>60</sub>, solid polymer product, was obtained by methods described above and the number of DOTA-lysine per polymer chain was determined by <sup>1</sup>H NMR (coupling efficiency 90%). To the DOTA-lysine(tetra-*t*-butyl ester)-*g*-PAA<sub>60</sub>-*b*-PS<sub>60</sub> was then attached NH<sub>2</sub>-PEG3000-COOH, by pre-activating the -COOH on the polymer chains, to afford HOOC-PEG3000<sub>4.0</sub>-*g*-DOTA-lysine<sub>3.2</sub>-*g*-PAA<sub>60</sub>-*b*-PS<sub>60</sub> (coupling efficiency 80%).



**Scheme 2.** Preparation of HOOC-PEG3000<sub>4.0</sub>-*g*-DOTA-lysine<sub>3.2</sub>-*g*-PAA<sub>60</sub>-*b*-PS<sub>60</sub>.

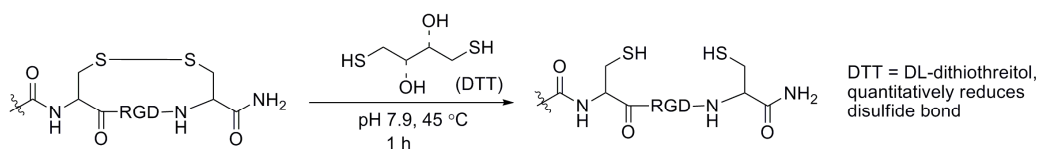
**General procedures for micelle assembly and SCK formation.** To a solution of the amphiphilic block copolymer (PAA-*b*-PS, mPEG2000-*g*-DOTA-lysine-*g*-PAA-*b*-PS or PEG-5-FAM-KCRGDC-*g*-mPEG2000-*g*-DOTA-lysine-*g*-PAA-*b*-PS) in THF or DMF, (*ca.* 1.0 mg/mL in polymer concentration), an equal volume of nanopure water was added dropwise *via* a syringe pump over 6 h. The reaction mixture was further stirred for *c.a.* 16 h at room temperature before transferring to a presoaked dialysis tubing (MWCO. 6,000-8,000 Da for PAA-*b*-PS; MWCO 50,000 Da for PEG-5-FAM-KCRGDC-*g*-mPEG2000-*g*-DOTA-lysine-*g*-PAA-*b*-PS), and dialyzed against nanopure water for 4 days, to afford a micelle solution with the final polymer concentration of 0.20-0.30 mg/mL.

**General procedures for the PAA Block Crosslinking to Form SCKs.** To a solution of micelle in nanopure water, was added dropwise a solution of 2,2'-(ethylenedioxy)bis(ethylamine) (*c.a.* 1.0 mg/mL) in nanopure water over 10 min. The reaction mixture was stirred for *c.a.* 2 h at room temperature. To this solution, was added dropwise *via* syringe pump over 30 min, a solution of 1-[3'-(dimethylamino)propyl]-3-ethylcarbodiimide methiodide in nanopure water. The reaction mixture was further stirred 20 h at room temperature before transferring to a presoaked dialysis tubing, and dialyzed against nanopure water for 4 days, to remove all of the impurities and afford the SCK solution. The nominal crosslinking extent (20% and 50%) were based on the stoichiometry of the crosslinker (2,2'-(ethylenedioxy)bis(ethylamine)) to that of the carboxylic acids on the PAA domain. The general stoichiometry employed to achieve 20% nominal crosslinking was 9:2.2:1 for carboxylic acid units : EDCI : crosslinker, and to achieve 50% nominal crosslinking, the stoichiometry was 3.6:2.2:1.

**General procedures for post-attaching KCRGDC/5-FAM-KCRGDC/PEG-5-FAM-KCRGDC onto micelle/SCK nanoparticles.** All micelle/SCK samples were pre-cooled

to 4 °C. Sulfo-NHS aqueous solution was then added, and the containers were shaken for *c.a.* 30 min. Freshly prepared EDCI aqueous solution was added and the reaction containers were shaken for 1.5 h in a 4 °C refrigerator. Here, the pH values of the solutions were adjusted to around 7.4 with pH 9.2 0.2 M phosphate buffer. KCRGDC/5-FAM-KCRGDC/PEG-5-FAM-KCRGDC solutions were then added. The pH of the reaction solutions were finally adjusted to around 7.4 (optimal pH for the coupling reaction to occur) and the reaction mixtures were kept shaking at 4 °C for 24 h. All reaction mixtures were then dialyzed against pH 7.4 5 mM PBS (after treatment of Chelax 100 resin) for 5 d.

**Reduction of disulfide bond on KCRGDC-NP to thiol.** Excess DTT (DL-dithiothreitol) was incubated with micelle/SCK nanoparticles labeled with the cyclic KCRGDC at 45 °C for 1h (Scheme 3). The reaction mixture was then dialyzed against nanopure water in pre-soaked MWCO 6-8000 Da dialysis tubing to remove unreacted DTT and for later quantification of thiol groups by Ellman's assay.



**Scheme 3.** Cleavage of disulfide bond on KCRGDC.

**Ellman's assay.** Cysteine (26.0 mg) is dissolved into 10.00 mL of reaction buffer (0.10 M sodium phosphate buffer, pH 8.0) to make the stock solution. Ellman's reagent (4.00 mg DTNB) was dissolved into 1.00 mL of reaction buffer. A series of cysteine standard solutions with different concentrations are then prepared from the stock

solution, with cysteine concentrations being 15.0 mM, 1.50 mM, 1.25 mM, 1.00 mM, 1.00 mM, 0.75 mM, 0.50 mM, 0.25 mM and 0.05 mM. The Ellman's reagent solution was then mixed with the cysteine standard solutions and the samples to be measured using the following volumetric quantities: 983  $\mu$ L buffer and 18  $\mu$ L Ellman's reagent for blank; 938  $\mu$ L buffer, 18  $\mu$ L of Ellman's reagent, and 45  $\mu$ L sample. After 15 minutes the absorbance of each sample was measured at 412 nm.

**Purifying aqueous nanoparticle samples using Sephadex<sup>®</sup> G75 gravity SEC columns.** Sephadex<sup>®</sup> G75 resin (superfine) (10 g) was pre-soaked in boiling water for *c.a.* 30 min to form a gel. After cooling to room temperature, the resin was packed into a glass column (30 cm  $\times$  2 cm) equipped with a stopcock. About 200 mL of the eluent (150 mM PBS, pH  $\sim$  7.4) was passed through the column prior to any sample loading. For each run, *c.a.* 4 mL of nanoparticle samples (with polymer concentration around 0.20-0.30 mg/mL) was loaded. The separation process was monitored by UV spectrometry. Columns were reused after being flushed with excess eluent. The desired fractions were collected and concentrated and solvent-exchanged into 5 mM PBS by using Centricon (MWCO 10000 Da, Millipore, MA) tubes.

#### APPENDIX IV

Sprague, JE; Peng, Y; Fiamengo, AL; Wooden, KS; Southwick, EA; Weisman, GR; Wong, EH; Golen, JA; Rheingold, AL; Anderson, CJ. "Synthesis, characterization and in vivo studies of  $^{64}\text{Cu}(\text{II})$ -labeled cross-bridged tetraazamacrocyclic-amide complexes as models of peptide conjugate imaging agents." *J. Med. Chem.* **2007**; 50 (10): 2527-2535.

## Synthesis, Characterization and In Vivo Studies of Cu(II)-64-Labeled Cross-Bridged Tetraazamacrocycle-amide Complexes as Models of Peptide Conjugate Imaging Agents

Jennifer E. Sprague,<sup>†</sup> Yijie Peng,<sup>‡</sup> Ashley L. Fiamengo,<sup>†</sup> Katrina S. Woodin,<sup>‡</sup> Evan A. Southwick,<sup>‡</sup> Gary R. Weisman,<sup>‡</sup> Edward H. Wong,<sup>‡</sup> James A. Golen,<sup>§</sup> Arnold L. Rheingold,<sup>||</sup> and Carolyn J. Anderson<sup>\*†</sup>

Mallinckrodt Institute of Radiology, Washington University School of Medicine, St. Louis, Missouri, Department of Chemistry, University of New Hampshire, Durham, New Hampshire, Department of Chemistry, University of Massachusetts, Dartmouth, Massachusetts, Department of Chemistry and Biochemistry, University of California, La Jolla, San Diego, California

Received February 21, 2007

Copper-64, a positron emitter suitable for positron emission tomography (PET), demonstrates improved in vivo clearance when chelated by the cross-bridged tetraazamacrocycle CB-TE2A compared to TETA. Good in vivo clearance was also observed for <sup>64</sup>Cu-CB-TE2A conjugated to a peptide, which converts one coordinating carboxylate pendant arm to an amide. To better understand the in vivo stability of peptide-conjugated CB-TE2A, cross-bridged monoamides were synthesized. Crystal structures of <sup>64</sup>Cu(II)-CB-TEAMA and <sup>64</sup>Cu(II)-CB-PhTEAMA revealed hexadentate, distorted octahedral coordination geometry. In vivo biodistribution showed clearance of all <sup>64</sup>Cu-radiolabeled cross-bridged monoamides from liver and bone marrow such that uptake at 24 h was <10% of uptake at 30 min. In contrast, >60% of 30 min uptake from <sup>64</sup>Cu-TETA was retained in these tissues at 24 h. Clearance of <sup>64</sup>Cu-cross-bridged monoamides from nontarget organs suggests good in vivo stability, thus supporting the use of CB-TE2A as a bifunctional chelator without modifications to the macrocycle backbone.

### Introduction

Copper-64 is a promising radionuclide for use in positron emission tomography (PET<sup>9</sup>) imaging as well as radiotherapy due to its half-life ( $t_{1/2} = 12.7$  h) and decay characteristics ( $\beta^+$  17.4%,  $E_{\beta^+max} = 656$  keV;  $\beta^-$  39%,  $E_{\beta^-max} = 573$  keV); it can be produced in high yield and high specific activity on a biomedical cyclotron.<sup>1–9</sup> Increasing use of <sup>64</sup>Cu and other copper radioisotopes in nuclear medicine has generated a need for strongly complexing chelators. Kinetic stability of Cu(II) complexes has been shown to be more predictive of in vivo stability than thermodynamic stability.<sup>10,11</sup> Macrocyclic chelators of Cu(II) such as TETA (1,4,8,11-tetraazacyclotetradecane-1,4,8,11-tetraacetic acid; Figure 1) demonstrate higher kinetic and thus in vivo stability relative to acyclic chelators such as EDTA (ethylene diamine tetraacetic acid).<sup>10–13</sup> However, biodistribution and metabolism studies in rats using TETA have demonstrated significant transchelation of <sup>64</sup>Cu to superoxide dismutase in liver and albumin in blood resulting in high background radioactivity.<sup>14,15</sup>

Several “cross-bridged” tetraamine ligands, where an ethylene (–CH<sub>2</sub>CH<sub>2</sub>–) bridge connects two nonadjacent nitrogens, have

been reported by Weisman and Wong.<sup>16–18</sup> A series of cross-bridged Cu(II) complexes have been prepared and characterized. Cross-bridged chelates were shown to have all four nitrogen lone pairs convergent on a cleft to coordinate Cu(II). Octahedral coordination geometry with the Cu(II) fully enveloped by the chelator was achieved by the addition of two carboxylate pendant arms to give Cu(II)-CB-TE2A (4,11-bis(carboxymethyl)-1,4,8,11-tetraazabicyclo[6.6.2]hexadecane; Figure 1).<sup>18</sup> Recently, we have established the exceptional kinetic inertness of this complex to aqueous acid decomplexation.<sup>19</sup> Busch and colleagues have reported additional cross-bridged Cu(II) complexes that also demonstrate high kinetic stability.<sup>20–22</sup> Studies in our laboratory have confirmed improved in vivo stability of <sup>64</sup>Cu-CB-TE2A compared to that of <sup>64</sup>Cu-TETA.<sup>14,18,23</sup>

Targeting radioactive metals to tumors or other tissues of interest can be accomplished by conjugation of a bifunctional chelator to a peptide or monoclonal antibody.<sup>24–26</sup> Conjugation of a macrocyclic chelator such as TETA converts one carboxylate arm of the chelator to an amide by reaction with either the N-terminus of a peptide or a lysine side chain. However, conjugation of CB-TE2A to a peptide results in a single free carboxylate to coordinate Cu(II); it was initially hypothesized that this would decrease its in vivo stability. To overcome this potential problem, Lewis et al. synthesized a CB-TE2A derivative in which a biotin molecule is covalently attached to the macrocycle backbone, leaving both carboxylate arms intact.<sup>27</sup> However, no kinetic or in vivo stability studies of Cu(II)-CB-TE2A-Bz-biotin were reported. We reported the in vivo biodistribution of <sup>64</sup>Cu-CB-TE2A conjugated to the cyclic somatostatin analogue Y3-TATE (Tyr3-octreotate, fCYwKTCT-OH).<sup>28</sup> Favorable clearance properties of <sup>64</sup>Cu-CB-TE2A-Y3-TATE in liver, blood, and bone marrow were all suggestive of improved in vivo stability of the <sup>64</sup>Cu-CB-TE2A-Y3-TATE relative to <sup>64</sup>Cu-TETA-Y3-TATE.<sup>28</sup>

Small molecule metabolites of <sup>64</sup>Cu- and <sup>67</sup>Cu-radiolabeled peptides or antibodies have not been well characterized due to the poor in vivo stability of Cu(II) chelates. As stated above,

\* To whom correspondence should be addressed. Mallinckrodt Institute of Radiology, Washington University School of Medicine, 510 S. Kingshighway Boulevard, Campus Box 8225, St. Louis, MO 63110. Phone: 314-362-8427. Fax: 314-362-9440. E-mail: andersoncj@wustl.edu.

<sup>†</sup> Washington University School of Medicine.

<sup>‡</sup> University of New Hampshire.

<sup>§</sup> University of Massachusetts.

<sup>||</sup> University of California.

Abbreviations: CB-TE2A, 4,11-bis(carboxymethyl)-1,4,8,11-tetraazabicyclo[6.6.2]hexadecane; CB-TEAMA, 4-acetamido-11-carboxymethyl-1,4,8,11-tetraazabicyclo[6.6.2]hexadecane; CB-MeTEAMA, 11-methylcarbamoylmethyl-1,4,8,11-tetraazabicyclo[6.6.2]hexadec-4-yl)-acetic acid; CB-PhTEAMA, 11-phenylcarbamoylmethyl-1,4,8,11-tetraazabicyclo[6.6.2]hexadec-4-yl)-acetic acid; CH<sub>3</sub>CN, acetonitrile; *n*-Phe<sup>1</sup>-octreotide, fCYwKTCT-OH; EDTA, ethylene diamine tetraacetic acid; ID, injected dose; log*P*, partition coefficients; PBS, phosphate buffered saline; PET, positron emission tomography; PI, post-injection; RT, retention time; TFA, trifluoroacetic acid; TETA, 1,4,8,11-tetraazacyclotetradecane-1,4,8,11-tetraacetic acid; Y3-TATE, Tyr3-octreotate, fCYwKTCT-OH.

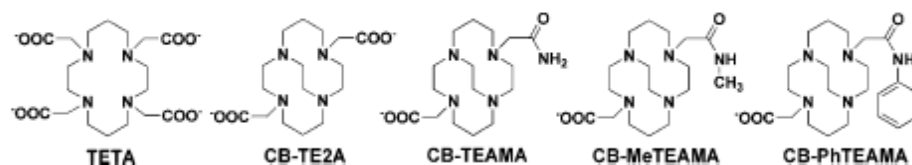
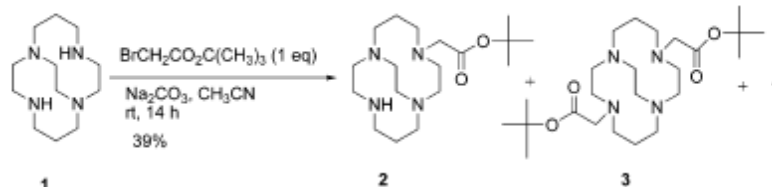


**Figure 1.** Structures of TETA, CB-TE2A, CB-TEAMA, CB-MeTEAMA, and CB-PhTEAMA.

**Scheme 1.** Synthesis of **2**



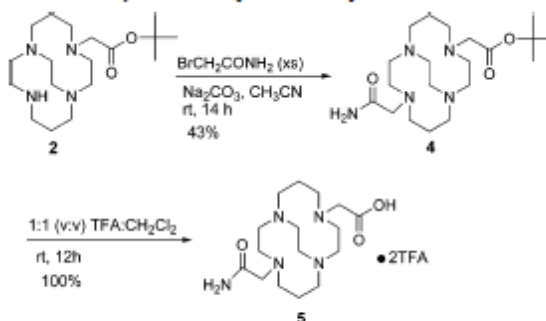
the primary radiometabolites of  $^{64}\text{Cu}$ -TETA and  $^{67}\text{Cu}$ -TETA-conjugated peptides and antibodies in liver and blood result from the dissociation of  $^{64,67}\text{Cu}$  from a peptide/antibody conjugate and subsequent binding to proteins.<sup>15,29</sup> This results in retention of the transchelated  $^{64}\text{Cu}$  in nontarget tissues such as liver.<sup>15</sup> However, the final metabolite of  $^{111}\text{In}$ -DTPA-D-Phe<sup>1</sup>-octeotide ( $\text{rCFwKTCT-OH}$ ), where  $^{111}\text{In}$ -DTPA forms a relatively stable chelate, has been identified as  $^{111}\text{In}$ -DTPA-D-Phe.<sup>30</sup> Similarly, the kidney metabolite of  $^{64}\text{Cu}$ -chelate antibody conjugates was reported to be  $^{64}\text{Cu}$ -chelate-lysine.<sup>31</sup> It is likely that the peptide portion of  $^{64}\text{Cu}$ -CB-TE2A-Y3-TATE will be degraded to yield  $^{64}\text{Cu}$ -CB-TE2A-D-Phe. To better understand the high in vivo stability of  $^{64}\text{Cu}$ -CB-TE2A-Y3-TATE, three simplified monoamide, monocarboxylate analogues of the CB-TE2A chelator were synthesized (Figure 1). In this study, the in vivo stabilities of  $^{64}\text{Cu}$ -CB-TEAMA,  $^{64}\text{Cu}$ -CB-MeTEAMA, and  $^{64}\text{Cu}$ -CB-PhTEAMA were compared to those of  $^{64}\text{Cu}$ -TETA and  $^{64}\text{Cu}$ -CB-TE2A.

**Results**

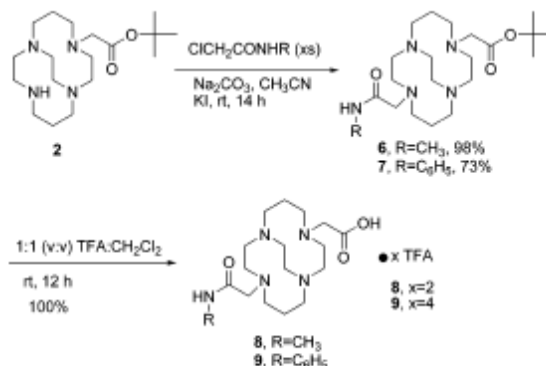
**Synthesis of Ligands CB-TEAMA, CB-MeTEAMA, and CB-PhTEAMA.** The title ligands were synthesized via synthetic intermediate **2**, which was prepared by statistical alkylation of cross-bridged cyclam **1**, as shown in Scheme 1. Thus, **1** was alkylated with 1 equiv of *t*-butyl bromoacetate in  $\text{CH}_3\text{CN}$  at room temperature to give a mixture consisting of **2** (45%–50% by NMR), dialkylated byproduct **3** (the precursor to CB-TE2A), and unreacted **1**. The desired mono-*t*-butyl ester **2** was isolated by flash chromatography in 39% yield. Treatment of **2** with an excess of 2-bromoacetamide in  $\text{CH}_3\text{CN}$  at room temperature gave cross-bridged cyclam **4** in 43% yield after workup (Scheme 2). Compound **4** was subsequently quantitatively deprotected in 1:1 (v/v)  $\text{CF}_3\text{CO}_2\text{H}(\text{TFA})/\text{CH}_2\text{Cl}_2$  to salt **5**·2TFA. Similarly, intermediates **6** and **7** were prepared by alkylation of **2** with 2-chloro-*N*-methylacetamide and 2-chloro-*N*-phenylacetamide in yields of 98 and 73%, respectively (Scheme 3). TFA deprotection of **6** and **7** gave **8** ([CB-MeTEAMA]H) and **9** ([CB-PhTEAMA]H) in quantitative yields as TFA salts.

**Copper(II) Complexes of CB-TEAMA and CB-PhTEAMA.** The copper(II) complexes of CB-TEAMA and CB-PhTEAMA were prepared and fully characterized as described in the Experimental Section. Their X-ray crystal structures are shown in Figure 2. In both complexes, Cu(II) is fully enveloped by four nitrogens from the ligand cleft and two oxygens, one from each pendant arm, resulting in a distorted octahedral geometry. Amide coordination is through the amide pendant arm's carbonyl oxygen. For Cu(II)-CB-TEAMA, the Jahn–

**Scheme 2.** Synthesis of H[CB-TEAMA]·2TFA



**Scheme 3.** Synthesis of H[CB-MeTEAMA]·2TFA and H[CB-PhTEAMA]·4TFA



Teller distortion is along the N(4)–Cu–O(1) axis, with elongated Cu–N and Cu–O bond lengths of 2.196(6) and 2.401(5) Å, respectively. Strong equatorial coordination is provided by N(2), N(3), O(2), and N(5). The *trans*-N(2)–Cu–N(5) and *cis*-N(3)–Cu–N(4) angles of 174.3(2) and 87.1(2) $^\circ$  are consistent with a reasonable ligand cleft–Cu(II) fit.

For Cu(II)-CB-PhTEAMA, the Jahn–Teller elongation is along the N(1)–Cu–O(2) axis, with long Cu–N and Cu–O bonds of 2.205(3) and 2.367(3) Å, respectively. The equatorial coordination plane consists of N(2), O(3), N(3), and N(4). The strongly bonded carboxylate is indicated by the short Cu–O(3) distance of 1.950(3) Å. The intra-cleft *trans*-N(2)–Cu–N(3) angle of 176.5(1) $^\circ$  and *cis*-N(1)–Cu–N(4) angle of 88.5(1) $^\circ$  also confirm the good fit of Cu(II) within this cross-bridged cyclam ligand cavity.

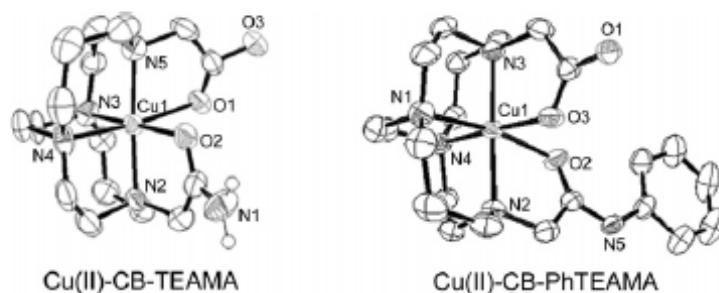


Figure 2. ORTEP drawing of the Cu-CB-TEAMA and Cu-CB-PhTEAMA complexes. Hydrogens were omitted for clarity except on the primary amide.

Table 1. Partition Coefficient for Each <sup>64</sup>Cu Complex

chelate	LogP
<sup>64</sup> Cu-TETA	-3.58 ± 0.18
<sup>64</sup> Cu-CB-TE2A	-2.07 ± 0.24
<sup>64</sup> Cu-CB-TEAMA	-2.35 ± 0.06
<sup>64</sup> Cu-CB-MeTEAMA	-2.08 ± 0.08
<sup>64</sup> Cu-CB-PhTEAMA	-1.35 ± 0.05

Solid-state IR as well as solution electronic spectral data are fully consistent with these structures. The asymmetric carboxylate stretch for Cu-CB-PhTEAMA is found at 1628 cm<sup>-1</sup>, while the amide carbonyl stretch appears at 1677 cm<sup>-1</sup>. Corresponding bands are observed at 1627 and 1677 cm<sup>-1</sup> for Cu-CB-TEAMA. Both complexes exhibit a single broad *d-d* band at 648 nm ( $\epsilon = 55 \text{ M}^{-1}\text{cm}^{-1}$ ) and 625 nm ( $\epsilon = 35 \text{ M}^{-1}\text{cm}^{-1}$ ), respectively, in their aqueous solution electronic spectra.

**Radiochemistry.** Consistent with previously reported results for radiolabeling CB-TE2A with <sup>64</sup>Cu(II),<sup>14</sup> radiolabeling CB-TEAMA, CB-MeTEAMA, and CB-PhTEAMA in aqueous solution (0.1 M NH<sub>4</sub>OAc, pH 8.0) resulted in the formation of several kinetically favored impurities, as evidenced by the presence of multiple peaks on radio-HPLC. However, using basic conditions in ethanol with C<sub>52</sub>CO<sub>3</sub>, as described by Boswell et al. for radiolabeling CB-TE2A,<sup>14</sup> single peaks were observed on radio-HPLC for <sup>64</sup>Cu-CB-TEAMA (RT = 17.1 min, 2.2–3.2 mCi/ $\mu$ mol), <sup>64</sup>Cu-CB-MeTEAMA (RT = 18.4 min, 53–73 mCi/ $\mu$ mol), and <sup>64</sup>Cu-CB-PhTEAMA (RT = 26.9 min; 51–74 mCi/ $\mu$ mol).

**Partition Coefficients.** The partition coefficients (octanol/PBS) were determined for each complex to evaluate relative lipophilicity (Table 1). The order of lipophilicity was as follows: <sup>64</sup>Cu-CB-PhTEAMA > <sup>64</sup>Cu-CB-MeTEAMA ~ <sup>64</sup>Cu-CB-TE2A > <sup>64</sup>Cu-CB-TEAMA > <sup>64</sup>Cu-TETA.

**Biodistribution Studies.** To examine the in vivo properties of <sup>64</sup>Cu-CB-TEAMA, <sup>64</sup>Cu-CB-MeTEAMA, and <sup>64</sup>Cu-CB-PhTEAMA, biodistribution studies were carried out in male Lewis rats. For comparison, biodistribution was also performed for <sup>64</sup>Cu-TETA and <sup>64</sup>Cu-CB-TE2A. Figure 3 shows the radioactivity uptake to 24 h postinjection (PI) in several organs. All five complexes cleared rapidly from blood between 30 min and 2 h PI (<15% of 30 min activity remaining at 2 h). However, between 2 and 24 h, blood-associated radioactivity decreased significantly more for each monoamide cross-bridged complex than for <sup>64</sup>Cu-TETA or <sup>64</sup>Cu-CB-TE2A (% 2 h uptake remaining at 24 h = 100 × [% ID/<sub>24h</sub> / % ID/<sub>2h</sub>]; <sup>64</sup>Cu-TETA, 80.5 ± 12.5%; <sup>64</sup>Cu-CB-TE2A, 61.9 ± 7.5%; <sup>64</sup>Cu-CB-TEAMA, 23.4 ± 5.4%; <sup>64</sup>Cu-CB-MeTEAMA, 17.2 ± 6.3%; <sup>64</sup>Cu-CB-PhTEAMA, 19.3 ± 3.5%;  $p < 0.01$ ). Kidney uptake decreased slowly between 30 min and 24 h for all five complexes such that 24 h kidney uptake was reduced to <10%

of the 30 min uptake value. This resulted in an excretion of the complexes in the urine (% ID in urine, 0–24 h PI, <sup>64</sup>Cu-TETA, 71.6 ± 5.3% ID; <sup>64</sup>Cu-CB-TE2A, 74.5 ± 6.1% ID; <sup>64</sup>Cu-CB-TEAMA, 66.9 ± 8.3% ID; <sup>64</sup>Cu-CB-MeTEAMA, 63.0 ± 12.2% ID; <sup>64</sup>Cu-CB-PhTEAMA, 44.6 ± 2.1% ID).

In the liver, <sup>64</sup>Cu-CB-MeTEAMA, initially (30 min PI) had 9.3-fold higher uptake than <sup>64</sup>Cu-TETA ( $p < 0.01$ ; Figure 3). Although not statistically significant, liver uptake was 7.4- and 5.8-fold higher for <sup>64</sup>Cu-CB-TEAMA and <sup>64</sup>Cu-CB-PhTEAMA, respectively, compared to <sup>64</sup>Cu-TETA. It was expected that liver uptake would reflect lipophilicity as determined by partition coefficients. Consistent with this hypothesis, all cross-bridged monoamides showed significantly higher 30 min liver uptake than the more hydrophilic <sup>64</sup>Cu-TETA. However, 30 min liver uptake of <sup>64</sup>Cu-CB-TE2A was even lower than for <sup>64</sup>Cu-TETA, despite a similar partition coefficient to <sup>64</sup>Cu-CB-MeTEAMA. This may be explained by the complex in vivo bioavailability, which reflects ongoing excretion as <sup>64</sup>Cu-CB-TE2A clears rapidly via the kidneys.

By 24 h, the liver uptake fell to 23.4 ± 5.0% for <sup>64</sup>Cu-CB-TE2A, 6.7 ± 0.9% for <sup>64</sup>Cu-CB-TEAMA, 7.8 ± 5.5% for <sup>64</sup>Cu-CB-MeTEAMA, and 1.3 ± 0.3% for <sup>64</sup>Cu-CB-PhTEAMA compared to 30 min uptake (Figure 3). In contrast, <sup>64</sup>Cu-TETA was retained in the liver to a much greater extent than cross-bridged complexes, resulting in a decrease in liver uptake to 66.2 ± 11.6% of 30 min uptake at 24 h ( $p < 0.001$ ). Similarly, bone marrow uptake fell significantly between 30 min and 24 h for <sup>64</sup>Cu-CB-TE2A, <sup>64</sup>Cu-CB-TEAMA, and <sup>64</sup>Cu-CB-PhTEAMA. Although marrow uptake for <sup>64</sup>Cu-CB-MeTEAMA does appear to decrease between 30 min and 24 h, this decrease is not statistically significant ( $p = 0.06$ ) due to high variability in 30 min uptake. In contrast, no significant change in marrow uptake was observed for <sup>64</sup>Cu-TETA over this period.

To further evaluate uptake and excretion of these <sup>64</sup>Cu complexes by the liver, radioactivity uptake in the gut was examined (Figure 4). Gastrointestinal tract biodistribution was performed without the removal of fecal contents. The GI tract was divided into four sections: stomach, proximal intestine, middle intestine, and distal intestine. The distal intestine included the cecum to the rectum; the remaining intestine (stomach to cecum) was divided in half to give the proximal and middle regions. For all cross-bridged complexes, minimal stomach uptake, high 30 min proximal intestine uptake that decreased with time, and increasing uptake in more distal parts of the intestine with time were suggestive of excretion by the liver into bile, with subsequent clearance as feces. At all time-points, intestinal uptake was highest for <sup>64</sup>Cu-CB-PhTEAMA, followed by <sup>64</sup>Cu-MeTEAMA and <sup>64</sup>Cu-CB-TEAMA. This pattern of uptake was not observed for <sup>64</sup>Cu-TETA. Radioactivity in the feces was <0.1% ID at 30 min, 1 h, and 2 h PI for all complexes.

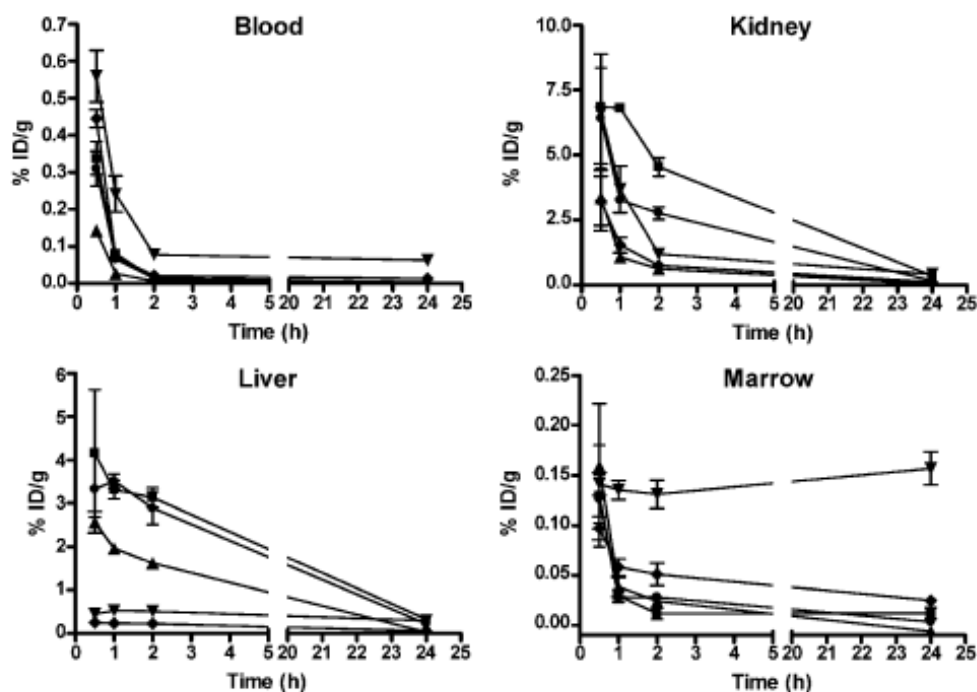


**Figure 3.** Selected organ biodistribution of  $^{64}\text{Cu}$ -TETA ( $\nabla$ ),  $^{64}\text{Cu}$ -CB-TE2A ( $\blacklozenge$ ),  $^{64}\text{Cu}$ -CB-TEAMA ( $\bullet$ ),  $^{64}\text{Cu}$ -CB-MeTEAMA ( $\blacksquare$ ),  $^{64}\text{Cu}$ -CB-PhTEAMA ( $\blacktriangle$ ) in 33–40 day old, male Lewis rats (30 min to 24 h,  $n = 4$ ;  $^{64}\text{Cu}$ -TETA 1 h marrow,  $n = 3$ , excluded by Q-test;  $^{64}\text{Cu}$ -CB-TE2A 2 h,  $n = 3$ , animal died prior to sacrifice). Note differences in scale.

By 24 h PI, amounts of  $^{64}\text{Cu}$  excreted as feces were as follows:  $^{64}\text{Cu}$ -TETA =  $3.1 \pm 0.7\%$  ID,  $^{64}\text{Cu}$ -CB-TE2A =  $3.5 \pm 0.9\%$  ID,  $^{64}\text{Cu}$ -CB-TEAMA =  $6.8 \pm 1.8\%$  ID,  $^{64}\text{Cu}$ -CB-MeTEAMA =  $11.2 \pm 1.2\%$  ID, and  $^{64}\text{Cu}$ -CB-PhTEAMA =  $39.3 \pm 3.7\%$  ID.

## Discussion

The group at Washington University has previously shown that the  $^{64}\text{Cu}$ -labeled cross-bridged chelator CB-TE2A has favorable biodistribution properties and good in vivo stability relative to  $^{64}\text{Cu}$ -TETA.<sup>14,23</sup> Subsequently, CB-TE2A was conjugated to the peptide Y3-TATE to evaluate its use as a bifunctional chelator.<sup>28</sup> Despite conversion of one carboxylate arm of CB-TE2A to a secondary amide upon peptide conjugation, it was found that  $^{64}\text{Cu}$ -CB-TE2A-Y3-TATE had superior in vivo clearance properties, suggestive of improved in vivo stability relative to  $^{64}\text{Cu}$ -TETA-Y3-TATE.<sup>28</sup> To investigate the in vivo biodistribution characteristics of the conjugated cross-bridged chelate independent of a peptide, three monoamide derivatives of CB-TE2A have been synthesized as models of a CB-TE2A-peptide conjugate.

High kinetic stability of a Cu(II) chelate has been shown to be predictive of in vivo stability.<sup>10,11</sup> It has been shown that the half-life of Cu(II)-CB-TE2A in 5 M HCl (90 °C) is approximately 2000-fold longer than for Cu(II)-TETA, indicating much higher kinetic stability.<sup>32</sup> Preliminary kinetic stability studies of Cu(II)-CB-TEAMA revealed that the harsh conditions caused hydrolysis of the amide bond, resulting in conversion back to Cu(II)-CB-TE2A. It was, therefore, not possible to determine directly the kinetic stability of these Cu(II) cross-bridged monoamide complexes.

Spectral data as well as X-ray crystal structures of both Cu(II)-CB-TEAMA and Cu(II)-CB-PhTEAMA confirmed their distorted octahedral coordination geometry as previously ob-

served for Cu(II)-CB-TE2A.<sup>18</sup> For both monoamides, the amide pendant arm was coordinated via the carbonyl oxygen. Although coordination geometries may change in solution, this increases the likelihood that a peptide-conjugated Cu(II)-CB-TE2A could also retain this distorted octahedral coordination geometry, thus accounting for the favorable in vivo clearance properties seen with  $^{64}\text{Cu}$ -CB-TE2A-Y3-TATE.<sup>28</sup>

Somewhat surprisingly, the logP values of  $^{64}\text{Cu}$ -CB-MeTEAMA ( $-2.08 \pm 0.08$ ) and  $^{64}\text{Cu}$ -CB-TE2A ( $-2.07 \pm 0.24$ ) were shown to be very similar. It was expected that the additional methyl group on  $^{64}\text{Cu}$ -CB-MeTEAMA would result in a more lipophilic complex than  $^{64}\text{Cu}$ -CB-TE2A. However, the difference in charge ( $^{64}\text{Cu}$ -CB-MeTEAMA = +1,  $^{64}\text{Cu}$ -CB-TE2A = 0) likely balances out the additional methyl group, resulting in similar partition coefficients. This is in contrast to a previously reported logP value for  $^{64}\text{Cu}$ -CB-TE2A ( $-2.42 \pm 0.04$ ).<sup>23</sup> However, the radiolabeling method for  $^{64}\text{Cu}$ -CB-TE2A has since been optimized, and the ligand used in the original study may have contained trace radio-impurities such as  $^{64}\text{Cu}$ -TE3A (predicted charge =  $-1$ ),<sup>33</sup> which would be less lipophilic than  $^{64}\text{Cu}$ -CB-TE2A. The order of lipophilicity for the remaining complexes was consistent with predictions.

Copper- $^{64}\text{Cu}$ -CB-TEAMA,  $^{64}\text{Cu}$ -CB-MeTEAMA, and  $^{64}\text{Cu}$ -CB-PhTEAMA cleared over time from blood, liver, and marrow despite initial high uptake in some organs. Previous studies have associated retention of radioactivity in nontarget tissues with poor in vivo stability and transchelation of  $^{64}\text{Cu}$  to proteins.<sup>3,15</sup> High liver uptake at 30 min, with subsequent excretion into feces, was not unexpected for  $^{64}\text{Cu}$ -CB-PhTEAMA given the structure and lipophilicity. Liver uptake and fecal clearance were similar for  $^{64}\text{Cu}$ -CB-MeTEAMA and  $^{64}\text{Cu}$ -CB-TEAMA, with fecal clearance being significantly less for both compared to  $^{64}\text{Cu}$ -CB-PhTEAMA ( $p < 0.001$ ). To account for the relatively high initial liver uptake with resultant low fecal excretion, we

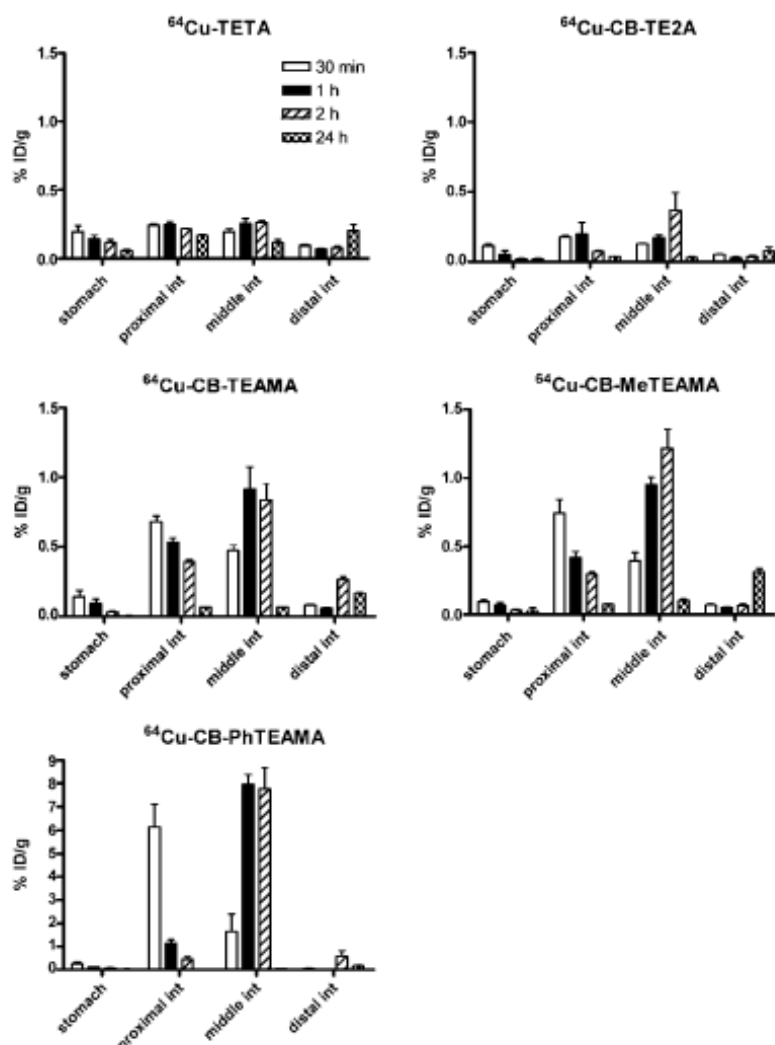


**Figure 4.** Gut biodistribution of <sup>64</sup>Cu-TETA, <sup>64</sup>Cu-CB-TE2A, <sup>64</sup>Cu-CB-TEAMA, <sup>64</sup>Cu-CB-MeTEAMA, and <sup>64</sup>Cu-CB-PhTEAMA in 33 to 40 day old, male Lewis rats (30 min to 24 h, *n* = 4; <sup>64</sup>Cu-CB-TE2A 2 h, *n* = 3, animal died prior to sacrifice). Intestines were removed and divided into three parts for counting without removal of fecal contents. Note differences in scale.

propose that <sup>64</sup>Cu-CB-TEAMA and <sup>64</sup>Cu-CB-MeTEAMA may have undergone enzymatic modification in the liver, such as hydrolysis of the amide to form <sup>64</sup>Cu-CB-TE2A. This might allow secretion of the radio-metabolite(s) into blood, with subsequent clearance via the kidneys.

The observation that all cross-bridged complexes demonstrate continuous clearance from blood, liver, and bone marrow is highly suggestive of improved *in vivo* stability compared to <sup>64</sup>Cu-TETA, as was shown previously for <sup>64</sup>Cu-CB-TE2A.<sup>14,23</sup> These data further support the observation that CB-TE2A can be used as a bifunctional chelator for <sup>64</sup>Cu-radiolabeled peptides without additional modifications to the macrocycle backbone. However, no studies have been conducted to examine the *in vivo* stability properties of <sup>64</sup>Cu-CB-TE2A conjugates to larger macromolecules, which would require imaging at later time points.

#### Experimental Section

**Materials and Methods.** Caution! Although we did not experience any difficulties, metal perchlorate salts with organic ligands

and in organic solvents are potentially explosive and should be prepared and handled only in small quantities and with great care. All work involving the use of radioactive materials at Washington University is conducted under Radiation Safety Committee approved authorizations in accordance with the University's Nuclear Regulatory Commission license and Missouri State registrations.

Copper-64 was produced on a CS-15 biomedical cyclotron at Washington University School of Medicine according to published procedures.<sup>9</sup> Copper chloride (CuCl<sub>2</sub>) was purchased from Johnson Matthey (West Deptford, NJ). All other chemicals were purchased from Sigma-Aldrich Chemical Co. (St. Louis, MO). All solutions were prepared using ultrapure water (18 MΩ/cm<sup>2</sup> resistivity). IR spectra were recorded on a Nicolet MX-1 FT spectrophotometer. UV-vis data were collected using a Cary 50 Bio UV-vis spectrophotometer. Elemental analyses were performed at Atlantic Microlab, Inc. (Norcross, GA). Analytical reversed-phase HPLC was performed on a Waters 600E (Milford, MA) chromatography system with a Waters 991 photodiode array detector and an Ortec Model 661 radioactivity detector (EG&G Instruments, Oak Ridge, TN). Radioactive samples were counted using a Beckman 8000

automated well-type gamma counter (Fullerton, CA). ES-MS was accomplished using a Waters Micromass ZQ (Milford, MA). Male Lewis rats (21 d old, 40–50 g) were purchased from Charles River Laboratories (Boston, MA).

**Ligand Synthesis.** Synthetic reactions were run under a nitrogen atmosphere. Solvents were removed by rotary evaporation under reduced pressure (water aspirator) and vacuum line (mechanical pump). 1,4,8,11-Tetraazabicyclo[6.6.2]hexadecane (cross-bridged cyclam 1) was prepared as previously reported.<sup>18</sup>

**4-Carbo-*r*-butoxymethyl-1,4,8,11-tetraazabicyclo[6.6.2]-hexadecane (2).** 1,4,8,11-Tetraazabicyclo[6.6.2]hexadecane (1; 100 mg, 0.441 mmol) was dissolved in dry CH<sub>3</sub>CN (4 mL), sodium carbonate (47.0 mg, 0.441 mmol) was added in one portion, and *t*-butyl bromoacetate (0.065 mL, 0.44 mmol) was added in one portion by syringe. The solution was stirred for 14 h at room temperature, followed by solvent removal. NMR indicated this crude product to be a mixture of monoester 2, diester 3, and residual tetraamine 1. Purification by flash chromatography (SiO<sub>2</sub>, MeOH/CH<sub>2</sub>Cl<sub>2</sub> = 1.5:10) yielded an oil that was dissolved in water (4 mL), adjusted to pH 14 (solid KOH), and extracted with benzene (3 × 50 mL). The combined extracts were dried (Na<sub>2</sub>SO<sub>4</sub>) and the solvent was removed to yield 2 as a light yellow oil (60.0 mg, 0.172 mmol, 39%): <sup>1</sup>H NMR (C<sub>6</sub>D<sub>6</sub>, 500 MHz) δ 1.20–1.32 (m, 2H), 1.38 (s, 9H, C(CH<sub>3</sub>)<sub>3</sub>), 1.41–1.52 (m, 2H), 1.94–2.01 (dm, 1H, *J* = 15.6 Hz), 2.08–2.14 (dm, 1H, *J* = 14.7 Hz), 2.19 (ddd, 1H, *J* = 13.4, 10.0, 3.4 Hz), 2.24–2.29 (dm, 1H, *J* = 12.9 Hz), 2.30–2.40 (m, 3H), 2.45 (td, 1H, *J* = 13.2, 3.7 Hz), 2.53 (td, 1H, *J* = 11.5, 5.4 Hz), 2.58–2.65 (ddm, 1H, *J* = 13.4, 5.9 Hz), 2.65–2.80 (m, 5H), 2.85–2.94 (m, 1H), 2.97–3.04 (m, 1H), 3.00 and 3.11 (AB, 2H, *J* = 16.4 Hz), 3.15–3.26 (m, 2H), 3.41–3.48 (m, 1H), 4.69 (m, 1H, NH); <sup>13</sup>C{<sup>1</sup>H} NMR (C<sub>6</sub>D<sub>6</sub>, 100.5 MHz) δ 25.73, 28.21 (C(CH<sub>3</sub>)<sub>3</sub>), 28.35, 48.79, 49.03, 49.07, 50.20, 53.67, 55.63, 55.71, 57.36, 57.59, 59.37, 60.75, 79.92 (OC(CH<sub>3</sub>)<sub>3</sub>), 171.24 (C=O); IR (neat) 1158, 1214, 1255, 1296, 1366, 1391, 1458, 1492, 1736(C=O), 2801, 2914, 3236 (NH) cm<sup>-1</sup>; HRFABMS (M + H)<sup>+</sup> exact mass calcd for C<sub>18</sub>H<sub>33</sub>N<sub>4</sub>O<sub>2</sub>, 341.2917; found, 341.2915 (error -0.1 mmu/-0.3 ppm).

**4-Acetamido-11-carbo-*r*-butoxymethyl-1,4,8,11-tetraazabicyclo[6.6.2]hexadecane (4).** 4-Carbo-*r*-butoxymethyl-1,4,8,11-tetraazabicyclo[6.6.2]hexadecane (2; 30 mg, 0.086 mmol) was dissolved in dry CH<sub>3</sub>CN (4 mL). Na<sub>2</sub>CO<sub>3</sub> (9.2 mg, 0.086 mmol) was then added, followed by 2-bromoacetamide (12 mg, 0.086 mmol). The mixture was stirred for 14 h at room temperature and then solvent was removed. The residue was dissolved in water (2 mL), adjusted to pH 14 (solid KOH) with cooling, and extracted with benzene (2 × 20 mL). The combined extracts were dried (Na<sub>2</sub>SO<sub>4</sub>) and solvent was removed to give 4 as an oil (15.0 mg, 0.0372 mmol, 43%): <sup>1</sup>H NMR (C<sub>6</sub>D<sub>6</sub>, 400 MHz) δ 1.01–1.40 (m, 4H), 1.39 (s, 9H, C(CH<sub>3</sub>)<sub>3</sub>), 2.00 (dt, 1H, *J* = 12.3, 4.1 Hz), 2.05–2.68 (m, 13H), 2.68–2.86 (m, 3H), 2.79 and 3.04 (AX, 2H, *J* = 16.4 Hz), 3.02 and 3.14 (AB, 2H, *J* = 16.4 Hz), 3.20 (td, 1H, *J* = 8.0, 4.1 Hz), 3.36 (td, 1H, *J* = 12.1, 4.5 Hz), 4.08 (ddd, 1H, *J* = 13.3, 8.2, 3.9 Hz), 6.37 (br s, 1H), 6.42 (br s, 1H); <sup>13</sup>C{<sup>1</sup>H} NMR (C<sub>6</sub>D<sub>6</sub>, 100.5 MHz) δ 28.04, 28.22, 28.40, 51.67, 52.27, 53.46, 53.86, 55.89, 56.76, 57.24, 57.52, 57.55, 58.65, 59.94, 61.06, 79.96, 171.18, 174.44; IR (CCl<sub>4</sub>) 3448, 2978, 2922, 2809, 1739, 1689, 1368, 1155, 1125 cm<sup>-1</sup>; HRFABMS (M + H)<sup>+</sup> exact mass calcd for C<sub>20</sub>H<sub>40</sub>O<sub>3</sub>N<sub>5</sub>, 398.3131; found, 398.3106 (error -2.5 mmu/-6.3 ppm).

**4-Acetamido-11-carboxymethyl-1,4,8,11-tetraazabicyclo[6.6.2]-hexadecane-2TFA (5-2TFA).** 4-Carbo-*r*-butoxymethyl-11-acetamido-1,4,8,11-tetraazabicyclo[6.6.2]hexadecane (4; 15 mg, 0.0372 mmol) was dissolved in a mixture of CF<sub>3</sub>CO<sub>2</sub>H (TFA) and CH<sub>2</sub>Cl<sub>2</sub> (TFA/CH<sub>2</sub>Cl<sub>2</sub> = 1:1, 6 mL), and the solution was stirred for 14 h at room temperature. Solvent was then removed to give 5 as a TFA salt (2 equiv TFA calculated on the basis of mass; 20 mg): <sup>1</sup>H NMR (D<sub>2</sub>O, 400 MHz, HOD peak set to 4.80) δ 1.72–1.80 (dm, 2H, *J* = 17.4 Hz), 2.30–2.45 (m, 2H), 2.70–2.84 (m, 2H), 3.00–3.36 (m, 16H), 3.42–3.72 (m, 4H), 3.56 and 4.08 (AX, 2H, *J* = 17.4 Hz), 3.63 and 4.08 (AX, 2H, *J* = 16.1 Hz); <sup>13</sup>C{<sup>1</sup>H} NMR (D<sub>2</sub>O, 100.5 MHz) δ 19.46, 19.47, 47.56, 47.82, 48.20, 48.30, 52.91,

53.23, 54.98, 55.11, 58.11, 58.13, 58.70, 58.93, 116.4 (q, *J* = 291.4 Hz, CF<sub>3</sub>COOH), 163.1 (q, *J* = 35.2 Hz, CF<sub>3</sub>COOH), 170.05, 171.77; IR (CH<sub>3</sub>CN) 3681, 3540, 3164, 3003, 2944, 1694, 1444, 1422, 1376, 1202, 1039, 918 cm<sup>-1</sup>; HRFABMS, *m/z* (M + H)<sup>+</sup> exact mass for C<sub>16</sub>H<sub>35</sub>N<sub>5</sub>O<sub>3</sub>, 342.2505; found, 342.2500 (error -0.5 mmu/-1.4 ppm).

**4-Carbo-*r*-butoxymethyl-11-(*N*-methylacetamido)-1,4,8,11-tetraazabicyclo[6.6.2]hexadecane (6).** Monoarmed ligand 2 (18 mg, 0.052 mmol) was dissolved in dry CH<sub>3</sub>CN (4 mL), Na<sub>2</sub>CO<sub>3</sub> (13 mg, 0.1226 mmol), KI (23 mg, 0.1385 mmol), and 2-chloro-*N*-methylacetamide (13 mg, 0.1209 mmol) were added sequentially, and the solution was stirred for 14 h at room temperature. Solvent was removed to yield crude product as a solid, which was dissolved in water (2 mL) and adjusted to pH 3 (3 M HCl with cooling). The aqueous phase was extracted with benzene (2 × 25 mL), and the retained aqueous phase was adjusted to pH 14 with solid KOH (with cooling). The basic aqueous phase was extracted with benzene (2 × 25 mL), the combined extracts were dried (Na<sub>2</sub>SO<sub>4</sub>), and the benzene was removed to yield 6, an oil (21 mg, 0.051 mmol, 98%, >94% purity by <sup>13</sup>C NMR): <sup>1</sup>H NMR (C<sub>6</sub>D<sub>6</sub>, 400 MHz) δ 1.05–1.40 (m, 4H), 1.40 (s, 9H, C(CH<sub>3</sub>)<sub>3</sub>), 2.02–2.16 (m, 2H), 2.17–2.36 (m, 2H), 2.36–2.66 (m, 8H), 2.64 (d, 3H, *J* = 5.1 Hz), 2.68–2.94 (m, 5H), 2.86 and 3.07 (AB, 2H, *J* = 16.2 Hz), 3.02 and 3.15 (AB, 2H, *J* = 16.4 Hz), 3.24 (td, 1H, *J* = 12.1, 4.3 Hz), 3.40 (td, 1H, *J* = 11.9, 4.3 Hz), 4.11 (ddd, 1H, *J* = 16.6, 10.0, 4.3 Hz), 6.59 (br s, 1H, NH); <sup>13</sup>C{<sup>1</sup>H} NMR (C<sub>6</sub>D<sub>6</sub>, 100.5 MHz) δ 25.77, 28.32, 28.53, 28.58, 51.96, 52.70, 53.83, 54.02, 56.29, 57.18, 57.76, 57.95, 58.81, 60.23, 61.58, 80.34, 171.53, 171.69; IR (CCl<sub>4</sub>) 3407, 2918, 2809, 1739, 1684, 1559, 1457, 1368, 1155, 1125 cm<sup>-1</sup>; HRFABMS (M + H)<sup>+</sup> exact mass calcd for C<sub>21</sub>H<sub>42</sub>N<sub>5</sub>O<sub>3</sub>, 412.3288; found, 412.3274 (error -1.4 mmu/-3.3 ppm).

**(11-Methylcarbamoylmethyl-1,4,8,11-tetraazabicyclo[6.6.2]-hexadec-4-yl)-acetic acid-2TFA (8-2TFA).** 4-(Carbo-*r*-butoxymethyl)-11-(*N*-methylacetamido)-1,4,8,11-tetraazabicyclo[6.6.2]hexadecane (6; 14 mg, 0.034 mmol) was dissolved in a mixture of TFA and CH<sub>2</sub>Cl<sub>2</sub> (TFA/CH<sub>2</sub>Cl<sub>2</sub> = 1:1, 8 mL), the solution was stirred for 16 h, and the solvent was removed to yield 8 as a TFA salt (20 mg): <sup>1</sup>H NMR (400 MHz, D<sub>2</sub>O, HOD peak set at 4.80) δ 1.70–1.80 (dm, 2H, *J* = 17.0 Hz), 2.30–2.46 (m, 2H), 2.70–2.85 (m, 2H), 2.74 (s, 3H, NCH<sub>3</sub>), 3.00–3.38 (m, 14H), 3.44–3.76 (m, 4H), 3.57 and 4.11 (AX, 2H, *J* = 17.4 Hz), 3.58 and 4.06 (AX, 2H, *J* = 16.1 Hz); <sup>13</sup>C{<sup>1</sup>H} NMR (100.5 MHz, D<sub>2</sub>O) δ 19.41 (2C), 25.95, 47.51, 47.87, 48.26, 48.32, 52.82, 53.29, 55.13 (2C), 58.07 (2C), 58.61, 58.93, 116.43 (q, *J*<sub>CF</sub> = 292.2 Hz, CF<sub>3</sub>COOH), 163.05 (q, *J*<sub>CF</sub> = 35.2 Hz, CF<sub>3</sub>COOH), 167.65, 171.74; IR (CH<sub>3</sub>CN) 3638–3538 (br), 3164, 3002, 2944, 1682, 1444, 1418, 1376, 1201, 1132, 1039 cm<sup>-1</sup>; HRFABMS *m/z* (M + H)<sup>+</sup> exact mass calcd for C<sub>17</sub>H<sub>34</sub>N<sub>5</sub>O<sub>3</sub>, 356.2662; found, 356.2664 (error +0.2 mmu/+0.5 ppm). The product is a di-TFA salt on the basis of the mass (no evidence of impurities by NMR).

**4-(Carbo-*r*-butoxymethyl)-11-(*N*-phenylacetamido)-1,4,8,11-tetraazabicyclo[6.6.2]hexadecane (7).** Monoarmed ligand 2 (20 mg, 0.058 mmol) was dissolved in dry CH<sub>3</sub>CN (4 mL), and Na<sub>2</sub>CO<sub>3</sub> (74 mg, 0.698 mmol), KI (13.4 mg, 0.0807 mmol), and 2-chloro-*N*-phenylacetamide (37 mg, 0.218 mmol) were added in single portions. The solution was stirred for 14 h at room temperature and solvent was removed by rotary evaporation to yield a solid, which was dissolved in water (2 mL). The pH was adjusted to 3 (3 M HCl with cooling), and the acidic solution was extracted with benzene (2 × 25 mL). The retained aqueous phase was adjusted to pH 14 (solid KOH with cooling) and extracted with benzene (2 × 25 mL), the combined benzene extracts were dried (Na<sub>2</sub>SO<sub>4</sub>), and the solvent was removed to yield 7 as an oil (20 mg, 0.042 mmol, 73%): <sup>1</sup>H NMR (C<sub>6</sub>D<sub>6</sub>, 500 MHz) δ 1.03–1.40 (m, 4H), 1.40 (s, 9H, C(CH<sub>3</sub>)<sub>3</sub>), 2.00–2.03 (m, 2H), 2.08 (dt, 1H, *J* = 13.0, 3.9 Hz), 2.12–2.23 (m, 2H), 2.24–2.35 (m, 2H), 2.48–2.55 (m, 2H), 2.55–2.66 (m, 4H), 2.71 (td, 1H, *J* = 8.8, 3.6 Hz), 2.76–2.86 (m, 2H), 2.85 and 3.09 (AX, 2H, *J* = 16.4 Hz), 2.97 (td, 1H, *J* = 11.7, 4.2 Hz), 3.01 and 3.13 (AB, 2H, *J* = 16.4 Hz), 3.25 (td, 1H, *J* = 13.2, 4.6 Hz), 3.33 (td, 1H, *J* = 12.0, 4.4 Hz), 4.17–4.24 (m, 1H), 6.92 (t, 1H, *J* = 8.6, 1.0 Hz), 7.14–7.22 (m,

**Table 2.** Crystal Data for [Cu-CB-TEAMA]ClO<sub>4</sub>·NaClO<sub>4</sub> and [Cu-CB-PhTEAMA]ClO<sub>4</sub>·MeOH

	[Cu-CB-TEAMA]ClO <sub>4</sub> ·NaClO <sub>4</sub>	[Cu-CB-PhTEAMA]ClO <sub>4</sub> ·MeOH
empirical formula	C <sub>16</sub> H <sub>22</sub> Cl <sub>2</sub> CuN <sub>3</sub> NaO <sub>11</sub>	C <sub>23</sub> H <sub>30</sub> ClCuN <sub>3</sub> O <sub>8</sub>
formula weight	623.86	609.56
temperature (K)	213(2)	100(2)
crystal system	orthorhombic	orthorhombic
space group	P2 <sub>1</sub> 2 <sub>1</sub> 2 <sub>1</sub>	Pbca
unit cell dimensions (Å)	a = 10.011(5) b = 12.346(6) c = 20.652(11)	a = 21.134(5) b = 10.7258(16) c = 23.111(4)
volume (Å <sup>3</sup> )	2553(2)	5238.6(15)
Z	4	4
density (calcd; Mg/m <sup>3</sup> )	1.623	1.546
absorption coefficient (mm <sup>-1</sup> )	1.145	0.993
crystal size (mm <sup>3</sup> )	0.20 × 0.20 × 0.05	0.40 × 0.30 × 0.08
crystal color, habit	blue, plate	blue, plate
reflections collected	12 979	22 661
independent reflections	4363 [R(int) = 0.0415]	4613 [R(int) = 0.0432]
completeness to theta = 25.00°	99.1%	99.0%
data/restraints/parameters	4363/0/325	4613/0/343
goodness-of-fit on F <sup>2</sup>	1.029	1.049
final R indices [I > 2σ(I)] (%)	R1 = 6.57, wR2 = 16.83	R1 = 5.42, wR2 = 13.03
absolute structure parameter	0.51(3)	NA
largest diff. peak, hole (e·Å <sup>-3</sup> )	0.893, -0.476	1.038, -0.461

2H), 7.91 (dd, 2H, J = 8.6, 1.0 Hz), 9.12 (br s, 1H, NH); <sup>13</sup>C{<sup>1</sup>H} NMR (C<sub>6</sub>D<sub>6</sub>, 100.5 MHz) δ 28.30, 28.57(C(CH<sub>2</sub>)<sub>3</sub>), 28.69, 51.87, 52.49, 53.84, 54.10, 56.13, 57.22, 57.46, 58.03, 58.36, 59.43, 60.40, 62.44, 80.39, 119.31, 124.24, 129.84, 139.48, 169.63, 171.49; IR (neat) 703, 739, 1126, 1156, 1265, 1368, 1443, 1521, 1601, 1684, 1732, 2818, 2925, 2979, 3053, 3308 cm<sup>-1</sup>; HSFABMS (M + H) exact mass calcd for C<sub>20</sub>H<sub>44</sub>N<sub>3</sub>O<sub>3</sub>, 474.3444; found, 474.3440 (error -0.4 mmu/-0.8 ppm).

**(11-Phenylcarbamoylmethyl-1,4,8,11-tetraazabicyclo[6.6.2]-hexadec-4-yl)-acetic acid-4TFA (9-4TFA).** 4-(Carbo-*t*-butoxy-methyl)-11-(*N*-phenylacetamido)-1,4,8,11-tetraazabicyclo[6.6.2]-hexadecane (7; 140 mg, 0.296 mmol) was dissolved in a mixture of TFA and CH<sub>2</sub>Cl<sub>2</sub> (TFA/CH<sub>2</sub>Cl<sub>2</sub> = 1:1, 20 mL), and the solution was stirred for 16 h. Solvent was then removed to yield **8** as a tetra-TFA adduct on the basis of mass (255 mg, quant; no impurities by NMR): <sup>1</sup>H NMR (CD<sub>3</sub>CN, 500 MHz, CHD<sub>2</sub>CN central peak set to 1.94) δ 1.63–1.72 (m, 2H), 2.20–2.34 (m, 2H), 2.68–2.76 (dm, 2H, J = 12.5 Hz), 2.94–3.02 (dm, 2H, J = 14.7 Hz), 3.03–3.22 (m, 12H), 3.27 (td, 1H, J = 12.9, 3.2 Hz), 3.40–3.61 (m, 4H), 3.62–3.72 (m, 2H), 4.05 (A of AX, 1H, J = 16.6 Hz), 4.23 (A of AX, 1H, J = 16.6 Hz), 7.12–7.17 (m, 1H), 7.31–7.36 (m, 2H), 7.57–7.61 (m, 2H), 10.02 (s, 1H, NH), 10.90 (br s, 2H), 11.06 (br s, 3H); <sup>13</sup>C{<sup>1</sup>H} NMR (CD<sub>3</sub>CN, 125.7 MHz, CD<sub>3</sub>CN central peak set to 1.39) δ 20.73, 20.81, 48.77, 48.98, 49.39, 49.43, 53.73, 53.91, 56.66, 57.70, 59.42, 60.40, 117.25 (q, J<sub>CF</sub> = 290.5 Hz, CF<sub>3</sub>CO<sub>2</sub>), 121.24, 125.88, 129.94, 138.79, 160.95 (q, J<sub>CF</sub> = 36.4 Hz, CF<sub>3</sub>CO<sub>2</sub>), 166.73, 171.91; IR (CH<sub>3</sub>CN) 3648, 3607, 3550, 3002, 2944, 1680, 1632, 1446, 1428, 1375, 1201, 1039, 918, 749 cm<sup>-1</sup>; HRFABMS (M + H)<sup>+</sup> exact mass calcd for C<sub>22</sub>H<sub>36</sub>N<sub>3</sub>O<sub>3</sub>, 418.2818; found, 418.2811 (error -0.7 mmu/-1.7 ppm).

**Synthesis of Cu-CB-PhTEAMA.** An amount of 9-4TFA (0.082 g, 0.99 mmol) was dissolved in 3 mL methanol. Copper perchlorate hexahydrate (0.056 g, 0.15 mmol) dissolved in 2 mL of methanol was added to give a light-blue solution. NaOH (6 equiv, 0.40 mL, 1.0 M) was added and the light-blue suspension was refluxed for 5 h to give a clear solution. Cooling to room temperature gave a light-blue precipitate that was filtered off and dried under reduced pressure to give 0.052 g (59% yield) of the complex. X-ray quality crystals were grown from a methanol solution of this product by ether diffusion. IR: 1677 (s, CO), 1628 (s, COO), 1116 (vs, ClO<sub>4</sub>) cm<sup>-1</sup>. Visible electronic spectrum (H<sub>2</sub>O): λ<sub>max</sub> 648 nm (ε = 55 M<sup>-1</sup>cm<sup>-1</sup>). Anal. Calcd for CuC<sub>22</sub>H<sub>34</sub>N<sub>3</sub>O<sub>3</sub>(ClO<sub>4</sub>)(H<sub>2</sub>O): C, 44.22; H, 6.07; N, 11.72; Cl, 5.93. Found: C, 44.47; H, 5.80; N, 11.68; Cl, 5.98.

**Synthesis of Cu-CB-TEAMA.** An amount of 5-2TFA (0.076 g, 0.19 mmol) was stirred in 10 mL of TFA overnight. After removal of volatiles under reduced pressure, the oily residue was

taken up in 10 mL of water and its pH adjusted to approximately 8. Copper perchlorate hexahydrate (0.080 g, 0.22 mmol) was dissolved in 5 mL of water and added to give a light-blue solution. This was heated to 80 °C overnight to give a dark-blue solution. After cooling to room temperature, this was evaporated to dryness under reduced pressure. The residue was treated with absolute ethanol and centrifuged to remove a small amount of insoluble material. Ether diffusion into the supernatant yielded 32 mg (31%) of the desired complex. X-ray quality crystals were grown from an acetonitrile solution of this product by ether diffusion. IR: 3475–3380 (w, br), 1677 (s, CO), 1628 (s, COO), 1098 (vs, ClO<sub>4</sub>) cm<sup>-1</sup>. Visible electronic spectrum (H<sub>2</sub>O): λ<sub>max</sub> 648 nm (ε = 55 M<sup>-1</sup>cm<sup>-1</sup>). Anal. Calcd for CuC<sub>16</sub>H<sub>20</sub>N<sub>3</sub>O<sub>3</sub>(ClO<sub>4</sub>)·0.3NaClO<sub>4</sub>: C, 35.58; H, 5.60; N, 12.96; Cl, 8.53%. Found: C, 35.52; H, 5.73; N, 12.89; Cl, 8.54%.

**X-ray Crystallography.** Crystallographic data are collected in Table 2. Both space groups were uniquely determined from systematic absences. Data collections for both structures were performed on a Bruker D8 platform diffractometer equipped with an APEX CCD detector using MoK(α) radiation. Data were corrected for absorption using empirical methods (SADABS). All nonhydrogen atoms were refined with anisotropic thermal parameters and hydrogen atoms were placed in idealized locations, except for those associated with the hydroxyl proton in the solvent MeOH for the PhTEAMA complex. Those hydrogens were ignored, but were included in computations of intensive properties. For the CB-TEAMA complex structure, refinement of the Flack parameter yielded a value of 0.51, which is interpreted as an indication that crystallization occurred as a racemic twin (further refinement with TWIN and BASF = 0.51 yielded identical results). All software was obtained from the SMART, SAINT, and SHELXTL Bruker libraries (Bruker-AXS, Madison, WI).

**Radiolabeling with <sup>64</sup>Cu.** Cu(II) complexes of CB-TEAMA, CB-MeTEAMA, and CB-PhTEAMA were prepared according to the method described previously for radiolabeling CB-TE2A-Y3-TATE with <sup>64</sup>Cu.<sup>28</sup> Briefly, CuCl<sub>2</sub> + <sup>64</sup>Cu (30 μCi) was added to each monoamide (1:1) in NH<sub>4</sub>OAc, pH 8.0. The reaction mixture was heated for 30 min at 95 °C. Complex formation was followed by radio-TLC. After sufficient time for radio-decay, formation of the correct complex was demonstrated by ES-MS (Cu(II)-CB-PhTEAMA (C<sub>22</sub>H<sub>34</sub>CuN<sub>3</sub>O<sub>3</sub>Cu) calcd m/z (M<sup>+</sup>), 479.20; found, 479.08; Cu(II)-CB-MeTEAMA (C<sub>17</sub>H<sub>22</sub>CuN<sub>3</sub>O<sub>3</sub>Cu) calcd m/z (M<sup>+</sup>), 417.18; found, 417.04). HPLC analysis of the monoamide complexes was accomplished using an Agilent Technologies C8 column (3.0 × 150 mm; Palo Alto, CA)<sup>33</sup> with the following gradient:

solvent A, H<sub>2</sub>O (0.1% formic acid); solvent B, CH<sub>3</sub>CN (0.1% formic acid; solvent B); 0% B to 50% B in 40 min (0.5 mL/min flow rate).

All monoamides, as well as CB-TE2A, were radiolabeled (no carrier added) with <sup>64</sup>Cu according to the method described by Boswell et al. for formation of <sup>64</sup>Cu-CB-TE2A.<sup>14</sup> TETA was radiolabeled with <sup>64</sup>Cu in 0.5 M NH<sub>4</sub>OAc, pH 6.5 (30 min at RT). Radio-HPLC for <sup>64</sup>Cu-CB-TEAMA, <sup>64</sup>Cu-CB-MeTEAMA, and <sup>64</sup>Cu-CB-PhTEAMA was performed as described above. For <sup>64</sup>Cu-CB-TE2A and <sup>64</sup>Cu-TETA, radio-HPLC was performed using an isocratic method (0.1% formic acid in H<sub>2</sub>O).

**Partition Coefficients.** The partition coefficients (logP) of <sup>64</sup>Cu-TETA, <sup>64</sup>Cu-CB-TE2A, <sup>64</sup>Cu-CB-TEAMA, <sup>64</sup>Cu-CB-MeTEAMA, and <sup>64</sup>Cu-PhTEAMA were determined using previously described methods.<sup>19</sup> Briefly, 4 μL of <sup>64</sup>Cu-labeled complex was added to 500 μL octanol + 500 μL PBS (obtained from a saturated octanol-PBS solution, *n* = 4). Solutions were shaken for 1 h at room temperature. For each sample, 50 μL was removed from each phase and counted separately in a gamma counter. The partition coefficient was calculated as a ratio of counts in the octanol fraction to counts in the PBS fraction.

**Biodistribution.** All animal experiments were performed in compliance with the Guidelines for the Care and Use of Research Animals established by Washington University's Animal Studies Committee. Male Lewis rats (33–40 d old) were injected intravenously with <sup>64</sup>Cu-radiolabeled complexes (43 μCi, 1 nmol ligand) via the tail vein. Tissue biodistribution data were obtained at 0.5, 1, 2, and 24 h PI according to previously described methods.<sup>5</sup> Rats in the 24 h group were maintained in metabolism cages; food and water were administered ad libitum. Urine and feces were collected.

**Statistical Methods.** All data are presented as mean ± standard deviation. For statistical classification, one-way ANOVA was used to determine statistically significant differences between the five complexes. Subsequently, Tukey's multiple comparison test (post-test) was used to compare individual data sets. Student's *t*-test (two-tailed, unpaired) was used to compare individual time points for a single complex. All statistical analysis was performed using GraphPad PRISM (San Diego, CA). All *p* values less than 0.05 were considered significant.

**Acknowledgment.** The authors acknowledge Todd A. Perkins and Deborah Sultan for production of <sup>64</sup>Cu and Laura Meyer, Chris Sherman, Nicole Fettig, and Lori Strong for their excellent technical assistance. This research was supported by NCI Grant R01 CA93375. The production of <sup>64</sup>Cu at Washington University School of Medicine is supported by the NCI Grant R24 CA86307. J.E.S. was supported by the Department of Defense Breast Cancer Research Program Grant W81XWH-04-1-0396.

**Supporting Information Available:** X-ray crystallographic information for Cu-CB-TEAMA and Cu-CB-PhTEAMA, including experimental crystal data, refinement details, final atomic position parameters, atomic thermal parameters, and complete bond distances and angles. This material is available free of charge via the Internet at <http://pubs.acs.org>.

## References

- Anderson, C. J.; Dehdashti, F.; Cutler, P. D.; Schwartz, S. W.; Laforest, R.; Bass, L. A.; Lewis, J. S.; McCarthy, D. W. Copper-64-TETA-octreotide as a PET imaging agent for patients with neuroendocrine tumors. *J. Nucl. Med.* 2001, 42 (2), 213–221.
- Connett, J. M.; Anderson, C. J.; Guo, L.-W.; Schwartz, S. W.; Zinn, K. R.; Rogers, B. E.; Siegel, B. A.; Philpott, G. W.; Welch, M. J. Radioimmunotherapy with a Cu-64 labeled monoclonal antibody: A comparison with Cu-67. *Proc. Natl. Acad. Sci. U.S.A.* 1996, 93, 6814–6818.
- Anderson, C. J.; Jones, L. A.; Bass, L. A.; Sherman, E. L. C.; McCarthy, D. W.; Cutler, D.; Lanahan, M. V.; Cristel, M. E.; Lewis, J. S.; Schwartz, S. W. Radiotherapy, toxicity and dosimetry of copper-64-TETA-octreotide in tumor-bearing rats. *J. Nucl. Med.* 1998, 39, 1944–1950.
- Lewis, J. S.; Lewis, M. R.; Cutler, P. D.; Srinivasan, A.; Schmidt, M. A.; Schwartz, S. W.; Morris, M. M.; Miller, J. P.; Anderson, C. J. Radiotherapy and dosimetry of <sup>64</sup>Cu-TETA-Tyr<sup>3</sup>-octreotide in a somatostatin receptor-positive, tumor-bearing rat model. *Clin. Cancer Res.* 1999, 5, 3608–3616.
- Lewis, J. S.; Srinivasan, A.; Schmidt, M. A.; Anderson, C. J. In vitro and in vivo evaluation of <sup>64</sup>Cu-TETA-Tyr<sup>3</sup>-octreotide. A new somatostatin analog with improved target tissue uptake. *Nucl. Med. Biol.* 1999, 26, 267–273.
- Zimmermann, K.; Grunberg, J.; Honer, M.; Ametamey, S.; Schubiger, P. A.; Novak-Hofer, I. Targeting of renal carcinoma with Cu-64/67-labeled anti-L1-CAM antibody chCE7: Selection of copper ligands and PET imaging. *Nucl. Med. Biol.* 2003, 30, 417–427.
- Wu, A. M.; Yazaki, P. J.; Tsai, S.; Nguyen, K.; Anderson, A.-L.; McCarthy, D. W.; Welch, M. J.; Shively, J. E.; Williams, L. E.; Raubitschek, A. A.; Wong, J. Y. C.; Toyokuni, T.; Phelps, M. E.; Gambhir, S. S. High-resolution microPET imaging of carcinoembryonic antigen-positive xenografts by using a copper-64 engineered antibody fragment. *Proc. Natl. Acad. Sci. U.S.A.* 2000, 97 (15), 8495–8500.
- Rogers, B. E.; Bigott, H. M.; McCarthy, D. W.; Manna, D. D.; Kim, J.; Sharp, T. L.; Welch, M. J. MicroPET imaging of a gastrin-releasing peptide receptor-positive tumor in a mouse model of human prostate cancer using a Cu-64-labeled bombesin analogue. *Bioconjugate Chem.* 2003, 14, 756–763.
- McCarthy, D. W.; Shefer, R. E.; Klinkowstein, R. E.; Bass, L. A.; Margeneau, W. H.; Cutler, C. S.; Anderson, C. J.; Welch, M. J. Efficient production of high specific activity Cu-64 using a biomedical cyclotron. *Nucl. Med. Biol.* 1997, 24, 35–43.
- Cole, W. C.; DeNardo, S. J.; Meares, C. F.; McCall, M. J.; DeNardo, G. L.; Epstein, A. L.; O'Brien, H. A.; Moi, M. K. Comparative serum stability of radiochelates for antibody radiopharmaceuticals. *J. Nucl. Med.* 1987, 28 (1), 83–90.
- Jones-Wilson, T. M.; Deal, K. A.; Anderson, C. J.; McCarthy, D. W.; Kovacs, Z.; Motekaitis, R. J.; Sherry, A. D.; Martell, A. E.; Welch, M. J. The in vivo behavior of copper-64-labeled azamacrocyclic complexes. *Nucl. Med. Biol.* 1998, 25, 523–530.
- Cole, W. C.; DeNardo, S. J.; Meares, C. F.; McCall, M. J.; DeNardo, G. L.; Epstein, A. L.; O'Brien, H. A.; Moi, M. K. Serum stability of <sup>67</sup>Cu chelates: Comparison with <sup>111</sup>In and <sup>57</sup>Co. *Nucl. Med. Biol.* 1986, 13 (4), 363–368.
- Moi, M. K.; Meares, C. F.; McCall, M. J.; Cole, W. C.; DeNardo, S. J. Copper chelates as probes of biological systems: Stable copper complexes with a macrocyclic bifunctional chelating agent. *Anal. Biochem.* 1985, 148 (1), 249–253.
- Boswell, C. A.; Sun, X.; Niu, W.; Weisman, G. R.; Wong, E. H.; Rheingold, A. L.; Anderson, C. J. Comparative in vivo stability of copper-64-labeled cross-bridged and conventional tetraazamacrocyclic complexes. *J. Med. Chem.* 2004, 47 (6), 1465–1474.
- Bass, L. A.; Wang, M.; Welch, M. J.; Anderson, C. J. In vivo transchelation of copper-64 from TETA-octreotide to superoxide dismutase in rat liver. *Bioconjugate Chem.* 2000, 11, 527–532.
- Weisman, G. R.; Rogers, M. E.; Wong, E. H.; Jasinski, J. P.; Paight, E. S. Cross-bridged cyclam protonation and Li<sup>+</sup> complexation in a diamond-lattice cleft. *J. Am. Chem. Soc.* 1990, 112, 8604–8605.
- Weisman, G. R.; Wong, E. H.; Hill, D. C.; Rogers, M. E.; Reed, D. P.; Calabrese, J. C. Synthesis and transition-metal complexes of new cross-bridged tetraamine ligands. *J. Chem. Soc., Chem. Commun.* 1996, 947–948.
- Wong, E. H.; Weisman, G. R.; Hill, D. C.; Reed, D. P.; Rogers, M. E.; Condon, J. P.; Fagan, M. A.; Calabrese, J. C.; Lam, K.-C.; Guzei, I. A.; Rheingold, A. L. Synthesis and characterization of cross-bridged cyclams and pendant-armed derivatives and structural studies of their copper(II) complexes. *J. Am. Chem. Soc.* 2000, 122, 10561–10572.
- Cutler, C. S.; Wuest, M.; Anderson, C. J.; Reichert, D. E.; Sun, Y.; Martell, A. E.; Welch, M. J. Labeling and in vivo evaluation of novel copper(II) diotetraazamacrocyclic complexes. *Nucl. Med. Biol.* 2000, 27, 375–380.
- Hubin, T. J.; Alcock, N. W.; Morton, M. D.; Busch, D. H. Synthesis, structure, and stability in acid of copper(II) and zinc(II) complexes of cross-bridged tetraazamacrocyclics. *Inorg. Chim. Acta* 2003, 348, 33–40.
- Hubin, T. J.; McCormick, J. M.; Alcock, N. W.; Clase, H. J.; Busch, D. H. Crystallographic characterization of stepwise changes in ligand conformations as their internal topology changes and two novel cross-bridged tetraazamacrocyclic copper(II) complexes. *Inorg. Chem.* 1999, 38, 4435–4446.
- Hubin, T. J.; McCormick, J. M.; Collinson, S. R.; Busch, D. H.; Alcock, N. W. Ultra rigid cross-bridged tetraazamacrocyclics as ligands—The challenge and the solution. *Chem. Commun.* 1998, 16, 1675–1676.

- (23) Sun, X.; Wuest, M.; Weisman, G. R.; Wong, E. H.; Reed, D. P.; Boswell, C. A.; Motekaitis, R. J.; Martell, A. E.; Welch, M. J.; Anderson, C. J. Radiolabeling and in vivo behavior of copper-64-labeled cross-bridged cyclam ligands. *J. Med. Chem.* 2002, 45, 469–477.
- (24) Li, W. P.; Lewis, J. S.; Kim, J.; Bugaj, J. E.; Johnson, M. A.; Erion, J. L.; Anderson, C. J. DOTA-D-Tyr<sup>1</sup>-octreotate: A somatostatin analogue for labeling with metal and halogen radionuclides for cancer imaging and therapy. *Bioconjugate Chem.* 2002, 13, 721–728.
- (25) de Jong, M.; Breeman, W.; Bakker, W.; Kooij, P.; Bernard, B.; Hofland, L.; Visser, T.; Srinivasan, A.; Schmidt, M.; Erion, J.; Bugaj, J.; Macke, H.; Krenning, E. Comparison of (111)In-labeled somatostatin analogues for tumor scintigraphy and radionuclide therapy. *Cancer Res.* 1998, 58 (3), 437–441.
- (26) de Jong, M.; Bakker, W. H.; Krenning, E. P.; Breeman, W. A. P.; van der Pluijm, M. E.; Bernard, B. F.; Visser, T. J.; Jermann, E.; Behe, M.; Powell, P.; Macke, H. R. Yttrium-90 and indium-111 labelling, receptor binding, and biodistribution of [DOTA<sup>0</sup>, D-Phe<sup>1</sup>, Tyr<sup>3</sup>]octreotide, a promising somatostatin analogue for radionuclide therapy. *Eur. J. Nucl. Med.* 1997, 24 (4), 368–371.
- (27) Lewis, E. A.; Boyle, R. W.; Archibald, S. J. Ultrastable complexes for in vivo use: A bifunctional chelator incorporating a cross-bridged macrocycle. *Chem. Commun.* 2004, 19, 2212–2213.
- (28) Sprague, J. E.; Peng, Y.; Sun, X.; Weisman, G. R.; Wong, E. H.; Achilefu, S.; Anderson, C. J. Preparation and biological evaluation of copper-64-labeled Tyr<sup>3</sup>-octreotate using a cross-bridged macrocyclic chelator. *Clin. Cancer Res.* 2004, 10 (24), 8674–8682.
- (29) Mirick, G. R.; O'Donnell, R. T.; DeNardo, S. J.; Shen, S.; Meares, C. F.; DeNardo, G. L. Transfer of copper from a chelated <sup>67</sup>Cu-antibody conjugate to ceruloplasmin in lymphoma patients. *Nucl. Med. Biol.* 1999, 26 (7), 841–845.
- (30) Bass, L. A.; Lanahan, M. V.; Duncan, J. R.; Erion, J. L.; Srinivasan, A.; Schmidt, M. A.; Anderson, C. J. Identification of the soluble in vivo metabolites of indium-111-diethylenetriaminepentaacetic acid-D-Phe<sup>1</sup>-octreotide. *Bioconjugate Chem.* 1998, 9, 192–200.
- (31) Rogers, B. E.; Anderson, C. J.; Connett, J. M.; Guo, L.-W.; Edwards, W. B.; Sherman, E. L. C.; Zinn, K. R.; Welch, M. J. Comparison of four bifunctional chelates for radiolabeling monoclonal antibodies with copper radioisotopes: Biodistribution and metabolism. *Bioconjugate Chem.* 1996, 7, 511–522.
- (32) Woodin, K. S.; Heroux, K. J.; Boswell, C. A.; Wong, E. H.; Weisman, G. R.; Niu, W.; Tomellini, S. A.; Anderson, C. J.; Zakharov, L. N.; Rheingold, A. L. Kinetic inertness and electrochemical behavior of copper(II)tetraazamacrocyclic complexes: Possible implications for in vivo stability. *Eur. J. Inorg. Chem.* 2005, 2005 (23), 4829–4833.
- (33) Boswell, C. A.; McQuade, P.; Weisman, G. R.; Wong, E. H.; Anderson, C. J. Optimization of labeling and metabolite analysis of copper-64-labeled azamacrocyclic chelators by radio-LC-MS. *Nucl. Med. Biol.* 2005, 32 (1), 29–38.

JM070204R

## References

1. Mankoff, D. A., A definition of molecular imaging. *J Nucl Med* **2007**, 48, (6), 18N, 21N.
2. Liu, S., Bifunctional coupling agents for radiolabeling of biomolecules and target-specific delivery of metallic radionuclides. *Advanced Drug Delivery Reviews* **2008**, 60, 1347-1370.
3. Ametamey, S.; Honer, M.; Schubiger, P. A., Molecular Imaging with PET. *Chemical Reviews* **2008**, 108, 1501-1516.
4. McQuade, P.; Rowland, D. J.; Lewis, J. S.; Welch, M. J., Positron-emitting isotopes produced on biomedical cyclotrons. *Current Medicinal Chemistry* **2005**, 12, (7), 807-818.
5. Phelps, M. E., Molecular imaging with positron emission tomography. *Annual Review of Nuclear and Particle Science* **2002**, 52, (1), 303-338.
6. Fass, L., Imaging and cancer: A review. *Molecular Oncology* **2008**, 2, (2), 115-152.
7. Weiner, R. E.; Thakur, M. L., Radiolabeled peptides in oncology: role in diagnosis and treatment. *BioDrugs* **2005**, 19, (3), 145-163.
8. Anderson, C. J.; Welch, M. J., Radiometal-labeled agents (non-Technetium) for diagnostic imaging. *Chemical Reviews* **1999**, 99, 2219-2234.
9. Reichert, D. E.; Lewis, J. S.; Anderson, C. J., Metal complexes as diagnostic tools. *Coord. Chem. Rev.* **1999**, 184, 3-66.
10. McCarthy, D. W.; Shefer, R. E.; Klinkowstein, R. E.; Bass, L. A.; Margeneau, W. H.; Cutler, C. S.; Anderson, C. J.; Welch, M. J., Efficient production of high specific activity  $^{64}\text{Cu}$  using a biomedical cyclotron. *Nuclear Medicine and Biology* **1997**, 24, (1), 35-43.
11. Linder, M. C.; Hazegh-Azam, M., Copper biochemistry and molecular biology. *Am J Clin Nutri Suppl* **1996**, 63, 797s-811s.

12. Moi, M. K.; Meares, C. F.; McCall, M. J.; Cole, W. C.; DeNardo, S. J., Copper chelates as probes of biological systems: stable copper complexes with a macrocyclic bifunctional chelating agent. *Anal Biochem* **1985**, 148, (1), 249-53.
13. Kume, M.; Tang, L.; Gaehle, G.; Willits, J.; Jenks, C. C.; Voller, T.; Carey, P. C.; Lapi, S.; Welch, M. J., Automated processing of copper and halogen radionuclides at Washington University. *Journal of Labelled Compounds and Radiopharmaceuticals* **2009**, 52, (S1), S254.
14. McCarthy, D. W.; Bass, L. A.; Cutler, P. D.; Shefer, R. E.; Klinkowstein, R. E.; Herrero, P.; Lewis, J. S.; Cutler, C. S.; Anderson, C. J.; Welch, M. J., High purity production and potential applications of copper-60 and copper-61. *Nuclear Medicine and Biology* **1999**, 26, 351-358.
15. Blower, P. J.; Lewis, J. S.; Zweit, J., Copper radionuclides and radiopharmaceuticals in nuclear medicine. *Nucl Med Biol* **1996**, 23, (8), 957-80.
16. Vavere, A. L.; Lewis, J. S., Cu-ATSM: a radiopharmaceutical for the PET imaging of hypoxia. *Dalton Trans* **2007**, (43), 4893-902.
17. Parker, D., Tumor targeting with radiolabeled macrocycle-antibody conjugates. *Chemical Society Reviews* **1990**, 19, 271-291.
18. Delgado, R.; Felix, V.; Lima, L. M.; Price, D. W., Metal complexes of cyclen and cyclam derivatives useful for medical applications: a discussion based on thermodynamic stability constants and structural data. *Dalton Trans* **2007**, (26), 2734-45.
19. Kaden, T. A., Functionalized tetraazamacrocycles: ligands with many aspects. *Advances in Supramolecular Chemistry* **1993**, 65-96.
20. Jurisson, S.; Berning, D.; Jia, W.; Ma, D., Coordination compounds in nuclear medicine. *Chemical Reviews* **1993**, 93, 1137-1156.
21. Rogers, B. E.; Anderson, C. J.; Connett, J. M.; Guo, L. W.; Edwards, W. B.; Sherman, E. L. C.; Zinn, K. R.; Welch, M. J., Comparison of Bifunctional Chelates for Radiolabeling Monoclonal Antibodies with Copper Radioisotopes: Biodistribution and Metabolism. *Bioconjugate Chemistry* **1996**, 7, 511-522.
22. Jones-Wilson, T. M.; Deal, K. A.; Anderson, C. J.; McCarthy, D. W.; Kovacs, Z.; Motekaitis, R. J.; Sherry, A. D.; Martell, A. E.; Welch, M. J., The *in vivo* behavior of

copper-64-labeled azamacrocyclic complexes. *Nuclear Medicine and Biology* **1998**, 25, (6), 523-530.

23. Wong, E. H.; Weisman, G. R.; Hill, D. C.; Reed, D. P.; Rogers, M. E.; Condon, J. S.; Fagan, M. A.; Calabrese, J. C.; Lam, K.-C.; Guzei, I. A.; Rheingold, A. L., Synthesis and Characterization of Cross-Bridged Cyclams and Pendant-Armed Derivatives and Structural Studies of Their Copper(II) Complexes. *Journal of the American Chemical Society* **2000**, 122, (43), 10561-10572.

24. Sprague, J. E.; Peng, Y.; Fiamengo, A. L.; Woodin, K. S.; Southwick, E. A.; Weisman, G. R.; Wong, E. H.; Golen, J. A.; Rheingold, A. L.; Anderson, C. J., Synthesis, characterization and in vivo studies of Cu(II)-64-labeled cross-bridged tetraazamacrocyclic-amide complexes as models of peptide conjugate imaging agents. *J Med Chem* **2007**, 50, (10), 2527-35.

25. Sprague, J. E.; Peng, Y.; Sun, X.; Weisman, G. R.; Wong, E. H.; Achilefu, S.; Anderson, C. J., Preparation and biological evaluation of copper-64-labeled tyr3-octreotate using a cross-bridged macrocyclic chelator. *Clin Cancer Res* **2004**, 10, (24), 8674-82.

26. Xiong, J. P.; Stehle, T.; Goodman, S. L.; Arnaout, M. A., Integrins, cations and ligands: making the connection. *Journal of Thrombosis and Haemostasis* **2003**, 1, (7), 1642-1654.

27. Hynes, R. O., Integrins: bidirectional allosteric signaling machines. *Cell* **2002**, 110, 673-687.

28. Hynes, R. O., Integrins: versatility, modulation, and signaling in cell adhesion. *Cell* **1992**, 69, (1), 11-25.

29. Kuphal, S.; Bauer, R.; Bosserhoff, A. K., Integrin signaling in malignant melanoma. *Cancer Metastasis Rev* **2005**, 24, (2), 195-222.

30. Bilato, C.; Curto, K. A.; Monticone, R. E.; Pauly, R. R.; White, A. J.; Crow, M. T., The inhibition of vascular smooth muscle cell migration by peptide and antibody antagonists of the  $\alpha$ v $\beta$ 3 integrin complex is reversed by activated calcium/calmodulin-dependent protein kinase II. *J Clin Invest* **1997**, 100, (3), 693-704.

31. Plow, E. F.; Haas, T. A.; Zhang, L.; Loftus, J.; Smith, J. W., Ligand Binding to Integrins. *J. Biol. Chem.* **2000**, 275, (29), 21785-21788.

32. Brooks, P. C.; Clark, R. A.; Cheres, D. A., Requirement of Vascular Integrin  $\alpha v\beta 3$  for Angiogenesis. *Science* **1994**, 264, 569-571.
33. Ruoslahti, E.; Reed, J. C., Anchorage dependence, integrins, and apoptosis. *Cell* **1994**, 77, 477-478.
34. Montgomery, A. M.; Reisfeld, R. A.; Cheres, D. A., Integrin alpha v beta 3 rescues melanoma cells from apoptosis in three-dimensional dermal collagen. *Proceedings of the National Academy of Sciences, U.S.A.* **1994**, 91, 8856-8860.
35. Kantlehner, M.; Schaffner, P.; Finsinger, D.; Meyer, J.; Jonczyk, A.; Diefenbach, B.; Nies, B.; Hölzemann, G.; Goodman, S. L.; Kessler, H., Surface coating with cyclic RGD peptides stimulates osteoblast adhesion and proliferation as well as bone formation. *ChemBioChem* **2000**, 1, (2), 107-114.
36. Liu, Z.; Wang, F.; Chen, X., Integrin  $\alpha v\beta 3$ -targeted cancer therapy. *Drug Development Research* **2008**, 69, (6), 329-339.
37. Kumar, C. C., Integrin alpha v beta 3 as a therapeutic target for blocking tumor-induced angiogenesis. *Curr Drug Targets* **2003**, 4, (2), 123-31.
38. Wilder, R. L., Integrin alpha V beta 3 as a target for treatment of rheumatoid arthritis and related rheumatic diseases. *Ann Rheum Dis* **2002**, 61, (90002), 96ii-99.
39. Mousa, S. A., Anti-integrin as novel drug-discovery targets: potential therapeutic and diagnostic implications. *Curr Opin Chem Biol* **2002**, 6, (4), 534-41.
40. Carron, C. P.; Meyer, D. M.; Pegg, J. A.; Engleman, V. W.; Nickols, M. A.; Settle, S. L.; Westlin, W. F.; Ruminiski, P. G., A peptidomimetic antagonist of the integrin alpha v beta 3 inhibits leydig cell tumor growth and the development of hypercalcemia of malignancy. *Cancer Res* **1998**, 58, (9), 1930-1935.
41. Ruoslahti, E., RGD and other recognition sequences for integrins. *Annual Review of Cell and Developmental Biology* **1996**, 12, 697-715.
42. Pierschbacher, M. D.; Ruoslahti, E., Influence of stereochemistry of the sequence Arg-Gly-Asp-Xxx on binding specificity in cell adhesion. *J. Biol. Chem.* **1987**, 262, 17294.

43. Hautanen, A.; Gailit, J.; Mann, D. M.; Ruoslahti, E., Effects of modifications of the RGD sequence and its context on recognition by the fibronectin receptor. *J. Biol. Chem.* **1989**, 264, 1437.
44. Bogdanowich-Knipp, S. J.; Chakrabarti, S.; Siahaan, T. J.; Williams, T. D.; Dillman, R. K., Solution stability of linear vs. cyclic RGD peptides. *The Journal of Peptide Research* **1999**, 53, (5), 530-541.
45. Goodman, S. L.; Holzemann, G.; Sulyok, G. A. G.; Kessler, H., Nanomolar small molecule inhibitors for  $\alpha_6\beta_6$ ,  $\alpha_5\beta_5$  and  $\alpha_v\beta_3$  integrins. *Journal of Medicinal Chemistry* **2002**, 45, (5), 1045-1051.
46. Kok, R. J.; Schraa, A. J.; Bos, E. J.; Moorlag, H. E.; Asgeirsdottir, S. A.; Everts, M.; Meijer, D. K. F.; Molema, G., Preparation and Functional Evaluation of RGD-Modified Proteins as  $\alpha_1\beta_2\beta_3$  Integrin Directed Therapeutics. *Bioconjugate Chemistry* **2002**, 13, (1), 128-135.
47. Boturyn, D.; Coll, J.-L.; Garanger, E.; Favrot, M.-C.; Dumy, P., Template Assembled Cyclopeptides as Multimeric System for Integrin Targeting and Endocytosis. *Journal of the American Chemical Society* **2004**, 126, (18), 5730-5739.
48. Ferrari, M., CANCER NANOTECHNOLOGY: OPPORTUNITIES AND CHALLENGES. *Nature Reviews Cancer* **2005**, 5, (3), 161-171.
49. Koos, O. M.; Rubinstein, I.; Onyuksel, H., Role of nanotechnology in targeted drug delivery and imaging: a concise review. *Nanomedicine: Nanotechnology, Biology, and Medicine* **2005**, 1, 193-212.
50. Liu, Y.; Miyoshi, H.; Nakamura, M., Nanomedicine for drug delivery and imaging: A promising avenue for cancer therapy and diagnosis using targeted functional nanoparticles. *International Journal of Cancer* **2007**, 120, (12), 2527-2537.
51. Hynes, R. O., Cell-matrix adhesion in vascular development. *Journal of Thrombosis and Haemostasis* **2007**, 5, (s1), 32-40.
52. Murthy, K. S.; Ma, Q.; Clark Jr, C. G.; Remsen, E. E.; Wooley, K. L., Fundamental design aspects of amphiphilic shell-crosslinked nanoparticles for controlled release applications. *Chemical Communications* **2001**, (8), 773-774.
53. Liu, S., The role of coordination chemistry in the development of target-specific radiopharmaceuticals. *Chem Soc Rev* **2004**, 33, (7), 445-61.

54. Liu, S.; Edwards, D. S., Bifunctional chelators for therapeutic lanthanide radiopharmaceuticals. *Bioconjug Chem* **2001**, 12, (1), 7-34.
55. Volkert, W. A.; Hoffman, T. J., Therapeutic radiopharmaceuticals. *Chem Rev* **1999**, 99, (9), 2269-92.
56. Mather, S. J., Design of radiolabelled ligands for the imaging and treatment of cancer. *Mol Biosyst* **2007**, 3, (1), 30-5.
57. Wadas, T. J.; Wong, E. H.; Weisman, G. R.; Anderson, C. J., Copper chelation chemistry and its role in copper radiopharmaceuticals. *Curr Pharm Des* **2007**, 13, (1), 3-16.
58. Qaim, S. M., Decay data and production yields of some non-standard positron emitters used in PET. *Q J Nucl Med Mol Imaging* **2008**, 52, (2), 111-20.
59. Cole, W. C.; DeNardo, S. J.; Meares, C. F.; McCall, M. J.; DeNardo, G. L.; Epstein, A. L.; O'Brien, H. A.; Moi, M. K., Comparative serum stability of radiochelates for antibody radiopharmaceuticals. *J Nucl Med* **1987**, 28, (1), 83-90.
60. Cole, W. C.; DeNardo, S. J.; Meares, C. F.; McCall, M. J.; DeNardo, G. L.; Epstein, A. L.; O'Brien, H. A.; Moi, M. K., Serum stability of <sup>67</sup>Cu chelates: comparison with <sup>111</sup>In and <sup>57</sup>Co. *Int J Rad Appl Instrum B* **1986**, 13, (4), 363-8.
61. Bass, L. A.; Wang, M.; Welch, M. J.; Anderson, C. J., In vivo transchelation of copper-64 from TETA-octreotide to superoxide dismutase in rat liver. *Bioconjug Chem* **2000**, 11, (4), 527-32.
62. Boswell, C. A.; Sun, X.; Niu, W.; Weisman, G. R.; Wong, E. H.; Rheingold, A. L.; Anderson, C. J., Comparative in vivo stability of copper-64-labeled cross-bridged and conventional tetraazamacrocyclic complexes. *J Med Chem* **2004**, 47, (6), 1465-1474.
63. Sun, X.; Wuest, M.; Weisman, G. R.; Wong, E. H.; Reed, D. P.; Boswell, C. A.; Motekaitis, R. J.; Martell, A. E.; Welch, M. J.; Anderson, C. J., Radiolabeling and In Vivo Behavior of Copper-64-Labeled Cross-Bridged Cyclam Ligands. *J Med Chem* **2002**, 45, 469-477.
64. Springborg, J., Adamanzanes - bi- and tricyclic tetraamines and their coordination compounds. *Dalton Transactions* **2003**, (9), 1653-1665.

65. Springborg, J.; Kofod, P.; Olsen, C. E.; Sotofte, I., Synthesis and Crystal Structure of a Small Bicyclic Tetraaza Proton Sponge, 1,4,7,10-Tetraazabicyclo[5.5.3]pentadecane Dibromide Perchlorate. *Acta Chem. Scand.* **1995**, 49, 547-554.
66. Prasanphanich, A. F.; Nanda, P. K.; Rold, T. L.; Ma, L.; Lewis, M. R.; Garrison, J. C.; Hoffman, T. J.; Sieckman, G. L.; Figueroa, S. D.; Smith, C. J., [64Cu-NOTA-8-Aoc-BBN(7-14)NH<sub>2</sub>] targeting vector for positron-emission tomography imaging of gastrin-releasing peptide receptor-expressing tissues. *Proc Natl Acad Sci U S A* **2007**, 104, (30), 12462-7.
67. Kukis, D. L.; Li, M.; Meares, C. F., Selectivity of antibody-chelate conjugates for binding copper in the presence of competing metals. *Inorganic Chemistry* **2002**, 32, (19), 3981-3982.
68. Liu, Z.; Li, Z. B.; Cao, Q.; Liu, S.; Wang, F.; Chen, X., Small-Animal PET of Tumors with 64Cu-Labeled RGD-Bombesin Heterodimer. *J Nucl Med* **2009**.
69. Velikyan, I.; Maecke, H.; Langstrom, B., Convenient preparation of 68Ga-based PET-radiopharmaceuticals at room temperature. *Bioconjug Chem* **2008**, 19, (2), 569-73.
70. Delgado, R.; Sun, Y.; Motekaitis, R. J.; Martell, A. E., Stabilities of divalent and trivalent metal ion complexes of macrocyclic triazatriacetic acids. *Inorganic Chemistry* **1993**, 32, (15), 3320-3326.
71. Bevilacqua, A.; Gelb, R. I.; Hebard, W. B.; Zompa, L. J., Equilibrium and thermodynamic study of the aqueous complexation of 1,4,7-triazacyclononane-N,N',N''-triacetic acid with protons, alkaline-earth-metal cations, and copper(II). *Inorganic Chemistry* **2002**, 26, (16), 2699-2706.
72. Wiegardt, K.; Bossek, U.; Chaudhuri, P.; Herrmann, W.; Menke, B. C.; Weiss, J., 1,4,7-Triazacyclononane-N,N',N''-triacetate (TCTA), a new hexadentate ligand for divalent and trivalent metal ions. Crystal structures of [CrIII(TCTA)], [FeIII(TCTA)], and Na[CuII(TCTA)].bul.2NaBr.bul.8H<sub>2</sub>O. *Inorganic Chemistry* **1982**, 21, (12), 4308-4314.
73. Moore, D. A.; Fanwick, P. E.; Welch, M. J., A novel hexachelating amino-thiol ligand and its complex with gallium(III). *Inorganic Chemistry* **1990**, 29, (4), 672-676.
74. McCarthy, D. W.; Shefer, R. E.; Klinkowstein, R. E.; Bass, L. A.; Margeneau, W. H.; Cutler, C. S.; Anderson, C. J.; Welch, M. J., Efficient production of high specific activity 64Cu using a biomedical cyclotron. *Nucl Med Biol* **1997**, 24, (1), 35-43.

75. Peng, Y. Doctoral Dissertation, University of New Hampshire, Durham, 2004.
76. Odendaal, A. Y. A modified synthesis, c-functionalization, resolution and racemization kinetics of cross-bridged tetraazamacrocycles. Doctoral Dissertation, University of New Hampshire, Durham, 2009.
77. Woodin, K. S.; Heroux, K. J.; Boswell, C. A.; Wong, E. H.; Weisman, G. R.; Niu, W.; Tomellini, S. A.; Anderson, C. J.; Zakharov, L. N.; Rheingold, A. L., Kinetic Inertness and Electrochemical Behavior of Copper(II)Tetraazamacrocyclic Complexes: Possible Implications for in Vivo Stability. *European Journal of Inorganic Chemistry* **2005**, 2005, (23), 4829-4833.
78. Heroux, K. J.; Woodin, K. S.; Tranchemontagne, D. J.; Widger, P. C.; Southwick, E.; Wong, E. H.; Weisman, G. R.; Tomellini, S. A.; Wadas, T. J.; Anderson, C. J.; Kassel, S.; Golen, J. A.; Rheingold, A. L., The long and short of it: the influence of N-carboxyethyl versus N-carboxymethyl pendant arms on in vitro and in vivo behavior of copper complexes of cross-bridged tetraamine macrocycles. *Dalton Trans* **2007**, (21), 2150-62.
79. Wadas, T. J.; Anderson, C. J., Radiolabeling of TETA- and CB-TE2A-conjugated peptides with copper-64. *Nat Protoc* **2006**, 1, (6), 3062-8.
80. Hubin, T. J.; Alcock, N. W.; Busch, D. H., Copper(I) and copper(II) complexes of an ethylene cross-bridged cyclam. *Acta Crystallogr C* **2000**, 56 (Pt 1), 37-9.
81. Anderson, C. J.; Jones, L. A.; Bass, L. A.; Sherman, E. L. C.; McCarthy, D. W.; Cutler, D.; Lanahan, M. V.; Cristel, M. E.; Lewis, J. S.; Schwartz, S. W., Radiotherapy, Toxicity and Dosimetry of Copper-64-TETA-Octreotide in Tumor-Bearing Rats. *J Nucl Med* **1998**, 39, 1944-1950.
82. Glukhova, M.; Deugnier, M. A.; Thiery, J. P., Tumor progression: the role of cadherins and integrins. *Mol Med Today* **1995**, 1, (2), 84-9.
83. Haubner, R.; Wester, H. J.; Reuning, U.; Senekowitsch-Schmidtke, R.; Diefenbach, B.; Kessler, H.; Stocklin, G.; Schwaiger, M., Radiolabeled alpha(v)beta3 integrin antagonists: a new class of tracers for tumor targeting. *J Nucl Med* **1999**, 40, (6), 1061-71.
84. Ojima, I.; Chakravarty, S.; Dong, Q., Antithrombotic agents: from RGD to peptide mimetics. *Bioorg Med Chem* **1995**, 3, (4), 337-60.

85. Carreiras, F.; Thiebot, B.; Leroy-Dudal, J.; Maubant, S.; Breton, M. F.; Darbeida, H., Involvement of  $\alpha_3\beta_1$  integrin and disruption of endothelial fibronectin network during the adhesion of the human ovarian adenocarcinoma cell line IGROV1 on the human umbilical vein cell extracellular matrix. *Int J Cancer* **2002**, 99, (6), 800-8.
86. Pidgeon, G. P.; Tang, K.; Cai, Y. L.; Piasentin, E.; Honn, K. V., Overexpression of platelet-type 12-lipoxygenase promotes tumor cell survival by enhancing  $\alpha(v)\beta_3$  and  $\alpha(v)\beta_5$  integrin expression. *Cancer Res* **2003**, 63, (14), 4258-67.
87. Marchisio, P. C.; Cirillo, D.; Naldini, L.; Primavera, M. V.; Teti, A.; Zamboni-Zallone, A., Cell-substratum interaction of cultured avian osteoclasts is mediated by specific adhesion structures. *J Cell Biol* **1984**, 99, (5), 1696-705.
88. Pierschbacher, M. D.; Ruoslahti, E., Cell attachment activity of fibronectin can be duplicated by small synthetic fragments of the molecule. *Nature* **1984**, 309, (5963), 30-3.
89. Ruoslahti, E., RGD AND OTHER RECOGNITION SEQUENCES FOR INTEGRINS. *Annual Review of Cell and Developmental Biology* **1996**, 12, (1), 697-715.
90. Haubner, R.; Finsinger, D.; Kessler, H., Sterioisomeric peptide libraries and peptidomimetics for designing selective inhibitors of the  $\alpha_3\beta_v$  integrin for a new cancer therapy. *Angew. Chem. Int. Ed. Engl.* **1997**, 36, 1374-1389.
91. Aumailley, M.; Gurrath, M.; Muller, G.; Calvete, J.; Timpl, R.; Kessler, H., Arg-Gly-Asp constrained within cyclic pentapeptides. Strong and selective inhibitors of cell adhesion to vitronectin and laminin fragment P1. *FEBS Lett* **1991**, 291, (1), 50-4.
92. Haubner, R.; Wester, H. J.; Burkhart, F.; Senekowitsch-Schmidtke, R.; Weber, W.; Goodman, S. L.; Kessler, H.; Schwaiger, M., Glycosylated RGD-containing peptides: tracer for tumor targeting and angiogenesis imaging with improved biokinetics. *J Nucl Med* **2001**, 42, (2), 326-36.
93. Harris, J. M.; Chess, R. B., Effect of pegylation on pharmaceuticals. *Nat Rev Drug Discov* **2003**, 2, (3), 214-21.
94. Schaffner, P.; Dard, M. M., Structure and function of RGD peptides involved in bone biology. *Cellular and Molecular Life Sciences* **2003**, 60, 119-132.

95. Chen, X.; Park, R.; Shahinian, A. H.; Bading, J. R.; Conti, P. S., Pharmacokinetics and tumor retention of <sup>125</sup>I-labeled RGD peptide are improved by PEGylation. *Nucl Med Biol* **2004**, 31, (1), 11-9.
96. van Hagen, P. M.; Breeman, W. A.; Bernard, H. F.; Schaar, M.; Mooij, C. M.; Srinivasan, A.; Schmidt, M. A.; Krenning, E. P.; de Jong, M., Evaluation of a radiolabelled cyclic DTPA-RGD analogue for tumour imaging and radionuclide therapy. *Int J Cancer* **2000**, 90, (4), 186-98.
97. Haubner, R.; Bruchertseifer, F.; Bock, M.; Kessler, H.; Schwaiger, M.; Wester, H. J., Synthesis and biological evaluation of a (99m)Tc-labelled cyclic RGD peptide for imaging the alphavbeta3 expression. *Nuklearmedizin* **2004**, 43, (1), 26-32.
98. Yoshimoto, M.; Ogawa, K.; Washiyama, K.; Shikano, N.; Mori, H.; Amano, R.; Kawai, K., alpha(v)beta(3) Integrin-targeting radionuclide therapy and imaging with monomeric RGD peptide. *Int J Cancer* **2008**, 123, (3), 709-15.
99. Wang, W.; McMurray, J. S.; Wu, Q.; Campbell, M. L.; Li, C., Convenient Solid-Phase Synthesis of Diethylenetriaminepenta-Acetic Acid (DTPA) and Conjugated Cyclic RGD Peptide Analogues. *Cancer Biotherapy & Radiopharmaceuticals* **2005**, 20, (5), 547-556.
100. Assa-Munt, N.; Jia, X.; Laakkonen, P.; Ruoslahti, E., Solution structures and integrin binding activities of an RGD peptide with two isomers. *Biochemistry* **2001**, 40, (8), 2373-8.
101. Craig, J. A.; Rexeisen, E. L.; Mardilovich, A.; Shroff, K.; Kokkoli, E., Effect of linker and spacer on the design of a fibronectin-mimetic peptide evaluated via cell studies and AFM adhesion forces. *Langmuir* **2008**, 24, (18), 10282-92.
102. Wu, Z.; Li, Z. B.; Cai, W.; He, L.; Chin, F. T.; Li, F.; Chen, X., <sup>18</sup>F-labeled mini-PEG spacers RGD dimer (<sup>18</sup>F-FPRGD2): synthesis and microPET imaging of alphavbeta3 integrin expression. *Eur J Nucl Med Mol Imaging* **2007**, 34, (11), 1823-31.
103. Sprague, J. E.; Kitaura, H.; Zou, W.; Ye, Y.; Achilefu, S.; Weilbaecher, K. N.; Teitelbaum, S. L.; Anderson, C. J., Noninvasive imaging of osteoclasts in parathyroid hormone-induced osteolysis using a <sup>64</sup>Cu-labeled RGD peptide. *J Nucl Med* **2007**, 48, (2), 311-8.
104. Qi, J.; Leahy, R. M., Resolution and noise properties of MAP reconstruction for fully 3-D PET. *IEEE Trans Med Imaging* **2000**, 19, (5), 493-506.

105. Strauss, L. G.; Conti, P. S., The applications of PET in clinical oncology. *J Nucl Med* **1991**, 32, (4), 623-48; discussion 649-50.
106. Haubner, R.; Wester, H. J., Radiolabeled tracers for imaging of tumor angiogenesis and evaluation of anti-angiogenic therapies. *Curr Pharm Des* **2004**, 10, (13), 1439-55.
107. Pfaff, M.; Tangemann, K.; Muller, B.; Gurrath, M.; Muller, G.; Kessler, H.; Timpl, R.; Engel, J., Selective recognition of cyclic RGD peptides of NMR defined conformation by alpha IIb beta 3, alpha V beta 3, and alpha 5 beta 1 integrins. *J Biol Chem* **1994**, 269, (32), 20233-8.
108. Su, Z. F.; He, J.; Rusckowski, M.; Hnatowich, D. J., In vitro cell studies of technetium-99m labeled RGD-HYNIC peptide, a comparison of tricine and EDDA as co-ligands. *Nucl Med Biol* **2003**, 30, (2), 141-9.
109. Su, Z. F.; Liu, G.; Gupta, S.; Zhu, Z.; Rusckowski, M.; Hnatowich, D. J., In vitro and in vivo evaluation of a Technetium-99m-labeled cyclic RGD peptide as a specific marker of alpha(V)beta(3) integrin for tumor imaging. *Bioconjug Chem* **2002**, 13, (3), 561-70.
110. Sutcliffe-Goulden, J. L.; O'Doherty, M. J.; Marsden, P. K.; Hart, I. R.; Marshall, J. F.; Bansal, S. S., Rapid solid phase synthesis and biodistribution of 18F-labelled linear peptides. *Eur J Nucl Med Mol Imaging* **2002**, 29, (6), 754-9.
111. Sivolapenko, G. B.; Skarlos, D.; Pectasides, D.; Stathopoulou, E.; Milonakis, A.; Sirmalis, G.; Stuttle, A.; Courtenay-Luck, N. S.; Konstantinides, K.; Epenetos, A. A., Imaging of metastatic melanoma utilising a technetium-99m labelled RGD-containing synthetic peptide. *Eur J Nucl Med* **1998**, 25, (10), 1383-9.
112. Smith, J. W.; Cheresch, D. A., The Arg-Gly-Asp binding domain of the vitronectin receptor. Photoaffinity cross-linking implicates amino acid residues 61-203 of the beta subunit. *J Biol Chem* **1988**, 263, (35), 18726-31.
113. Bloch, S.; Xu, B.; Ye, Y.; Liang, K.; Nikiforovich, G. V.; Achilefu, S., Targeting Beta-3 integrin using a linear hexapeptide labeled with a near-infrared fluorescent molecular probe. *Mol Pharm* **2006**, 3, (5), 539-49.
114. Janssen, M.; Oyen, W. J. G.; Massuger, L. F. A. G.; Frielink, C.; Dijkgraaf, I.; Edwards, D. S.; Radjopadhya, M.; Corstens, F. H. M.; Boerman, O. C., Comparison of a monomeric and dimeric radiolabeled RGD-peptide for tumor targeting. *Cancer Biotherapy and Radiopharmaceuticals* **2002**, 17, (6), 641-646.

115. Janssen, M. L.; Oyen, W. J.; Dijkgraaf, I.; Massuger, L. F.; Frielink, C.; Edwards, D. S.; Rajopadhye, M.; Boonstra, H.; Corstens, F. H.; Boerman, O. C., Tumor targeting with radiolabeled alpha(v)beta(3) integrin binding peptides in a nude mouse model. *Cancer Res* **2002**, 62, (21), 6146-51.
116. Thumshirn, G.; Hersel, U.; Goodman, S. L.; Kessler, H., Multimeric cyclic RGD peptides as potential tools for tumor targeting: solid-phase peptide synthesis and chemoselective oxime ligation. *Chemistry* **2003**, 9, (12), 2717-25.
117. Poethko, T.; Schottelius, M.; Thumshirn, G.; Hersel, U.; Herz, M.; Henriksen, G.; Kessler, H.; Schwaiger, M.; Wester, H. J., Two-step methodology for high-yield routine radiohalogenation of peptides: (18)F-labeled RGD and octreotide analogs. *J Nucl Med* **2004**, 45, (5), 892-902.
118. Liu, S., Radiolabeled multimeric cyclic RGD peptides as integrin  $\alpha\beta 3$  targeted radiotracers for tumor imaging. *Molecular Pharmaceutics* **2006**, 3, (5), 472-487.
119. Boswell, C. A.; Eck, P. K.; Regino, C. A.; Bernardo, M.; Wong, K. J.; Milenic, D. E.; Choyke, P. L.; Brechbiel, M. W., Synthesis, characterization, and biological evaluation of integrin  $\alpha\beta 3$ -targeted PAMAM dendrimers. *Mol Pharm* **2008**, 5, (4), 527-39.
120. Mitra, A.; Coleman, T.; Borgman, M.; Nan, A.; Ghandehari, H.; Line, B. R., Polymeric conjugates of mono- and bi-cyclic  $\alpha\beta 3$  binding peptides for tumor targeting. *J Control Release* **2006**, 114, (2), 175-83.
121. Almutairi, A.; Rossin, R.; Shokeen, M.; Hagooly, A.; Ananth, A.; Capoccia, B.; Guillaudeu, S.; Abendschein, D.; Anderson, C. J.; Welch, M. J.; Frechet, J. M., Biodegradable dendritic positron-emitting nanoprobe for the noninvasive imaging of angiogenesis. *Proc Natl Acad Sci U S A* **2009**, 106, (3), 685-90.
122. Henry, C.; Moitessier, N.; Chapleur, Y., Vitronectin receptor  $\alpha(V)\beta(3)$  integrin antagonists: chemical and structural requirements for activity and selectivity. *Mini Rev Med Chem* **2002**, 2, (6), 531-42.
123. Kerr, J. S.; Slee, A. M.; Mousa, S. A., Small molecule  $\alpha(v)$  integrin antagonists: novel anticancer agents. *Expert Opin Investig Drugs* **2000**, 9, (6), 1271-9.
124. Kerr, J. S.; Slee, A. M.; Mousa, S. A., The  $\alpha v$  integrin antagonists as novel anticancer agents: an update. *Expert Opin Investig Drugs* **2002**, 11, (12), 1765-74.

125. Tucker, G. C., Inhibitors of integrins. *Curr Opin Pharmacol* **2002**, 2, (4), 394-402.
126. Harris, T. D.; Kalogeropoulos, S.; Nguyen, T.; Dwyer, G.; Edwards, D. S.; Liu, S.; Bartis, J.; Ellars, C.; Onthank, D.; Yalamanchili, P.; Heminway, S.; Robinson, S.; Lazewatsky, J.; Barrett, J., Structure-activity relationships of <sup>111</sup>In- and <sup>99m</sup>Tc-labeled quinolin-4-one peptidomimetics as ligands for the vitronectin receptor: potential tumor imaging agents. *Bioconjug Chem* **2006**, 17, (5), 1294-313.
127. Coleman, P. J.; Duong, L. T., Ligands to the integrin receptor alpha(v)beta(3). *Expert Opin Ther Patents* **2002**, 12, (7), 1009-1021.
128. Harris, T. D.; Kalogeropoulos, S.; Nguyen, T.; Liu, S.; Bartis, J.; Ellars, C.; Edwards, S.; Onthank, D.; Silva, P.; Yalamanchili, P.; Robinson, S.; Lazewatsky, J.; Barrett, J.; Bozarth, J., Design, synthesis, and evaluation of radiolabeled integrin alpha v beta 3 receptor antagonists for tumor imaging and radiotherapy. *Cancer Biother Radiopharm* **2003**, 18, (4), 627-41.
129. Temming, K.; Schiffelers, R. M.; Molema, G.; Kok, R. J., RGD-based strategies for selective delivery of therapeutics and imaging agents to the tumour vasculature. *Drug Resist Updat* **2005**, 8, (6), 381-402.
130. Craig, W. S.; Cheng, S.; Mullen, D. G.; Blevitt, J.; Pierschbacher, M. D., Concept and progress in the development of RGD-containing peptide pharmaceuticals. *Biopolymers* **1995**, 37, (2), 157-75.
131. Dechantsreiter, M. A.; Planker, E.; Matha, B.; Lohof, E.; Holzemann, G.; Jonczyk, A.; Goodman, S. L.; Kessler, H., N-Methylated cyclic RGD peptides as highly active and selective alpha(V)beta(3) integrin antagonists. *J Med Chem* **1999**, 42, (16), 3033-40.
132. Kang, Y. K.; Jhon, J. S., Preferred conformations of a linear RGD tripeptide. *J Pept Res* **2000**, 56, (6), 360-72.
133. Ruoslahti, E.; Pierschbacher, M. D., New perspectives in cell adhesion: RGD and integrins. *Science* **1987**, 238, (4826), 491-7.
134. Saudek, V.; Atkinson, R. A.; Pelton, J. T., Three-dimensional structure of echistatin, the smallest active RGD protein. *Biochemistry* **1991**, 30, (30), 7369-72.
135. Main, A. L.; Harvey, T. S.; Baron, M.; Boyd, J.; Campbell, I. D., The three-dimensional structure of the tenth type III module of fibronectin: an insight into RGD-mediated interactions. *Cell* **1992**, 71, (4), 671-8.

136. Adler, M.; Lazarus, R. A.; Dennis, M. S.; Wagner, G., Solution structure of kistrin, a potent platelet aggregation inhibitor and GP IIb-IIIa antagonist. *Science* **1991**, 253, (5018), 445-8.
137. Krezel, A. M.; Wagner, G.; Seymour-Ulmer, J.; Lazarus, R. A., Structure of the RGD protein decorsin: conserved motif and distinct function in leech proteins that affect blood clotting. *Science* **1994**, 264, (5167), 1944-7.
138. Smith, K. J.; Jaseja, M.; Lu, X.; Williams, J. A.; Hyde, E. I.; Trayer, I. P., Three-dimensional structure of the RGD-containing snake toxin albolabrin in solution, based on <sup>1</sup>H NMR spectroscopy and simulated annealing calculations. *Int J Pept Protein Res* **1996**, 48, (3), 220-8.
139. Rahman, S.; Aitken, A.; Flynn, G.; Formstone, C.; Savidge, G. F., Modulation of RGD sequence motifs regulates disintegrin recognition of  $\alpha$ IIb  $\beta$ 3 and  $\alpha$ 5  $\beta$ 1 integrin complexes. Replacement of elegantin alanine-50 with proline, N-terminal to the RGD sequence, diminishes recognition of the  $\alpha$ 5  $\beta$ 1 complex with restoration induced by Mn<sup>2+</sup> cation. *Biochem J* **1998**, 335 ( Pt 2), 247-57.
140. Verrier, S.; Pallu, S.; Bareille, R.; Jonczyk, A.; Meyer, J.; Dard, M.; Amedee, J., Function of linear and cyclic RGD-containing peptides in osteoprogenitor cells adhesion process. *Biomaterials* **2002**, 23, (2), 585-96.
141. Pierschbacher, M. D.; Ruoslahti, E., Influence of stereochemistry of the sequence Arg-Gly-Asp-Xaa on binding specificity in cell adhesion. *J Biol Chem* **1987**, 262, (36), 17294-8.
142. Samanen, J.; Ali, F.; Romoff, T.; Calvo, R.; Sorenson, E.; Vasko, J.; Storer, B.; Berry, D.; Bennett, D.; Strohsacker, M.; et al., Development of a small RGD peptide fibrinogen receptor antagonist with potent antiaggregatory activity in vitro. *J Med Chem* **1991**, 34, (10), 3114-25.
143. Wu, Y.; Zhang, X.; Xiong, Z.; Cheng, Z.; Fisher, D. R.; Liu, S.; Gambhir, S. S.; Chen, X., microPET imaging of glioma integrin  $\alpha$ <sub>v</sub> $\beta$ <sub>3</sub> expression using (64)Cu-labeled tetrameric RGD peptide. *J Nucl Med* **2005**, 46, (10), 1707-18.
144. Chen, X.; Park, R.; Tohme, M.; Shahinian, A. H.; Bading, J. R.; Conti, P. S., MicroPET and autoradiographic imaging of breast cancer  $\alpha$ <sub>v</sub>-integrin expression using <sup>18</sup>F- and <sup>64</sup>Cu-labeled RGD peptide. *Bioconjug Chem* **2004**, 15, (1), 41-9.
145. Haubner, R.; Wester, H. J.; Weber, W. A.; Mang, C.; Ziegler, S. I.; Goodman, S. L.; Senekowitsch-Schmidtke, R.; Kessler, H.; Schwaiger, M., Noninvasive imaging of

alpha(v)beta3 integrin expression using 18F-labeled RGD-containing glycopeptide and positron emission tomography. *Cancer Res* **2001**, 61, (5), 1781-5.

146. Edwards, W. B.; Akers, W. J.; Ye, Y.; Cheney, P. P.; Bloch, S.; Xu, B.; Laforest, R.; Achilefu, S., Multimodal imaging of integrin receptor-positive tumors by bioluminescence, fluorescence, gamma scintigraphy, and single-photon emission computed tomography using a cyclic RGD peptide labeled with a near-infrared fluorescent dye and a radionuclide. *Mol Imaging* **2009**, 8, (2), 101-10.

147. Caswell, P. T.; Norman, J. C., Integrin trafficking and the control of cell migration. *Traffic* **2006**, 7, (1), 14-21.

148. Fani, M.; Psimadas, D.; Zikos, C.; Xanthopoulos, S.; Loudos, G. K.; Bouziotis, P.; Varvarigou, A. D., Comparative evaluation of linear and cyclic 99mTc-RGD peptides for targeting of integrins in tumor angiogenesis. *Anticancer Res* **2006**, 26, (1A), 431-4.

149. Brooks, P. C.; Clark, R. A.; Cheres, D. A., Requirement of vascular integrin  $\alpha v \beta 3$  for angiogenesis. *Science* **1994**, 264, (5158), 569-571.

150. Creamer, D.; Sullivan, D.; Bicknell, R.; Barker, J., Angiogenesis in psoriasis. *Angiogenesis* **2002**, 5, (4), 231-6.

151. Bishop, G. G.; McPherson, J. A.; Sanders, J. M.; Hesselbacher, S. E.; Feldman, M. J.; McNamara, C. A.; Gimple, L. W.; Powers, E. R.; Mousa, S. A.; Sarembock, I. J., Selective alpha(v)beta(3)-receptor blockade reduces macrophage infiltration and restenosis after balloon angioplasty in the atherosclerotic rabbit. *Circulation* **2001**, 103, (14), 1906-11.

152. Chavakis, E.; Riecke, B.; Lin, J.; Linn, T.; Bretzel, R. G.; Preissner, K. T.; Brownlee, M.; Hammes, H. P., Kinetics of integrin expression in the mouse model of proliferative retinopathy and success of secondary intervention with cyclic RGD peptides. *Diabetologia* **2002**, 45, (2), 262-7.

153. Jens Gille, R. A. S., Integrins: Role in Cell Adhesion and Communication. *Anal. NY Acad. Sci.* **1996**, 797, (Microbial Pathogenesis and Immune Response II), 93-106.

154. Seftor, R. E.; Seftor, E. A.; Gehlsen, K. R.; Stetler-Stevenson, W. G.; Brown, P. D.; Ruoslahti, E.; Hendrix, M. J., Role of the  $\alpha v \beta 3$  integrin in human melanoma cell invasion. *Proc. Natl. Acad. of Sci. USA.* **1992**, 89, (5), 1557-1561.

155. Montgomery, A. M.; Reisfeld, R. A.; Cheresch, D. A., Integrin  $\alpha_v\beta_3$  rescues melanoma cells from apoptosis in three-dimensional dermal collagen. *Proc. Natl. Acad. of Sci. USA*. **1994**, 91, (19), 8856-8860.
156. Ruoslahti, E.; Pierschbacher, M. D., New perspectives in cell adhesion: RGD and integrins. *Science* **1987**, 238, (4826), 491-497.
157. Pasqualini, R.; Koivunen, E.; Ruoslahti, E.,  $\alpha_v$  Integrins as receptors for tumor targeting by circulating ligands. *Nat. Biotech.* **1997**, 15, (6), 542-546.
158. Arap, W.; Pasqualini, R.; Ruoslahti, E., Cancer Treatment by Targeted Drug Delivery to Tumor Vasculature in a Mouse Model. *Science* **1998**, 279, (5349), 377-380.
159. Ellerby, H. M.; Arap, W.; Ellerby, L. M.; Kain, R.; Andrusiak, R.; Rio, G. D.; Krajewski, S.; Lombardo, C. R.; Rao, R.; Ruoslahti, E.; Bredesen, D. E.; Pasqualini, R., Anti-cancer activity of targeted pro-apoptotic peptides. *Nat Med* **1999**, 5, (9), 1032-8.
160. Cai, W.; Niu, G.; Chen, X., Imaging of Integrins as Biomarkers for Tumor Angiogenesis. *Curr. Pharm. Design* **2008**, 14, 2943-2973.
161. Lim, E. H.; Danthi, N.; Bednarski, M.; Li, K. C. P., A review: Integrin  $\alpha_v\beta_3$ -targeted molecular imaging and therapy in angiogenesis. *Nanomedicine: Nanotechnology, Biology and Medicine* **2005**, 1, (2), 110-114.
162. Zhou, Q.; Wulfkuhle, J.; Ouatas, T.; Fukushima, P.; Stetler-Stevenson, M.; Miller, F. R.; Steeg, P. S., Cyclin D1 overexpression in a model of human breast premalignancy: Preferential stimulation of anchorage-independent but not anchorage-dependent growth is associated with increased cdk2 activity. *Breast Cancer Research and Treatment* **2000**, 59, (1), 27-39.
163. King C.P. Li, M. D. B., Vascular-targeted molecular imaging using functionalized polymerized vesicles. *J. Magn. Reson. Imaging*. **2002**, 16, (4), 388-393.
164. Dubey, P. K.; Mishra, V.; Jain, S.; Mahor, S.; Vyas, S. P., Liposomes Modified with Cyclic RGD Peptide for Tumor Targeting. *J. Drug Target*. **2004**, 12, (5), 7-264.
165. Marko, K. L., M.; Mezo, G.; Mihala, N.; Kutnyanszky, E.; Kiss, E.; Hudecz, F.; Madarasz, E., A Novel Synthetic Peptide Polymer with Cyclic RGD Motifs Supports Serum-Free Attachment of Anchorage-Dependent Cells. *Bioconjugate Chem.* **2008**, 19, (9), 1757-1766.

166. Nagai, Y.; Hasegawa, M.; Shinmi, K.; Kishi, C.; Tsushima, Y.; Endo, K.; Okabe, K.; Suzuki, K.; Ishikawa, O., Nephrogenic systemic fibrosis with multiple calcification and osseous metaplasia. *Acta Derm Venereol FIELD Full Journal Title:Acta dermatovenereologica* **2008**, 88, (6), 597-600.
167. Chen, R.; Curran, S. J.; Curran, J. M.; Hunt, J. A., The use of poly(L-lactide) and RGD modified microspheres as cell carriers in a flow intermittency bioreactor for tissue engineering cartilage. *Biomaterials* **2006**, 27, (25), 4453-4460.
168. Montet, X.; Funovics, M.; Montet-Abou, K.; Weissleder, R.; Josephson, L., Multivalent Effects of RGD Peptides Obtained by Nanoparticle Display. *J. Med. Chem.* **2006**, 49, (20), 6087-6093.
169. Kang, H.; Alam, M. R.; Dixit, V.; Fisher, M.; Juliano, R. L., Cellular Delivery and Biological Activity of Antisense Oligonucleotides Conjugated to a Targeted Protein Carrier. *Bioconjugate Chem.* **2008**, 19, (11), 2182-2188.
170. J. L. Turner, D. P., R. Plummer, Z. Chen, A. K. Whittaker, K. L. Wooley, Synthesis of Gadolinium-Labeled Shell-Crosslinked Nanoparticles for Magnetic Resonance Imaging Applications. *Adv. Funct. Mater.* **2005**, 15, (8), 1248-1254.
171. Becker, M. L.; Liu, J.; Wooley, K. L., Functionalized Micellar Assemblies Prepared via Block Copolymers Synthesized by Living Free Radical Polymerization upon Peptide-Loaded Resins. *Biomacromolecules* **2005**, 6, (1), 220-228.
172. Sun, G.; Hagooly, A.; Xu, J.; Nystrom, A. M.; Li, Z.; Rossin, R.; Moore, D. A.; Wooley, K. L.; Welch, M. J., Facile, efficient approach to accomplish tunable chemistries and variable biodistributions for shell cross-linked nanoparticles. *Biomacromolecules* **2008**, 9, (7), 1997-2006.
173. Sprague, J. E.; Kitaura, H.; Zou, W.; Ye, Y.; Achilefu, S.; Weillbaecher, K. N.; Teitelbaum, S. L.; Anderson, C. J., Noninvasive Imaging of Osteoclasts in Parathyroid Hormone-Induced Osteolysis Using a <sup>64</sup>Cu-Labeled RGD Peptide. *J. Nucl. Med.* **2007**, 48, (2), 311-318.
174. Xu, J.; Sun, G.; Rossin, R.; Hagooly, A.; Li, Z.; Fukukawa, K.-I.; Messmore, B. W.; Moore, D. A.; Welch, M. J.; Hawker, C. J.; Wooley, K. L., Labeling of Polymer Nanostructures for Medical Imaging: Importance of Cross-Linking Extent, Spacer Length, and Charge Density. *Macromolecules* **2007**, 40, (9), 2971-2973.

175. Hosseinkhani, H.; Tabata, Y., PEGylation enhances tumor targeting of plasmid DNA by an artificial cationized protein with repeated RGD sequences, *Pronectin® J. Controlled Release* **2004**, 97, (1), 157-171.
176. Okarvi, S. M., Peptide-based radiopharmaceuticals: future tools for diagnostic imaging of cancers and other diseases. *Med Res Rev* **2004**, 24, (3), 357-97.
177. Smith, S. V., Molecular imaging with copper-64. *Journal of Inorganic Biochemistry* **2004**, 98, (11), 1874-1901.
178. Kukis, D. L.; Li, M.; Meares, C. F., Selectivity of antibody-chelate conjugates for binding copper in the presence of competing metals. *Inorganic Chemistry* **1993**, 32, (19), 3981-3982.
179. Becker, M. L.; Liu, J.; Wooley, K. L., Functionalized micellar assemblies prepared via block copolymers synthesized by living free radical polymerization upon peptide-loaded resins. *Biomacromolecules* **2005**, 6, (1), 220-8.
180. Weisman, G. R.; Wong, E. H.; Hill, D. C.; Rogers, M. E.; Reed, D. P.; Calabrese, J. C., Synthesis and transition-metal complexes of new cross-bridged tetraamine ligands. *J. Chem. Soc. Chem. Commun.* **1996**, 947-948.
181. Wong, E. D.; Weisman, G. R., *J. Am. Chem. Soc.* **2000**, 122, 10561-10572.

*Curriculum Vitae*  
Ashley Lauren Fiamengo

**ADDRESS:** Washington University School of Medicine  
Department of Radiological Sciences  
510 S. Kingshighway Blvd.  
Campus Box 8225  
St. Louis, MO 63110

**PHONE:** 314.362.8473 (work)  
314.362.9940 (fax)

**EMAIL:** fiamengoa@mir.wustl.edu

**EDUCATION:**

2004-2009: Washington University in St. Louis, St. Louis, MO  
Ph.D. candidate in Chemistry, August 2009  
Relevant course work: Inorganic Chemistry, Organometallic Chemistry,  
Inorganic Biochemistry, Chemical Biology, Principles and Applications of  
Biological Imaging, Contrast Agents for Biological Imaging, Nanomedicine

2000-2004: Austin College, Sherman, TX  
Bachelor of Arts, *magna cum laude*, Honors in Chemistry  
Concentrations: Biochemistry, French

2003: San Jose State University, San Jose, CA  
ACS/DOE Nuclear and Radiochemistry Summer School

**RESEARCH EXPERIENCE:**

2005-2009: Washington University in St. Louis, MO  
Ph.D. graduate research, Advisor: Carolyn J. Anderson  
Topic: Structurally diverse <sup>64</sup>Cu-labeled RGD peptide conjugates for PET  
imaging of  $\alpha_v\beta_3$  expression

2003-2004: Austin College, Sherman, TX  
Undergraduate Honors Thesis Research, Advisor: Andrew J. Carr  
Topic: Synthesis and *in vitro* characterization of quaternary ammonium  
antibacterial agents

2002-2003: Austin College, Sherman, TX  
Undergraduate Research, Advisor: Andrew J. Carr  
Topic: Synthesis, spectral analysis, and thermodynamic studies of bis-urea  
organogelators

2000-2001: Oregon Health & Science University, Portland, OR  
High School Research and Undergraduate Summer Research,  
Advisor: Gail M. Clinton  
Topic: Cloning, expression, and purification of Herstatin intron 8 protein  
isoforms

**TEACHING EXPERIENCE:**

2005-2006, 2009: Graduate Teaching Assistant, Washington University in St. Louis, MO  
General Chemistry II (Chem 112a)  
General Chemistry Laboratory I and II (Chem 151 and 152)  
Inorganic Chemistry Laboratory (Chem 470)

2001-2004: Undergraduate Teaching Assistant, Austin College, TX  
Introduction to Chemistry Laboratory (Chem 15)  
Chemical Equilibria Laboratory (Chem 16)  
Organic Chemistry Laboratory I and II (Chem 35 and 36)  
General and Organic Chemistry tutoring

**HONORS AND AWARDS:**

Teaching Citation, Teaching Center at Washington University in St. Louis (July 2009)  
DOE Travel Award to attend the 18<sup>th</sup> International Symposium on Radiopharmaceutical Sciences (2009)  
DOD Breast Cancer Research Program pre-doctoral traineeship award (2006-2008)  
GSAS Tuition Scholarship, Washington University (2004-2009)  
ACS/DOE Nuclear and Radiochemistry Summer School Fellowship (2003)  
Austin College Dean's List (Fall 2000, Spring 2002, Spring 2003, Spring 2004)  
Austin College State Fellowship (2000-2004)

**PROFESSIONAL ACTIVITIES:**

2001-present: American Chemical Society  
ACS National member (since 2004)  
Division of Nuclear Chemistry and Technology member (since 2004)  
ACS Student Affiliate (2001-2004)  
2006-present: American Academy for the Advancement of Science member

**POSTERS AND PRESENTATIONS:**

**Fiamengo, AL;** Ye, Y; Achilefu, S; Anderson, CJ. " In vitro and in vivo evaluation of structurally diverse <sup>64</sup>Cu-labeled RGD peptides for PET imaging of expression." 18<sup>th</sup> International Symposium on Radiopharmaceutical Sciences, July 2009, Edmonton (AB), Canada. (oral)

**Fiamengo, AL;** Ye, Y; Achilefu, S; Anderson, CJ. "Binding affinity and cellular internalization of  $\alpha_v\beta_3$ -targeting ligands for molecular imaging of cancer and cardiovascular disease." 236<sup>th</sup> American Chemical Society National Meeting, August 2008, Philadelphia, PA. (oral)

**Fiamengo, AL;** Sprague, JE; Ye, Y; Achilefu, S; Anderson, CJ. "Binding affinity determination of  $\alpha_v\beta_3$ -targeting ligands for imaging of osteolysis." DOD Era of Hope Meeting, June 2008, Baltimore, MD. (poster)

**Fiamengo, AL;** Li, Z; Sun, G; Xu, J; Wooley, KL; Anderson, CJ. "Binding affinity determination of RGD-functionalized shell crosslinked nanoparticles to  $\alpha_v\beta_3$  and  $\alpha_v\beta_5$  integrins." 234<sup>th</sup> American Chemical Society National Meeting, August 2007, Boston, MA. (oral)

- Fiamengo, AL**; Capretto, DA; Sprague, JE; Peng, Y; Weisman, GR; Wong, EH; Anderson, CJ. "In vivo evaluation of  $^{64}\text{Cu}$ -labeled cross-bridged tetraazamacrocyclic complexes with amide and/or carboxylate functional groups." 7<sup>th</sup> International Symposium on Technetium in Chemistry and Nuclear Medicine, September 2006, Bressanone (BZ), Italy. (poster)
- Fiamengo, AL**; Carr, AJ. "Synthesis and characterization of tetraalkyl ammonium, urea-based hydrogelators." National Conferences on Undergraduate Research, April 2004, Indianapolis, IN. (poster)
- Fiamengo, AL**; Carr, AJ. "Synthesis of urea-based organogelators." American Chemical Society Southwest Regional Meeting, November 2002, Austin, TX. (poster)

#### PUBLICATIONS:

- Fiamengo, AL**; Ye, Y; Achilefu, S; Anderson, CJ. "In vitro and in vivo evaluation of structurally diverse  $^{64}\text{Cu}$ -labeled RGD peptides for PET imaging of  $\alpha_v\beta_3$  expression." Manuscript in preparation.
- Shokeen, MS; Pressly, ED; Ramos, N; Zheleznyak, A; **Fiamengo, AL**; Hawker, CJ; Anderson, CJ. "Tunable synthesis and *in vitro* evaluation of multifunctional,  $\alpha_v\beta_3$ -targeted nanoparticles comprised of amphiphilic block graft copolymers." Manuscript in preparation.
- Li, Z; **Fiamengo, AL**; Xu, J; Sun, G; Xu, J; Liu, Y; Welch, MJ; Leonard, J; Anderson, CJ; Wooley, KL. "Preparation, Purification, and *In Vitro* Characterization of RGD-Functionalized Shell Crosslinked Nanoparticles." Manuscript in preparation.
- Ferdani, R; Stigers, D; **Fiamengo, AL**; Wei, L; Wong, EH; Weisman, GR; Anderson, CJ. "Synthesis, Cu(II) complexation,  $^{64}\text{Cu}$ -labeling and biological evaluation of 1,4,8,11-tetraazacyclotetradecane-1,8-di(methanephosphonic acid) (CB-TE2P): Comparison with CB-TE2A, NOTA and Diamsar." Manuscript in preparation.
- Sprague, JE; Peng, Y; **Fiamengo, AL**; Wooden, KS; Southwick, EA; Weisman, GR; Wong, EH; Golen, JA; Rheingold, AL; Anderson, CJ. "Synthesis, characterization and in vivo studies of  $^{64}\text{Cu}$ (II)-labeled cross-bridged tetraazamacrocyclic-amide complexes as models of peptide conjugate imaging agents." *J. Med. Chem.* 2007; 50 (10): 2527-2535.
- Fiamengo, AL**; Capretto, DA; Sprague, JE; Peng, Y; Weisman, GR; Wong, EH; Anderson, CJ. "In vivo evaluation of  $^{64}\text{Cu}$ -labeled cross-bridged tetraazamacrocyclic complexes with amide and/or carboxylate functional groups." Technetium, Rhenium and Other Metals in Chemistry and Nuclear Medicine, 7th Ed. Mazzi, U. (ed), Servizi Grafici Editoriali, Padova, 2006, pp. 235-236.



